Title
Hadean-Archean transitions: Constraints from the Jack Hills detrital zircon record

Author
Bell, Elizabeth Ann

Publication Date
2013

Peer reviewed|Thesis/dissertation

UNIVERSITY OF CALIFORNIA

Los Angeles

Hadean-Archean transitions: Constraints from the Jack Hills detrital zircon record

A dissertation submitted in partial satisfaction of the requirements for the degree Doctor of Philosophy in Geochemistry

by

Elizabeth Ann Bell

2013

ABSTRACT OF THE DISSERTATION

Hadean-Archean transitions: Constraints from the Jack Hills detrital zircon record

by

Elizabeth Ann Bell

Doctor of Philosophy in Geochemistry

University of California, Los Angeles, 2013

Professor T. Mark Harrison, chair

Detrital zircons from the Jack Hills (Yilgarn Craton, Western Australia) range from ca. 4.4 to 3.0 Ga in age and constitute the most complete known record for the pre-4 Ga (i.e., Hadean) Earth. Many past investigations have established the geochemistry of the Hadean zircons: their Hf isotope compositions suggest dominant sourcing from ancient felsic crust, while their low Ti crystallization temperatures (average ca. 680˚C) and commonly igneous internal zonation suggests granitic origins. In addition, their dominant mineral inclusion assemblage of quartz + muscovite, along with a large minority of zircons displaying heavy $\delta^{18}O$ reminiscent of meta-sedimentary input, has led to their interpretation as largely sourced from S-type granites. Concordant Hadean zircons, however, make up only ca. 5% of the Jack Hills population, and the few investigations of the younger zircons have hinted at somewhat different provenances.

We investigate the <4 Ga history of the Jack Hills zircons and their provenance(s), finding both important geochemical similarities and differences between the post-Hadean and

Hadean populations. The average crystallization temperature of ca. 680˚C does not appear notably different from the Hadean population, indicating continued dominance of granitic protoliths. However, the younger zircons are overall both more radiogenic in Lu-Hf and have a more restricted, mantle-like $\delta^{18}O$ distribution with no obvious evidence for meta-sedimentary magma sources. Further investigation of the sparsely populated time period 4.0-3.6 Ga reveals that this restriction in $\delta^{18}O$ occurs fairly suddenly after 3.8 Ga. This time period is also marked by the disappearance of an ancient felsic crustal component (at ca. 3.7 Ga) and evidence for juvenile input from the mantle (at ca. 3.8 Ga), reminiscent of Hf isotope patterns seen in Phanerozoic subduction-related orogens. We interpret the Hf isotope record as evidence for subduction-related recycling of much of the ancient Hadean crust at ca. 3.8-3.7 Ga. A distinctive group of zircons with trace element geochemistry and internal textures consistent with metamorphic recrystallization occurs just before this point at ca. 3.91-3.84 Ga. The coincidence of this apparent event with our proposed subduction event soon thereafter and/or with the hypothesized Late Heavy Bombardment of the inner solar system are both interesting, but causal relationships are not entirely clear with the present evidence. Overall, however, the changeover from the prevailing Hadean provenance(s) to a different source(s) for the younger zircons occurs in a series of geochemical transitions between 3.9 and 3.7 Ga, likely reflecting important tectonic (or exogenic) events in the ancestral Jack Hills crust.

Investigation of the Hadean population itself reveals interesting patterns of post-Hadean alteration: we employ Xe isotopic systematics to investigate the zircons' original Pu/U ratios and later Xe loss histories. ^{244}Pu and ^{238}U spontaneously fission to produce characteristic isotopic components of Xe, while irradiation with thermal neutrons induces fission of ^{235}U to create a third component. Deconvolution of fission Xe from irradiated zircons into these end-member

components allows for estimation of both the original Pu/U of the zircons and the U-Xe age. Nearly all investigated zircons in this and a previous study have post-Hadean U-Xe ages, and in this study they range as young at ca. 1.8 Ga. This finding underscores the long history of post-Hadean thermal events that affected the zircons. Pu/U is a potential indicator for aqueous mobilization of the more soluble U, but the near ubiquity of subchondritic Pu/U in this population may be mostly due to the effects of Xe loss. The higher range of Pu/U in younger relative to older Hadean zircons in this and a previous study, coupled with other trace element indicators for more compositionally evolved melts, may however suggest that the Pu/U was partly controlled by magmatic processes. A larger set of samples with minimal Xe loss, however, would be needed to confirm this observation.

Finally, we have begun building a model of free subduction in order to test whether this process would be more or less likely to occur in a warmer mantle (as expected for the early Earth) – a contentious subject with various contradictory model results in the literature. Results for our initial Cartesian model are of uncertain applicability to the Earth given the ubiquity of 2-sided rather than 1-sided subduction in the models. However, the model results do suggest that for oceanic plates of modern thickness (ca. 100 km), warmer mantle temperatures may indeed enhance the tendency toward subduction. Thinner plates, as proposed by some workers, do not subduct as readily and are more likely to show slab breakoff events, while thicker plates subduct more readily than modern slabs. Slab geometry appears to be a function of both mantle temperature and the maximum lithospheric viscosity allowed by each model, and has implications for the preservation of subduction-related lithologies on the upper plate.

The dissertation of Elizabeth Ann Bell is approved.

Axel K. Schmitt

Alice Shapley

Edward D. Young

T. Mark Harrison, Committee Chair

University of California, Los Angeles

2013

For Mom, Dad, and Julia

Table of Contents

Acknowledgments

Many people have helped me immensely along the way in conducting my doctoral research and writing this dissertation. Dianne Taylor, Karen Ziegler, Sarah Crowther, and Issaku Kohl provided invaluable help and instruction in analyzing my samples. Discussions with Patrick Boehnke regarding my statistical analysis in ch. 3 were very helpful in improving its rigor, and my interpretations were helped greatly by discussions with Matthew Wielicki and Sunshine Abbott. Many of the oxygen isotope analyses presented in ch. 4 and Appendix G were collected by Haibo Zhou. Discussions with Rita Economos, Jason Kaiser, Carolyn Crow, and others were crucial to much of the trace element discussion in ch. 4-5. In addition to my committee member David Stegman, Robert Petersen was instrumental in helping me to use the geodynamic code in ch. 6 and in interpreting the results thereof.

My committee and many other faculty members have been wonderful in both providing instruction on analytical or computational techniques and in guiding my research. Alice Shapley's observations on the manuscript and thoughtful questions have been very useful in putting together the final version of this dissertation. Ed Young provided both the laboratory for making my Lu-Hf-Pb measurements and immense guidance in understanding isotope geochemistry, both in the classroom and in my research. Kevin McKeegan's SIMS class was very helpful in establishing me as a user of the ion probe. Axel Schmitt has patiently taught me the workings of the ion microprobe and also required that I learn independence on the machine for several measurements, which has been very valuable both for not only my ability to analyze samples but also my understanding of the SIMS and the data I've collected thereby. Dave Stegman introduced me to geodynamic modeling and adapted the version of StagYY I employ in ch. 6. He has been crucial to the results and interpretations I report here and to the future work

outlined in ch. 6. My advisor, Mark Harrison, has not only guided me in the course of this project but has also provided an invaluable model of skeptical analysis, creativity, and effective scientific writing that has profoundly influenced my view of science as both a field of inquiry and as a community with its strengths and weaknesses.

The ion microprobe facility at UCLA is partly supported by a grant from the Instrumentation and Facilities Program, Division of Earth Sciences, National Science Foundation. This research was conducted with support from a grant to T. Mark Harrison from NSF-EAR's Petrology/Geochemistry Program and an NSF Graduate Research Fellowship to Elizabeth A. Bell.

Ch. 2 was published in *Geochimica et Cosmochimica Acta* as

Bell, E.A., Harrison, T.M., McCulloch, M.T., Young, E.D., 2011. Early Archean crustal evolution of the Jack Hills Zircon source terrane inferred from Lu-Hf, $^{207}Pb/^{206}Pb$, and $\delta^{18}O$ systematics of Jack Hills zircons. *Geochim. Cosmochim. Acta*., 75, 4816-4829.

Ch. 3 was published in *Earth and Planetary Science Letters* as

Bell, E.A., Harrison, T.M., 2013. Post-Hadean transitions in Jack Hills zircon provenance: A signal of the Late Heavy Bombardment? *Earth Planet. Sci. Lett.*364, 1-11.

Ch. 4 is a modified version of a manuscript under review at *Geology* as

Bell, E.A., Harrison, T.M., Kohl, I.E., Young, E.D., Hf isotopic evidence for Hadean-Eoarchean transitions in crustal evolution. Under review at *Geology*.

Ch. 5 is based on a manuscript in preparation for submission:

Bell, E.A., Gilmour, J.D. Harrison, T.M., Turner, G., Crowther, S.A., Origins of variable Xe loss and Pu/U among Hadean Jack Hills zircons. *In prep*.

Vita

Education

2008: B.Sc. in geology, University of South Carolina, Columbia
GPA: 3.979
Thesis title: *A Novel Provenance Method for Detrital Calcareous Sediments by Single-Grain Stable Isotope and Elemental Geochemistry*

Research Experience

2008 – present: graduate student researcher (advisor: Prof. Mark Harrison), UCLA

2006: internship in Seismology and Tectonics Laboratory (PI: Prof. William Holt), SUNY Stony Brook, as part of the Mineral Physics Institute Summer Scholars Program (an NSF-affiliated REU)

2005 – 2008: undergraduate research assistant, Tectonics and Sedimentation Laboratory (PI: Prof. David Barbeau), University of South Carolina

Grants and Awards

2012: CIDER Group Research Project grant, "The Late Veneer: Constraints on Composition, Mass, and Mixing Timescales" -- $4500

2011: Eugene B. Waggoner Scholarship, Dept. of Earth and Space Sciences, UCLA

2010: National Science Foundation Graduate Research Fellowship

2008: Dorothy Radcliffe Dee Scholarship, Dept. of Earth and Space Sciences, UCLA

2008: Institute of Geophysics and Planetary Physics Fellowship, UCLA

2007: Barry M. Goldwater Scholarship

Peer-Reviewed Publications

Bell, E.A., Harrison, T.M., McCulloch, M.T., Young, E.D., 2011. Early Archean crustal evolution of the Jack Hills Zircon source terrane inferred from Lu-Hf, $^{207}Pb/^{206}Pb$, and $\delta^{18}O$ systematics of Jack Hills zircons. *Geochim. Cosmochim. Acta*., 75, 4816-4829.

Bell, E.A., Harrison, T.M., 2013. Post-Hadean transitions in Jack Hills zircon provenance: A signal of the Late Heavy Bombardment? *Earth Planet. Sci. Lett.*364, 1-11.

Publications Submitted or in Preparation

Bell, E.A., Harrison, T.M., Kohl, I.E., Young, E.D., Hf isotopic evidence for Hadean-Eoarchean transitions in crustal evolution. Under review at *Geology*.

Bell, E.A., Gilmour, J.D. Harrison, T.M., Turner, G., Crowther, S.A., Origins of variable Pu/U among Hadean Jack Hills zircons. In prep.

Selected Meeting Presentations

(*indicates I presented)

*Bell, E.A.; Harrison, T.M.; Kohl, I.E.; Young, E.D.; Hadean-Eoarchean transitions in crustal evolution from Hf isotopic evidence. AGU Fall Meeting December 2013.

*Bell, E.A.; Gilmour, J.D.; Harrison, T.M.; Turner, G.; Crowther, S.A.; Origins of variable Pu/U among Hadean Jack Hills zircons, 44th Annual Lunar and Planetary Science Conference, March 2013.

*Bell, E.A., Harrison, T.M., Mojzsis, S.J.; Mid-Proterozoic detrital zircons and the depositional history of the Jack Hills (Narryer Gneiss Complex, Western Australia), AGU Fall Meeting December 2012.

Prescher, C., Allupeddinti, D, Bell, E.A., Bello, L., Cernok, A., Ghosh, N., Tucker, J., Wielicki, M., Zahnle, K.; Origin and mixing timescale of the Earth's late veneer, AGU Fall Meeting December 2012.

*Bell, E.A., Harrison, T.M.; Jack Hills zircons record a thermal event coincident with the hypothesized Late Heavy Bombardment, Goldschmidt 2012.

*Bell, E.A., Harrison, T.M.; Trace Elements Reveal a Possible Link Between some Jack Hills detrital zircons and the Late Heavy Bombardment, 43rd Annual Lunar and Planetary Science Conference, March 2012.

*Bell, E.A., Harrison, T.M.; Possible link between detrital Jack Hills zircons and the Late Heavy Bombardment. AGU Fall Meeting, December 2011.

Tailby N., Trail D., Cates N., Mojzsis S., Bell E., Harrison, T.M., Watson, E.B.; Direct Measurement of Ce^{3+}/Ce^{4+} and Eu^{2+}/Eu^{3+} in Hadean Zircons by XANES, Goldschmidt 2011.

*Harrison, T.M.; Bell, E.A.; Jack Hills Lu-Hf revisited, Goldschmidt 2011.

*Bell, E.A.; Harrison, T.M.; A change in igneous conditions of the Jack Hills zircon source(s) ca. 3.9 Ga, AGU Fall Meeting December 2010.

*Bell, E.A.; Harrison, T.M.; Early Archean crustal evolution from Jack Hills detrital zircons, Goldschmidt 2010.

*Bell, E.A.; Wielicki, M.M.; Abbott, S.S.; Mojzsis, S.J.; Harrison, T.M.; Do the Jack Hills zircons record evidence of the Late Heavy Bombardment? AGU Fall Meeting December 2009.

*Bell, E. A.; Harrison, T. M.; Lovera, O. M.; McCulloch, M. T.; Young, E. D.; Early Archean crustal evolution in the Yilgarn: Constraints from Lu-Hf in Jack Hills zircons, Goldschmidt 2009.

Chapter One: Introduction – Hadean-Archean Transitions

The Earth exhibits several striking differences from other terrestrial bodies in that it loses heat through plate tectonics, supports liquid water over much of the surface and subsurface environment, and appears uniquely (so far as is known) supportive of life. The reasons that these conditions prevail only on Earth are only partially clear. In contrast, the apparently wet and possibly life-supporting early period(s) on now arid and seemingly abiotic Mars raises the question of when this divergence began. Knowledge of this timing would then help constrain the mechanisms responsible for the very different evolution of terrestrial planetary environments. An important step in drawing these comparisons is constraining the early history of Earth's crust and surficial environments and understanding how they changed during the planet's first few hundred million years. Over the past decade, empirical evidence from early detrital mineral records has dramatically reshaped our view of this period, including showing that, much like early Mars, there was likely a hydrosphere present during much of the Hadean (>4 Ga) eon on Earth. However, before 4.03 Ga (Bowring and Williams, 1999) there is no rock record (cf. O'Neil et al., 2008), limiting our ability to peer into the planet's earliest state.

The oldest solids in our solar system condensed at 4.573±0.001 Ga (Bouvier and Wadhwa, 2010; Connelly et al., 2008) with Earth forming and differentiating within the following ~30 to 70 Ma (Kleine et al., 2009; refs. therein). The oldest known rocks on Earth are components of the Acasta Gneiss with ages up to ~4.03 Ga (zircon U-Pb, Bowring and Williams, 1999), although an age of up to ~4.4 Ga has been purported for cummingtonite-bearing amphibolites of the Nuvvuagittuq Greenstone Belt based on ^{146}Sm-^{147}Sm/^{142}Nd-^{143}Nd systematics (O'Neil et al., 2013; cf. Cates et al., 2013). Either way, given the altered nature of those rocks, this leaves the first several hundred million years of planetary history essentially

unrecorded. The rock record since ~3.8 Ga is more readily interpretable in terms of geologic and environmental conditions, although many mysteries remain. For example, the geodynamics and tectonic regime of this period are uncertain (see Davies, 2006 vs. Davies, 1992 and Stern, 2007 for contrasting views on the operation of plate tectonics on the early Earth), as is the history of the silicate Earth's differentiation into early reservoirs and their loss or preservation with time.

Although there are a wealth of speculations regarding Earth's geodynamic and geochemical behavior during the Hadean, empirical information about the period is rare and comes almost exclusively from the sparse detrital zircon record. Zircons from the Jack Hills (Yilgarn craton, Western Australia; Compston and Pidgeon, 1986) have been especially fruitful in terms of identifying early crustal processes and materials. In the Jack Hills, a ca. 3 Ga conglomeratic sandstone contains zircons spanning the age range ~4.4 – 3.0 Ga (e.g., Peck et al., 2001; Crowley et al., 2005). Zircons in the sandstone form a dominant age population at 3.6-3.3 Ga and a minor population at 4.3-3.8 Ga. Zircons of other ages are rare, particularly >4.3 Ga and 3.8-3.6 Ga (see fig. 1.1). Approximately 10% of concordant grains are older than 3.8 Ga and ~5% are older than 4.0 Ga (e.g. Crowley et al., 2005; Holden et al., 2009).

Most work on the Jack Hills zircons has focused on the Hadean period, revealing evidence suggesting a hydrosphere, granitic melting, and a continental-like reservoir of material (see section 1.1). Much of this evidence complements that found in the whole-rock record by 3.8-3.5 Ga, which shows a planet with oceans and evolved granitic rocks. Whether there were any substantial changes between the Hadean and the early to middle Archean are uncertain from the fragmentary nature of the evidence. Arguments abound about not only the environmental conditions at the Earth's surface during this period but also whether plate tectonics or other tectonothermal regimes operated. The Jack Hills zircons provide a virtually continuous record of

magmatic conditions in one region of early crust through the Hadean and into the middle Archean, and thus represent our currently best known resource for investigating this period of history.

In this thesis, we present new evidence from the Jack Hills zircons relevant to both conditions during the Earth's first billion years and showing important transitions in magmatic sources at ca. 3.8 Ga that are relevant to the evolution and (lack of) preservation of the Hadean crust. This study is broken into 5 chapters (ch. 2-6).

First (ch. 2), we took a random survey of the Hf-Pb isotope systematics of the Jack Hills population using one 400-grain mount from the study of Holden et al. (2009). We also analyzed for $\delta^{18}O$ and Ti thermometry for added petrologic context. This survey revealed that the dominant 3.6-3.3 Ga zircon age population is different from the Hadean population in several respects: it shows an overall more radiogenic Lu-Hf composition and lacks the highly unradiogenic portions of the Hadean record. This population also displays much more mantle-like $\delta^{18}O$ with no obvious evidence for meta-sedimentary input. However, Ti-in-zircon temperatures still indicate near minimum-melt granitic origins. This points to a change in the formation environment of the zircons at some point between 4.0 and 3.6 Ga, but the 3.8-3.6 Ga age gap makes pinning the timing and nature of the transitions difficult with a random survey alone.

Next (ch. 3), we surveyed the period 4.0-3.6 Ga in particular for U-Pb ages, $\delta^{18}O$, and trace element geochemistry, to find evidence for geochemical transitions in zircon formation environment. We document a likely Pb loss event associated with distinctive chemistry reminiscent of solid-state transgressive recrystallization (Hoskin and Black, 2000) in ca. 3.91-

3.84 Ga zircons, an age range similar to estimates for the hypothesized Late Heavy Bombardment of the inner solar system (Tera et al., 1974). This study also established that the truncation of the concordant zircons' $\delta^{18}O$ distribution occurs at ca. 3.8 Ga.

Following on this track, we surveyed the period 4.0-3.6 Ga for Lu-Hf systematics (ch. 4), which revealed an abrupt discontinuity in the Hf record at ca. 3.8-3.7 Ga. The younger population lacks model ages >4.3 Ga, whereas these are very common beforehand. An apparent juvenile addition to the crust at ca. 3.8 Ga and the overall shifting of the population to more radiogenic compositions after this "sawtooth" event is reminiscent of Phanerozoic subduction-related orogens (Collins et al., 2011), and we interpret this as evidence for a subduction-like process operating at ca. 3.8-3.7 Ga that recycled much of the original Hadean crust in the Jack Hills ancestral terrane.

We investigated the xenon geochemistry of >4 Ga zircons in order to reveal patterns of post-Hadean alteration (ch. 5) and evaluate the use of Xe isotopes to identify Hadean aqueous mobilization of uranium vs. other processes to fractionate U from the other actinides. We also present preliminary results from modeling the feasibility of subduction under a warmer Hadean-Archean mantle and its plausible physical and chemical consequences for the early Earth's mineral record and crust (chapter 6).

Put together, these five studies provide a much clearer picture of the Jack Hills crust's evolution from Hadean to Archean times, and better constrain the geodynamic and geochemical environment of the early Earth.

1.1 Uncertainties in Hadean and Archean Conditions

Despite the presence of some clear signals for formation environment among the Hadean zircons, significant uncertainties remain as to the aqueous (or non-) and tectonic environment of the Jack Hills ancestral crust. A relative lack of data for the pre-4 Ga zircon formation environment, exacerbated by the 3.8-3.6 Ga gap in zircon ages, has also heretofore obscured any Hadean-Archean transitions that might be recorded in the Jack Hills zircon record.

1.1.1 Hadean Magmatic Compositions and Environment

The isotopic record of the Jack Hills zircons has been particularly useful in forming a Hadean narrative, particularly the stable isotopes of oxygen and the radiogenic ^{176}Lu-^{176}Hf system. Magmas with high δ^{18}O relative to the mantle value (5.3±0.3‰ SMOW; Valley, 2003) are interpreted in Phanerozoic zircons as deriving partially from sedimentary material. Sediments typically have high δ^{18}O, due to deriving from low-temperature aqueous weathering of their precursor rocks to form (δ^{18}O-enriched) clays. Jack Hills range in δ^{18}O from ~3-8‰ SMOW, with a substantial number higher than the mantle value (e.g., Mojzsis et al., 2001; Peck et al., 2001). This is probably evidence for their derivation from sediment-including magmas, and this interpretation has led to the idea of a Hadean hydrosphere. A mineral inclusion assemblage dominated by quartz and muscovite (Hopkins et al., 2008, 2010) and the low crystallization temperatures of the zircons (ca. 680˚C on average; Watson and Harrison, 2005; Harrison et al., 2008) bolsters the interpretation of hydrous granitic melts. However suggestive, these lines of evidence do not definitively demonstrate a Hadean hydrosphere (especially given the detrital, out-of-context nature of the existing Hadean mineral record), and it is useful to search for corroborating geochemical systems to distinguish among hydrous and anhydrous origins of the zircons' characteristics. Another potential geochemical indicator for water-rock interaction is uranium mobility. Uranium is soluble in water under a much larger range of

environmental conditions (i.e. in eH and pH) than the other light actinides Th and Pu (Maher et al., 2012). It thus may be possible from actinide behavior to further ascertain the effect of liquid water in the formation of Hadean zircon-bearing rocks. Investigation of the zircons' original Pu/U ratios (accomplished through xenon isotopic studies) may yield another control on Hadean environment and water-involved processes. Xenon isotopic studies also allow for calculation of a U-Xe age, further constraining any thermal events causing Xe loss among the zircons post-4 Ga.

It is also worth considering whether the zircon $\delta^{18}O$ record would be much affected by a very different seawater $\delta^{18}O$ composition for the early Earth. If, for instance, seawater (and by extension the meteoric waters derived from it) was significantly more enriched in ^{18}O, might the skewing of the Hadean zircon population toward high $\delta^{18}O$ represent remelting of protoliths with some limited water-rock interactions rather than significant metasedimentary input? Conversely, for a Hadean ocean significantly more depleted in ^{18}O than today, any low-$\delta^{18}O$ signature might not necessarily represent remelting of heavily hydrothermally altered magma sources, as it does today (e.g., Bindeman et al., 2006). Fig. 1.2 shows the hypothetical evolution of seawater $\delta^{18}O$ as a result of changing hydrothermal flux. Today, seawater $\delta^{18}O$ is buffered by both hydrothermal circulation at mid-ocean ridges, which tends to drive water towards higher $\delta^{18}O$, and low-temperature weathering on the seafloor (as well as subaerially on the continents), which tends to drive seawater $\delta^{18}O$ lower (Muehlenbachs and Clayton, 1976). Today these fluxes are in balance, but seawater may have increased in $\delta^{18}O$ by ca. 8 ‰ over the course of the Phanerozoic (Veizer et al., 1999) and its compositional evolution beforehand is more uncertain. The presence of muscovite inclusions in the zircons is an independent piece of evidence suggesting highly aluminous parent melts, so the conclusion of metasediments-including magmas is not based only

on the zircon oxygen isotope composition. However, further investigations of the possible Hadean hydrosphere, including by the Pu-U-Xe system mentioned above, will be useful.

The radiogenic ^{176}Lu-^{177}Hf system is a powerful tracer for mantle melting and the ages of crustal reservoirs. ^{176}Lu decays to ^{176}Hf with a half-life ~37 Ga (Soderlund et al., 2004). Deviations from chondritic^{176}Hf/^{177}Hf are used to determine model mantle extraction ages for Earth materials. Similar to the Sm/Nd system, mantle melting fractionates Lu and Hf so that melts have lower Lu/Hf ratio than the starting mantle material; the residue, with higher Lu/Hf, grows to higher ^{176}Hf/^{177}Hf ratios. Thus over time the depleted upper mantle has evolved to have ^{176}Hf/^{177}Hf ~18 epsilon units (parts per 10^4) higher than chondrites owing to higher time-integrated ^{176}Lu/^{177}Hf. Continental materials tend toward lower ^{176}Hf/^{177}Hf, often negative when normalized to the chondritic value ("ε_{Hf}"). Jack Hills zircons display dominantly negative ε_{Hf}, suggestive of a continental setting.

Jack Hills Hadean zircons also display extreme Hf isotopic compositions with both highly positive (~+15 epsilon at 4.2 Ga, Harrison et al., 2005) and highly negative (~-5 at 4.3 Ga) ε_{Hf}. The latter, highly unradiogenic group includes several zircons 4.3-4.0 Ga in age that fall within error of the solar system initial hafnium composition. Their existence necessitates the early formation of a very low Lu/Hf reservoir within the Earth. It is unclear from the zircon evidence how long this reservoir persisted or how large it was. Zircons as young as 4.0 Ga have ε_{Hf} within error of solar system initial ^{176}Hf/^{177}Hf (Harrison et al., 2008), but there is little evidence for the reservoir afterwards (Amelin et al., 1999) – although the 3.8-3.6 Ga age gap is a confounding factor that may obscure this signal.

1.1.2 Early Tectonothermal Regime

One constraint on planetary thermal evolution during Hadean-Archean times is the rapidly changing amount of radioactive heating. Based on the modeled present amounts of U, Th, and K in the solid Earth, the solid Earth at 4 Ga should have had ~4x the radioactive heating as our planet today (e.g., Harrison, 2009). Given ^{235}U and ^{40}K's half-lives of ~700 Ma and ~1 Ga, respectively, ~75% of the Earth's original complement of radioactive heat-producing elements (HPE) would have decayed away by ~3.9-3.6 Ga.

There remain serious questions (e.g., Davies, 1992) about the viability of subduction in a warmer mantle, but there is little consensus on the topic. Some work has suggested that higher Archean and Hadean mantle temperatures would have supported plate tectonics (e.g., Korenaga, 2013), perhaps with plate rates faster or slower than today, or perhaps characterized by much smaller plates (Davies, 2006). It is also possible that instead of modern-style subduction a subduction-like underthrusting regime may have formed convergent plate boundaries during some periods of Earth history, complicating our search for the "earliest evidence of subduction" with a continuum of subduction-like regimes on the early Earth, which may or may not share the above-mentioned characteristic geology with modern subduction zones (Sizova et al., 2009). A similar open question is the amount of continental crust existing on the Earth during Hadean and Archean times. Various models proposed over the past few decades include voluminous Hadean crust (Warren, 1989) or almost no continental crust until later in the Archean (e.g. McLennan and Taylor, 1982). The continental crust may have an insulating effect on the mantle beneath it but will also take up HPEs from the mantle during its formation; its overall effects on geodynamics are uncertain.

1.1.3 What is the earliest evidence for subduction?

Past subduction is often diagnosed by the identification of rock types formed uniquely in subduction settings. The underthrusting of oceanic crust in subduction zones often leads to the obduction of slices of oceanic crust – termed ophiolites – onto the overlying plate. The low-temperature, high-pressure conditions in downgoing oceanic slabs lead uniquely to blueschist facies and ultra-high pressure metamorphism. Ophiolites and blueschist terranes are known from as early as the Neo-Proterozoic record (Stern, 2007, 2008), but such direct evidence for subduction is either absent, or no longer present, in the geologic record earlier than the Neo-Proterozoic (except for a few possible older ophiolites; Stern, 2008). More indirectly, the production of calc-alkaline granitoids is characteristic of modern subduction zones. Calc-alkaline granitoids are found on Earth dating to >3.5 Ga, although they did not begin to dominate the preserved granitoid record of (presumed) convergent margins until ca. 2.5 Ga (Condie, 2008). The lower heavy rare earth element (HREE) contents and higher ratio of light to heavy REE among Archean compared to later granitoids (Martin, 1986) probably indicate differences in the residual phases during partial melting to form the granitoids' magmatic precursors. Martin (1986) argues that higher amounts of garnet and hornblende were present in the Archean melting residues, and that this can be traced to melting of hydrous basalt (which he infers is in a subducting slab, although the necessity of this is not obvious) rather than to a metasomatized mantle wedge which is the source of most primitive melts in today's arcs.

Tying the presence of subduction to the presence of certain markers in the rock record runs the serious risk of false negatives for much of Earth history, and increasingly so in the earliest times. Lithologies and mineral markers characteristic of subduction zones and continental collision zones, such as jadeitite and ruby (the "plate tectonic gemstones" of Stern et al., 2013), form in environments very hostile to continued preservation where large amounts of subduction

erosion and mantle recycling or uplift and erosion of the continental crust occur. On the other hand, a uniformitarian perspective that the present tectonic regime of Earth can be assumed to continue into the past, *sans* contradicting evidence, becomes increasingly suspect as the age of the geologic record increases and the number of clear indicators for both solid earth and environmental conditions decrease. The inherent limitations of the early geologic record give numerical modeling an important place in answering this question and more self-consistent simulations of subduction under warmer early Earth conditions will help establish its feasibility or lack thereof.

Plate tectonics and stagnant lid mantle convection should have different implications not only for the geology of the lithosphere but also for the preservation of heterogeneities within the mantle. Although the magma ocean(s) that probably characterized the very earliest Earth and the aftereffects of the moon-forming impact are traditionally considered to homogenize the silicate Earth, recent evidence suggests that very early-formed materials survived several billions of years intact. Touboul et al. (2012) report a tungsten isotopic anomaly in 2.8 Ga komatiites related to the short-lived ^{182}Hf/^{182}W system which must have formed within the solar system's first ~30 Ma. Its preservation for this period of time demonstrates that some material from this time remains intact despite the extensive convective stirring that large impact(s) in early Earth history should have wrought (or reflects a late veneer). Similarly, Debaille et al. (2013) demonstrate a ^{142}Nd anomaly in a 2.7 Ga tholeiitic lava flow, a reservoir necessarily formed before ~4.2 Ga. Debaille et al. (2013) interpret this as evidence for a lack of sustained plate tectonics before 3 Ga, arguing that plate tectonics would homogenize the mantle too efficiently and would effectively destroy such heterogeneities. However, the extent of convective stirring in the early Earth is dependent upon the plate motions and convective vigor of the early mantle.

While classical scalings of mantle temperature, heat flow, and plate velocities suggest very high early heat flow, vigorous early convection, and fast plate motions, alternative scalings such as assuming a constant heat flow through Earth history allow for only moderate rises in mantle temperature and convective vigor (e.g., Korenaga, 2013), and account for some of the petrologic evidence of mantle temperature through time (Herzberg et al., 2010). Also potentially significant is the fact that the >4 Ga Jack Hills zircons record large heterogeneities in Hf isotopic composition that are not seen in the later Archean record (e.g., Harrison et al., 2005, 2008), suggesting their later destruction or re-mixing.

1.1.4 Meteorite Impacts

Bolide impacts should have been more numerous early in the solar system's history, when many small bodies were yet to be accreted to the various planets. Crater counting of the surfaces of many terrestrial bodies seems to corroborate this projection. Geochemical arguments point to a "Late Veneer" of meteoritic materials accreted to the Earth since the moon-forming impact (e.g., Holzheid et al., 2000). This conclusion is based on the elevated concentrations of highly siderophile elements in Earth's mantle – several orders of magnitude above projections from a pure core/mantle differentiation scenario – that are interpreted to represent the mixing in of later-accreted material amounting to ~1% of the mass of the Earth (Dauphas and Marty, 2002).

The ubiquitous disturbance of isotopic ages in lunar samples returned by the Apollo missions has led to the hypothesis of a spike in meteorite impact rates in the inner solar system ca. 3.9 Ga (Tera et al., 1974). This event is usually termed the Late Heavy Bombardment (LHB), and if it occurred, the Earth by virtue of its gravitational cross-section should have attracted ~20x the mass of impactors as the Moon. This event would have caused widespread thermal effects in the

lithosphere. Abramov and Mojzsis (2009) and Abramov et al. (2013), for instance, conclude that while only a few percent of the lithosphere would have experienced temperature increases of 1000 K or more, ~20% of the lithosphere would have seen temperature increases of 100 K. In addition, areas proximal to an impactor may record voluminous melt sheets and target rock homogenization (e.g., Darling and Moser, 2012).

1.1.5 Post-Hadean Changes and Transitions

The high $\delta^{18}O$ and very unradiogenic ε_{Hf} displayed by some Hadean zircons may or may not be a continuous feature in the 4.4-3.0 Ga Jack Hills record. Although zircons from other terranes show a preponderance of heavy oxygen signatures by 3 Ga (Dhuime et al., 2012; with the timing based on Lu-Hf model ages rather than crystallization ages), the detrital record before this is dominated by zircons with mantle affinities – even Hadean zircons at Jack Hills show mostly mantle-like $\delta^{18}O$.–The period 4.0-3.6 Ga in particular has not been highly sampled. There is independent evidence from the sedimentary record for oceans in the early- to mid-Archean (Nutman, 2006), so any possible lack of obvious sediment-derived magmas during this period is not based on the lack of a hydrosphere. Instead, if post-Hadean zircons lack high $\delta^{18}O$, this probably reflects a local change in magmatic compositions and may be important for reconstructing the geology and tectonics of this slice of ancient crust. Oxygen isotopes are a possible line of evidence about the nature of any Hadean-Archean transitions and possible changing characters of continental magmas produced during this time.

We will also search for transitions in the Hf isotopic record. The extreme hafnium reservoirs at Jack Hills – very positive ε_{Hf} and zircons within error of the solar system initial $^{176}Hf/^{177}Hf$ alike – do not obviously persist in the Jack Hills record after 4 Ga (Amelin et al., 1999), and they

are not found in materials from other Archean cratons (e.g., Amelin et al., 2000; Pietranik et al., 2008; Guitreau et al., 2012). The solar system initial Hf ratio today is ~ -104ε relative to the chondritic uniform reservoir (using the chondritic values of Bouvier et al., 2008), a value not approached by materials in the known continental record. Likely, the ancient unradiogenic reservoir seen in the Jack Hills zircons has been remixed into the mantle since the Hadean – an event(s) of uncertain timing but which may have taken place during the Hadean-Archean transition or the early Archean. The highly radiogenic materials seen in the Hadean (for example, +10ε at 4.1 Ga and +15ε at 4.2 Ga; Harrison et al., 2005) are also rare in the more recent record, but not unheard of. Some MARID kimberlitic xenolith materials show ε_{Hf} as positive as +110ε today (Choukroun et al., 2007), which is similar to how a +10ε reservoir at 4.1 Ga would plot if it continued evolving for the past 4.1 Ga with a $^{176}Lu/^{177}Hf$ ~0.07 (the value necessary for it to evolve to its highly radiogenic composition by 4.1 Ga, assuming reservoir formation at 4.55 Ga). The MARID xenoliths are interpreted to have formed partly by metasomatism of the mantle by melts or fluids in contact with ancient garnet-bearing slab materials. The mineral garnet forms with high Lu/Hf ratios, and thus garnet-rich materials can reach highly radiogenic $^{176}Hf/^{177}Hf$ over geologic time. It is possible that a garnet-rich reservoir may have yielded the highly radiogenic Hadean zircons. It is possible, but not necessarily the case, that this reservoir persists to today based on the MARID evidence (the reservoir need not be the same one from the Hadean). On the other hand, the more extreme +15 value at 4.2 Ga (Harrison et al., 2005), when treated similarly, evolves to a more extreme value of ~207ε today, which is not seen in the geologic record.

Guitreau et al. (2012) find that the $^{176}Lu/^{177}Hf$ and ε_{Hf} of juvenile Archean tonalite-trondjemite-granodiorite (TTG) terranes, which make up much of the continental Archean

granitoid record, more or less track chondritic (or, assumed bulk silicate earth) evolution. Reworked crustal materials display more negative ε_{Hf}. The Hadean Jack Hills zircons in particular seem to be dominated by subchondritic $^{176}Lu/^{177}Hf$ ratios (Harrison et al., 2005; 2008), perhaps pointing to their derivation in a somewhat different setting, although Blichert-Toft and Albarede (2008) interpreted them as deriving from the remelting products of TTGs. Differences in the Jack Hills zircon Lu-Hf systematics through the Hadean-Archean transition may be able to answer some questions about changes in crustal preservation and tectonic style during this time.

1.2 Summary: Important Questions

Many important aspects of both the Hadean and the Hadean-Archean transition have yet to be explored. As outlined at the beginning of the chapter, this contribution focuses on several questions:

1. Do the various geochemical records at Jack Hills – oxygen isotopes, Hf isotopes, Ti thermometry, other trace elements – show changes after the Hadean? Are these relatable to geodynamic transitions or tectonic events?

2. Do the Jack Hills zircons show evidence for the hypothesized Late Heavy Bombardment?

3. Can the Xe isotope geochemistry of the Hadean zircons (e.g., U-Xe ages) help constrain post-Hadean alteration of the zircons? Can xenon-derived $(Pu/U)_O$ estimates provide another line of evidence for a Hadean hydrosphere?

4. Is subduction feasible on the early Earth? Would early Earth subduction systems yield heat flows like those inferred for Hadean zircons? What other subduction-related lithologies could we expect to form or fail to form in a warmer mantle on the early Earth?

Chapter One Figures

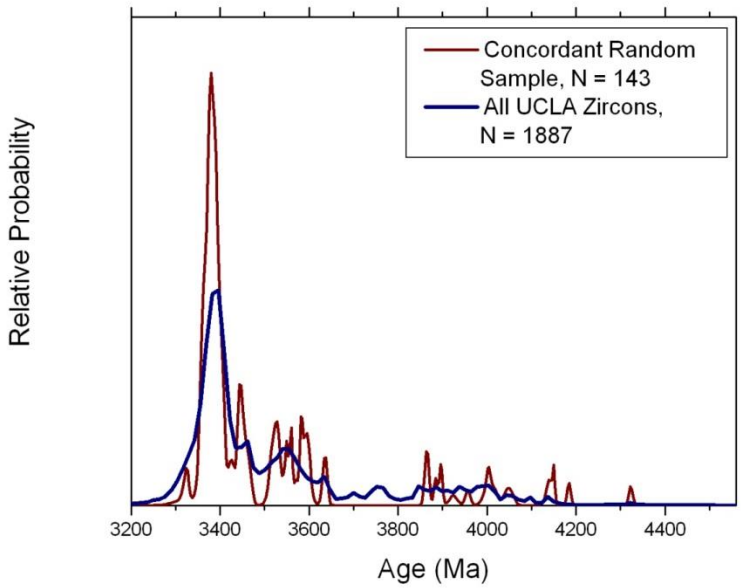

Fig. 1.1: Age population of Jack Hills zircons as measured on the CAMECA *ims*1270 ion microprobe at UCLA, 2008-2013. "All UCLA Zircons" category is mostly made up of shorter $^{207}Pb/^{206}Pb$ measurements on without accompanying concordance information, from which population zircons ca. 4.0-3.6 Ga were selected for full U-Pb analysis (survey procedure described in ch. 3). This category also excludes zircons identified as >3.8 Ga in the survey of Holden et al. (2009), and so underestimates this proportion of the population (in reality ca. 10%).

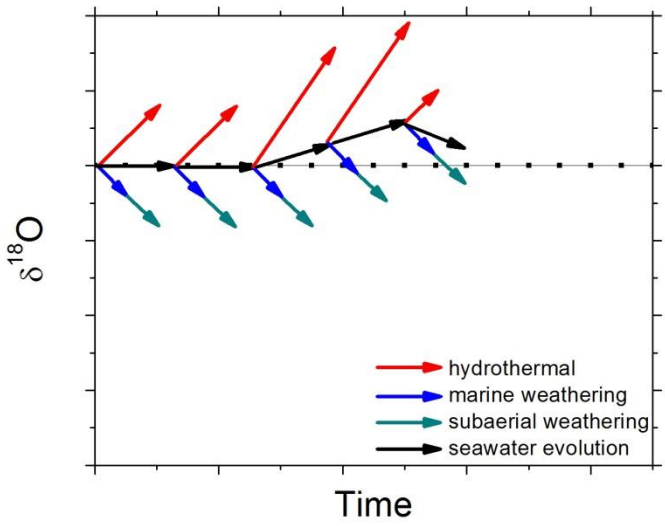

Fig. 1.2: Hypothetical evolution of seawater $\delta^{18}O$ by changes to the hydrothermal flux at mid-ocean ridges. Hydrothermal circulation adds net ^{18}O to seawater, while both marine and subaerial low-temperature weathering subtracts net ^{18}O from seawater (Muehlenbachs and Clayton, 1976). Thus, relatively higher rates of hydrothermal alteration relative to other types of weathering might be expected to move seawater toward higher $\delta^{18}O$, while relatively lower hydrothermal flux might be expected to move seawater toward lower $\delta^{18}O$. Complementary compositional evolution might occur for changes to the low-temperature weathering fluxes.

Chapter Two: Early Archean crustal evolution of the Jack Hills Zircon source terrane

Abstract

Several lines of isotopic evidence – the most direct of which is from Hadean Jack Hills zircons – suggest a very early history of crust formation on Earth that began by about 4.5 Ga. To constrain both the fate of the reservoir for this crust and the nature of crustal evolution in the sediment source region of the Jack Hills, Western Australia, during the early Archean, we report here initial $^{176}Hf/^{177}Hf$ ratios and $\delta^{18}O$ systematics for <4 Ga Jack Hills zircons. In contrast to the significant number of Hadean zircons which contain highly unradiogenic $^{176}Hf/^{177}Hf$ requiring a near-zero Lu/Hf reservoir to have separated from the Earth's mantle by 4.5 Ga, Jack Hills zircons younger than ca. 3.6 Ga are more radiogenic than –13ε (CHUR) at 3.4 Ga in contrast to projected values at 3.4 Ga of –20ε for the unradiogenic Hadean reservoir indicating that some later juvenile addition to the crust is required to explain the more radiogenic younger zircons. The shift in the Lu-Hf systematics together with a narrow range of mostly mantle-like $\delta^{18}O$ values among the <3.6 Ga zircons (in contrast to the spread towards sedimentary $\delta^{18}O$ among Hadean samples) suggests a period of transition between 3.6 and 4 Ga in which the magmatic setting of zircon formation changed and the highly unradiogenic low Lu/Hf Hadean crust ceased to be available for intracrustal reworking. Constraining the nature of this transition provides important insights into the processes of crustal reworking and recycling of the Earth's Hadean crust as well as early Archean crustal evolution.

2.1 Introduction

The suggestion that the silicate Earth differentiated to form a continental-like crust during its first few hundred million years was, until recently, highly controversial. In contrast to the traditional paradigm of continental growth occurring largely since 4 Ga or later (e.g., Taylor and McLennan, 1985), isotopic evidence has recently emerged suggesting that enriched, possibly continental reservoirs developed substantially before that time during the so-called Hadean eon. For example, evidence for very early (>4.35-4.53 Ga) differentiation of the silicate earth has been inferred from $^{142}Nd/^{144}Nd$ variations in terrestrial samples (Caro et al., 2003) and the contrast between $^{142}Nd/^{144}Nd$ in chondrites and the silicate Earth (Boyet and Carlson, 2005), although this is also explicable in terms of a non-chondritic bulk silicate Earth (Dauphas and Chaussidon, 2011). Nd isotopic evidence for a region of enriched Hadean crust is inferred from $^{142}Nd/^{144}Nd$ data for amphibolites from the Nuvvuagittuq Greenstone Belt (O'Neil et al., 2008), but inconsistent with other data (e.g., Cates and Mojzsis, 2009).

Independent evidence for early felsic crust comes from the $^{176}Hf/^{177}Hf$ compositions of detrital Jack Hills zircons, Narryer Gneiss Complex, Western Australia (Harrison et al., 2005, 2008; Blichert-Toft and Albarede, 2008). Zircons tend toward low Lu/Hf ratios, such that the ingrowth of ^{176}Hf from beta decay of ^{176}Lu is typically minimal. Thus zircons reflect, with minimal correction for radiogenic ingrowth, the initial $^{176}Hf/^{177}Hf$ ratio of their host rock. A significant number of Hadean Jack Hills zircons contain highly unradiogenic hafnium, suggestive of derivation from a near-zero Lu/Hf reservoir formed almost immediately following accretion of the planet (Harrison et al., 2005, 2008). In addition, the zircons record oxygen isotope and trace element signatures interpreted to imply the existence of surface

water (e.g., Mojzsis et al., 2001) and water-saturated granitic melting conditions (Watson and Harrison, 2005) by 4.3 Ga, which are also suggestive of continental crust.

One interesting aspect of the Nd and Hf isotopic evidence for early crust formation is that the inferred early enriched reservoir(s) has apparently not been significantly reworked and sampled by younger rocks. Also, only very small quantities of Hadean materials bearing this signature survive. It is likely that this early enriched crust has been destroyed well before the present day, but examination of the <4 Ga portion of the Jack Hills detrital zircon population should shed light on the extent and longevity of this reservoir in the Jack Hills source terrane(s) during the early Archean.

Although the vast majority of Lu-Hf isotopic analyses (Harrison et al., 2005, 2008; Blichert-Toft and Albarede, 2008) have concentrated on the >4 Ga Jack Hills zircons, the detrital population ranges in age from ~3 to nearly 4.4 Ga (Holden et al., 2009). In this paper, we present the largest dataset to date (130 analyses) of Lu-Hf measurements of <4 Ga Jack Hills zircons and use this record to investigate how late into Earth's history the early low Lu/Hf reservoir is evident in the Jack Hills detrital population. We also evaluate the relative importance of crustal growth versus reworking over the ca. 1 billion year detrital zircon Lu-Hf isotope record in an effort to constrain the chemical and tectonic evolution of the Yilgarn Craton.

2.2 Geologic Setting

The Jack Hills are located in the northwestern corner of the Yilgarn Craton, Western Australia, within the Narryer Gneiss Complex (Fig. 2.1). The Narryer complex consists of Early to Late Archean orthogneisses and several metasedimentary associations, some of which host >4 Ga zircons. The relationship between the metasediments and orthogneisses in

the Jack Hills and throughout the Narryer terrane is uncertain. The present contacts between the crystalline and metasedimentary units are thought to be tectonic rather than depositional (Nutman et al., 1991; Spaggiari, 2007). Despite broad agreements between the ages of younger detrital zircons in Jack Hills metasediments and the ages of Narryer gneisses (Maas and McCulloch, 1992; Nutman et al., 1991), whole-rock REE geochemistry (Maas and McCulloch, 1992) of the metasediments and more detailed comparison of the age distributions (Maas and McCulloch, 1992; Amelin, 1998) suggest that the presently exposed Narryer gneisses are distinct from the source of Archean zircons in the Jack Hills population. It is therefore best to consider the detrital zircon and Narryer gneiss record separately for the purpose of constraining crustal evolution in the region.

The largest concentrations of Hadean grains are found within apparently fluvial (Williams and Myers, 1987) pebble metaconglomerates likely deposited at ~3 Ga (Spaggiari et al., 2007). U-Pb age surveys of the population tend to reveal maxima in the age distribution at 3.4 and 4.1 Ga, the younger being much more prominent, and a gap (or minimum) in the distribution between about 3.6 and 3.8 Ga (Kober et al., 1989; Amelin, 1998; Crowley et al., 2005; Holden et al., 2009). Automated SHRIMP age analysis of >100,000 zircons has revealed that concordant Hadean (>4 Ga) grains make up approximately 5% of the metaconglomerate population (Holden et al., 2009).

Observable magmatic rocks in the Narryer Gneiss Complex span ages from 2.6 to 3.73 Ga (Nutman et al., 1991; Spaggiari et al., 2007) (Fig. 2.1). A widespread unit, the Meeberrie gneiss, contains protoliths ranging from 3.73 Ga tonalites to 3.6 Ga granitoids (Nutman et al., 1991) with a prominent monzogranitic unit at 3.68 Ga (Myers, 1988a) (Fig. 2.1). The Manfred gabbro-anorthosite complex at 3.73 Ga is included in several of the younger gneisses

(Myers, 1988a,b). The 3.44-3.49 Ga tonalitic Eurada gneisses and the ~3.38 Ga syeno- to monzogranitic Dugel gneisses occupy the time period most heavily sampled by detrital zircons (Myers, 1988a; Nutman et al., 1991). Several granites and pegmatites dating from ~3.0-3.3 Ga are also found within the Narryer Complex (Bennett et al., 1990). Finally, 2.6-2.7 Ga granites intrude the region concomitantly with widespread metamorphism, faulting, and folding (Myers 1988a; Nutman et al., 1991).

Previous work on crustal evolution of the Narryer Terrane focused on the Sm-Nd and U-Pb compositions of exposed orthogneisses. Maas and McCulloch (1992) recalculated T_{DM} from earlier work (DeLaeter et al., 1985) on the Meeberrie, Eurada and Dugel gneisses and 3.0-3.3 Ga granitoids. The tonalitic portions of the Meeberrie appear to be sourced from relatively juvenile materials, whereas the monzogranitic younger Meeberrie, Dugel, and 3.3 Ga granitoids appear to be sourced largely from older (but <4 Ga) reworked crust with little juvenile input (Maas and McCulloch, 1992). The Eurada gneiss and the 3.0 Ga granitoids appear to be formed from the reworking of distinct sources extracted from the depleted mantle more recently than the Meeberrie (Maas and McCulloch, 1991). The high apparent source μ of the 3.73 Ga Manfred Complex may suggest a substantial component of >4 Ga crust (Fletcher et al., 1988).

Despite the unclear relationship between the sources for Jack Hills detrital zircons and the known geology of the Narryer Gneiss Complex, it is clear that the isotopic characteristics of some Archean Narryer gneisses record evidence for crustal evolution since Hadean times. A large dataset of Lu-Hf data for the younger detrital zircons may provide a parallel, but more detailed, account of crustal evolution in the region for the early and middle Archean.

2.3 Methods

We sampled the Jack Hills zircon distribution with the goal of obtaining a more complete picture of the age, internal textures, and isotope geochemistry among the younger detrital population. We selected an epoxy mount (RSES51) from the study of Holden et al. (2009) containing approximately 255 randomly picked zircons from the Jack Hills detrital population at the discovery site (Compston and Pidgeon, 1986) from the large collection of Jack Hills grains analyzed at the Australian National University. The dating protocol of Holden et al. (2009) employs automated sampling of each grain for several seconds to establish an estimate of $^{207}Pb/^{206}Pb$. Full U-Pb analysis was done only for grains with apparent $^{207}Pb/^{206}Pb$ ages >3.95 Ga. Therefore most grains employed in this study were not precisely dated. One hundred and twenty nine grains on mount RSES51 were analyzed for both Lu-Hf isotopes and $^{207}Pb/^{206}Pb$ age, with the only further selection being for grains with a large enough uncracked surface area to be used for laser ablation Lu-Hf analyses. This approach, we believe, provides an essentially random sample of that portion of the zircon population large enough for laser ablation sampling.

2.3.1 Imaging for Textures

Imaging was mainly accomplished using a scanning electron microscope. A combination of BSE imaging and EDAX were used to identify mineral inclusions (several of which were further studied by electron microprobe for stoichiometry) within the zircons. Cathodoluminescence (CL) imaging was used to elucidate internal structures and zoning. Zircons were sorted into zoning-style categories following the suggestions of Corfu et al. (2003). Categories included 1) oscillatory zoning, 2) core/rim geometry, 3) patchy or irregular zoning, 4) sector zoning, and 5) no (or too faint to be distinguishable) zoning. Inhomogeneous zircons with uncertain patterns were sorted into the “patchy/irregular”

category, which became a catchall for ambiguous grains. Due to the possibility for zoning patterns to be rendered uncertain by grain fragmentation during sedimentary cycling, the patchy/irregular category is most likely over-represented.

2.3.2 Coupled Hf-Pb Measurements

We measured Lu-Hf systematics and $^{207}Pb/^{206}Pb$ ages for the zircons by laser ablation multicollector inductively coupled plasma mass spectrometry (LA-MC-ICPMS), employing ThermoFinnigan NEPTUNE MC-ICPMS and associated lasers at the Australian National University and UCLA. A combination of magnet switching and zoom optics switching were used to switch between Lu-Hf and Pb isotopic measurements, adapted for the NEPTUNE from the procedure of Woodhead et al. (2004). This method gives us the potential to deconvolve the results of the semi continuous analyses into definable Hf-Pb domains, increasing the accuracy of the interpretations. Though we do not sample the Lu-Hf and Pb mass sets simultaneously as in the work of, e.g., Xie et al. (2008) (who employ a laser ablation line leading to two separate mass spectrometers), we are able to determine coherent age-Hf domains by bracketing our Hf analyses with Pb analyses showing the same $^{207}Pb/^{206}Pb$ age. One disadvantage of the approach is the lack of information regarding U-Pb discordance. Despite its limitations, however, this combined Hf-Pb approach is more useful for correlating Lu-Hf systematics with an applicable age than the more traditional in situ analysis of U-Pb and Lu-Hf information on separate volumes of material. Despite our fairly large laser spot size (80-100 μm) which runs the risk of overlapping multiple age domains in the horizontal direction, our in situ sampling and ability to detect age domains in the vertical direction gives us a significant advantage also over solution U-Pb and Lu-Hf methods.

We identified separate Hf-Pb age domains on the basis of the $^{207}Pb/^{206}Pb$ ratio, requiring the presence of a plateau in $^{207}Pb/^{206}Pb$ ages for at least three Pb counting cycles. For age domains in the interior of crystals, only Lu-Yb-Hf data (two back-to-back cycles) bracketed by consistent Pb data (three cycles) were considered. Using this method we identified 130 separate Hf-Pb domains among the grains analyzed. Analyses were accomplished during two sessions: Session One took place at ANU in September 2007 and Session Two at UCLA in April 2009. Background subtraction was accomplished online, and all further data reduction was done offline.

2.3.2.1 Session One

Fifty-nine grains (totaling 61 Hf-Pb domains) were analyzed using a 193 nm laser with a circular spot 80 μm in diameter. 10 seconds of counting on the Yb, Lu, Hf mass set (i.e., 171, 173-179, 181) alternated with three seconds of counting on the Pb mass set, with 4 seconds of magnet settling time between each mass set. A total of 130 seconds counting time was given to each analysis. See Harrison et al. (2005, 2008) for details of the analytical methods.

2.3.2.2 Session Two

Session Two took place over three days in April of 2009 at UCLA. Statistics related to the accuracy of the peak stripping and mass fractionation corrections were calculated on a day-to-day basis. Sixty-six grains (totaling 69 Hf-Pb domains) were analyzed by laser ablation using an Excistar ArF excimer laser with a circular spot 100 μm in diameter. Eleven seconds of counting on the Yb, Lu, and Hf mass set alternated with five seconds of counting on the Pb mass set (204, 206, 207, 208), and the first 2 seconds of counting on each mass set were disregarded during data reduction in order to ensure a two-second settling time for the

magnet. This leaves 9 seconds counting on the Yb, Lu, and Hf masses alternating with 3 seconds counting on Pb considered for the final analysis. A maximum of 160 seconds (120 used for data) was given to each analysis. Blanks were run before each analysis in this session.

2.3.2.3 Interference and Mass Fractionation Correction

Despite its advantages (e.g., lesser destructivity to the sample), sampling of Lu and Hf in zircon by laser ablation rather than in solution precludes chemical removal of isobaric interferences. Yb, which occurs in zircon at the trace level (Finch and Hanchar, 2003), presents interferences with Hf at masses 174 and 176. Isotopes of Lu and Hf at mass 176, the relevant isotopes involved in the Lu-Hf decay system, also mutually interfere. Analysis by laser ablation thus necessitates peak-stripping to deconvolve the signals at mass 174 and 176. Details of the Hf isotopic analysis and peak stripping procedures for isobaric interference of Yb and Lu on Hf isotopes are given in Harrison et al. (2005, 2008) and Taylor et al. (2009). We tested the accuracy of the peak stripping and fractionation corrections (normalized to (^{179}Hf/^{177}Hf = 0.7325) by comparing the corrected ^{174}Hf/^{177}Hf and ^{178}Hf/^{177}Hf values for each analysis against the accepted values (0.008657±5 and 1.46735±16 respectively, ±2σ) of Thirlwall and Anczkiewicz (2004) (Fig. 2.2). Our corrected values for ^{174}Hf/^{177}Hf, which is highly sensitive to the veracity of the ^{174}Yb stripping, agree well on average with the reference value (Fig. 2.2c,d).

In Session 1, four analyses out of 102 (~4%) fell more than 3σ from the reference value. In Session 2, four analyses out of 139 (~3%) fell more than 3σ from the reference value: one analysis on Day 1 (N=34), one analysis on Day 2 (N=50), and two analyses on Day 3 (N=55). Our corrected values for ^{178}Hf/^{177}Hf are uniformly low by 0.85 ε for Session 1 and

by 1.29 ε for Day 1 of Session 2, which occurred one week before days 2 and 3 of Session 2. During the ANU session, nine out of 102 analyses (including both unknowns and standards) fell more than 3σ from the reference value (Fig. 2.2a,b). Statistics for the peak-stripping accuracy for the UCLA session were calculated on a day-by-day basis.

This higher than expected incidence of analyses inconsistent with standard values for the isotope ratios is balanced by fractionation- and interference-corrected $^{176}Hf/^{177}Hf$ values for the AS3 and Mud Tank standard zircons that agree well with the reference values of Woodhead and Hergt (2005) (see Fig. 2.3). In both sessions, mass-discrimination corrections were interpolated from the standard values' offsets and applied to the unknowns bracketed by each set of standards. The standards AS3, Temora-2, and Mudtank were used for calculating $^{176}Hf/^{177}Hf$ offsets; only AS3 and Temora-2 were used for calculating $^{176}Lu/^{177}Hf$ owing to Mudtank's very low Lu/Hf ratio compared to our unknowns (nearly two orders of magnitude below Temora-2 and AS3; Woodhead and Hergt, 2005). The results compare well between the two sessions (see Fig. 2.4), lending confidence to our conclusion that the data reduction and correction procedures have yielded accurate results. In addition to the standard zircons, the NIST610 standard glass was used as a secondary $^{207}Pb/^{206}Pb$ standard. $^{207}Pb/^{206}Pb$ of standards was sensitive to the ^{207}Pb average signal, becoming unreliable at a threshold of 10 millivolts (Fig. 2.5). The standards with ^{207}Pb signals above the threshold fell within two percent of their known values, whereas standards with lower signals were considerably more inaccurate (Fig. 2.5). Only standards falling above the threshold were considered; all unknowns fell above the threshold as well. Only NIST610 and AS3 standards fell above the threshold and were subsequently used for comparing to unknowns. This result is unsurprising: the Mudtank and Temora-2 zircon standards are much younger than AS3 (732

and 417 Ma compared to 1099 Ma, respectively) and they consequently have lower Pb contents. The Mudtank and Temora-2 Pb data reflect the physical limitations of the technique at low Pb signal – notably lower signal than any of our unknowns or than the relatively Pb-rich AS3 and NIST610 standards. Because of the good agreement of the high-signal standards with their accepted $^{207}Pb/^{206}Pb$ ages, we did not apply a mass fractionation correction to any of our Pb data. We analyzed at mass 204 and 208, and found no appreciable ^{204}Pb in our samples. $^{208}Pb/^{206}Pb$ values did not display any trend indicative of common Pb contamination (see e.g., Blichert-Toft and Albarede, 2008). Given the lack of noticeable common Pb contamination among our zircons, we did not apply a common Pb correction to the data.

Fractionation - and interference-corrected $^{176}Lu/^{177}Hf$ for the standard zircons AS3 and Temora-2 compare well with the reference values of Woodhead and Hergt (2005). In-day averages for $^{176}Lu/^{177}Hf$, $^{176}Hf/^{177}Hf$, and $^{207}Pb/^{206}Pb$ of standard zircons are tabulated together with the accepted values in Table 1. Uncertainties are based both on internal uncertainty and the reproducibility of the relevant standards for each quantity.

All ε_{Hf} values are calculated using the CHUR values of Bouvier et al. (2008), and a decay constant for ^{176}Lu of 1.867×10^{-11} yr^{-1} (Soderlund et al., 2004). CHUR was likely not a physical reservoir for long in the early Archean, and so we adopt it only as a well-defined reference value. ε_{Hf} uncertainties include uncertainties in $^{176}Hf/^{177}Hf$, $^{176}Lu/^{177}Hf$, contemporaneous CHUR values of these ratios, and uncertainty in the ^{176}Lu decay constant using the error propagation formulae of Harrison et al. (2008). Lu-Yb-Hf/Pb data for all standards and unknowns are shown in electronic annex EA-1.

2.3.3 Oxygen isotopes

Analyses of oxygen isotopes in 85 selected grains were made using the CAMECA *ims*1270 ion microprobe at UCLA in March of 2009. A spot size of ~20 μm and primary beam current of ca. 1.5 nA were used (see Trail et al, 2007b for further analytical details). The AS3 zircon standard ($\delta^{18}O_{SMOW}$ = 5.34‰; Trail et al., 2007b) was used for correction of raw $^{18}O/^{16}O$ ratios. Oxygen isotope measurements made on grains for which multiple Hf-Pb domains were found are attributed to the Hf-Pb domain closest to the surface of the grain, where the oxygen measurements were made. Data for all oxygen standards and unknowns are shown in Appendix A.

2.3.4 Ti thermometry

Ti concentrations for Ti-in-zircon thermometry (Watson and Harrison, 2005) on selected grains were made using the CAMECA *ims*1270 ion microprobe at UCLA in March and August of 2009. Details of the temperature-calculating procedure are given in Watson and Harrison (2005) and analytical conditions for Ti measurement in Harrison and Schmitt (2007). We estimated uncertainties in our temperature calculations by quadratic addition of the roughly 10°C uncertainty from the model of Watson and Harrison (2005) to uncertainty in our Ti concentrations. In calculating apparent T^{xlln} we assume that the TiO_2 and SiO_2 activity of the melt were 1 during zircon growth. The ubiquity of quartz among mineral inclusions (see section 4.1) provides support for the latter assumption. Crystallization temperatures calculated for grains for which multiple Hf-age domains were found are attributed to the Hf-Pb domain closest to the surface of the grain, where the Ti measurements were made.

2.4 Results

2.4.1 Grain Textures and Zoning

The zircons display several zoning styles under cathodoluminescence imaging. Whereas 57 grains show no zoning, 32 show oscillatory zoning and 2 of the zircons show sector zoning. Chaotic or patchy zoning is evident in 50 grains. Zircons with no zoning tend to be dark-to-medium in CL brightness. Several 3.4-3.7 Ga grains have a well-defined rim-and-core geometry evident under CL. Obvious igneous (oscillatory or sector) zoning and pronounced rim/core geometry are rare in grains older than 3.6 Ga. Around 10% of zircons contain identifiable mineral inclusions at the surface, among which quartz and K-feldspar dominate. Quartz, K-feldspar, muscovite and biotite are present in 3.4 Ga zircons while quartz is found in the 3.5-3.75 Ga zircons. One ilmenite inclusion was found in a 3.75 Ga zircon. All CL and inclusion information are given in electronic Appendix B.

2.4.2 Coupled Hf-Pb Analyses

Results from the two analysis sessions agree well in both Lu-Hf systematics and ages despite their collection in different laboratories (Fig. 2.4), highlighting the accuracy of the peak-stripping protocol. Nearly all of the 130 Hf-Pb domain data points fall at realistic values of $^{176}Lu/^{177}Hf$ for zircon (<~0.001). Four analyses fall above 0.002 in $^{176}Lu/^{177}Hf$, which may indicate inaccuracies in the peak-stripping procedure for these few analyses (4/130; ~3%). These analyses are marked in all figures. One of these suspect analyses has a $^{207}Pb/^{206}Pb$ age of ~2.9 Ma and lies at ~-28ε. It is noticeably younger than the vast majority of zircons found in previous studies of the Jack Hills; this apparent age probably reflects ancient Pb loss. Its patchy zonation may also suggest alteration. Though its great distance from DMM in ε_{Hf} space may suggest a highly unradiogenic source, its high Lu/Hf renders further interpretation of the data point suspect. We do not include it in most of our figures. Ages resemble the distribution shown in previous studies (e.g. Crowley et al., 2005) with a large age peak ca. 3.4

Ga and minor peaks ca. 3.45 and 3.55 Ga (Fig. 2.6). Fig. 2.7 displays the same data with the Hf-Pb domains grouped by the zonation style of their zircons.

We refer to the solar system initial $^{176}Hf/^{177}Hf$ ratio, below which no solar system samples should plot, as the Primordial Hafnium Bound (PHB) for the rest of this work and compare our analyses to this bound. The proportion of domains displaying highly unradiogenic Hf (i.e., plotting near PHB) decreases with decreasing age, such after 3.8 Ga few plot near PHB (see Fig. 2.7). Less than 4 Ga zircons within a few ε units of PHB display textures under CL suggestive of a metamorphic origin, so the significance of their unradiogenic hafnium in terms of igneous activity in the source terrane(s) is uncertain. The distribution in $^{207}Pb/^{206}Pb$ ages compares well to that observed in the rest of the Jack Hills distribution, with a major peak near 3.4 Ga and a minimum between 3.6 and 3.8 Ga (Holden et al., 2009; Crowley et al., 2005; see Fig. 2.6). Hf-Pb data for all samples can be seen in Appendix A.

2.4.3 Oxygen Isotopes

$\delta^{18}O_{SMOW}$ values for the zircons average 5.49±0.43‰ (1σ), in good agreement with the average mantle value of ~5.3±0.3‰ (1σ, Valley, 2003). Ten zircons fall outside the range of common mantle values: seven zircons have $\delta^{18}O$ above 5.9‰ and three zircons are below 4.7‰. There is no clear correlation of $\delta^{18}O$ with age, ε_{Hf} or crystallization temperature (see Fig. 2.8). $\delta^{18}O$ values for all samples are shown in Appendix A.

2.4.4 Ti Thermometry

Ti abundances in the zircons range from 0.89 to 36 ppm, indicating crystallization temperatures (T^{xlln}) ranging from 567 to 935 ºC. Crystallization temperatures average

679±124ºC (2σ). There is no apparent correlation between T^{xlln} and age, ε_{Hf} or $\delta^{18}O$ (see Fig. 2.8). Values of [Ti] and T^{xlln} for all samples are shown in Appendix B.

2.5 Discussion

There are several notable differences in ε_{Hf}, $\delta^{18}O$, and T^{xlln} between the Hadean zircon record in the Jack Hills and the younger zircons sampled here. The age distribution in our zircons displays several discrete peaks rather than the more homogeneous age distribution seen in the Hadean (see Fig. 2.6). Zircons in the 3.4 Ga age peak exhibit a narrow range in age with a wide range in ε_{Hf} (–6 to –14). Minor age peaks at 3.45 and 3.5-3.6 Ga demonstrate similar behavior. These groups behave similarly in $\delta^{18}O$, exhibiting a range in $\delta^{18}O$ from 4.5 to 6.5 ‰ SMOW. There is no correlation between ε_{Hf} and $\delta^{18}O$ within each of the age groups. All groups exhibit large ranges in T^{xlln}, indistinguishable from the Hadean record.

Interestingly, our finding of almost exclusively mantle-like $\delta^{18}O$ among the <3.8 Ga zircons differs from the results for similarly aged Jack Hills zircons reported by Peck et al. (2001). Peck et al.'s 3.3-3.6 Ga zircons average ~6.3‰ SMOW (n = 32 spot analyses on 16 grains). The discrepancy between these two datasets may owe partly to undersampling in the earlier study – whereas Peck et al. analyzed only 16 crystals with ages between 3.3-3.6 Ga for a total of 32 analyses, we have analyzed 76 individual crystals between the ages of 3.2 and 3.8 Ga, likely yielding a more representative sample. It is also the case that we do not pre-screen our samples for U-Pb concordance, and given Trail et al.'s (2007b) and Booth et al.'s (2005) finding that discordant Jack Hills zircons tend toward lower $\delta^{18}O$ there is some danger that these grains may not reflect primary magmatic $\delta^{18}O$. However, the similarity of our average $\delta^{18}O$ to that of 214 concordant Hadean Jack Hills zircons previously analyzed by ion microprobe (Cavosie et al., 2005; Harrison et al., 2008; Peck et al., 2001; Trail et al., 2007b)

suggests that any systematic error in the younger, non-screened zircons is likely not significant. Interestingly, several of our zircons fall below 5‰ SMOW (though within the range of values found by previous studies), and may indicate the remelting of higher temperature, hydrothermally altered materials. However, it is not clear from the small sample size whether this is a significant part of the younger zircon population, which mostly clusters about mantle values.

The variables of age, ε_{Hf} and $\delta^{18}O$ can be used for provenance interpretations for the <4 Ga zircons. It is likely that the large spreads in ε_{Hf} at each age peak are due to the mixing of material from multiple sources at different initial $^{176}Hf/^{177}Hf$ ratios to form the magma in question. This is consistent with the spread in $\delta^{18}O$, which could reflect minor source variations in $\delta^{18}O$ about a mantle value. The distinct clusters may suggest a low number of discrete source units. The ages of the younger clusters are consistent with the ages of some orthogneiss units in the Narryer Gneiss Complex (Kinny et al., 1988; Myers, 1988; Nutman et al., 1991). Zircons from the Dugel Gneiss reveal a crystallization age of 3375±26 Ma, the Eurada Gneiss yields zircon ages of ~3.45-3.49 Ga, and zircons from the various portions of the Meeberrie Gneiss range from younger than 3.40 to ~3.73 Ga (Nutman et al., 1991). In comparison to the <3.6 Ga zircons, the Hadean record would be more suggestive of derivation from a multitude of sources. This smoother distribution in the Hadean detrital zircons could be effected also if the Hadean zircons have undergone multiple sedimentary cycles – the population thus likely deriving from a larger total area and number of protoliths.

Despite these consistent ages, others (e.g., Maas and McCulloch, 1992) have pointed to geochemical discrepancies between the detrital zircon-bearing metasediments and the Narryer orthogneisses that may indicate the gneisses are not the source of the younger detrital zircons.

The Narryer orthogneisses display HREE depletion and widely variant positive and negative Eu anomalies, in contrast to the unfractionated HREE and consistently negative Eu anomaly in the metasediments. However, these differences could be balanced by a high proportion of mafic sediment (also suggested by detrital chromite and high Cr, Ni in the metasediments). A more relevant dataset for comparison was compiled by Kemp et al. (2010), who report age and Lu-Hf information for 70 metaigneous zircons separated from gneisses in the Narryer Gneiss Complex. Fig. 2.9 shows our data in the context of both a) earlier studies of detrital Jack Hills zircons and b) the meta-igneous zircons of Kemp et al. (2010). Narryer orthogneiss zircons range in age from 2.6-3.75 Ga and overlap with the more radiogenic of the <3.8 Ga Jack Hills zircons, though there are slight discrepancies in the peak ages. It appears that a large proportion of the more radiogenic <4 Ga Jack Hills zircons are at least consistent with derivation from local gneisses. The lack of more unradiogenic zircons among the Narryer gneisses would prove more puzzling in this context, perhaps requiring a less radiogenic reservoir of material, no longer outcropping in the area, which recorded many of the same events 3.3-3.75 Ga as the Narryer gneisses. It may be that the metasediments' derivation from this wider set of source lithologies accounts for the chemical discrepancies observed by Maas and McCulloch (1992), though the large mafic component needed to balance the REE discrepancies between Narryer gneisses and the metasediments may not be an excellent source for the large component of radiogenic zircons. However, due to the still unconstrained nature of the relationship between the Jack Hills source terrane(s) and the extant Narryer gneisses, for this study we consider the identity of the younger zircons' protoliths to remain an open question. For the remainder of this paper we will draw conclusions about the

geochemistry and crustal evolution of the source region for the Jack Hills metaconglomerate, whatever this source(s) might be in terms of extant rock units.

2.5.1 Implications of Initial Hafnium Isotopes and Model Extraction Ages

Model mantle extraction ages for the crust represented in any zircon population are dependent upon the choice of $^{176}Lu/^{177}Hf$ ratio for the crust. In the case of detrital zircon populations, the original host rocks are not available for analysis and reasonable assumptions must be made regarding $^{176}Lu/^{177}Hf$ for the grains in question. The simplest method involves assuming a uniform $^{176}Lu/^{177}Hf$ for the population in the absence of contrary evidence. We consider several models with differing values (Fig. 2.10a-c). The first model (Fig. 2.10a) uses $^{176}Lu/^{177}Hf = 0.01$, which is close to the average for volcanic rocks from the GEOROC database (http://georoc.mpch-mainz.gwdg.de/georoc/Start.asp; see Sarbas, 2008) and consistent with the bulk crust value of 0.008 preferred by Rudnick and Gao (2003). A second model (Fig. 2.10b) explores the possibility of a mafic origin for the zircons with $^{176}Lu/^{177}Hf = 0.022$. A third model (Fig. 2.10c) uses a value derived by fitting a reservoir evolution line to the least radiogenic of the <3.8 Ga zircons with igneous zonation, which yields a value of ~0.006. Depleted mantle parameters were calculated by extrapolating from an assumed present ε_{Hf} value of +18 to a value of zero at 4.56 Ga, assuming no appreciable external changes to the $^{176}Lu/^{177}Hf$ of the reservoir apart from the decay of ^{176}Lu over geologic time. As an additional note of caution, in the case of source mixing during magma formation, as is likely for igneous zircons at 3.4 Ga, the model age for any particular zircon may not have much significance and model ages for zircons from the extreme ends of the ε_{Hf} distribution will be most significant in terms of source material extraction age.

2.5.1.1 Uniform Models

The two more felsic models with $^{176}Lu/^{177}Hf = 0.01$ (average felsic volcanics) and $^{176}Lu/^{177}Hf = 0.006$ (best fit to younger distribution) generally yield depleted mantle extraction ages (T_{DM}'s) for the <3.6 Ga materials between 3.8 and 4.3 Ga. At ~3.8 Ga there is a fairly abrupt transition in both models in the average T_{DM}. Formation of all 3.4-3.45 Ga zircons directly from a long-lived mafic reservoir of $^{176}Lu/^{177}Hf = 0.022$ (a value derived by Amelin et al., 1999 from the slope of their age, ε_{Hf} array) is unlikely given the unrealistically high model ages of >4.56 Ga for the most unradiogenic zircons. The most unradiogenic 3.4 Ga zircons are also (as shown in Fig. 2.7) magmatically zoned, demonstrating that they represent igneous materials rather than older material metamorphosed at 3.4 Ga, which is a likely origin for the patchily zoned <4 Ga zircons plotting near PHB. A direct mafic source is also inconsistent with the observed granitic mineral inclusions (quartz+K-feldspar+micas) and with minimum melting conditions inferred from low T^{xlln} among the zircons.

2.5.1.2 More Complex Extraction Age Models

One possibility for the derivation of the younger zircons is a granitic source only recently remelted from an older, long-lived mafic source. In the above calculations and Fig. 2.10a-c we assume that each modeled reservoir was extracted directly from the mantle. This is a simplified model, as direct mantle melts would have typical basaltic Lu/Hf ratios (higher than felsic, but with variations depending on garnet content). The two lower Lu/Hf reservoirs would most likely have formed from a mafic reservoir that was extracted from the mantle at some unspecified time in the past – and thus the calculated extraction ages for the two lower Lu/Hf reservoirs should be viewed as minimum model ages. This does not, however, erase the necessity for the most unradiogenic Hadean zircons and the far more radiogenic <3.6 Ga zircons to be derived from distinct source reservoirs.

Fig. 2.10d shows the evolution of hypothetical reservoirs that might form the basis for a more complex model of Jack Hills source terrane(s) development, including reservoirs with the same $^{176}Lu/^{177}Hf$ ratios investigated in the uniform-composition models. Felsic and mafic reservoirs isolated at planet formation permissively bracket the more unradiogenic among the sampled Jack Hills materials, though as shown in Fig. 2.10d no <3.6 Ga magmatic grains approach the felsic evolution line. Mafic reservoirs extracted at 4.56 and 4.0 Ga bracket most 3.5-4.0 Ga zircons and the more unradiogenic 3.4-3.5 Ga zircons, though some felsic history is required for zircons below ~-10ε at 3.45 and 3.4 Ga (many of which display igneous zonation). A variety of possible source terrane evolutions are shown. For example, a hypothetical history involving the extraction of a felsic reservoir from a 4.56 Ga mafic reservoir is shown to be consistent with the <3.6 Ga data; so also would be mixtures (of varying degrees) of ancient mafic and felsic reservoirs.

Despite the many working hypotheses consistent with these data, several things are clear from this figure. First, the <3.6 Ga materials must be derived largely from different sources than the unradiogenic Hadean zircons – either younger materials with a long felsic history or felsic materials derived more recently from a very ancient mafic reservoir. Fig. 2.10d shows the latter scenario for the derivation of unradiogenic 3.4 Ga magmas. The most unradiogenic Hadean material is not unambiguously sampled after 3.6 Ga. At the same time, model ages show that the more unradiogenic zircons (below -10ε at 3.4 Ga) must have been sourced from a reservoir with Lu/Hf lower than typical mafic rocks, though not inconsistent with ancient remelts of mafic crust. Second, unlike most of the sampled Hadean zircons (Kemp et al., 2010; Harrison et al., 2005, 2008), the more radiogenic materials among the <3.8 Ga distribution require juvenile mantle melts at some point in the late Hadean to post-

Hadean history of the source terrane (with the present zircons sourced partially from reworkings of these mantle melts). Using Fig. 2.9, estimates of the timing for the simplest model – a direct mafic source – fall ~4 Ga.

2.5.2 Formation Environment and Petrogenesis

The relatively narrow distribution of the zircons about a mantle-like $\delta^{18}O$ value (5.49±0.43‰ $\delta^{18}O_{SMOW}$, ±1σ) suggests little systematic contribution to the host rocks from materials involved in low-temperature aqueous alteration. For the igneous zircons, this likely precludes a large degree of (meta-) sediment assimilation into host magmas. These results are in contrast to the much more variant Hadean oxygen record which despite the similar average $\delta^{18}O_{SMOW}$ value of 5.72‰ has a higher degree of variation at ±0.8‰ (±1σ). The Hadean record contains many grains falling above 6.5‰ that likely reflect significant contributions from older sedimentary materials (see Fig. 2.8a).

The crystallization temperatures recorded in the zircon Ti abundances of 679±62ºC (1σ) suggest that, like the majority of Hadean zircons, the younger population if igneous represent close to minimum melting conditions of intermediate to felsic magmas. An igneous origin is indeed suggested by the oscillatory zoning evident in 32 grains. The 107 grains displaying patchy, irregular, or no zoning are more ambiguous in origin. The 50 patchily-zoned grains may have undergone recrystallization or metamorphic overprinting (Corfu et al., 2003), which might obscure the original igneous Hf and O isotopic compositions, but nevertheless except in the noted cases of highly unradiogenic patchy grains these apparently metamorphic grains do not differ systematically from other zircons in their geochemistry. Though there is no apparent systematic relationship among the distributions of $\delta^{18}O$ or ε_{Hf} and zoning style, grains with T^{xlln} <600ºC tend to display either no zonation or patchy/irregular

zonation, though these zonation categories also include higher-T^{xlln} grains. From 3.4 to 3.6 Ga, patchily and irregularly zoned zircons occur in the same age intervals as the apparently more pristine oscillatorily zoned zircons, and zircons with no zoning occur alongside them.

2.5.3: Global Comparison

Pietranik et al. (2008) compiled a Lu-Hf-age dataset of zircons from several Archean cratons and interpret it to reveal several pulses of continental growth between 4.5 and 2.8 Ga. Many zircons in this compilation are contemporaneous with the younger Jack Hills zircons and may provide a comparison for other regions where early Archean crustal evolution left some lithic record. We plot our age vs. ε_{Hf} data with Pietranik et al.'s (2008) data for Slave Craton detrital zircons and Amelin et al.'s (2000) data for detrital zircons from the Acasta Gneiss, Barberton Mountain Land, Pilbara Craton and Itsaq Gneiss (Fig. 2.11). We have normalized all hafnium compositions to the CHUR values of Bouvier et al. (2008) for comparison. Zircons with ε_{Hf} values as low as –10 occur in the Acasta Gneiss from 3.6-3.4 Ga. Interestingly, the sampled Acasta Gneiss zircons overlap considerably in ε_{Hf} with zircons from our 3.55 Ga broad age peak and may indicate parallel crustal reworking histories in the two terranes for this time period.

Pietranik et al. (2008) interpret Mid- to Late-Archean zircons from the Slave Craton to lie along a mafic reservoir evolution line that suggests a mantle extraction age of ~4.2 Ga. Many of our samples are also compatible with origins from a remelted mafic Hadean reservoir and overlap the reported compositions of Slave and Superior province zircons. However, our 3.4 Ga zircons reach much more unradiogenic compositions than those found in other cratons for the same time period. It is likely that the unusually unradiogenic younger Jack Hills zircons are a unique resource in determining the fate of early felsic crust. This is compounded by the

apparent lack of highly unradiogenic signatures among detrital zircons of similar age from the nearby Mt. Narryer (Nebel-Jacobsen et al., in press).

2.5.4 Synthesis: Crustal Evolution from 3.0 to 4.0 Ga

While a powerful approach for elucidating juvenile crustal addition versus remelting of older crust, Lu-Hf isotopic data do not constrain the tectonic environment in which the metaconglomerate catchment area evolved. The apparent contrasts between older and younger zircons in both Lu-Hf and oxygen isotope systematics may suggest different magmatic settings and possibly different reservoirs of material for <3.6 Ga and >4 Ga protoliths. Further study of <4 Ga Jack Hills zircons and the Narryer Gneiss Complex may be needed to constrain the specific geologic context in which the Hadean grains have been preserved and the younger grains formed, but some constraints are evident now.

The change in Lu-Hf systematics with age precludes the preservation or remelting of significant amounts of the most enriched sampled Hadean materials (that falling on or near the PHB) into younger magmas and requires at least some contribution from late- to post-Hadean juvenile crust. Why this unradiogenic reservoir ceased to be available for reworking is unclear. Solutions involving the erosion and loss of this crustal material (for instance, by some form of tectonic denudation) are intriguing but await further analysis of the period between 3.6 and 4.0 Ga to determine whether any magmatic zircons bearing this signature are evident in a more representative sampling. This period is sparsely sampled at present due to its coincidence with a minimum in the zircon age distribution at 3.6-3.8 Ga.

Despite the transition in the Lu-Hf systematics with time, a large separation in model ages for Hadean and younger zircons is only achieved with a felsic precursor for the younger magmas. The isotopic evidence does not rule out an alternate scenario in which most <3.6 Ga

zircons derive from a remelted mafic Hadean precursor indistinguishable from the more radiogenic of the sampled Hadean materials. Derivation from remelting of mafic Hadean materials is also consistent with the Lu-Hf systematics of contemporaneous zircons from several spatially distinct cratons (Amelin et al., 2000; Pietranik et al., 2008; Fig. 2.11), and is likely a common petrogenesis among Early Archean crust. We must also consider the possibility of a mixture of various sources, Hadean and younger, in the production of younger magmas. Further sampling 3.6-4 Ga will constrain the form of the distribution and determine whether the younger Jack Hills zircons are indeed best modeled by magmas derived from felsic or mafic precursor materials (or a mixture).

Whether the melts from which the <3.6 Ga Jack Hills zircons formed are remelts of mafic or felsic materials they appear to be largely felsic themselves. Ti-in-zircon T^{xlln} throughout the age distribution suggest close to minimum melting conditions. There is no obvious distinction between the Hadean and younger populations in T^{xlln}. The mineral inclusion suite is only well characterized for the 3.4 Ga age peak, but here appears largely consistent with a granitic melt: quartz and K-feldspar dominate. The largely mantle-like $\delta^{18}O$ among <3.6 Ga zircons suggest little contribution of sedimentary material to the magmas. This is corroborated for grains in the 3.4 Ga age peak by the smaller proportion of muscovite among mineral inclusions compared to the Hadean (e.g., Hopkins et al., 2008, 2010). The apparently granitic T^{xlln} combined with the mantle-like $\delta^{18}O$ of most grains suggests the <3.6 Ga zircons are likely derived from I-type granitic melts. In contrast, a significant proportion of the Hadean grains appear on the basis of mineral inclusions to be from S-type melts (Hopkins et al., 2008, 2010). This suggests a transition to a different magmatic style with possible tectonic implications. Both the Lu-Hf systematics and other geochemical indicators

of petrogenesis independently suggest a transition between the Hadean and <3.6 Ga source areas. Whether this is due to the zircons deriving from separate tectonic terranes or one region undergoing continuous geologic evolution away from S-type granite production is yet unclear.

2.6 Conclusions

Age, ε_{Hf}, and $\delta^{18}O$ results for <3.8 Ga zircons in the Jack Hills detrital record reveal important differences between the Hadean and younger zircon populations. Whereas the majority of igneous zircons from both time periods appear to result from minimum melting of a low Lu/Hf source, the <3.6 Ga zircons lack the highly unradiogenic materials sampled in the Hadean, require at least some juvenile input not seen among the Hadean zircons, and appear less likely to reflect aqueous alteration (hydrothermal or low-T) among their source materials. This indicates a substantial provenance difference between the Hadean and younger grains. Whether this indicates separate tectonic terranes remains to be seen. For petrogenesis of the <3.6 Ga magmas by remelting of an older felsic source, there is an abrupt transition of the ε_{Hf} distribution at 3.6-3.8 Ga; models based on the remelting of Hadean mafic materials for some of the younger zircons remove the abrupt transition but still require disappearance of the most unradiogenic Hadean materials. A larger dataset for the period from 3.6-4 Ga will clarify the fate of the unradiogenic Hadean component and further constrain possible tectonic scenarios accounting for the ε_{Hf} distribution in the younger Jack Hills record. Further surveys of geochemistry among the older and younger zircon populations will also help to elucidate the relationship between the two groups. The 3.6-4 Ga portion of the Jack Hills record is potentially one of the best resources on the planet for probing this poorly understood period of early Earth history, especially given that <3.6 Ga zircons preserve some of the most

unradiogenic hafnium seen in the early Archean. Further constraining the geologic behavior of the source region 3.6-4 Ga will have important implications for the tectonic evolution of this fragment of the very early continental crust.

Chapter Two Tables and Figures

Quantity	Accepted	Session 1	2σ	Sess. 2 d. 1	2σ	Sess. 2 d. 2	2σ	Sess. 2 d. 3	2σ
				Temora-2					
$^{176}Hf/^{177}Hf$	0.282686	0.282696	5.4e-5	0.282631	5e-6	0.282625	7.1e-5	0.282574	1.5e-4
$^{176}Lu/^{177}Hf$	0.00109	0.001059	8.1e-4	0.001055	6.8e-4	0.000932	4.5e-4	0.001039	6.4e-4
				Mud Tank					
$^{176}Hf/^{177}Hf$	0.282507	0.282486	2.1e-5	0.282487	2.2e-5	0.282464	3.9e-5	0.282471	3.3e-5
$^{176}Lu/^{177}Hf$[a]	0.000042	0.000049	2.4e-6	6.08e-6	1.0e-6	6.54e-6	1.3e-6	1.26e-5	1.5e-5
				AS3					
$^{176}Hf/^{177}Hf$	0.282184	0.282161	4.2e-5	0.282124	4.3e-5	0.282148	6.6e-5	0.282160	3.9e-5
$^{176}Lu/^{177}Hf$	0.001262	0.001178	5.8e-4	0.000931	1.9e-4	0.001292	8.5e-4	0.001136	4.2e-4

(a) not used for corrections

Table 2.1: In-day averages for $^{176}Lu/^{177}Hf$ and $^{176}Hf/^{177}Hf$ of the standard zircons AS3, Temora-2 and Mud Tank. The reference values of Woodhead and Hergt (2005) shown for comparison. AS3 is called "FC-1" by Woodhead and Hergt. Italics indicate the zircon was not used as a standard for the relevant quantity.

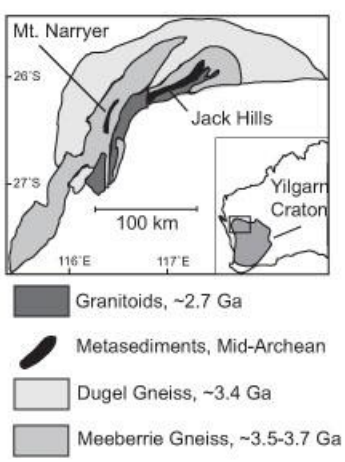

Fig. 2.1: Geologic sketch map of the Narryer Gneiss Complex, after Myers (1988a). Location of Jack Hills and Mt. Narryer indicated.

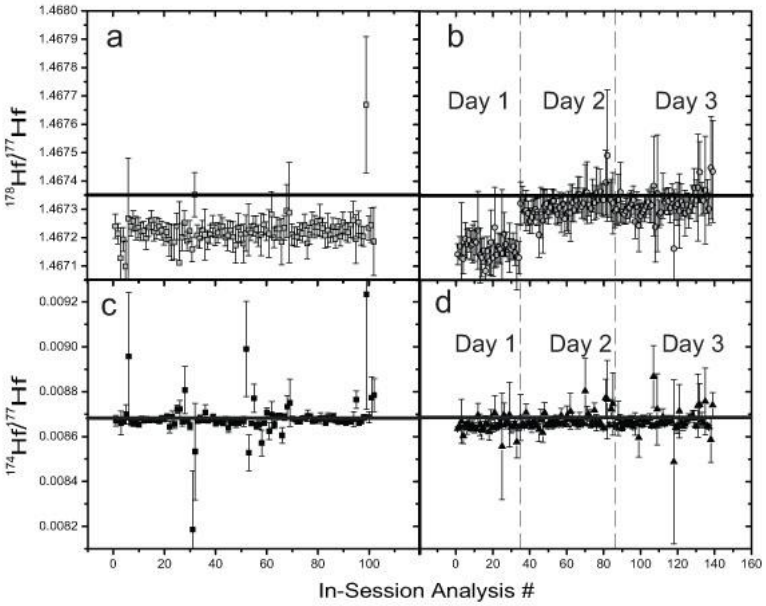

Fig. 2.2: Hafnium isotopic results for two uniform ratios in nature. A,B) ^{174}Hf/^{177}Hf results after mass fractionation correction for both analysis sessions. C,D) ^{178}Hf/^{177}Hf results after mass fractionation correction for both analysis sessions. Results for Session One and Day One of Session Two are uniformly low compared to the accepted value (Thirlwall and Anczkiewicz, 2004). Deviation from the accepted value for ^{178}Hf/^{177}Hf does not appear to correlate with either deviation from the reference value for ^{174}Hf/^{177}Hf or from the standards' accepted values for ^{176}Hf/^{177}Hf.

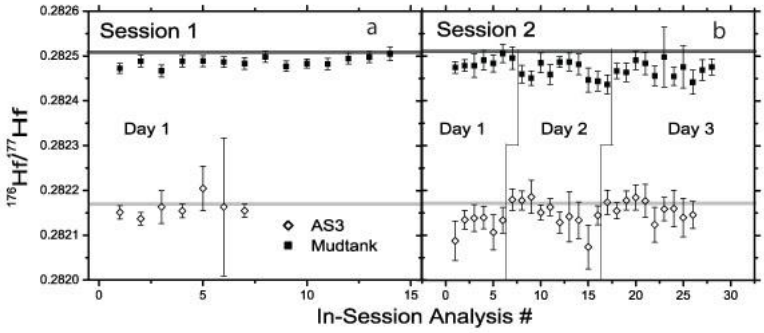

Fig. 2.3: ^{176}Hf/^{177}Hf results for the standard zircons AS3 and Mudtank, for which analytical conditions are closest to the unknowns. A) Session One data were collected in September 2007 at ANU; B) Session Two data were collected in April 2009 at UCLA.

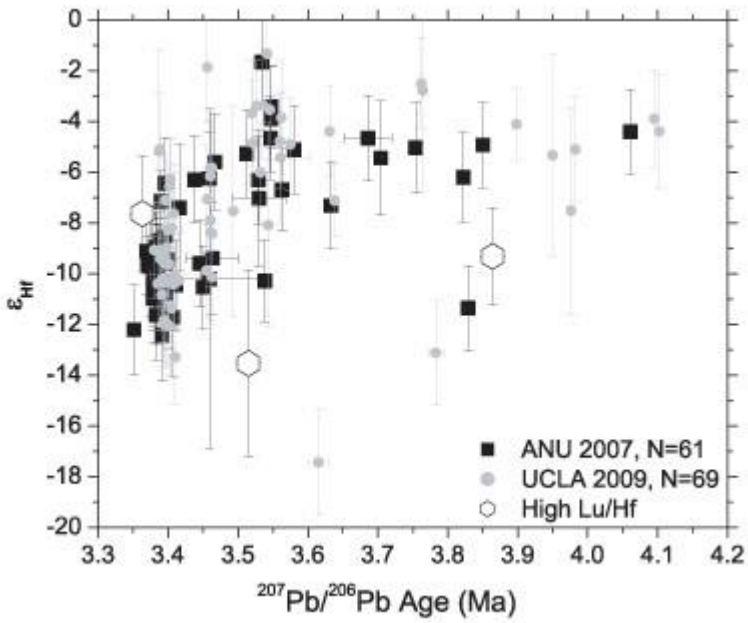

Fig. 2.4: Comparison of results from ANU and UCLA Hf-Pb sessions in ε_{Hf} vs. age space. One high Lu/Hf measurement at 2.88 Ga, -28ε was omitted for space purposes.

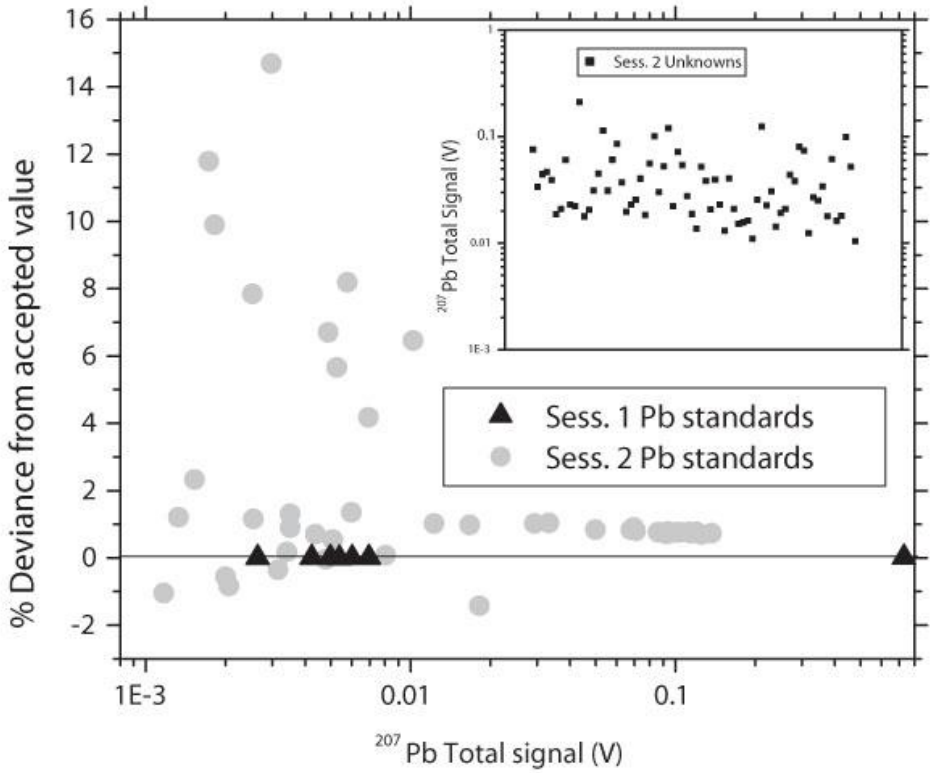

Fig. 2.5: All Pb standard analyses in % deviance (from expected value) vs. total ^{207}Pb signal (V) space. No standards were omitted for Session 1, but Session 2 standards below 0.01 V were omitted. Inset: Session 2 unknowns; all are >0.01 V.

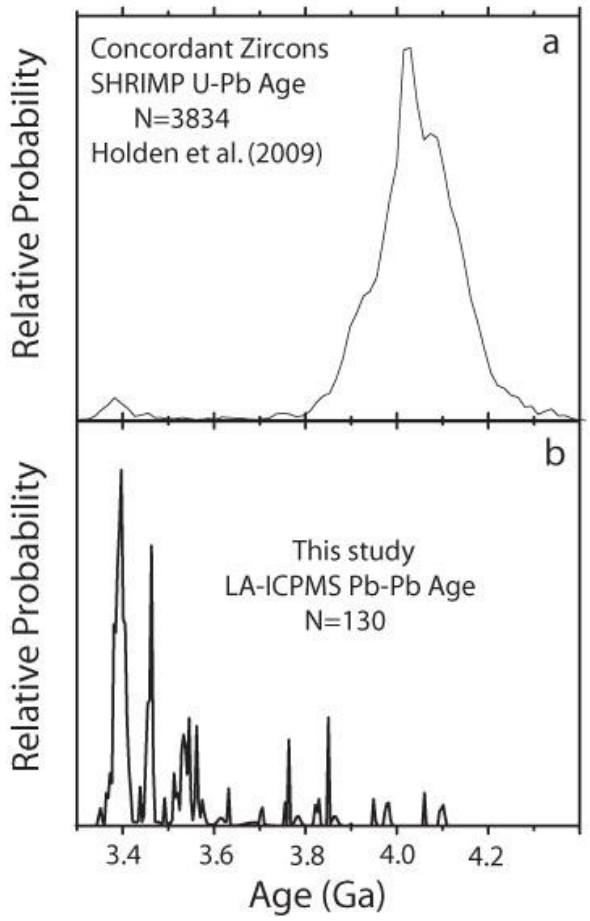

Fig. 2.6: Distributions in $^{207}Pb/^{206}Pb$ ages in the Jack Hills zircons from A) Holden et al. (2009)'s survey of Hadean Jack Hills zircons using SIMS U-Pb dating and B) ages from this study. The small <4 Ga peaks (e.g., at 3.4 Ga) in the Holden et al. (2009) data represent zircons with initially Hadean-appearing $^{207}Pb/^{206}Pb$ ages that upon closer analysis had younger cores.

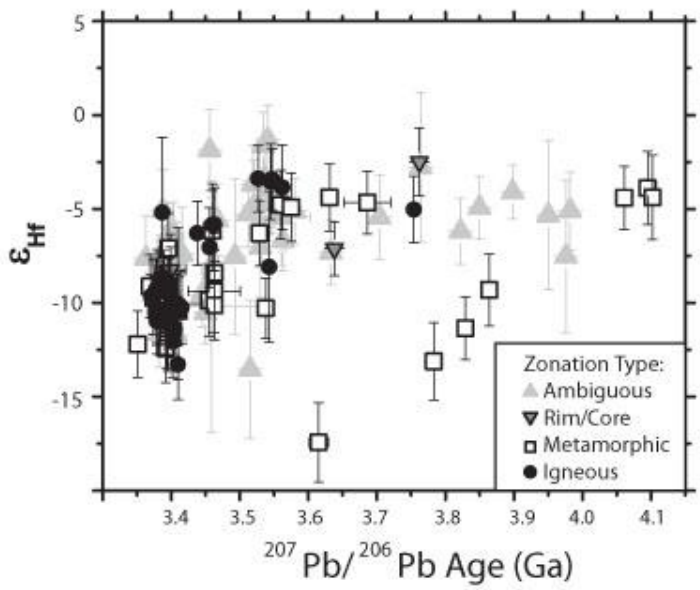

Fig. 2.7: Jack Hills zircons from this study in ε_{Hf} vs. age space, with zircons grouped by textures as imaged by cathodoluminescence. The "metamorphic" group consists of zircons with patchy or disrupted zoning; the "igneous" group consists of zircons with oscillatory or sector zoning (or both). Oscillatory zonation is rare >3.6 Ga. Interestingly the most unradiogenic zircons <4 Ga display metamorphic textures, indicating that their hafnium compositions probably do not reflect source terrane magmatic evolution.

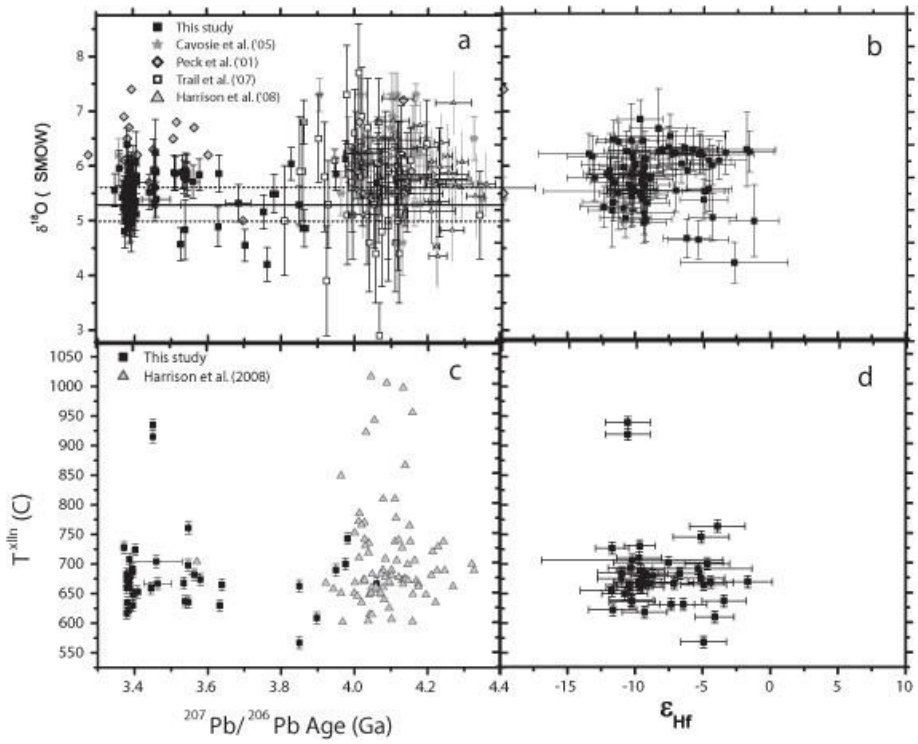

Fig. 2.8: Indicators for environment of formation among the studied Jack Hills zircons. A) age vs. $\delta^{18}O$, B) ε_{Hf} vs. $\delta^{18}O$, C) age vs. T^{xlln}, D) ε_{Hf} vs. T^{xlln}. No correlations are apparent.

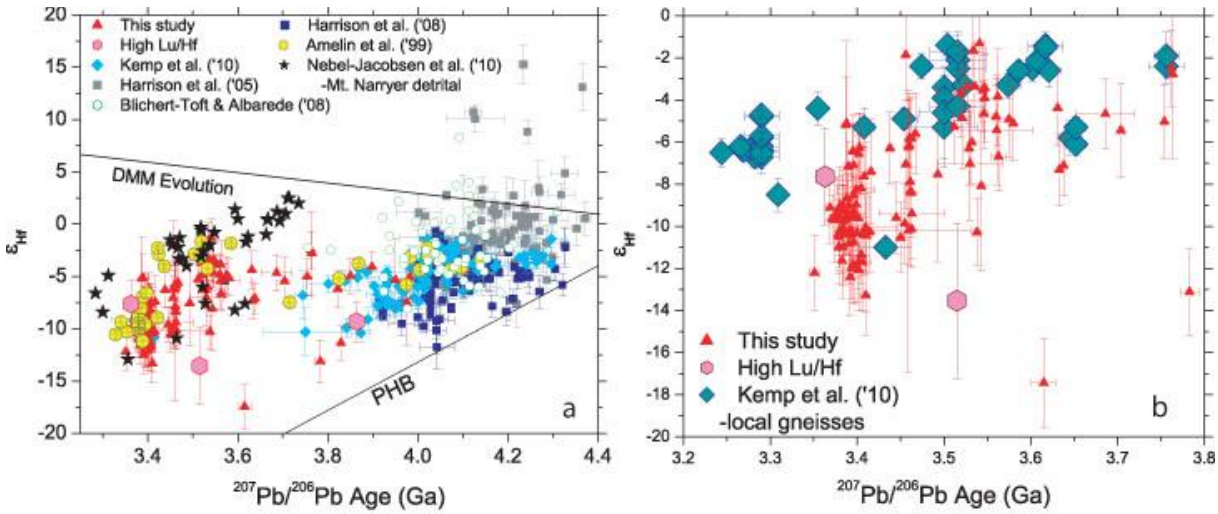

Fig. 2.9: Jack Hills zircons in age vs. ε_{Hf} space from this and several previous studies. A) Our data compared to other Jack Hills detrital zircon studies. The "PHB" line represents the evolution of a reservoir with the stated $^{176}Lu/^{177}Hf$ separated from CHUR at 4560 Ga. As in Fig. 4, a high Lu/Hf analysis at 2.88 Ga, -28ε is omitted. B) Our 3.2 - data shown with metaigneous zircon analyses from the Narryer Gneiss Complex. Data from several of these studies were normalized to slightly different CHUR values; we have renormalized to the CHUR values of Bouvier et al. (2008) for a more apt comparison to our data.

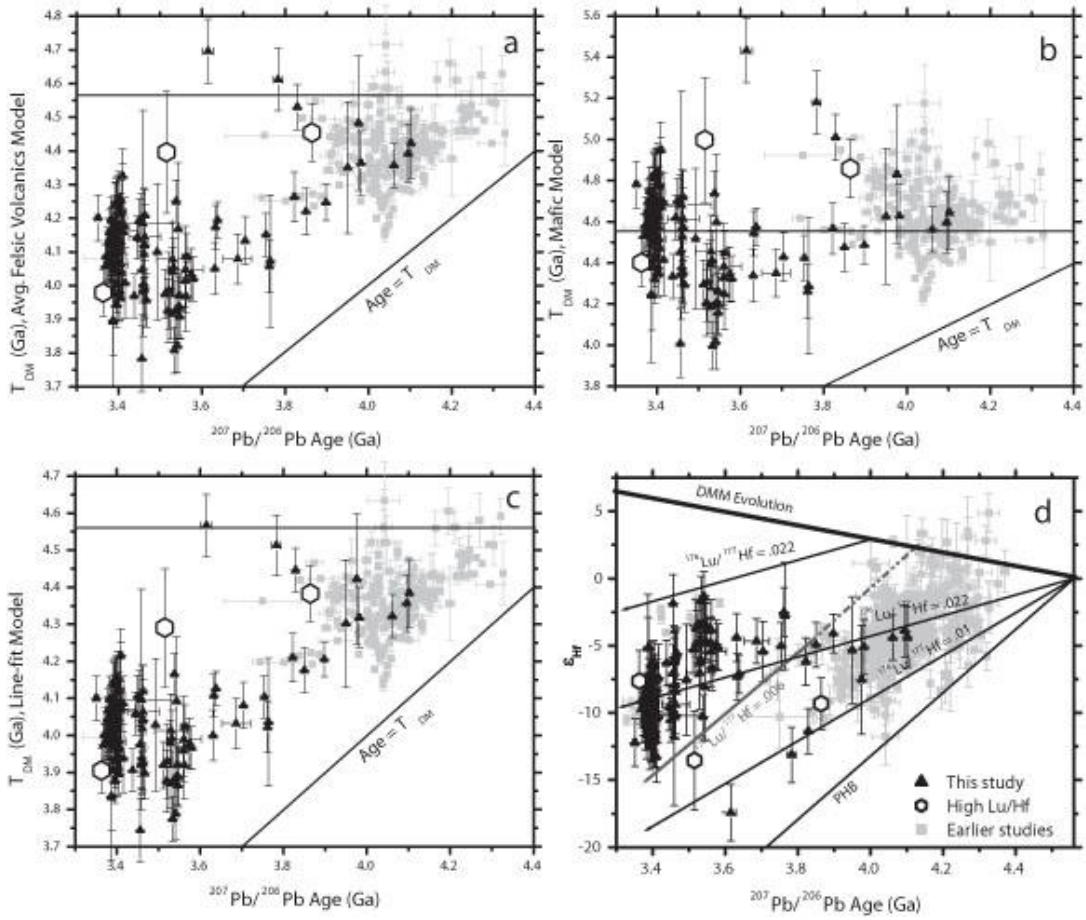

Fig. 2.10: Several models for zircon Lu-Hf extraction ages. A)Uniform model with $^{176}Lu/177Hf$ = 0.01, B) Uniform $^{176}Lu/^{177}Hf$ = 0.022, C)Uniform $^{176}Lu/^{177}Hf$ = 0.006. D) A basis for more complex models incorporating multiple past reservoirs. See the text in Section 5.1.2. Felsic and mafic reservoirs are shown originating at 4.56 Ga, along with a necessary juvenile reservoir sometime <4.2 Ga and a hypothetical $^{176}Lu/^{177}Hf$ = 0.006 reservoir fit to the <3.6 Ga distribution. Analyses with unusually high $^{176}Lu/^{177}Hf$ are marked with gray hexagons and should be regarded with caution; one at 2.88 Ga and -28ε is omitted. The data marked "earlier studies" are the detrital zircon data shown in Fig. 9a from Amelin et al. (1999), Blichert-Toft and Albarede (2008), Harrison et al. (2005, 2008), and Kemp et al. (2010).

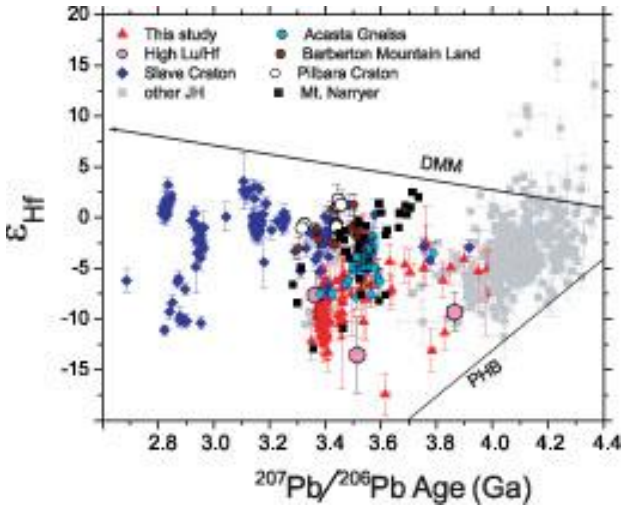

Fig. 2.11: Jack Hills detrital zircons from this and previous studies compared with zircons of similar age from other Archean cratons. Slave Craton data are from Pietranik et al. (2008); Acasta Gneiss, Barberton Mountain Land, and Pilbara Craton zircons are from Amelin et al. (2000); Mt. Narryer detrital zircon data are from Nebel-Jacobsen et al (in press); earlier Jack Hills detrital zircon data as for Fig. 10d. We normalized all Lu-Hf data to the CHUR parameters of Bouvier et al. (2008) for comparison to our data.

Chapter Three: Post-Hadean transitions in Jack Hills zircon provenance: A signal of the Late Heavy Bombardment?

Abstract. Hadean Jack Hills (Western Australia) detrital zircons represent the best documented terrestrial resource with which to observe the pre-4 Ga Earth. The >4 Ga component of this semi-continuous 4.38 to 3.0 Ga zircon record has been investigated in detail for age, $\delta^{18}O$, Lu-Hf systematics, and Ti thermometry. The more abundant post-Hadean population is less well-characterized, but our investigations in ch. 2 of this study suggests a more restricted range of $\delta^{18}O$ source materials together with a ca. 4.0-3.6 Ga discontinuity in Lu-Hf evolution. These differences could reflect a transformation in the character of the older zircon source region or their sourcing from different terranes entirely. The relative scarcity of 4.0-3.6 Ga zircons corresponds to a discontinuity in Lu-Hf evolution after which $^{176}Hf/^{177}Hf$ in zircon reverts to more radiogenic values relative to the >4 Ga population. We present new oxygen isotope, titanium, and trace element results for 4.0-3.6 Ga Jack Hills zircons in a search for apparent transitions in petrological conditions. Post-3.8 Ga zircons show a marked decrease in the occurrence of heavy oxygen (>6.5 ‰), but remain close to the average of the Hadean distribution despite their restricted range. This may point to the decreased importance of sedimentary materials in post-3.8 Ga magmas. Ca. 3.9 Ga zircons fall into two categories: "Group I" displays temperatures and compositions similar to the Hadean zircons whereas "Group II" zircons have higher U and Hf, and lower (Th/U), Ce and P. Group II zircons also have anomalously low Ti, and are remarkably concordant in the U-Pb system. Group II's geochemical characteristics are consistent with formation by transgressive recrystallization (Hoskin and Black, 2000), in which non-essential structural constituents are purged during high-grade thermal metamorphism. The restricted age range of Group II occurrence (3.91-3.84) and its coincidence with the postulated

intense bolide flux in the inner solar system (i.e., Late Heavy Bombardment; 3.95-3.85) may have causal significance.

3.1. Introduction

The pre-3.6 Ga terrestrial rock record is sparse. Surviving rocks older than 4 Ga are even rarer and consist of components of the Acasta Gneiss (ca. 4.03 Ga, Bowring and Williams, 1999) and, possibly, amphibolites from the Nuvvuagittuq greenstone belt (ca. 4.3 Ga, O'Neil et al., 2008). Arguably the most complete record of the Hadean is found in detrital zircons from the Jack Hills, Western Australia, whose ages semi-continuously span the period 4.38-3.0 Ga (Compston and Pidgeon, 1986; Holden et al., 2009; Harrison, 2009). Investigations of these zircons have revealed the presence of heavy oxygen in some, perhaps reflecting evidence for sedimentary cycling and low-temperature water-rock interactions in the protolith (Peck et al., 2001; Mojzsis et al., 2001). Ti-in-zircon crystallization thermometry of Hadean zircons yields apparent crystallization temperatures (T^{xlln}) that average ~700ºC (Fu et al., 2008; Watson and Harrison, 2005) suggestive of granitic minimum melting conditions (Watson and Harrison, 2005; cf. Fu et al., 2008). Rare earth element (REE) patterns and Lu-Hf systematics (Trail et al., 2007b; Harrison et al., 2008; Harrison, 2009) also suggest felsic igneous origins for the majority of the zircons. Although Kemp et al. (2010) argued for sourcing of the zircons from hydrous low-temperature remelting of a primary Hadean basaltic crust, they did not consider the full spectrum of constraints on their origin (see Harrison, 2009) .

As a consequence of the sparse lithological record of early Earth, we currently have no clear view of the nature of the transition between conditions prevailing during the Earth's first few 100s of millions of years and those during the later, and more accessible, parts of the Archean – or indeed if globally there were significant differences between the two periods. The

Jack Hills detrital record is an invaluable resource for investigating this poorly known time period as it provides a semi-continuous history of its source terrane(s) spanning more than a billion years. In this paper, we geochemically investigate this poorly understood transition and find significant differences between pre- and post-4 Ga zircons that may bear on the Earth's impact history.

3.2. Geologic Transitions at the Hadean-Archean Boundary

Jack Hills zircons are found in ca. 3 Ga metaconglomerates deposited in a deltaic environment (Spaggiari et al., 2007) sourced from mature clastic sediments. The range of protolith compositions and P-T histories experienced by Jack Hills zircons are likely representative of the catchment area of this drainage (barring selection effects of sedimentary transport, for instance if some of the zircons are polycyclic as suggested for some younger Jack Hills sedimentary units by Grange et al., 2010), but not necessarily of the whole Earth. Consequently, changes with time in the Jack Hills zircon record are potentially due to either changes to their local geological environment or possible planet-wide effects. Discerning positively whether the cause of a particular change in the Jack Hills provenance was global or local may not be possible. However, catastrophic meteorite bombardment – as in the hypothesized Late Heavy Bombardment – would be expected to have effects on both a local and a planet-wide scale.

3.2.1 Apparent Geochemical Transitions in Jack Hills Zircons

Comparisons of pre-4 Ga and 3.6-3.4 Ga Jack Hills zircons show several apparent differences in formation conditions and protolith sources. In ch. 2 of this study we found a $\delta^{18}O_{SMOW}$ distribution among the younger zircons that clustered around mantle equilibrium

values (i.e., 5.3‰, Valley, 2003) with none containing unambiguously heavy oxygen (cf. Peck et al., 2001). By contrast, the Hadean record contains a significant proportion of zircons with heavy $\delta^{18}O_{SMOW}$, consistent with incorporation of hydrous sediments (Mojzsis et al., 2001; Cavosie et al., 2005; Trail et al., 2007b). The most unradiogenic (with respect to CHUR) Hf isotopic signatures in Hadean zircons are generally not observed among the <4 Ga zircons, such that even if the younger zircons are derived from broadly the same source terrane as their Hadean counterparts, some of the more unradiogenic source materials had either become inaccessible to protolith magmas or destroyed by 3.6 Ga (this study, ch. 2).

Due to a paucity of detrital Jack Hills zircons between ca. 3.8-3.6 Ga, a prior survey (this study, ch. 2) was unable to adequately sample that interval and thus did not document precisely when and how differences between Hadean and younger zircons began to be preserved (whether gradually or more suddenly). A sudden transition in $\delta^{18}O$ distribution, for instance, might signal a rapid change in geological conditions. Similarly, although Hadean and 3.6-3.4 Ga (the dominant peak in the Jack Hills zircon population) zircons yield similar Ti-in-zircon T^{xlln} distributions (this study, ch. 2), any deviations from the prevailing, apparently granitic source during this period may also reflect changes in the sediment source during late Hadean-early Archean time.

3.2.2 The Late Heavy Bombardment

The Earth-Moon system, and likely the entire inner solar system, appears to have been subjected to an intense flux of impactors at ca. 3.9 Ga (Tera et al., 1974). The first recognition of this event came from isotopic disturbances seen in lunar samples (Tera et al., 1974). Specifically, Rb-Sr, U-Pb and K-Ar systems were reset at ca. 4.0-3.85 Ga (*e.g.*, Tera et al., 1974;

Turner, 1977; Maurer et al., 1978; Ryder et al., 2000; Kring and Cohen, 2002). The hypothesis that emerged was of a discrete Late Heavy Bombardment (LHB) in the period 3.95-3.85 Ga (Tera et al., 1974), although it remains unclear whether this was instead the tail of a decreasing bolide flux (*e.g.*, Hartman, 1975). The lack of an identifiable signature in the fragmentary terrestrial rock record from the LHB era has limited the study of this period of solar system history almost entirely to extraterrestrial samples. Given its scaling to the Moon in terms of mass and surface area, the Earth should have experienced approximately 20 times the impact flux of the Moon (*e.g.*, Grieve et al., 2006), leading to heating of a significant proportion of the crust.

As hypothesized (*e.g.*, Gomes et al., 2005; Abramov and Mojzsis, 2009), the LHB would have been sufficiently pervasive and intense to create a distinctive set of geological conditions characterized by widespread metamorphism and hydrothermal alteration. For example, although the proportion of the crust predicted by Abramov and Mojzsis (2009) to have experienced thermal disruptions of >1000°C is small (ca. 2%), their model suggests that ~20% of the lithosphere would have been heated by 100°C or more. More locally, large impacts would result in the generation of impact melt sheets.

Zircons grown from impact melt sheets are unlikely to crystallize at the predominantly minimum melting conditions inferred for Hadean detrital zircons (see Harrison, 2009), but instead form at significantly higher temperatures (Darling et al., 2009; Wielicki et al., 2012). Thermal metamorphism may or may not form new zircon (Hoskin and Schaltegger, 2003) depending on petrological conditions, but metamorphically grown and metamorphically overprinted zircons may be identifiable by their patchy internal zonation (Corfu et al., 2003), although this is not universal and some specific alteration mechanisms result in different internal

structures. Low (Th/U) ratios are common among metamorphic zircons, whether newly grown (often <0.01; c.f. Wan et al., 2011) or recrystallized originally igneous zircons, which decrease in Th/U with respect to their protolith zircons but may not reach values as low as 0.01 (Hoskin and Schaltegger, 2003). Zircons recrystallized during metamorphic heating and/or fluid ingress show a variety of textural and chemical features (*e.g.*, Pidgeon, 1998; Vavra et al., 1999; Hoskin and Black, 2000). Vavra et al. (1999) found zones of recrystallization in zircons from high-grade metamorphic rocks in the Ivrea Zone that showed bright regions of recrystallization under cathodoluminescence that had lost both Pb and U, resetting the U-Pb age. Pidgeon et al. (1998) observed that during metamorphism, zircons can develop both lobate low-U regions and trace element rich bands, cross-cutting previous zircon internal structures. Hoskin and Black (2000) found that zircons recrystallized under granulite-facies metamorphic conditions can contain recrystallized regions transgressing previous structures that are homogeneous or display faint relicts of magmatic textures. These transgressively recrystallized regions of their zircons typically display increased contents of trace elements compatible in the zircon lattice (*e.g.*, U, Hf) and decreased contents of zircon-incompatible trace elements (*e.g.*, P, LREE).

Unfortunately, much of the evidence of an LHB-type event would be indistinguishable from endogenic geological processes that operated at smaller spatial scales (*e.g.*, regional metamorphism). Proof of a connection to a period of heavy bombardment may not be possible when considering the Jack Hills zircon record alone. That said, the absence of a distinctive signal consistent with a global impact cataclysm would argue against the source terrane having experienced LHB-related effects, so a partial hypothesis test of a terrestrial occurrence of the LHB may yet be possible. In this paper, we apply both the Ti-in-zircon crystallization temperature (T^{xlln}), an element of zircon petrogenesis that is well-established for the Hadean

population, and other trace element analyses to 4.0-3.6 Ga zircons to seek evidence of some change or disruption in geological conditions with time in the Jack Hills source region(s).

3.3. Methods

Many U-Pb ages of zircons studied here were undertaken using the SHRIMP I instrument at the Australian National University and reported in Holden et al. (2009). Additional dating was carried out using UCLA's CAMECA *ims*1270 ion microprobe. All analytical results for those data are given in Appendix C together with summarized ages for the previously analyzed samples. Oxygen isotope and trace element measurements were all carried out using the UCLA ion microprobe.

All samples were mounted in epoxy and polished to reveal a flat surface. At UCLA, Jack Hills detrital zircons were surveyed using a rapid (5-10 cycle) method that measured only the masses ^{204}Pb, ^{206}Pb, ^{207}Pb, and ^{208}Pb, providing a ^{207}Pb/^{206}Pb age estimate but no concordance information. Those zircons with apparent ages from 3.6-4.0 Ga were then more precisely analyzed using our standard U-Th-Pb protocol (Trail et al., 2007b). During the several analysis sessions at UCLA from June 2009 to May 2010 we used primary O^- beam intensities ranging from 8-13 nA corresponding to analysis spot sizes of 30 to 40 μm. We used zircon U-Pb age standard AS3 (1099±1 Ma; Paces and Miller, 1993) during all analysis sessions. In addition, some zircons analyzed for other variables were from the collection of Holden et al. (2009).

Ti measurements on 4.0-3.6 Ga zircons were carried out in multicollector (MC) electron multiplier mode detecting $^{48}Ti^+$ and $^{30}SiO^+$ under a 30-40 μm primary O^- beam of ~10 nA at high mass resolution power (MRP; m/Δm ~ 8,000). The analyses were carried out in three sessions in August 2009, September 2009, and May 2010. The concentration of Ti was determined based on

analysis of several standard materials, including the standard zircons AS3 and SL13 (22 ppm and 6.3 ppm, respectively; Aikman, 2007) as well as NIST610 glass. We determined T^{xlln} from the Ti measurements using the Ti-in-zircon thermometer (Watson and Harrison, 2005) as formulated by Ferry and Watson (2007).

Ti-in-zircon measurements were also undertaken in peak switching (PS) mode in the course of a more extensive analysis of trace elements (REE, Hf, Th, U, Ti) for a selected, smaller group of zircons at ca. 3.9 Ga, as well as several Hadean zircons (discussed in section 4.2). These analyses were carried out using the CAMECA *ims*1270 ion microprobe at UCLA in one session during January 2011. Primary O^- beam intensities of ~15 nA were used, the spot size was 30µm, and secondary ions were detected at low MRP ($m/\Delta m \sim 2{,}000$) and high energy offset (-100 eV) using $^{49}Ti^+$. Only those analyses determined by later electron microscope imaging to not lie on cracks or inclusions were included in this study. NIST610 standard glass was used for calibration. We refer to these analyses as 'PS mode' (after the peak-switching protocol) to distinguish them from the multicollector ('MC') Ti measurements.

Oxygen isotope measurements were undertaken in two sessions during January and July of 2010. Analyses were made in Faraday multicollection mode with a Cs^+ primary beam of ~1.5-2.2 nA focused into a ~30 µm spot. For more details on the analytical method see Trail et al. (2007b). The AS3 zircon standard (5.34‰; Trail et al., 2007b) was used for sample-standard comparison.

3.4. Results

Zircons between 4.0 and 3.6 Ga broadly resemble the Hadean zircon population but differ in some important aspects of their trace element compositions. Ti-in-zircon temperatures and

several other elements of interest reveal a group of zircons at ca. 3.9 Ga that differ substantially from the Hadean population.

3.4.1 Ti-in-Zircon Thermometry

154 T^{xlln}_{MC} measurements are displayed in Fig. 3.1 (and reported in Appendix C). Statistics discussed herein are elaborated upon in Appendix D. Calculated T^{xlln} vs. age for all samples from 4.0-3.6 Ga analyzed using the MC protocol are shown in Fig. 3.1a in the context of data previously generated from Hadean Jack Hills zircons (Harrison et al., 2008). Given the danger that the placement of ion probe analysis spots over cracks may yield an artificially high Ti measurement (Harrison and Schmitt, 2007), we have attempted to check the analysis spots for cracks through later imaging. Clearly imaged spots seen to be over cracks are excluded and were systematically higher in Ti than the clearly imaged spots with no cracks, which mostly display Hadean-like and lower temperatures (Fig. 3.1). Samples for which there is some question due to ambiguous images are marked in Fig. 3.1, but they are statistically indistinguishable from the well-imaged samples and we include them in our discussion. Both the clearly imaged and ambiguous datasets have a small high-temperature tail similar to that seen in the Hadean (Harrison et al., 2008; Watson and Harrison, 2006), with somewhat more in the poorly imaged samples.

Significant trends observed in the Ti survey formed the basis for subsequent targeting of trace element measurements. Although T^{xlln} among 4.0-3.6 Ga zircons ranges from similar to cooler than average Hadean T^{xlln}, one time period ~3.9 Ga stands out as distinct (shown in greater detail in Fig. 3.1b). A number of zircons with ages between 3.91-3.84 Ga display low Ti and apparent T^{xlln} that range well below 600°C, as well as a scattering of higher-Ti zircons with

apparent T^{xlln} above 700°C. Zircons below 650°C in this period are with one exception >90% concordant, whereas several higher-Ti zircons are >10% discordant (discordance calculated as 100 x ($t_{207/206}/t_{206/238}$ - 1)). As revealed by the Wilcoxon Rank Sum Test, the T^{xlln} distribution in the period 3.91-3.84 Ga is statistically distinguishable from both the Hadean distribution (Harrison et al., 2008; p-value of 0.01) and from the 3.84-3.6 and 3.91-4.0 Ga zircons analyzed in this study (both p-values ~0.02). The Wilcoxon test compares two samples of non-specified distribution in a particular variable and tests the hypothesis that their probability distributions are distinct (see McClave and Sincich, 2006). The distributions of T^{xlln} in the age range 3.84-3.6 and 4.0-3.91 Ga both cluster about an average apparent T^{xlln} of ~690°C and are statistically indistinguishable from the Hadean distribution (with p-values >0.5). A few scattered zircons at 3.8-3.6 Ga fall at or below 600°C but do not represent a robust population. On the basis of the distinctly low Ti distribution in the age range 3.91-3.84 Ga, trace element analyses were targeted in this time period to search for other distinctive geochemical differences.

3.4.2 Trace Element Results

Zircons from the period 3.91-3.84 Ga were targeted for comprehensive trace element analysis, including REE, Hf, Th, U, and a second Ti measurement in PS (peak-switching) mode. All trace element results for 3.91-3.84 Ga zircons and 14 Hadean zircons for comparison are compiled in Appendix E. Various trace elements for the 30 zircons with accepted analyses in Appendix E are shown in Fig. 3.2. The 33 accepted analyses are those whose SIMS analysis pits were found to be free of cracks and inclusions (3 grains have 2 accepted analyses, which are similar and are averaged for interpretation). The zircon data appear to fall into two groupings within this time period (Group I and Group II), picked based on the two clusters in Fig. 3.2a (U_t vs. T^{xlln}; X_t refers to quantity X corrected to time of formation). Figure 3.3 shows chondrite-

normalized REE results for the Group I and II zircons. Most zircons show the low LREE/HREE, positive Ce anomalies, and negative Eu anomalies common to most terrestrial zircons. There is little overall difference between the groups in HREE contents, but Group II is somewhat lower on average than Group I in several LREE, including Ce. Two zircons show elevated contents of some LREEs, which may point to the analysis pit overlapping small LREE-rich inclusions (*e.g.* phosphates), although the analysis pits show no visible evidence for this. For the low-Ti MC measurements (<650°C), the two T^{xlln} estimates are typically consistent (Fig. 3.4). However, for the zircons that showed high Ti (>700°C) in the MC measurement, the PS estimate is often lower, leading to a Hadean-like distribution about apparent T^{xlln} ~680°C (Harrison, 2009). The disagreeing Ti measurements may be due to inadvertent sampling of multiple Ti domains, and indeed five of the eight zircons with disagreeing Ti measurements reveal zonation in cathodoluminescence imaging (see section 4.3). To reduce such a risk we attempted to place the measurement spots in the same structural domain as the age measurements; the few exceptions are noted in Appendix E. It appears that the existence of a distinct low-Ti signature during this time period (now considered part of Group II) is robust, but a distinct high-Ti signature, relative to the Hadean distribution, is not.

The Wilcoxon Rank Sum Test (see McClave and Sincich, 2006) shows that Groups I and II are distinct in the variables U_t, $(Th/U)_t$, Hf, Ce, and P at the 95% confidence level (see Appendix D). Although Group I compositions are similar to those of Hadean Jack Hills zircons (see Fig. 3.5), Group II is distinct and apparently unique in the Jack Hills record. Group II U contents are higher than Group I and range from 50-480 ppm (U_t = 100-1050 ppm), with most grains having U>200 ppm (Fig. 3.2a, Fig. 3.5). The high U contents displayed by Group II zircons contrast with the Hadean Jack Hills zircons, which typically have U below 200 ppm

(*e.g.*, Crowley et al., 2005; Harrison, 2009). (Th/U) ratios of the Group II zircons are typically below Group I (Fig. 3.2b) and (Th/U) appears to vary with U content. Another notable minor element is Hf (Fig. 3.2c), which is higher in Group II than Group I and covaries weakly with U (R^2 = 0.42). Fig. 3.2d shows the light REE Ce, for which Group II displays lower values than Group I. Phosphorus behaves similarly to Ce in the two groups.

Discriminant analysis using the variables U_t, Hf, $(Th/U)_t$, P, and Ce and the discriminant function given in Appendix D confirms these groupings, sorting all of the zircons in the 3.91 - 3.84 Ga age range into their respective groups based on our original estimated identifications from Fig. 3.2a. Leave-one-out cross-validation (to test the robustness of the discriminant classification; see, *e.g.*, Klecka, 1980) also confirms this result. Trace element results for 14 Hadean Jack Hills zircons mostly fall within Group I (Fig. 3.5; U_t vs. Hf) and this is also shown by the discriminant analysis (see Appendix D).

3.4.3 Imaging for Morphologies and Internal Textures

Zircon morphologies range from irregularly shaped grains to those with at least one pyramidal termination. Zircons also range from angular to well-rounded. Many are highly cracked, although on most grains we were able to measure Ti on uncracked regions of the surface. Internal textures as shown by cathodoluminescence (CL) imaging include oscillatory zonation (common among magmatic grains), patchy zonation (commonly caused by metamorphic alteration), and concentric broad zones of an uncertain origin (but which may reflect altered or blurred oscillatory zonation). Many grains are homogeneous in CL. One grain (RSES73-3.7, 3831±35 Ma, T^{xlln}_{MC}= 716°C) shows possible sector zonation. Fig. 3.6 and 3.7 show representative CL images of zircons in Group I and Group II, respectively, along with

SIMS analysis spots. Additional CL images for all grains in Groups I and II are found in Appendix E.

3.4.4 Oxygen Isotopes

Figure 3.8 shows $\delta^{18}O$ results for concordant 4.0-3.6 Ga zircons. All oxygen isotope data are tabulated in Appendix C. Like the Ti_{MC} results, we imaged the spots and excluded those found to be collected on cracks. Higher-confidence measurements were collected on demonstrably pristine surfaces and lower-confidence measurement spots could not be imaged well enough for certainty, although there is no distinguishable difference between the two populations. Concordant zircons in this age range have an average $\delta^{18}O_{SMOW}$ of ~5.5‰, similar to that of the Hadean population (see, *e.g.*, Cavosie et al., 2005; Trail et al., 2007b; Harrison et al., 2008). Unlike the trace element record, the $\delta^{18}O$ distribution in the period 3.91-3.84 Ga is not distinct from the Hadean. After 3.8 Ga, however, the $\delta^{18}O_{SMOW}$ distribution is more restricted: there are few zircons with oxygen compositions resolvably heavier than the mantle value (5.3‰, Valley, 2003), consistent with the findings of ch. 2 for post-Hadean Jack Hills zircons. The two exceptions are RSES72-1.3 (7.23±1.15‰ at 3.60 Ga) and RSES72-17.8 (1.10±1.16‰ at 3.64 Ga), although the highly imprecise measurement on sample RSES72-1.3 is within error of the prevailing ~4.5-6.5‰ population at this time period. Several discordant zircons (not pictured on Fig. 3.8 but listed in Appendix C) also fall below the mantle value along with RSES72-17.8 between 3.8 and 3.6 Ga.

3.5. Discussion

The age distribution of the Jack Hills zircons is dominated by a) a small population 4.3-3.8 Ga (peaking at 4.1 Ga) and b) a dominant population 3.6-3.3 Ga (peaking at 3.4 Ga), with a

sparsely populated age minimum in between (see this study, ch. 2; Crowley et al.; 2005; Holden et al., 2009). These two populations have somewhat different properties, indicating changes in provenance between the two time periods: despite similar T^{xlln} signatures, the more restricted $\delta^{18}O$ distribution among younger zircons points to a different magmatic environment (this study, ch. 2).

Detailed investigation of zircons from the sparsely represented age range from 4.0-3.6 Ga sheds some light on this transition. Although the average $\delta^{18}O$ is not very different from that seen in previous studies of the Hadean zircons, the restricted range after 3.8 Ga (and lack of unambiguously heavy $\delta^{18}O$) may point to a decreased importance of aqueous alteration or sediment inclusion in post-3.8 Ga Jack Hills protoliths. Although the overall T^{xlln} distribution is similar for much of the Jack Hills zircon record, the period 3.91-3.84 Ga shows anomalously low Ti. Low-Ti zircons in this period were sorted (along with others) into Group II following more comprehensive trace element analysis (see section 4.2), a group that appears unique in the Jack Hills record in several geochemical characteristics.

3.5.1 Group II: The Case for a Distinct Origin

A distinct distribution of highly incompatible trace elements for some zircons ("Group II") suggests that many of these grains have a separate origin from the majority of other Jack Hills zircons in the variables U_t, $(Th/U)_t$, Hf, P, and Ce. Other samples from the period 3.91-3.84 Ga ("Group I") have trace element signatures strongly resembling those of the Hadean Jack Hills zircons (see discriminant results in section 4.2), such that a discriminant analysis based on the function and variables given in Appendix D sorts the Hadean zircons into Group I. The 4.0-3.6 Ga distribution outside of this ~70 Ma period is indistinguishable from the Hadean

distribution in apparent T^{xlln}. Group II $^{207}Pb/^{206}Pb$ ages (of which 14 out of 17 grains are within 10% of concordia; all are within 15%) span the period 3.91 – 3.84 Ga.

3.5.1.1 Provenance Interpretations

The discriminant analysis described in section 4.2 indicates at least two distinct groups of Jack Hills zircons during the period 3.91-3.84 Ga; we interpret these groups as having separate origins, of which Group II is apparently unique in the Jack Hills record. Group I likely derives from similar provenance(s) as the Hadean zircons on the basis of T^{xlln}, U_t, Hf, and $(Th/U)_t$, Ce, and P, probably indicating a continuance of similar geological conditions in the source region(s) at least until 3.84 Ga. Group I consists of zircons with both apparently magmatic, oscillatory zonation (4 of 13), patchy (apparently metamorphic or altered) internal features (7 of 13), and two zircons of more ambiguous internal structure: a homogeneous grain (RSES 54-15.11) and one displaying wide concentric banding of uncertain origins, which may be faded or blurred oscillatory zonation (RSES 55-5.13) (see Fig. 3.6 and Appendix E). The zircons display typical igneous REE patterns of low LREE/HREE, positive Ce anomalies, and negative Eu anomalies (Hoskin and Schaltegger, 2003), although one does display somewhat unusually elevated LREE (see Fig. 3.3). $(Th/U)_t$ values of 0.27±0.08 are within the range of typical igneous (Th/U) values (Hoskin and Schaltegger, 2003) and similar to if slightly lower than most Hadean Jack Hills zircons. Group I zircons are probably igneous in origin (or igneous with some later alteration, as with the patchily textured grains) and derive from a provenance(s) similar to the Hadean Jack Hills zircons.

Group II displays distinctly higher U_t and Hf than Jack Hills Hadean zircons and lower average $(Th/U)_t$, Ce, and P. The average $(Th/U)_t$ of 0.15±0.05 is significantly below Group I and

the Hadean zircons. Group II also contains both zircons with consistently low apparent T^{xlln} along with zircons that have conflicting (MC vs. PS) T^{xlln} estimates. REE patterns for the majority of these zircons appear to have all the characteristics of typical igneous zircon (as does Group I, though Group II has somewhat lower LREE as shown here by Ce abundances). Group II consists of 8 homogeneous and 7 patchy grains (see Fig. 3.7 and Appendix E). Two zircons (RSES 56-10.17, RSES 59-6.12) display a wide concentric banding that is of uncertain origins, but may be faded or blurred oscillatory zonation. On the basis of REE and structural data, we conclude that most of these zircons are ultimately igneous in origin with variable amounts of later alteration.

3.5.1.2 Origins of Group II Zircons

Several models for Group II petrogenesis are possible. If Group II zircons are igneous and relatively unaltered, then their higher U_t and Hf would suggest derivation from relatively more evolved or later-stage melts than those that yielded the Hadean and Group I zircons. Their very low Ti contents (and therefore low apparent T^{xlln}) are consistent with this, since rare (possibly sub-solidus) zircons with apparent T^{xlln}<600°C are nearly always found in highly evolved felsic rocks (*e.g.*, Fu et al., 2008). On first consideration, a relatively low degree of alteration for these zircons might be suggested by their high degree of concordance – homogeneous grains and grains with wide concentric zoning (possibly faded oscillatory zonation?) are mostly within 5% of concordia. By contrast, Holden et al. (2009)'s survey of Jack Hills zircons shows that during this time period only ~60% of the overall population are within 10% of concordia. However, the high degree of concordance for these high-uranium zircons, compared to the higher degrees of discordance found among other contemporary Jack Hills zircons, is puzzling. If Group II zircons are largely unaltered, it is likely that they resided in a

higher temperature environment for much of their history between formation and deposition at ca. 3 Ga in order for accumulated radiation damage to be annealed, thus forestalling metamictization and Pb loss. The lack of clear igneous textures among Group II zircons is notable if an origin of the group as unaltered igneous zircons is to be seriously considered.

Another possible origin for Group II zircons is by metamorphic recrystallization of originally igneous zircons, perhaps even of similar or identical provenance to the prevailing 4.2-3.6 Ga population (though not necessarily so). Originally igneous zircons that subsequently recrystallized during metamorphism have distinct chemistries from neo-formed metamorphic zircon as well as different internal structures (Hoskin and Schaltegger, 2003). While several types of metamorphic recrystallization have been identified that flush Pb from the zircon lattice and thus re-set the U-Pb clock (*e.g.*, Hoskin and Black, 2000; Vavra et al., 1999), transgressive recrystallization (Hoskin and Black, 2000) is the type most likely to account for Group II. Transgressive recrystallization occurs under high-temperature conditions and involves the migration of recrystallization across a zircon (transgressing earlier structures), which results in the flushing of more incompatible trace elements (*e.g.*, LREE, P, Th) from the lattice as well as an increase in more compatible elements (*e.g.*, Hf, U), consistent with Group II chemistry. Many other types of alteration yield zircon with trace element chemistries at odds with the general trends for Group II: for instance, Pidgeon et al. (1998) found recrystallized regions with either low U or high levels of many trace elements including U, Pb, and P. Vavra et al. (1999) observed mostly CL-bright, U-depleted regions among their U-Pb disturbed zircon domains. Complete recrystallization tends to blur or erase original compositional zoning, often leading to transgressive dark, homogeneous regions of zircon (Hoskin and Black, 2000; Hoskin and Schaltegger, 2003), so that zircons with obviously altered/metamorphic zoning (*e.g.*, patchy)

may represent only partially altered, rather than completely recrystallized, samples. Following this, CL-bright regions are also likely not transgressively recrystallized.

The chemistry of Group II is consistent with the general trends observed following transgressive solid-state recrystallization of zircon during high-grade metamorphism (*e.g.*, Hoskin and Black, 2000; Hoskin and Schaltegger, 2003): cation pumping removes incompatible trace elements from the structure but tends to enhance more compatible elements, leading to increases in the concentrations of, *e.g.*, Hf and U, in recrystallized areas. Less compatible elements in the zircon lattice tend to be expelled leading to recrystallized regions displaying lower Th/U ratios. The recrystallized zircons studied by Hoskin and Black (2000) displayed Th/U ratios lower than unaltered protolith zircons, but at the lower end of the magmatic range rather than the values <0.01 often observed in neo-formed metamorphic zircon. Complete recrystallization will also reinitialize U-Pb ages by removing radiogenic Pb from the zircon crystal structure (*e.g.*, Hoskin and Schaltegger, 2003). Group II's dark, homogeneous zircons are similar to what Hoskin and Black (2000) observed in recrystallized regions, although Group II zircons lack obvious alteration fronts and un-recrystallized areas for chemical comparison which would make their identification more certain. Some Group II zircons display patchy (if faintly so) regions that are probably not fully recrystallized via transgressive recrystallization or may have been subjected to other modes of alteration. It is significant that several of these patchy zircons are also among the most U-Pb discordant of the Group II grains.

Given the Group II zircons' U-Pb systematics, internal structures, and compositional traits, we consider transgressive recrystallization of originally igneous zircons to be the most likely scenario for Group II formation. The protoliths are unknown but could perhaps be a population similar to the Group I/Hadean Jack Hills zircons. The trace chemical characteristics

of Group II are consistent with its derivation from the Group I/Hadean population by transgressive crystallization, and the low degree of discordance despite the high U contents is explained by increased lattice stability and U-Pb clock resetting following cation pumping during recrystallization. The zircons with alteration structures were likely not completely recrystallized and radiogenic Pb was only partially lost. Under this interpretation, the unusually low Ti contents of Group II zircons do not reflect formation temperatures but instead cation-pumping during partial to total recrystallization. Higher-Ti domains sampled during MC analysis may represent zones that escaped thorough recrystallization; 3 out of the 6 Group II zircons with disagreeing MC and PS Ti measurements display patchy zonation indicative of regions that escaped thorough recrystallization. For a population of protolith zircons with uniform age and similar (Th/U), transgressive recrystallization, as described by Hoskin and Black (2000), would be expected to lead to correlations between (Th/U) and apparent age. However, as the original igneous provenance of Group II zircon is likely highly inhomogeneous both in age and trace element contents (similar to the Group I/Hadean Jack Hills zircon population) then the lack of correlation between $(Th/U)_t$ and age is not a compelling argument against the transgressive recrystallization hypothesis. Given the likely multi-source nature of the detrital zircons, it is unclear if the ~70 Ma period (from the range of Group II ages, 3.91-3.84 Ga) represents one long-duration thermal event, or a series of thermal events. The high degree of U-Pb concordance of Group II zircons indicates that it is unlikely that recrystallization occurred much more recently than the apparent grain ages, although given the nature of the recrystallization process and the possibility of only partial resetting (probably not significant, again, given the concordance of the zircons) the individual zircon ages may be slight overestimates for the period of resetting.

Hoskin and Black (2000) suggest that high concentrations of trace elements exert strain in the zircon crystal structure which is relieved by recrystallization. The higher U contents in Group II relative both to Group I and the prevailing 4.2-3.6 Ga population may suggest that these zircons were already high in trace element abundances. Higher U contents in particular also predispose a zircon to metamictization, which may facilitate recrystallization and other alteration. However, given that transgressive recrystallization also leads to increased U contents in recrystallized regions of the zircon, the original trace chemistry of these grains is unclear.

3.5.2 Are these observations consistent with an LHB signature?

If Group II zircons indeed recrystallized during a thermal event(s) at ca. 3.9 Ga in the Jack Hills zircon source(s) as discussed in section 5.1.2, then the Late Heavy Bombardment provides a plausible, though not necessary, mechanism for the heating event(s). Expected effects of an intense meteorite bombardment of the magnitude proposed for the LHB (*e.g.*, Abramov and Mojzsis, 2009) include low-grade metamorphism throughout much of the crust and high grade metamorphism – including temperature increases of ≥300°C through up to ~10% of the crust – creating locally pervasive impact-related melting (Abramov and Mojzsis, 2009). Of these effects, metamorphism is most likely to be widespread enough to leave a signal in the detrital record. The inferred metamorphic event(s) suggested by Group II at ca. 3.91-3.84 Ga are consistent with the LHB, although endogenic causes for metamorphism cannot with the present data be excluded.

Although the detrital nature of our samples precludes examination of zircon protoliths, it does allow for a wide sampling of conditions in the Jack Hills source terrane ca. 3.9 Ga. One expected effect of bolide impact that is notably absent in the Jack Hills zircon record is the development of shock structures. The apparent absence of these in today's Jack Hills zircons

may be due to preferential destruction of shocked grains during sedimentary transport. While Cavosie et al. (2010) documented the ability of shocked zircons to survive riverine transport from their basement source, the possibility of multi-cycle clastic sediments containing such zircons seems remote.

The existence of two distinct provenance groups among the ca. 3.9 Ga zircons, one distinct from the apparently dominant group from the Hadean, is interesting in light of an LHB origin model: Group I zircons represent a provenance contemporaneous with and not noticeably affected by the likely high-temperature conditions experienced by Group II and probably represent a continuation of the same petrogenetic processes ongoing in the Jack Hills source area prior to 3.91 Ga – probably intermediate to felsic magmatism near minimum melting conditions (*e.g.*, Trail et al., 2007b; Watson and Harrison, 2005). At first glance, the continuity of Group I/Hadean-style zircon petrogenesis during the period 3.91-3.84 Ga seems problematic for a scenario in which Group II formed by transgressive recrystallization during heating. However, Group II zircons could have been derived from the portions of the source region that experienced higher temperatures – perhaps deeper in the crust or laterally closer to sources of heat at ca. 3.9 Ga – and Group I from areas that experienced less thermal intensity.

Lastly, we note that if our results are truly a consequence of the LHB, the observation of a unique zircon population bounded between 3.91 and 3.84 Ga would support the original hypothesis by Tera et al. (1974) of a relatively brief event at ca. 3.9 Ga rather than the termination of a protracted cataclysm (*e.g.*, Hartman, 1975).

3.5.3 Comparison of Timing from Other Studies of the LHB

The concept of a Late Heavy Bombardment originated with the observation that U-Pb and Rb-Sr systems in Apollo and Luna samples were reset at ca. 3.95-3.85 Ga (Tera et al., 1974). $^{40}Ar/^{39}Ar$ dating of more randomly derived lunar meteorites has also been interpreted to indicate a Moon-wide cataclysm (Cohen et al., 2000) and the estimated ages of the largest lunar impact basins are restricted to ~3.82 to 4.0 Ga (Ryder, 2002). Meteorites from several large asteroid families (the mesosiderites, HED achondrites, and ordinary chondrites) also appear to have undergone impact degassing at ~3.9 Ga (Kring and Cohen, 2002).

In addition, several studies have identified a period at ca. 3.9 Ga when Jack Hills zircons grew epitaxial rims – likely due to a heating event. Trail et al. (2007a) found epitaxially grown rims on >4 Ga Jack Hills zircons, with rim $^{207}Pb/^{206}Pb$ ages ranging from 3.85-3.97 Ga, permissively bracketing the Group II age range. These rims are in general highly discordant and have Th/U significantly different than the zircon cores. Recurring ages in the Trail et al. (2007a) study fall into the range 3.93-3.97 Ga, slightly older than Group II (but some rim ages are within error of 3.91 Ga). In a follow-up study, Abbott et al. (2012) found ca. 3.95-3.85 Ga rims grown on Hadean Jack Hills zircon cores. Abbott et al. (2012) extracted additional information from these rims by depth-profiling the zircons using a technique that combined traditional U-Th-Pb analysis (Trail et al., 2007a) with analysis of Ti, allowing for continuous profiles of both age and T^{xlln}. Most rims in the period 3.95-3.85 Ga displayed average apparent T^{xlln} ~850°C, much higher than the Hadean average (ca. 680°C) but consistent with prevailing T^{xlln} displayed by zircons formed in melt sheets associated with large impacts (Wielicki et al., 2012). This high-T^{xlln} signature is seen only in the period 3.85-3.95 Ga (Abbott et al., 2012), and is notably different than the lower T^{xlln} seen among many Group II zircons in the same period. This suggests that these rims probably formed by new zircon growth at 3.95-3.85 Ga under high

temperature conditions, rather than by the solid-state, transgressive recrystallization of protolith zircon that we interpret in our Group II zircon cores. Cavosie et al. (2004) documented rims with ages of 3.7-3.4 Ga on >4 Ga Jack Hills zircons; they did not find clear evidence for rims at ca. 3.9 Ga. However, they did not depth profile the zircons but collected multiple U-Pb spot analyses on each of several >3.8 Ga grains. Rims on their zircons therefore had to be large to be noticeable; the <10 μm zones discovered by Trail et al. (2007a) would not be accessible to spot analysis. It appears that whatever event(s) occurred at ca. 3.9 Ga did not cause the noticeable growth of many rims larger than several μm in the pre-existing Jack Hills zircons. Although there is no exact match between the periods of epitaxial rim formation (Abbott et al., 2012; Trail et al., 2007a) and apparent recrystallization of our Group II zircons, they do largely coincide and may point toward the same thermal event or series of events ca. 3.9 Ga in the Jack Hills source region(s). If Group II zircons display transgressive recrystallization, that likely points toward a high-temperature event: Hoskin and Black (2000) made the observations of this alteration type in granitoids that had undergone granulite-facies metamorphism. While this information is in itself insufficient to distinguish between a meteoritic versus endogenic origins for this apparent period of heating in the Jack Hills source terrane(s), the occurrence of a high-temperature metamorphic event ca. 3.9 Ga is an expected effect of the LHB and Group II Jack Hills zircons may be some of the first terrestrial evidence for it. Investigation of the few other localities on Earth where >3.8 Ga rocks or zircons are found may shed further light on this important interval in Earth history.

3.6. Conclusions

The period between ca. 3.91-3.84 Ga appears unique in the >3.6 Ga Jack Hills zircon record in having at least two distinct provenance groupings based on trace elements. The

existence of a distinct high-U (and Hf), low-Ti (and Ce, P, Th/U) zircon provenance ("Group II") is specific to this era. Other zircons in this period (trace element "Group I") resemble the majority of Hadean zircons both in apparent T^{xlln} distribution and various other aspects of trace element chemistry. These patterns in trace element depletion and enrichment, the seemingly paradoxical coincidence of the highest U contents with high degrees of concordance, and the homogeneous nature or very faint zoning found in many Group II grains, lead us to interpret Group II as products of transgressive recrystallization at ca. 3.91-3.84 Ga (see Hoskin and Black, 2000; Hoskin and Schaltegger, 2003), likely resulting from a significant thermal event(s). Previously discovered ca. 3.9 Ga rims on older zircon cores (Abbott et al., 2012; Trail et al., 2007a) may also be related to this event. Group II makes up a large proportion of the ca. 3.9 Ga zircon record, and the existence of a prominent distinct group here (as compared to the rest of the 3.8-4.3 Ga Jack Hills record) suggests this event may have been unique in intensity during the Hadean and early Archean of the Jack Hills source terrane. The curious coincidence of an apparent thermal event with the time period suggested for the Late Heavy Bombardment (LHB) (i.e., ca. 3.9 Ga) suggests this portion of the Jack Hills detrital zircon record may be evidence of the LHB on Earth.

Chapter Three Figures

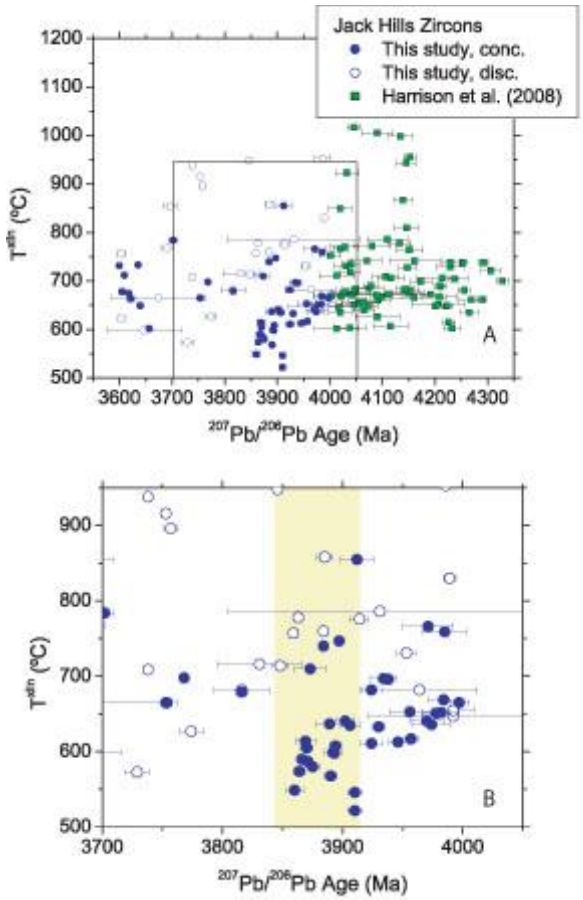

Fig. 3.1: T^{xlln}_{MC} vs. age for Jack Hills zircons. A) All ≥90% concordant samples from this study for the period 3.5 – 4.0 Ga, along with a Hadean dataset from Harrison et al. (2008). Rectangular area is the region of the plot shown in 1b. B) Focusing on this study's data for the time period 3.70 – 4.05 Ga, with Hadean data excluded. The period 3.84-3.91 Ga – with many low-Ti zircons – is shaded for emphasis. Samples from this study are divided into "higher confidence" analyses, which have ion probe pits on demonstrably pristine surfaces, and "lower confidence" analyses, where the pits are not able to be identified with a pristine versus cracked surface. There is no systematic difference between the two (see Appendix D). Spots found to be on cracks were excluded due to the danger of artificially high Ti measurements (Harrison and Schmitt, 2007).

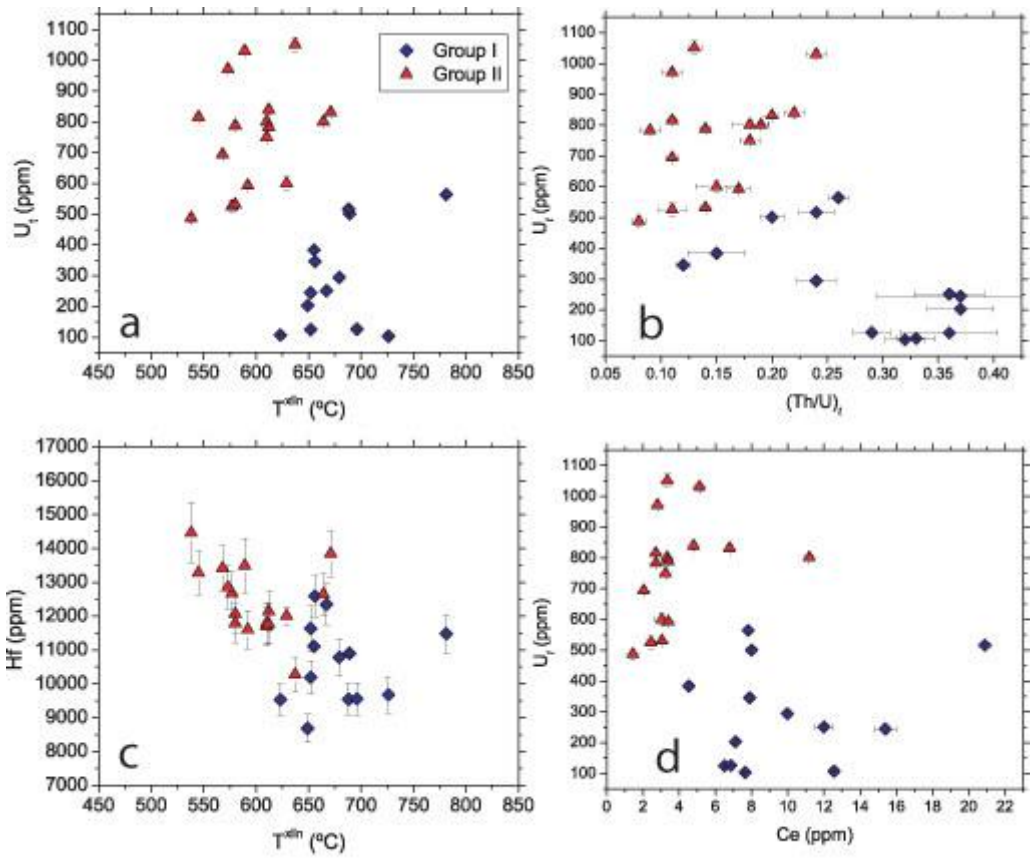

Fig. 3.2: 3.91-3.84 Ga zircons classified into two groups (I and II) as defined in section 4.2, plotted in various trace element quantities for which the groups are notably different. A) U_t (age-corrected uranium concentration; see section 4.2) vs. T^{xlln}_{PS}; B) U_t vs. $((Th/U))_t$ (time-corrected ^{232}Th over time-corrected U); C) Hf vs T^{xlln}_{PS}; D) U_t vs. Ce.

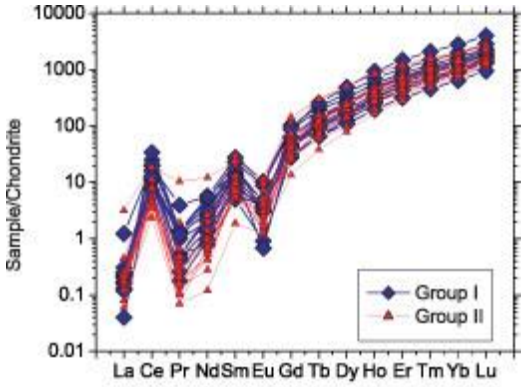

Fig. 3.3: Rare earth element analyses for Group I and Group II zircons. The analyses resemble typical terrestrial continental zircons with prominent Ce and Eu anomalies and high

HREE/LREE; elevated LREE in two analyses are unusual and may indicate the presence of microscopic phases not seen in our search for imperfections on the sample surface.

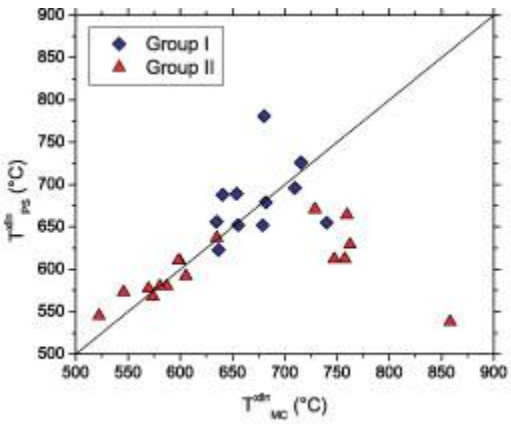

Fig. 3.4: A comparison of the temperature estimates using Ti data from both multicollection (MC) and peak switching (PS) during the full trace element analysis.

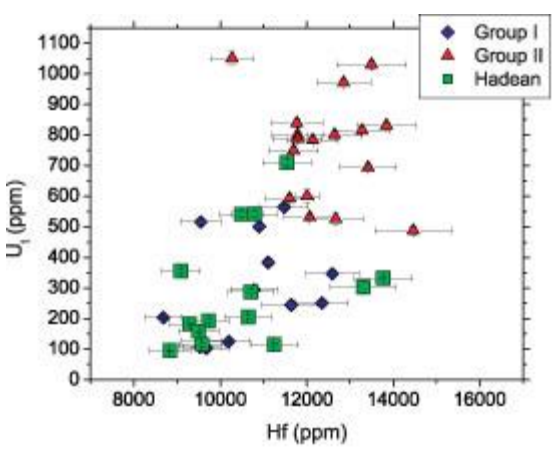

Fig. 3.5: Group I and II zircons in U_t vs. Hf space, with a set of Hadean zircons also analyzed in this study for comparison (all PS trace element data in Appendix E). Note the greater similarity with Group I than Group II of the 13 out of 14 studied Hadean zircons.

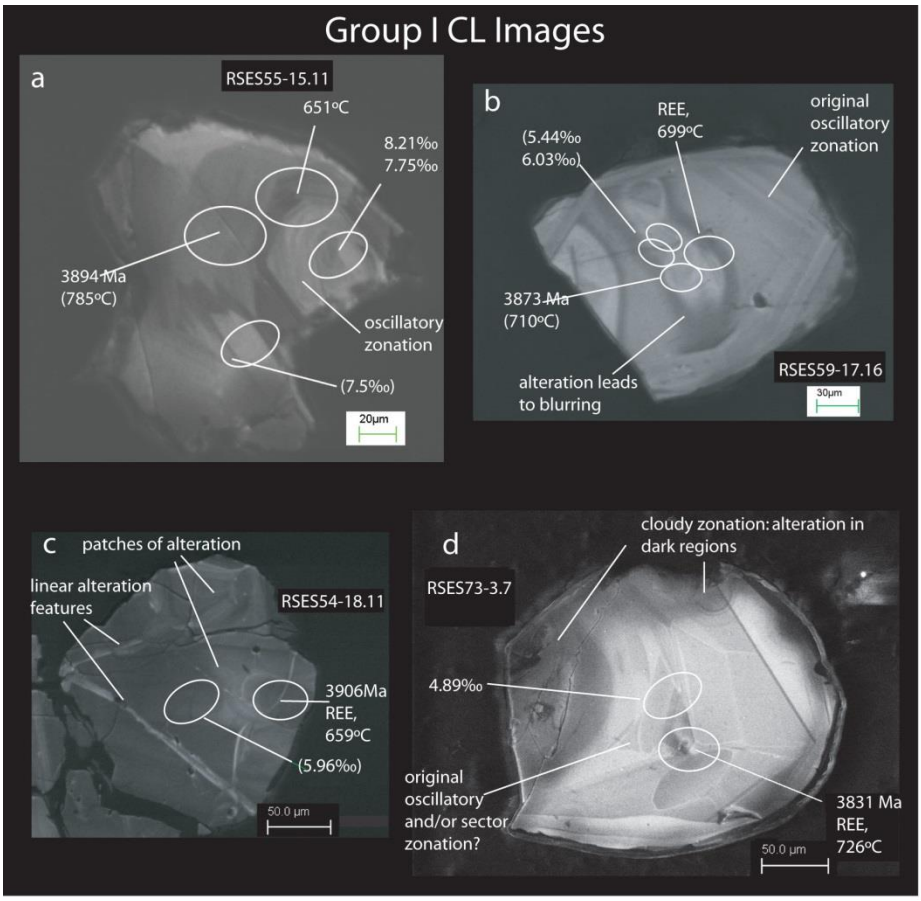

Fig. 3.6: Representative cathodoluminescence images of the 13 zircons in Group I. Each scale bar is 50 µm unless otherwise specified. The locations of U/Pb analysis spots are labeled with their associated $^{207}Pb/^{206}Pb$ ages. The locations of trace element analyses are labeled with "REE" and their associated Ti-in-zircon temperatures. Several spots in which Ti alone was measured are labeled with their associated temperatures (these are the "MC" spots discussed in section 4.1). The locations of oxygen isotope spots and their associated $\delta^{18}O$ values are also noted. Values in parentheses were later found to have been collected over a crack. Additional images for Group I zircons are shown in Appendix E.

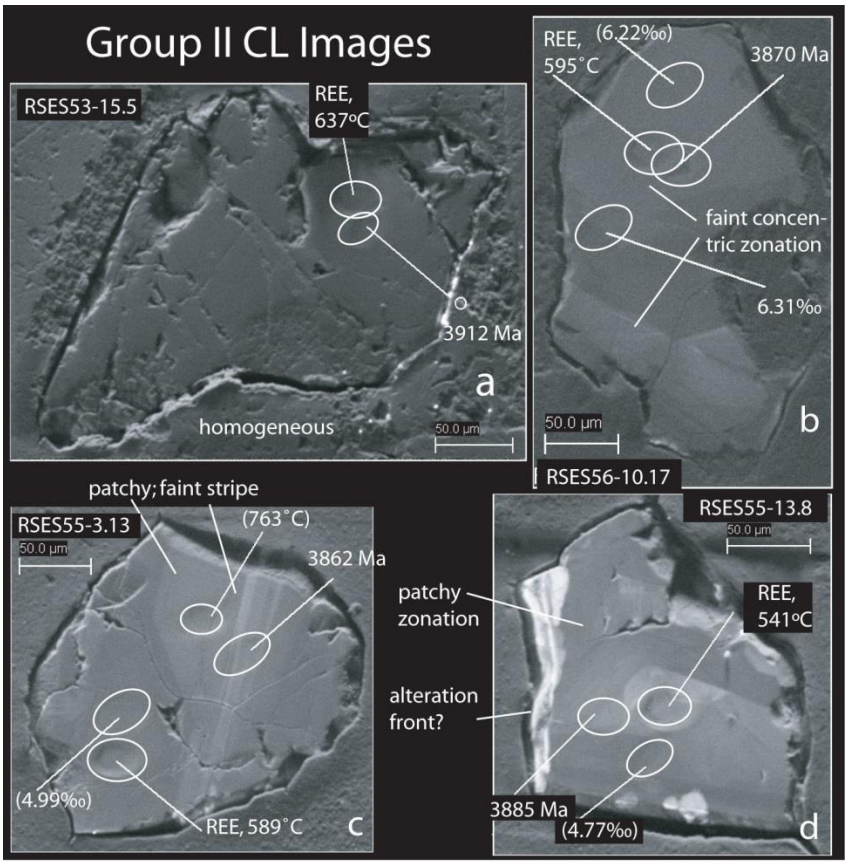

Fig. 3.7: Representative cathodoluminescence images of the 17 zircons in Group II. Values and analysis spot annotations for $^{207}Pb/^{206}Pb$ ages, T^{xlln}, and $\delta^{18}O$ are shown as in Fig. 3.6. Additional images for Group II zircons are shown in Appendix E.

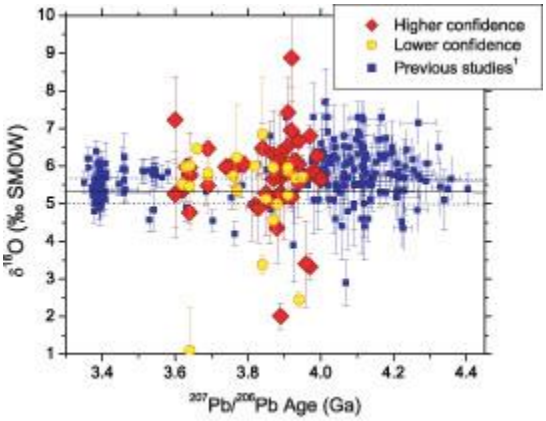

Fig. 3.8: $\delta^{18}O$ vs. age for U-Pb-concordant samples in this study, with earlier studies for comparison. After 3.8 Ga, zircons rarely fall above the mantle value (solid line; dashed lines are 1σ above and below). As in Fig. 3.1, samples from this study are divided into "well imaged" and

"poorly imaged" analyses. [1]The several previous studies include: Cavosie et al. (2005), Trail et al. (2007b), Harrison et al. (2008) (Hadean), and this study (ch. 2) (post-Hadean).

Chapter Four: Late Hadean-Eoarchean Transitions in Crustal Evolution

Abstract

The evolution of the Earth's earliest crust remains largely unknown due to the dearth of Hadean (>4 Ga) rocks, with most observational evidence of the planet's first few hundred million years deriving from geochemical studies of 4.4-4.0 Ga detrital zircons from Narryer Gneiss Complex (Yilgarn craton). Previous Lu-Hf investigations of these zircons suggested to us that continental-like (low Lu/Hf) crust formation began by ~4.4-4.5 Ga and continued for several hundred million years. The most isotopically primitive crust represented in the Jack Hills population was preserved until at least ~4 Ga. However, evidence for the involvement of Hadean materials in later crustal evolution is sparse, and even in the Jack Hills zircon population, the most unradiogenic, ancient isotopic signals have not been identified in the younger (<3.9 Ga) rock and zircon record. We present new Lu-Hf results from <4 Ga Jack Hills zircons that indicate a significant transition in Yilgarn crustal evolution between 4.0 and 3.6 Ga. The Jack Hills zircon protolith evolves largely by internal reworking through the period 4.0 to 3.8 Ga, and both the most ancient and unradiogenic components of the crust are missing from the record after ~4 Ga. New juvenile additions to the crust at ~3.8-3.7 Ga are accompanied by the disappearance of crust with model ages of >4.3 Ga. Additionally, a combination of prior oxygen isotope measurements along with new trace element measurements shows that this period is also characterized by a restriction in $\delta^{18}O$ (see ch. 3), the appearance and disappearance of a group with unique zircon chemistry (see ch. 3), and an overall shift in several zircon trace element characteristics ca. 4.0-3.6 Ga. The simultaneous loss of ancient crust accompanied by juvenile crust addition ca. 3.8-3.7 Ga is best explained by a mechanism similar to subduction, by which both processes are effected on the modern Earth. The other geochemical information also

supports a transition in zircon formation environment in this period, although it is less sensitive to processes like crustal recycling. We interpret these data as consistent with the action of destructive plate boundary interactions by Eoarchean times, and with initiation of plate boundaries by ~3.8-3.7 Ga.

4.1. Introduction: Empirical Constraints on Hadean-Archean Transitions

Conditions on the early Earth are difficult to constrain due to the fragmentary Eoarchean and essentially absent Hadean rock record (cf. O'Neil et al., 2008). Of particular interest is the nature of the early crust and the tectonic processes operating on it. Speculation on the viability of subduction and other plate-boundary processes in the early Earth has been rife (e.g., Davies, 1992, 2006; van Hunen and van den Berg, 2008; Sizova et al., 2010). Various lines of isotopic and mineral evidence from several cratons have been interpreted to show substantial changes in crustal evolution ~3 Ga, possibly connected with the onset of plate tectonics (Dhuime et al., 2012; Naeraa et al., 2012; Shirey et al., 2011; Debaille et al., 2013). However, the search for older evidence of tectonic regime is limited by the dearth of samples. This is compounded by the efficacy of plate tectonics at recycling older crust in subduction zones (e.g., Scholl and von Huene, 2007), if such features existed during this time.

Despite the absent Hadean rock record, various aspects of the >4 Ga Jack Hills zircons' geochemistry have been used to infer their formation in low-temperature, hydrous, granite-like melting conditions (e.g., Harrison et al., 2008; Mojzsis et al., 2001; Peck et al., 2001; Watson and Harrison, 2005; see also chapter 1). In particular, previous work on the Lu-Hf isotopic systematics of Jack Hills zircons (see Fig. 4.1) demonstrated a dominantly unradiogenic Hadean population (Amelin et al., 1999; Blichert-Toft and Albarede, 2008; Harrison et al., 2005, 2008;

Kemp et al., 2010) with isolation of low-Lu/Hf (enriched) reservoirs as early as 4.5 Ga and persistence of that material in the crust until at least ~4 Ga (Harrison et al., 2008). The large range in initial ε_{Hf} (initial $^{176}Hf/^{177}Hf$ normalized to the chondritic uniform reservoir, or CHUR) between the solar system initial $^{176}Hf/^{177}Hf$ and CHUR (also depleted mantle) may suggest additional later extraction, perhaps to ~4.0-3.9 Ga (Blichert-Toft and Albarede, 2008; Harrison et al., 2005; cf. Kemp et al., 2010).

However, the dominant Jack Hills age group at ~3.6-3.3 Ga is distinct from the Hadean population in several important geochemical systems, suggesting that an important transition(s) occurred between 4.0 and 3.6 Ga in the Yilgarn crust. <3.6 Ga zircons have considerably more radiogenic ε_{Hf} as a whole, suggesting a loss of ancient Hadean crust in the zircon source area at some point before 3.6 Ga (Amelin et al., 1999; this study, ch. 2). In addition, some post-Hadean juvenile input to the crust is required for the most radiogenic <3.6 Ga zircons (This study, ch. 2). The Jack Hills oxygen isotope record also changes during the Eoarchean: although concordant Hadean zircons range in $\delta^{18}O_{SMOW}$ ~3-8‰ (Peck et al., 2001; Mojzsis et al., 2001; Cavosie et al., 2005; Trail et al., 2007b), the <3.8 Ga population appears more mantle-like (this study, ch. 2; this study, ch. 3). Although Peck et al. (2001) found elevated $\delta^{18}O$ largely above the mantle value among younger zircons (with 32 analyses on 16 crystals), ch. 2 and ch. 3 of this study analyzed >200 <4 Ga samples in total and found that while 4.0-3.8 Ga zircons do not differ from the Hadean population in $\delta^{18}O$, zircons resolvably different from the mantle value become rare in the Jack Hills record after 3.8 Ga (see fig. 4.2). This probably points to a smaller diversity of aqueous alteration histories among the younger zircons.

Trace element-based indicators are also useful for monitoring the changing petrogenesis of the Jack Hills zircons; application of the Ti-in-zircon thermometer to the Hadean population

revealed average crystallization temperatures (T^{xlln}) ~680˚C – similar to wet granitic melting, and notably lower than the majority of zircons from mafic magmas (Watson and Harrison, 2005; Harrison and Watson, 2007; cf. Fu et al., 2008). In ch. 2 and ch. 3 of this study we report T^{xlln} among 4.0-3.3 Ga zircons similar to the Hadean distribution, with the curious exception of the period ~3.91-3.84 Ga, in which a large group of concordant zircons displays average apparent T^{xlln} ~600˚C, with values extending as low as 525˚C (this study, ch. 3). These are subsolidus temperatures in the vast majority of magmatic systems. Other geochemical peculiarities of zircons in this time period led us to interpret this distinct group as resulting from solid-state recrystallization (Hoskin and Black, 2000) likely due to a ca. 3.9 Ga thermal event in the zircon source terrane(s). The application of more comprehensive trace element analyses to other 4.0-3.6 Ga zircons, along with cathodoluminescence imaging and previous Ti-thermometry and oxygen isotope measurements (presented in ch. 3) in this time period, will allow for better determination of the nature of these samples (metamorphic, magmatic) and their relationship to crustal evolution.

The Jack Hills population is poorly sampled outside of these 2 prominent age groups (especially in a prominent age gap 3.8-3.6 Ga), so the true nature of this crustal evolution has remained uncertain. We present 118 new coupled Lu-Hf-Pb isotopic measurements (Woodhead et al., 2004) on mostly 4.0-3.6 Ga zircons which clarify the nature of the distribution in this period and demonstrate an important transition in crustal evolution that was not distinguishable from previous sampling. We also present 34 new trace element measurements on <4 Ga Jack Hills zircons and compare the record of change in the Lu-Hf system to the oxygen isotope, trace element, and Ti thermometry records to further constrain the nature of these transitions in the Eoarchean Yilgarn crust.

4.2. Methods

Samples were taken from the sample sets of ch. 2 and ch. 3. Zircons from the latter sample set were previously dated by ion microprobe using the U-Pb method by either this study (ch. 3) or Holden et al. (2009), and were analyzed for Ti and $\delta^{18}O$ (ch. 3). Using a similar analytical method as in ch. 2, we carried out coupled Hf-Pb LA-ICPMS measurements for a random sample of the Jack Hills distribution, giving coupled $^{207}Pb/^{206}Pb$ age (no concordance information) and Hf isotope composition for each zircon (dominantly 3.6-3.3 Ga). We also present additional ion probe trace element measurements for zircons from the sample sets of ch. 2 and 3.

4.2.1 Trace Element Measurements

We carried out analyses for Ti, P, REE, Hf, U, and Th using the CAMECA *ims*1270 ion microprobe at UCLA in three sessions during December of 2008, January of 2011, and May of 2012. Primary O^- beam intensities of ~15 nA and a spot diameter of 30µm were used. Secondary ions were detected at low MRP ($m/\Delta m \sim 2{,}000$) and high energy offset (-100 eV). NIST610 standard glass was used for calibration.

4.2.2 Lu-Hf-Pb Measurements

We used backscattered electron and cathodoluminescence images of zircons within 10% of U-Pb concordia (and 18 >10% discordant zircons) to target the placement of 69 µm laser ablation pits made using a Photon Machines 193nm ArF ATL laser coupled to a Thermo-Finnigan Neptune MC-ICPMS at UCLA. We also analyzed 25 zircons from local ~2.65 Ga meta-igneous units similarly. These measurements were accomplished over 7 days in April and May of 2013. We used the coupled Hf-Pb analysis developed by Woodhead et al. (2004) to

switch between measuring a Yb-Lu-Hf mass set (^{171}Yb, ^{173}Yb, ^{174}Yb/^{174}Hf, ^{175}Lu, ^{176}Yb/^{176}Lu/^{176}Hf, ^{177}Hf, ^{178}Hf, ^{179}Hf) for Lu-Hf systematics to a Pb mass set (204, 206, 207, 208) for estimating age, using the analysis sequence described by Ch. 2. Briefly, this involves measuring for 11 seconds on the Yb-Lu-Hf mass set and for 5 seconds on the Pb mass set; the first 2 seconds of each set were disregarded to allow for magnet settling.

All detrital zircon ages presented for this study are those measured during ICP-MS analysis, which with few exceptions agree with ion probe ages for the grain within error. Our meta-igneous zircons are forced to an age of 2.67 Ga to avoid the artificially older ages that result from common Pb contamination (considerable for some units). All data and correction procedures are presented in Appendix F. We have omitted from our figures all datapoints from this study with 2σ error bars >4ε, but these 12 analyses do not qualitatively change the εHf-age distribution and are tabulated along with the graphed data in Appendix F. We have time-corrected our Hf isotope ratios using the ^{176}Lu decay constant of Soderlund et al. (2004) and the CHUR parameters of Bouvier et al. (2008). All data from previous work are evaluated using the same parameters, sometimes requiring a recalculation of ε_{Hf} from the original study.

4.3. Results

Zircons in the period 4.0-3.6 Ga differ from the prevailing Hadean and <3.6 Ga Jack Hills zircon populations in several geochemical variables relevant to petrogenesis and crustal history. Although ~70% of zircons within the main 4.2-3.8 and 3.6-3.3 Ga populations have U-Pb systems less than 10% discordant, within the 3.8-3.6 Ga age minimum only ~50% of zircons are <10% discordant. As pointed out by Ch. 3, the period <3.8 Ga displays a much more truncated oxygen isotope distribution than the Hadean population. The period 3.9-3.6 Ga is distinct in

several important trace element variables. Also important is the restriction in the range of $\delta^{18}O$ that occurs ca. 3.8 Ga, such that younger zircons are only rarely distinct from the mantle value (see fig. 4.2).

4.3.1 Trace Elements

Fig. 4.3 shows various trace element concentrations and ratios versus $^{207}Pb/^{206}Pb$ crystallization age. Zircons from the period 4.0-3.6 Ga differ from both the Hadean and <3.6 Ga populations by their higher incidence of elevated Hf and U_t. $(Th/U)_t$ values are generally magmatic although they range <0.1 for several ca. 3.9 Ga zircons (Group II of This study, ch. 3; interpreted as recrystallized zircons). $(Th/U)_t$ values >0.6 are rare >3.6 Ga but characterize ~1/3 of measured zircons <3.6 Ga. All time periods look similar in P contents. Fig. 4.4 shows the HREE ratio Yb/Gd versus $(Th/U)_t$, a plot that traces progressive zircon crystallization with magmatic evolution (towards higher-Yb/Gd and lower-Th/U liquids; trends shown in, e.g., Claiborne et al., 2010). Although zircons from all periods populate the space between Yb/Gd ~10-30 and $(Th/U)_t$ ~0.2-0.4, zircons with $(Th/U)_t > 0.4$ are for the most part limited to the periods 3.8-3.7 Ga and <3.6 Ga. Zircons with $(Th/U)_t > 0.4$ display Yb/Gd < 18.

4.3.2 Lu-Hf-Pb

Fig. 4.5 shows our data in ε_{Hf} vs. age space, along with the previous Jack Hills zircon Hf measurements shown in Fig. 4.1 (Amelin et al., 1999; This study, ch. 2; Blichert-Toft and Albarede, 2008; Harrison et al., 2005, 2008; Kemp et al., 2010). Our 4.0-3.8 Ga samples define a distribution similar to that of the majority of Hadean zircons in both range and trajectory in ε_{Hf} vs. age space. Neither the most radiogenic (within error of a projected depleted mantle evolution line) nor the most unradiogenic (within error of the solar system initial $^{176}Hf/^{177}Hf$ ratio) portions

of the Hadean population are abundantly sampled by Jack Hills zircons after ~4 Ga. Although this may reflect in part the limits of our sampling at younger ages (137 4.0-3.8 Ga zircons, vs. 307 >4.0 Ga zircons in this and other studies), it seems that these portions of the Hadean crust are at least much less prominent in the later record. After 3.7 Ga, the zircon population at Jack Hills becomes strikingly more radiogenic, losing the most unradiogenic portion of the >3.8 Ga record as well as requiring post-Hadean juvenile input.

4.4 Discussion

The coincidence between the discontinuities in the Jack Hills Hf isotopic record and the truncation of oxygen isotope compositions, coupled with various trace element indicators for changing geologic conditions during zircon formation, all point to the Eoarchean and especially the interval 3.9-3.7 Ga as an important period in the evolution of early Yilgarn crust.

4.4.1 Model Ages and Crustal Reservoirs

In all, the Jack Hills ε_{Hf} distribution is best explained by the mixing of several low-Lu/Hf (i.e., felsic) reservoirs (see Fig. 4.6a), some of which appear to be lost from the zircon record in discrete steps between 4.0 and 3.7 Ga. The unradiogenic ε_{Hf} of the majority of Jack Hills zircons, along with their low Ti-in-zircon crystallization temperatures (e.g., Watson and Harrison, 2005), elevated $\delta^{18}O$ in some grains (e.g., Mojzsis et al., 2001; Peck et al., 2001) and granitoid inclusion assemblages (Hopkins et al., 2008, 2010; Mojzsis et al., 2001), are all consistent with felsic sources for the Jack Hills zircons. The average $^{176}Lu/^{177}Hf$ of Archean granites (~0.01; Condie, 1993) is similar to the median $^{176}Lu/^{177}Hf$ of felsic volcanic rocks (~.014) compiled in the GeoROC database (http://georoc.mpch-mainz.gwdg.de/georoc/), and the evolution of such reservoirs in ε_{Hf} vs. age space is broadly consistent with most of the Jack Hills

zircon record (Fig. 4.6a). Because melting of the mantle yields broadly mafic material (modeled in Fig. 4.6a with $^{176}Lu/^{177}Hf$ ~ 0.021 based on average early Archean basalt; Condie, 1993), modeling the evolution of the early Jack Hills crust with only felsic reservoirs will not capture the entirety of its history. Although ultimately the felsic reservoirs we invoke will have resulted from a more complicated earlier history involving mantle melting at some stage(s), this does not qualitatively change our interpretation. We therefore calculate depleted mantle model ages (T_{DM}) for all zircons using this simplified felsic model (probability density contoured in Fig. 4.6b), with $^{176}Lu/^{177}Hf$ of 0.01.

We identify several likely reservoirs on Fig. 4.6a. The most unradiogenic compositions identified by previous studies are within error of the solar system initial $^{176}Hf/^{177}Hf$, with concordant U-Pb ages between 4.35 and 4.0 Ga (Harrison et al., 2005, 2008). They require the isolation of a reservoir of essentially zero Lu/Hf by ~4.5 Ga (Harrison et al., 2008), which we refer to as Reservoir A. Materials with T_{DM} between 4.5 and 4.2 Ga evolve by internal recycling and mixing between their formation and 3.7 Ga. Given the broad distribution of T_{DM} between 4.2 and 4.5 Ga, it is uncertain if this material, which makes up the majority of the Hadean distribution, represents continuous extraction from the mantle or mixing between different crustal reservoirs (4.5 and 4.2 Ga felsic reservoirs; older felsic and mafic reservoirs; or some combination of these). Because 4.3 Ga T_{DM} are evident continuously between 4.3 and 3.4 Ga, we infer either a long-lived 4.3 Ga felsic reservoir or remelting of a long-lived older basaltic reservoir after 3.7 Ga (Reservoir C). The most radiogenic <4.3 Ga Hadean zircons probably represent mixing between Reservoir C and more juvenile material. Finally, the more radiogenic <3.7 Ga crust, characterized by T_{DM} of 4.3-3.7 Ga, probably represents mixing between Reservoir C and a new reservoir extracted at some point $\geq$3.7 Ga (Reservoir D). Detrital zircons

from Mt. Narryer, another Narryer Gneiss Complex (NGC) location, reveal the presence of juvenile crust ~3.8-3.7 Ga (see Fig. 4.5; MN data: Nebel-Jacobsen et al., 2010). Given the coincidence between the juvenile nature of these zircons and the youngest model ages among younger Jack Hills zircons, it is likely that they sample crust derived from the same event. Most of these reservoirs are consistent with sources identified in previous studies of Jack Hills zircons, with the exception of the highly unradiogenic Reservoir A, which is evident in Harrison et al. (2005, 2008) but not seen in Kemp et al. (2010). This is almost certainly due to the small number of zircons (n=51) analyzed by Kemp et al. (2010) relative to that of Harrison et al. (2005, 2008; n=230) and the very small fraction of the Hadean zircon population represented by Reservoir A (ca. 2%).

4.4.2 Magma Types and Alteration History of the Jack Hills Source

4.4.2.1 Trace Element and Oxygen Isotope Data

Trace elements show a great deal of similarity among zircons throughout the Jack Hills detrital record, but the period 3.9-3.6 Ga does stand out in several respects. High concentrations of U (>600 ppm) and Hf (>12,500 ppm) are more common during this period, particularly ~3.91-3.84 Ga, ~3.75 Ga, and ~3.63 Ga (see Fig. 4.3). Ch. 3 attribute high U_t and Hf contents in ~3.91-3.84 Ga zircons to solid-state transgressive recrystallization (Hoskin and Black, 2000) of originally igneous zircon, shown also by these zircons' lower $(Th/U)_t$ and lower levels of LREE and P. However, the lack of a similar low-P and –LREE signature among high-U and -Hf zircons 3.8-3.6 Ga (and higher Th/U among 3.8-3.7 Ga zircons) suggests less of a role for recrystallization among the younger group and may point instead to magmatic effects – for instance, zircon U and Hf concentrations and the Yb/Gd ratio generally rise (and the Th/U falls) as magmas evolve through fractional crystallization (e.g., Claiborne et al., 2010), with variable

behavior in P based on the co-crystallization of other accessory phases. A comparison of zircons from various time periods on a plot of Yb/Gd vs. $(Th/U)_t$ (Fig. 4.4), which roughly shows crystallization during progressive magmatic evolution toward low Th/U and high Yb/Gd, reveals that lesser-evolved signals – higher Th/U and lower Yb/Gd – are seen at both 3.8-3.7 Ga (dominant signal) and 3.6-3.3 Ga (~1/3 of signal with present dataset).

The trace element data seem to indicate a provenance of less-evolved magmas for most ~3.8-3.7 Ga zircons and for many 3.6-3.3 Ga zircons. The similar, low average T^{xlln} of ~700°C throughout much of the record suggests mainly granitoid sources. Trace elements suggest that these time periods were characterized by a higher incidence of hydrous remelting of basaltic materials (as opposed to remelting of felsic crust), with the possible exception of a few high-U, Hf grains at ~3.75 Ga. This is supported by the beginning of more radiogenic crust in the Hf record at ca. 3.8 Ga. The more evolved magmatic signal at ~3.63 Ga accompanied by a few zircons with high $\delta^{18}O$ probably points to more felsic sources involved in magma production, including supracrustal materials.

4.4.2.2 Integrating Hf and Trace Element Data

As shown in Fig. 4.7a, the two trace element groups among ca. 3.9-3.8 Ga zircons have distinct Hf isotopic signatures. Group I, which is indistinguishable from Hadean zircons except in age, constitutes the most unradiogenic crust represented in this time period, with ε_{Hf} of -7 to -11 (part of Reservoir B). Group II, whose distinct chemistry probably points to solid-state recrystallization (ch. 4), represents the most radiogenic crust at this time (Reservoir C), with most zircons displaying ε_{Hf} of -2 to -6. Two Group II zircons (RSES53-3.4, RSES58-13.14) are more similar to Group I. Because Hoskin and Schaltegger (2003) report that zircons altered by

solid-state recrystallization do not appear to display changes in Hf isotopic composition, we consider only the artificially young ages to have a likely effect on ε_{Hf} among Group II zircons – and artificially young ages should yield artificially *low* ε_{Hf} rather than the more radiogenic signature seen here. We therefore interpret this more radiogenic nature as a primary feature of Group II.

The two groups' distinct Hf compositions demonstrate derivation from different crustal reservoirs, calling into question the interpretation that Group II was derived from Hadean/Group I-type zircons through recrystallization. Their distinct Hf composition makes it possible that they sample an anomalous reservoir, perhaps with chemical properties leading to unusually cool or TiO_2 – undersaturated melts, leading to the uniquely low-Ti nature of Group II. However, an analysis of the Hadean zircon data in Harrison et al. (2008), which also includes Ti and Th/U measurements on the zircons, indicates that the more radiogenic portion of the Hadean record does not display lower Ti than the prevailing Hadean population (Fig. 4.7b). Similarly, the lower Th/U and higher U among Group II is not matched by lower average Th/U or higher U among the more radiogenic Hadean zircons that are more likely to derive from similar reservoir(s) of crustal material (Fig. 4.7c,d). Group II's unique properties don't appear to be expressed in the geologic record until ca. 3.9 Ga, and thus likely reflect an event (either a thermal event causing recrystallization or the new production of low-Ti or unusually low-temperature melts from Reservoir C) rather than chemical inheritance. The presence of a smattering of low-Ti zircons (with similar low Th/U and high Hf and U as Group II) among the more unradiogenic zircons ca. 3.63 Ga (Fig. 4.b-d) could be reasonably attributed to a similar process to that forming Group II (or perhaps to inheritance of some of Reservoir C's Group II-like characteristics if these reflect some change to the whole rock rather than the zircon recrystallization suggested in ch. 4). The

ca. 3.63 Ga zircons' high P contents relative to Group II zircons (elements lost during solid-state recrystallization; Hoskin and Black, 2000) may cast doubt on solid-state recrystallization during this time period, or may point to the protolith zircons having unusually high P contents.

If these chemical differences do indeed point to the origins of Group II chemistry by recrystallization, then one likely interpretation is that the differing histories of Groups I and II reflect contrasting spatial positions of these two reservoirs to a source of heating. If Reservoirs B and C were emplaced in different regions of the Hadean crust, this could explain why only certain zircons preserved from this time experienced apparent recrystallization from a heating event. Since Reservoir B is apparently lost from the Jack Hills record within 200 million years of this apparent event, while the Hf record is consistent with preservation of Reservoir C, one possibility is the residence of Reservoir C deeper in the crust than Reservoir B. In this way Reservoir C would have been at a higher temperature than B such that, other factors being equal, Reservoir C zircons could be preferentially subject to even greater temperatures in a thermal pulse. Subsequent uplift and erosion would also have then destroyed Reservoir B preferentially to Reservoir C. One future avenue for evaluating this hypothesis may be geobarometry on mineral inclusions (similar to the work of Hopkins et al., 2008, 2010, if suitable inclusion phases are found) coupled with Hf isotopic analyses of the host zircons during this time period.

4.4.3 Eoarchean Yilgarn Crustal Evolution

The sharp discontinuity in the zircon Hf record at ~3.8-3.7 Ga is characterized by both the loss of Hadean felsic crust and the addition of juvenile crust. Based on the Mt. Narryer detrital zircons, this probably involved melting of the depleted mantle (Nebel-Jacobsen et al., 2010). The Manfred Complex in the extant NGC, which comprises the remnants of a ~3.7 Ga

layered mafic intrusion (Fletcher et al., 1988), is another indication of juvenile input to the Yilgarn crust at this time. Based on processes operating on the modern Earth, the most obvious mechanism to accomplish this discontinuity is subduction, which today both recycles significant amounts of continental material (Scholl and von Huene, 2007) and causes the production of juvenile mantle melts. At ~4.0 Ga, the last appearance of both material as unradiogenic as the solar system initial $^{176}Hf/^{177}Hf$ (Harrison et al., 2008) and of material within error of depleted mantle (Blichert-Toft and Albarede, 2008; Harrison et al., 2005) may signal a similar process, although the small number of samples representing this most ancient unradiogenic reservoir renders interpretations about the timing of loss more uncertain.

Although our specific model ages are dependent upon a particular assumed $^{176}Lu/^{177}Hf$, this sawtooth-like pattern of crustal loss (and gain) at ~3.8-3.7 Ga is not dependent upon the felsic model: unradiogenic materials present until 3.7 Ga and absent thereafter cannot be reconciled with continuous crustal growth and mixing, but require crustal loss. Many of the more radiogenic Jack Hills zircons <3.8 Ga would be consistent with a long-lived Hadean mafic reservoir, but the presence of similarly-aged, clearly juvenile material among zircons at nearby Mt. Narryer makes it clear that juvenile addition was occurring in the NGC at this time. Although other mechanisms for producing this pattern of crustal evolution as reflected in the Hf isotopic distribution are difficult to find on Earth today, the record is possible to reconcile with a diapirism-based tectonic regime proposed by some workers for the Archean Earth (e.g., Hamilton, 1998) if the downwelling of ancient crustal material resulted in its foundering into the mantle and juvenile melts formed with similar timing. A large enough meteorite impact, obliterating part of the crust and inducing mantle melting, is another alternative.

In light of this sawtooth pattern in the Hf isotopes beginning at ~3.8 Ga, it is worth considering the coincidence between the sawtooth and the event(s) represented by Group II. Chapter four recognizes the similarity in timing between concordant Group II ages and the hypothesized spike in bolide flux called the Late Heavy Bombardment (LHB). The production of Group II zircon chemistry in this restricted time period suggests that this period was unique in either its thermal conditions (at least those affecting Reservoir C) or in the production of uniquely low-Ti or low-temperature melts in Reservoir C not seen before in the record. If these do indeed reflect recrystallization during a heating event(s), then the $^{207}Pb/^{206}Pb$ ages of the Group II zircons represent intermediate ages between crystallization and resetting unless complete Pb loss occured. The ~100 Myr age spread may reflect multiple resetting events during or after the period 3.91-3.84 Ga or varying degrees of Pb loss during an event at or after 3.84 Ga.

Given the introduction of more juvenile material ~3.8 Ga, the causes of the sawtooth pattern and the probable resetting of Group II zircons may be linked. The heating event may be exogenic or endogenic. Subduction initiation is a poorly understood process, but both induced and spontaneous nucleation of subduction zones are likely to have significant thermal effects in the upper plate. Stern (2004) suggests that induced subduction initiation will involve significant compression in the upper plate before subduction begins, while spontaneously nucleated subduction zones will display pre-subduction rifting in the upper plate. Both scenarios should lead to significant heating of portions of the upper plate. However, thermal effects would also accrue in the case of an impact or diapirism. One question regarding the plausibility of these latter two hypotheses is the amount of mafic crust that could have been generated in this manner and whether it is sufficient to account for the ancient crust required elsewhere in the Yilgarn. It is also true that if the Hf record at ca. 4 Ga also shows a similar introduction of juvenile crust and

loss of ancient crust, the 3.8-3.7 Ga period doesn't represent a unique event in the record – and the earlier event is unaccompanied by Group II-like signatures (low Ti, Th/U, P; high U, Hf) despite the well-studied Hadean T^{xlln} (e.g. Harrison et al., 2008; Trail et al., 2007b; Watson and Harrison, 2005) and somewhat less well-studied Hadean trace element record (e.g. Crowley et al., 2005; Peck et al., 2001).

4.4.3.1 Post-Eoarchean Yilgarn Evolution

We consider the most likely mechanism to create this discontinuity to be a subduction-like process operating at 3.8-3.7 Ga. Subduction simultaneously recycles crust while introducing juvenile melts into the crust, and in the Phanerozoic, subduction-related orogens are often expressed in the zircon Lu/Hf record as an excursion toward more positive ε_{Hf} and the loss of highly negative ε_{Hf} (Collins et al., 2011). At ~4.0 Ga, the last appearance of zircons from sources both as unradiogenic as the solar system initial $^{176}Hf/^{177}Hf$ (Harrison et al., 2008) and within measured uncertainty of depleted mantle (Blichert-Toft and Albarede, 2008; Harrison et al., 2005) may signal a similar process, although the concomitant shift toward more positive ε_{Hf} is not in evidence. A broad survey of detrital zircon Hf isotope compositions in modern Yilgarn craton drainages (Griffin et al., 2004) identifies several zircon populations consistent with the internal reworking of 3.8 Ga felsic crust until ~2.6 Ga, and a few zircons at ~2.6 Ga may point to older felsic crust (see Fig. 4.8), although they derive from other regions of the Yilgarn craton and their identification with Jack Hills crust is uncertain at best. The composition of the Jack Hills zircon source is uncertain after 3.3 Ga due to the relatively few grains sampled, but zircons from the ca. 2.65 Ga granitoids in the Narryer Gneiss Complex (NGC; from SIMS U-Pb ages; see Appendix F) range between -5 and -20ε, overlapping with the wider Yilgarn distribution but demonstrating the persistence of some more ancient or more felsic crust within the NGC (Fig.

4.8). The episodic loss of ancient crust in this terrane probably reflects separate episodes of recycling and appears to show an increase in crustal residence times with decreasing age: crust within error of the solar system initial Hf composition resides in the crust for at least 0.5 Ga; >4.3 Ga crust is lost at 3.7 Ga (0.5-0.8 Ga); 4.3 Ga crust is expressed until at least 3.3 and perhaps 2.6 Ga (1-1.7 Ga). This trend may reflect increasing crustal stability in a cooling Earth.

4.4.4 Subduction in the Early Earth

The existence of subduction-like processes during the Eoarchean – and even its viability in the Neoproterozoic – is contentious (see Stern, 2007). The higher heat content of the early Earth, due to higher radioactivity and accretional energy, would undoubtedly have influenced mantle convection and its expression on the lithosphere. Models variously support (e.g., Davies, 2006; Sizova et al., 2010; van Hunen and van den Berg, 2008; Korenaga, 2013) or deny (e.g., Davies, 1992) the role of early subduction on a warmer Earth. Some models suggest instead the existence of quasi-subduction regimes involving shallow underthrusting of oceanic crust (Sizova et al., 2010) or only short episodes of intermittent subduction (e.g., O'Neill et al., 2007; van Hunen and van den Berg, 2008) during the Archean. Empirical evidence has been limited due to the sparse Archean and absent Hadean rock records, although thermobarometry on mineral inclusions in the Jack Hills zircons has been interpreted as evidence for an underthrusting, subduction-like regime at 4.2-4.0 Ga (Hopkins et al., 2008, 2010).

Our Hf isotope data support an episode of crustal recycling and juvenile addition in a piece of the ancestral Yilgarn craton at ~3.8-3.7 Ga, along with a possible episode(s?) at ≥ 4.0 Ga (see Hopkins et al., 2008, 2010). The episodic loss of Hadean crust in two apparent steps 4.0-3.7 Ga, the apparent absence of >4.3 Ga crust (our felsic-model ages) in the Archean crust exposed today in the Yilgarn craton (based on data of Griffin et al., 2004), and the relatively

short-lived period of juvenile input ca. 3.8-3.7 Ga are suggestive of episodic rather than continuous crustal replacement in the Yilgarn during the Archean. However, since the Jack Hills zircons represent an unknown portion of the Archean crust, our data cannot distinguish between episodic, short-lived destructive plate boundaries in one region – similar to many convergent boundaries today – and the continuous operation of such a mechanism during the Archean but in different regions around the planet. Finally, the likely heating event(s) shown by some ca. 3.9-3.8 Ga zircons may also be linked to this transition. Although the zircons' similar ages to the LHB may be suggestive of an exogenic origin, the existence of an apparent endogenic mechanism in the same time period may represent a simpler explanation.

4.5. Conclusions

The Lu-Hf systematics of Jack Hills zircons indicate an important transition in crustal evolution during the Eoarchean. >4 Ga crust evolved by internal recycling and mixing among various reservoirs until 3.8 Ga, when the appearance of more radiogenic materials (mirrored at the Mt. Narryer site, Nebel-Jacobsen et al., 2010) indicates new juvenile addition to the crust. Much of the Hadean crust was lost from the zircon record after 3.7 Ga, and <3.7 Ga zircon ε_{Hf} compositions are consistent with mixing between the remaining more radiogenic Hadean crust and the new juvenile addition. The coincident loss of ancient crust and input of juvenile crust is best explained by an episode of subduction ca. 3.8-3.7 Ga, suggesting the operation of some form of plate tectonics at least by the Eoarchean. The loss of ancient crust and occurrence of juvenile crust at ca. 4 Ga may point to a similar episode, but the small number of samples with which this ancient reservoir is represented limits confidence in the timing of its disappearance. Comparison of ancient Narryer Gneiss Complex zircons from detrital and meta-igneous units

with detrital zircons in the modern Yilgarn craton reveals that Hadean crust was lost from the craton in stepwise fashion, much of it within 0.5-0.8 Ga of Earth's formation.

Chapter Four Tables and Figures

Reservoir	T_{DM}	$^{176}Lu/^{177}Hf$	Behavior	Persists To	Residence Time
A	≥4.5 Ga	Very low	mixes with B?	~4 Ga	~0.5 Ga
B (perhaps multiple)	≥4.5-4.2 Ga	<0.021; mixes with A and C?	Mixing with C? Multiple extractions mixed?	3.7 Ga	0.5-0.8 Ga
C	4.3 Ga	4.2 Ga felsic or felsic remelt of older mafic	<3.7 Ga: mixes with B? >3.7 Ga: mixes with D	≤3.3 Ga	≥0.9 Ga
D	3.8-3.7 Ga	Mafic? felsic?	Mixes with C	?	?

Table 4.1: A description of our posited crustal reservoirs in the Jack Hills detrital zircon record.

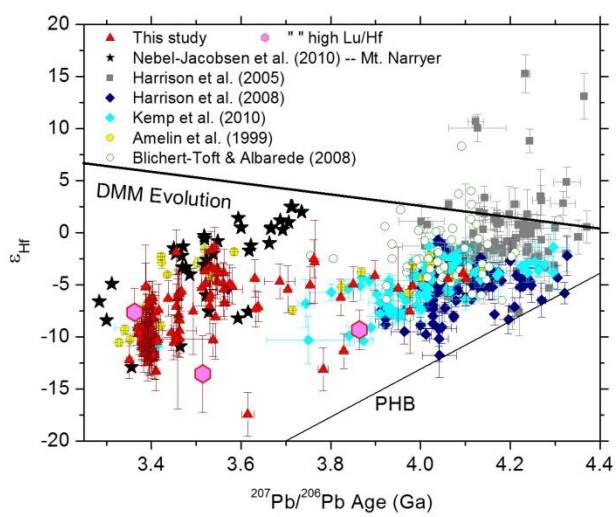

Fig. 4.1: Jack Hills and Mt. Narryer zircons from several studies in ε_{Hf} vs. age space. Reproduction of Fig. 4.6.9a. Note the majority negative values for ε_{Hf}. "Lu/Hf=0" denotes the ε_{Hf} of the solar system initial $^{176}Hf/^{177}Hf$ ratio (i.e., evolved forward in time with no radiogenic ingrowth). "DM Evolution" denotes the evolution of a theoretical depleted mantle-like reservoir formed at 4.55 Ga. Most zircons fall between the solar system initial ratio and the DM. Several Hadean zircons plot well above the DM, while several plot within error of the solar system initial ratio. These extreme compositions are not seen in the rest of the known Archean record.

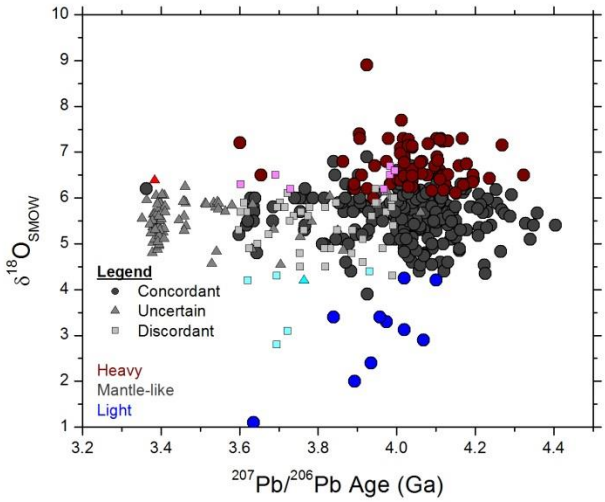

Fig. 4.2: All oxygen isotope analyses from Fig. 4.8 plus discordant zircons from the same study, with error bars removed and color-coded for oxygen isotope composition. 150 additional Hadean zircon analyses are shown (collected in Appendix G). Gray = mantle-like compositions, defined as within error (1σ) of the range 4.7 – 4.9 ‰. Red = high $\delta^{18}O$, not within error of the mantle range. Blue = low $\delta^{18}O$, not within error of the mantle range. Circles denote analyses within 10% of U-Pb concordia, squares samples >10% discordant, and triangles samples of unknown concordance (mostly from the study of This study, ch. 2). Of six <3.8 Ga samples with heavy oxygen compositions, only two are known to be concordant and fall ~3.63 Ga. A small low- $\delta^{18}O$ tail 4.1-3.8 Ga resembles the low- $\delta^{18}O$ tail among some discordant 3.8-3.6 Ga samples, but the disturbance to their U-Pb systems makes their ultimate crystallization ages uncertain. This figure omits the 32 analyses on 16 <3.6 Ga grains carried out by Peck et al. (2001), which were on average higher than the mantle range because the larger dataset shown here for that time period seems to contradict those authors' findings.

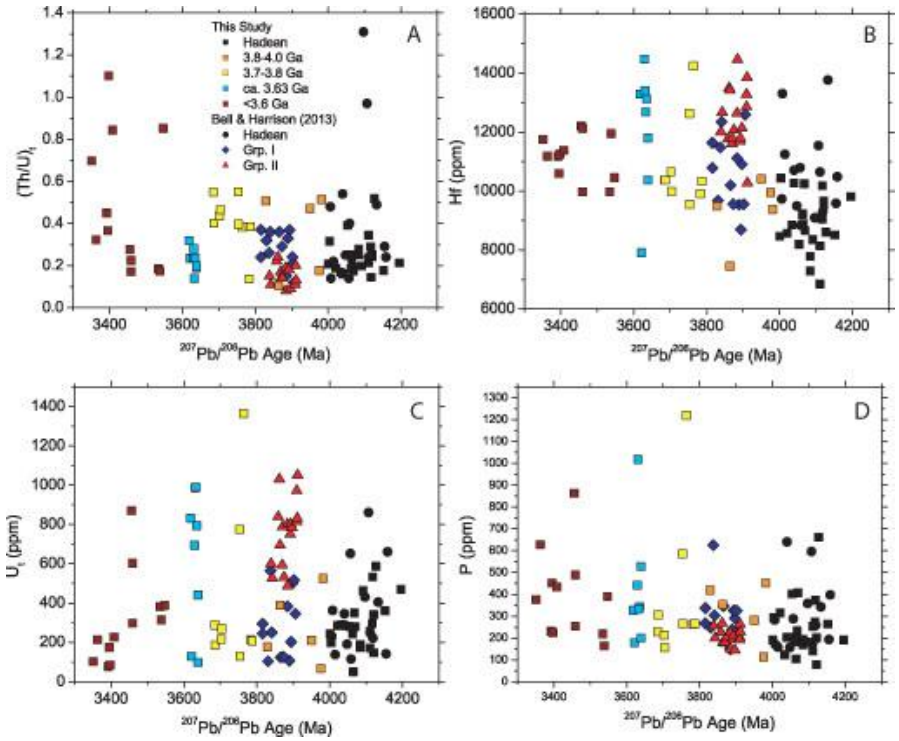

Fig. 4.3: various trace element concentrations and ratios for the Jack Hills zircons vs. crystallization age. Data collected in Appendix G. A) U_t vs. age plot shows that zircons in the period 4.0-3.6 Ga are enriched in U relative to other periods in the Jack Hills record. B) Hf vs. age plot shows Hf-enriched zircons are also more abundant 4.0-3.6 Ga. In addition, many Hadean zircons from ch. 2 (this study) are poorer in Hf than is seen elsewhere in the record. C) $(Th/U)_t$ vs. age plot shows that $(Th/U)_t$ values > 0.06 are most common <3.6 Ga (a few also in the Hadean). 3.8-3.7 Ga zircons have higher $(Th/U)_t$ ~0.5 relative to the largely <0.4 values seen in adjacent time periods. D) P vs. age plot shows little change in P contents with time.

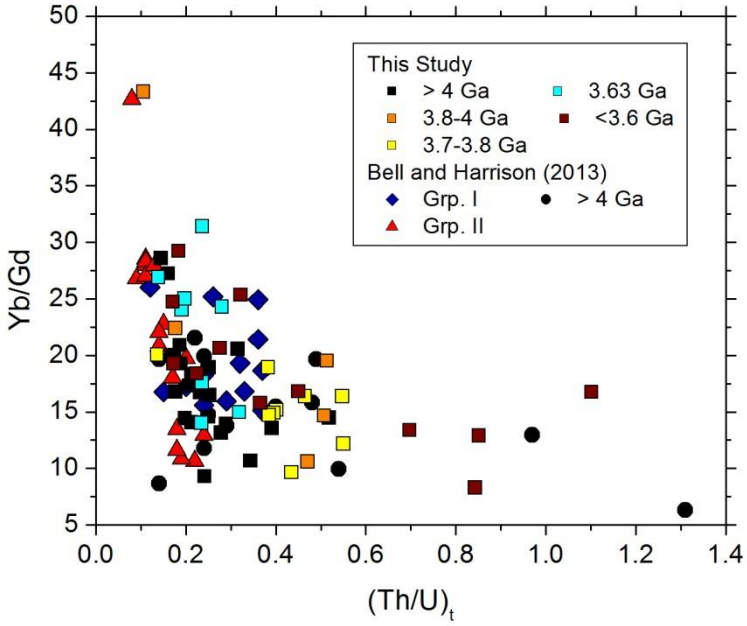

Fig. 4.4: Yb/Gd vs. $(Th/U)_t$ for Jack Hills zircons sorted by age. Less-evolved magmatic liquids appear to dominate the record ~3.75-3.63 Ga and appear to make up a significant proportion of <3.6 Ga zircons.

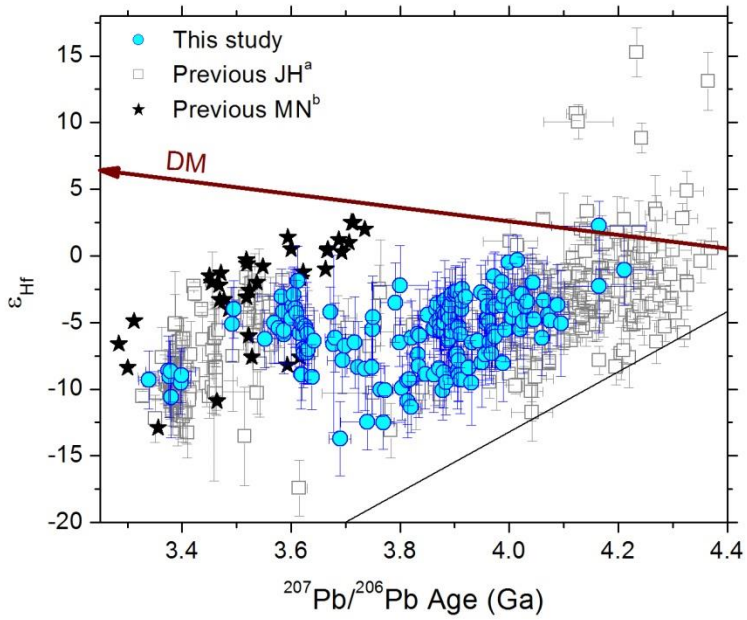

Fig. 4.5: Our data plotted in ε_{Hf} vs. crystallization age space along with a database of detrital zircons measured in previous studies of Archean metasediments in the Jack Hills and nearby Mt.

Narryer localities. DM evolution curve calculated by linearly projecting the current DM ε_{Hf} of +18 to zero at 4.56 Ga.
[a]Data for previous Jack Hills detrital zircons from Amelin et al. (1999), Ch. 2, Blichert-Toft and Albarede (2008), Harrison et al. (2005, 2008), and Kemp et al. (2010).
[b]Data for Mt. Narryer detrital zircons from Nebel-Jacobsen et al. (2010)

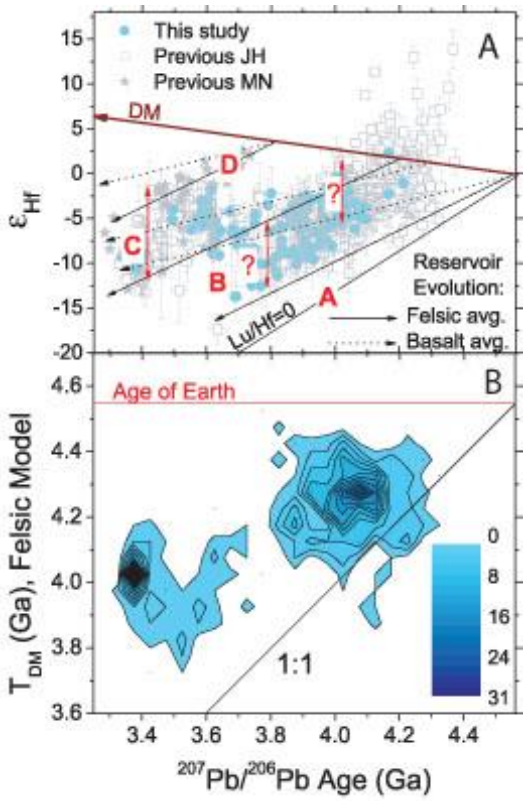

Fig. 4.6: Potential source reservoirs and contoured depleted mantle extraction ages (TDM) of all Jack Hills zircons shown on Fig. 1. A) The zircon record modeled by a mixture of hypothetical basaltic and felsic reservoirs (see text for explanation). B) Jack Hills detrital zircon data contoured in TDM vs. $^{207}Pb/^{206}Pb$ age space assuming $^{176}Lu/^{177}Hf = 0.01$. A discontinuity at ca. 3.8-3.7 Ga sees loss of reservoir B and afterwards more radiogenic crust on average.

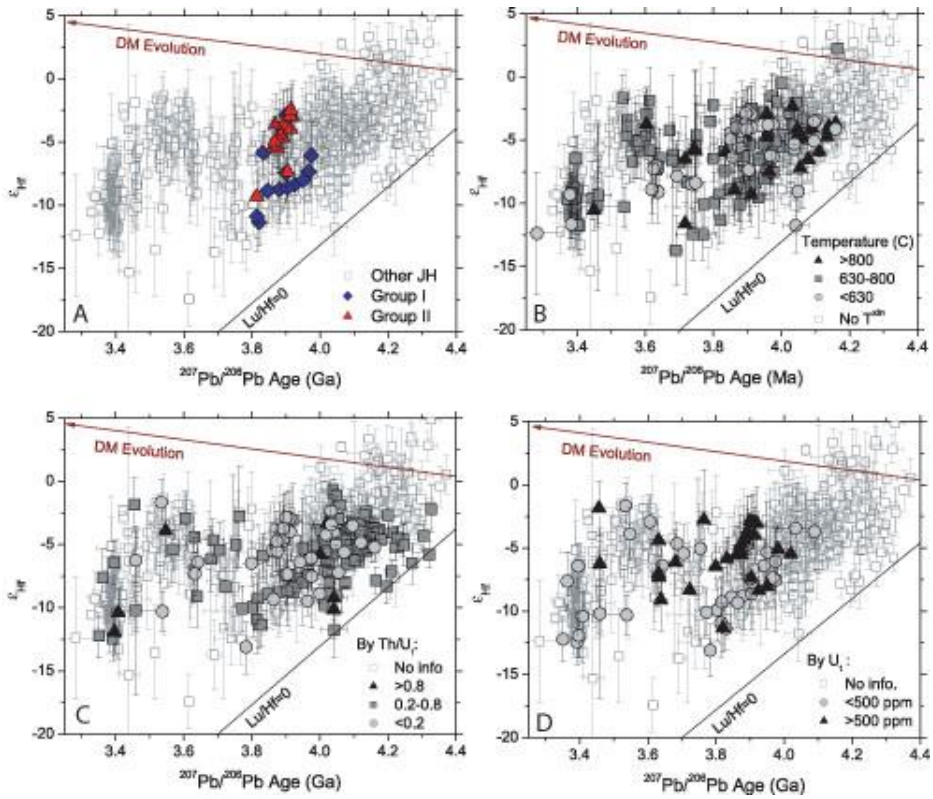

Fig. 4.7: A) Group I and II zircons in age vs. eHf space along with other analyses from the Jack Hills; B) Similar plot, with zircons analyzed for [Ti] highlighted and grouped by T^{xlln}; C) zircons analyzed for Th/U (including Harrison et al., 2008) highlighted and grouped by Th/U_t; D) zircons analyzed for U highlighted and grouped by U_t. Radiogenic Hadean population doesn't display a higher incidence of Group II-like characteristics (e.g., low Ti) than the prevailing Hadean population, suggesting that simple chemical inheritance from Reservoir C (in the case of low Ti reflecting not crystallization temperature or flushing during recrystallization but formation in magma with low a_{TiO2}) doesn't explain Group II's properties.

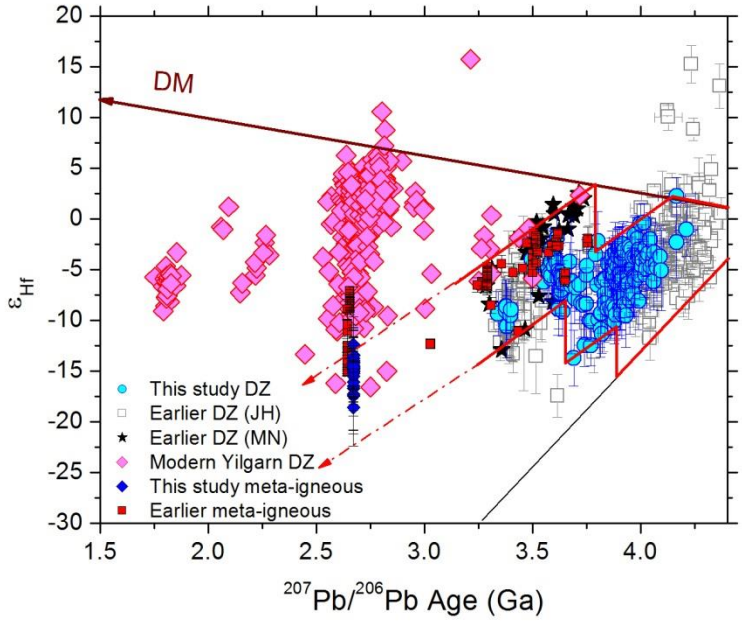

Fig. 4.8: NGC meta-igneous (Kemp et al., 2010; this study) and detrital zircons along with 1.5-3.8 Ga detrital zircons within 10% of U-Pb concordia from modern drainages in the Yilgarn craton (Griffin et al., 2004). Unlabeled symbols are as on Fig. 1. Red arrows represent the εHf, age evolution trajectories for 3.8 and 4.2 Ga felsic reservoirs, which bound the <3.7 Ga Jack Hills distribution. There is little evidence for felsic Hadean crustal involvement in the sources of <3 Ga zircons.

Chapter Five: Origins of variable Xe loss and Pu/U in Hadean Jack Hills zircons

Abstract

Initial Pu/U ratios in >4 Ga terrestrial zircons from the Jack Hills, Western Australia, yield values both above and below the most recent estimate of initial solar system Pu/U. Given that U becomes oxidized to the soluble uranyl ion (UO_2^{2+}) under even mildly oxidized aqueous conditions while the solubility of Pu is generally much lower, this variation has been suggested as a possible indicator of aqueous alteration in the precursors to Jack Hills zircon magmas. However, the lack of extant natural Pu since ca. 4 Ga has limited insights into its behavior in terrestrial settings. Thus an aqueous history may not be the only potential cause of Pu/U variations, and the potential effects of magmatic compositional evolution (similar to that seen in evolving zircon Th/U ratios) and secondary alteration of the zircons need to be considered. In order to unravel the causes of Jack Hills Pu/U variations, we collected a multivariate dataset on 11 zircons consisting of Xe isotopic analyses along with U-Pb age, trace element, and oxygen isotopes, to assess the relative effects of these processes in causing Pu/U variations. Pu/U does not display obvious correlations with other geochemical indicators, with the exception of Nd/U. High-Nd/U zircons display only low Pu/U, while low Nd/U zircons show more heterogeneous Pu/U. The high-Nd/U group appears less magmatically evolved than other Hadean zircons, has REE patterns permissive of some degree of alteration, and consists of solely low-Pu/U zircons with a mixture of Hadean and Proterozoic U-Xe ages. The higher diversity of Pu/U among the rest of the population suggests more complex and heterogeneous origins, including possible primary Pu/U variations from a variety of processes that cannot be well-constrained by the present data. The spread in U-Xe ages from ca. 4.3 to 1.8 Ga shows a great diversity in Xe loss

and underscores the intensity of the post-Hadean to Proterozoic thermal histories of the Jack Hills zircons.

5.1 Introduction

Among the most significant geochemical signatures recognized in >4 Ga Jack Hills (Western Australia) zircons is the presence of heavy oxygen – many display $\delta^{18}O$ resolvably heavier than that of unaltered mantle-derived rocks (e.g., Mojzsis et al., 2001; Peck et al., 2001; Cavosie et al., 2005; Trail et al., 2007b). Among Phanerozoic zircons, "heavy" oxygen in a magmatic rock and its constituent zircons is taken as evidence that the magma's precursors included sediments (or more generally, materials altered by aqueous interaction at low temperatures; Valley, 2003). Applying this interpretation to Hadean zircons may indicate a terrestrial hydrosphere since at least 4.3 Ga (Mojzsis et al., 2001). The existence of Hadean rock-water interactions is corroborated by the low crystallization temperatures of Hadean zircons near the wet granite solidus (Watson and Harrison, 2005).

One other possibly hydrosphere-related feature observed among the Hadean Jack Hills zircons is an apparent variability in $(Pu/U)_o$ (i.e., Pu/U corrected to the age of the solar system). Although ^{244}Pu is now extinct in our solar system ($t_{1/2}$ =≈ 80.0±1.2 Ma; Chechev, 2011), the $(Pu/U)_o$ can be observed from Xe remanant in zircon from the spontaneous fission of the nuclides ^{244}Pu and ^{238}U (Hohenberg et al., 1967; Turner et al., 2004, 2007). Due to its similar size and charge relative to the long-lived actinides ^{232}Th and ^{238}U, Pu is favorably partitioned into the zircon lattice (Burakov et al., 2002). A hydrosphere might be expected to fractionate Pu from U, similarly to the Th/U fractionation that occurs during fluid flow through oxidized crust due to their contrasting solubilities (e.g., Mojzsis and Harrison, 2002). Both Th and Pu tend to occur in nature as water-insoluble tetravalent cations, in part because Pu^{4+} reacts quickly with

solid surfaces to form essentially insoluble Pu^{3+} (Kersting et al., 1999). U has an additional 6+ oxidation state, which, depending on pH, can form the soluble uranyl (UO_2^{2+}) ion under most crustal oxidation conditions (Langmuir, 1978; Sverjensky and Lee, 2010)).

Previous studies of fission Xe in Hadean zircons (Turner et al., 2004, 2007) found $(Pu/U)_o$ that varied from 0.012 to zero. For comparison, estimates for solar system $(Pu/U)_O$, based mainly on the St. Severin chondrite, range from 0.015 to 0.004 with the most recent estimate being 0.0068 (Hudson et al., 1989). Because no geochemical variables were measured in these zircons apart from U-Pb age and Xe isotopes, it is unclear whether this variability can be positively attributed to the actions of a Hadean hydrosphere or if it is indicative of magmatic differentiation, fractional crystallization, or other processes. In this paper we present new fission Xe measurements on a suite of irradiated zircons which have also been analyzed for U-Pb age, oxygen isotopes, and trace element abundances in order to determine the origin(s) of Hadean Pu/U variability. Our results suggest that apparent Pu/U from the Xe measurements reflects mostly secondary alteration. We discuss the ways in which primary Pu/U variations in zircons – if positively identified in future work – could reflect various processes operating on the Hadean Earth.

5.2. Interpreting Xe Isotope Signatures

Turner et al. (2007) established a framework for the interpretation of fissiogenic Xe in irradiated zircons and we follow here their format. Xenon in zircons is produced by the spontaneous fission of ^{238}U and ^{244}Pu. Irradiation by thermal neutrons inducing ^{235}U fission yields a third fission Xe component, allowing for estimation of U-Xe age and Xe loss. These processes are most readily visualized in the ternary $^{132}Xe/^{134}Xe$ vs. $^{131}Xe/^{134}Xe$ diagram (Fig. 5.1).

If the Xe system has been closed since zircon crystallization, the ratio Xe_{244Pu}/Xe_{238U}, measured as the projection from the ^{235}U end-member through the zircon's Xe composition and onto the ^{238}U-^{244}Pu join, will reflect the $(Pu/U)_o$ ratio of the zircon at its formation (*original* to A; Fig. 5.1). Xe_{235U}/Xe_{238U} will reflect the age of formation, and is measured as the projection from the ^{244}Pu end-member through the zircon's Xe composition and onto the ^{235}U-^{238}U join (*original* to B; Fig. 5.1). The U-Xe ages to which the various Xe_{235U}/Xe_{238U} ratios correspond is a function of the $^{235}U \rightarrow Xe$ conversion factor during neutron bombardment and will vary for each irradiation. Thus the ternary diagram cannot be used to visually compare, for instance, our data to that of Turner et al. (2007). Fig. 5.2 shows the effect of different irradiation parameters: Turner et al. (2007)'s data with the actual neutron fluence received during irradiation and the Xe isotope ratios if their samples had received 2x or 4x the neutron dose.

For zircons that have undergone later Xe loss, only approximate values for $(Pu/U)_O$ and U-Xe degassing age can be calculated except in specific circumstances as illustrated on Fig. 5.1. Xenon loss draws the isotope composition toward the ^{235}U-^{238}U join corresponding to the age of degassing (*current* to C, with age read as B' and $(Pu/U)_O$ read as A'; Fig. 5.1). For complete degassing, we will measure $(Pu/U)_O = 0$ and a U-Xe age equal to the time of Xe loss. For partial Xe loss at time B, the projected U-Xe age (location B) overestimates the actual age of Xe loss (which is time C). Thus, the projected $(Pu/U)_O$ underestimates the actual $(Pu/U)_O$ (at position *original*). The extent of lowering the apparent $(Pu/U)_O$ depends on the timing of Xe loss – recent loss moves the zircon toward the ^{235}U end-member in Xe three-isotope space, thus preserving the $(Pu/U)_o$ information. Ancient loss leads to more significant lowering of the apparent $(Pu/U)_O$.

5.3. Actinide geochemistry: mechanisms of Pu-U fractionation

We begin by establishing a framework in which to interpret the significance of Pu/U in natural samples. First to consider is the geochemical behavior of Pu, and second, the various means of fractionating the two elements in both aqueous and magmatic environments. Lastly, we consider whether there should be meaningful differences between the interpretation of Pu/U and the more widely used actinide ratio Th/U.

5.3.1 Geochemical Behavior of Pu

In studies of both meteorites (e.g. Lugmair and Marti, 1977, Wasserburg et al., 1977) and nuclear materials (e.g. Koelling, 1985), Pu is commonly considered similar in chemistry to the light rare earth elements (LREE). Among the metal alloys and other compounds used for nuclear fuel, cerium exhibits similar bonding behavior to the middle actinides Np, Pu, and Am (Koelling, 1985), and is often used as a proxy for Pu in experimental work (Metz, 1957). Despite the vast differences between the chemistry of these compounds and of naturally occurring rocks, natural meteoritic samples seem to bear out this Pu-LREE similarity (e.g. Lugmair and Marti, 1977, Wasserburg et al., 1977). Natural terrestrial systems differ from meteoritic systems in many ways, including the production of evolved felsic magmas in oxidized environments, so while not all aspects of meteorite studies will be applicable to terrestrial zircon petrogenesis and development of variable Pu/U, some may be useful.

5*.3.1.1 Meteorite Studies*

The preservation ^{244}Pu relicts in some meteorites inspired investigations of the cosmochemistry of Pu using natural samples and laboratory experiments. Lugmair and Marti (1977) and Wasserburg et al. (1977) both suggested that little to no fractionation occurs between Pu and Nd during nebular processes. Jones and Burnett (1987) confirmed through experiment that Pu and Sm are not significantly fractionated between diopside or whitlockite and melt under

reducing conditions. They surmised that, given the relative geochemical behavior of other LREE such as Ce and Nd, there would be even less fractionation between Pu and these elements. They also noted, however, that the behavior of Pu is modified by the addition of a few wt.% of P_2O_5 to the melt, such that $^{Pu}D_{cpx}$ changes by a factor of two.

The case of meteorite metamorphism is quite different. Although highly metamorphosed meteorites contained live Pu, LREE, and U all concentrated in various phosphate phases, less metamorphosed ordinary chondrite (H3-H5) phosphates were rich in Pu while U and REE are concentrated in other phases (Murrell and Burnett, 1983). Increasing REE and U contents are seen in the phosphates with increasing metamorphism, with the REE migrating into the phosphates more quickly than U (Murrell and Burnett, 1983). There is substantial variation in Pu/U (as well as Pu/Nd), then, among the various phases in unequilibrated meteorites.

5.3.1.2 Terrestrial Magmatic Processes

Terrestrial igneous processes differ from meteoritic environments largely by the greater range in composition and oxygen fugacity. Whereas even differentiated meteorites rarely display igneous materials more felsic than basalt, remelting of basaltic and more felsic materials in the Earth's crust dominantly yields granitoids. Differing oxygen fugacities among granitoids are often revealed by accessory minerals, as in the magnetite-ilmenite series of Ishihara (1977). Often in the Phanerozoic rock record, these variations can be traced to the tectonic/sedimentary setting of the source, although uncertainties about the tectonic regime(s) operating in the Hadean and Early Archean make similar distinctions less clear for such ancient samples.

The abundance of Pu relative to other trace elements is likely to change throughout the course of magmatic crystallization, similar to the behavior of other incompatible trace elements. Incompatible trace elements (including lanthanides and actinides, among others) are generally

concentrated in the melt as modal phases largely exclude them. Zircon elemental abundances and ratios appear to track magmatic temperature and elemental ratio evolution (Claiborne et al., 2010), although the overall abundance of REEs appears not to change significantly during the course of granitoid magma crystallization (Hoskin et al., 2000). Claiborne et al. (2010) found increasing Hf abundance, decreasing Th/U, and increasing Yb/Gd with decreasing Ti-in-zircon crystallization temperature (T^{xlln}) in zircons from the Spirit Mountain batholith (Nevada, USA), reflecting a complex magmatic evolution including multiple recharge events. Linnen and Kepler (2002) determined the solubility of zircon and hafnon ($HfSiO_4$) in granitic melts and predict that zircon crystallization in most granitic magmas will lead to a decrease in the Zr/Hf ratio in the remaining liquid, such that with increasing melt differentiation zircons become more Hf-rich (also noted by Claiborne et al., 2010).

The increasing Yb/Gd ratio with decreasing T^{xlln} seen by Claiborne et al. (2010) probably reflects the effects of the lanthanide contraction – systematic changes in chemical behavior and compatibility of the trivalent lanthanides resulting from the systematic decrease in ionic radius with atomic number – on the compatibility of the various REE in major and minor mineral phases. For instance, the common accessory mineral monazite (present as inclusions in Jack Hills zircons) concentrates Th preferentially to U and LREE preferentially to HREE. Increasing melt crystallization can exacerbate these differences absent an HREE-concentrating phase other than zircon (*e.g.*, garnet). The actinides also show this contraction, and the decreasing Th/U with decreasing T^{xlln} (Claiborne, 2010) may be a similar effect, but it certainly also reflects the evolving Th/U ratio of the melt caused by the crystallization of other mineral phases. By analogy the Pu/U ratio should also increase in the remaining liquid fraction during differentiation. The trends in compatibility of lanthanides in zircon in particular versus ionic

radius are shown in Fig. 5.3. This is a candidate mechanism for producing zircons with primary super-chondritic Pu/U ratios from evolved magmas. Complementary sub-chondritic Pu/U ratios would then be found in cumulate materials, a supposition which is supported by higher Th/U ratios among cumulate zircons in the Spirit Mountain batholith (Claiborne, 2010). Given, however, the variety of both super- and subchondritic Th/U ratios found in terrestrial crustal materials today, straightforward comparison of primary magmas with the chondritic ratio may not be possible. Other possible fractionation mechanisms include remelting the separated high- and low-Pu/U products of previous magmatic episodes and aqueous alteration.

5.3.1.3 Aqueous Alteration and Metamorphism

U displays different geochemical behavior from the other light actinides under even mildly oxidizing aqueous conditions: it oxidizes to form the water-soluble uranyl ion (UO_2^{2+}) while Pu and Th remain in nonsoluble tetravalent form (Kersting et al., 1999; Langmuir, 1978; Sverjensky and Lee, 2010). Because of this differing behavior, substantial Th/U and Pu/U fractionation may occur in most aqueous systems. Thus materials that have been leached by reactions with water will tend to lose U relative to Th and Pu. Eventual precipitation of this dissolved UO_2^{2+} then lead to deposits with a U excess relative to Th and Pu. Thus aqueous alteration is a possible mechanism for the generation of both super- and subchondritic Pu/U ratios.

Reactions with meteoric water tend to lower a rock's $\delta^{18}O$ (while reactions with seawater at mid-ocean ridge hydrothermal systems can have more varied effects: Valley, 2003; Gregory and Taylor, 1981). Low temperature exchange of oxygen isotopes between clay minerals and water results in elevated mica $\delta^{18}O$. $\delta^{18}O_{SMOW}$ of some Jack Hills zircons above the mantle value of ~5.3‰ (Valley, 2003) have generally been interpreted as due to hydrous minerals in the

protolith of the granitoids from which the Jack Hills zircons were derived (*e.g.*, Mojzsis et al., 2001; Peck et al., 2001; Trail et al., 2007b). Thus a search for correlations between Pu/U and $\delta^{18}O$ in our zircons may lead to evidence of aqueous effects either in the zircons themselves (secondary alteration) or in the magma protoliths. Water-rock interactions have been proposed to explain some oxygen isotope compositions in Jack Hills zircons.

5.3.2. Primary Pu/U Signatures vs. Effects of Recrystallization and Xe Loss

An important caveat is that determinations of Pu/U using Xe isotopes can only give an apparent Pu/U ratio at the time of formation. The behavior of Xe during zircon recrystallization is poorly known, but we can assume that its inert nature results in its release from the structure during this processs. Thus our observation of apparent Pu/U may not reflect expectations for the geochemical behavior of Pu/U but could instead result from Xe loss during alteration (cf. Honda et al., 2003).

The effects of Xe loss are compounded by the relatively short half-life of ^{244}Pu, in that this radionuclide was effectively extinct by ca. 4 Ga. Thus, total loss of Xe after ^{244}Pu extinction results in a total loss of the Pu signal whereas ^{238}U decay continues to accumulate radiogenic Xe until today (see Fig. 5.1). Partial loss instead yields a Pu/U intermediate between zero and the grain's true value, along with a U-Xe age intermediate between the age of zircon crystallization and the time of Xe loss (the illustrated as dashed line in Fig. 5.1).

Xenon loss while Pu was still live will also yield artificially low Pu/U estimates. This is because the rapid decay of ^{244}Pu relative to ^{238}U means that after Xe loss, a zircon's newly ingrown Xe will never "catch up" to its previous plutogenic Xe content owing to the progressively smaller amount of Pu in existence as time passes. This effect is exacerbated as the period between crystallization and Xe loss increases. Thus an approach is needed to distinguish

between lowered apparent Pu/U due to Xe loss and actual, primary Pu/U variations. A comparison of U-Xe and $^{207}Pb/^{206}Pb$ ages can distinguish zircons with Xe loss and the maximum age of that loss. Indeed, Turner et al. (2007) found that deviations (both positive and negative) from chondritic estimates for Pu/U among their Hadean zircon samples were more common among those zircons with the highest discordancy between U-Xe and Pb-Pb ages, suggesting that these variations reflected Xe loss. Another method developed by Turner et al. (2007) involves the estimation of Pu/U by two methods. First, by taking the ratio of plutogenic Xe to uranogenic Xe, and second by taking the ratio of plutogenic Xe to Xe that formed from the induced fission of ^{235}U under thermal neutron bombardment. Xe loss during the zircon's lifetime also includes the loss of uranogenic Xe, but as ^{235}U does not produce Xe naturally, it is unaffected by natural Xe loss over geologic time. Thus Xe loss yields differing Pu/U estimates depending upon the uranogenic Xe end-member used. Agreement between the two would indicate that the zircon has has remained a closed system (or in some cases, that it has lost all of its plutogenic Xe and thus both ratios are zero). Mechanisms for Xe loss both pre- and post-Hadean include heating (to induce postulated diffusion of Xe out of the zircon) and recrystallization, either solid-state or fluid-mediated. Little data exist on the diffusion behavior of Xe in zircon, but a study by Shukolyukov et al. (2009) suggests that non-metamict zircon is highly retentive of Xe and thus recrystallization may be much more effective as a Xe loss mechanism.

As discussed, various processes may lead to artificially low Pu/U estimates due to Xe loss. It is also be possible for a zircon to obtain a higher than original igneous Pu/U through certain types of recrystallization. Solid-state transgressive recrystallization in originally igneous zircons from a granulite terrane tends to sweep zircon-incompatible elements out of the zircon lattice in favor of more compatible elements (Hoskin and Black, 2000). Given their respective

ionic radii (see Fig. 5.3), this leads to an enhancement of tetravalent actinides in the zircon lattice relative to trivalent. The greater compatibility of U relative to Th leads to an decrease in Th/U in recrystallized regions (Hoskin and Black, 2000). By similar reasoning, transgressively recrystallized zircon should also have higher Pu/U ratios than the unrecrystallized zircon due to its higher projected compatibility in the zircon lattice due from its smaller ionic radius (see Fig. 5.3). The incompatible nature of Xe in zircon should result in its being flushed from recrystallized regions. While the loss of Xe will lead to an lowering of apparent Pu/U, a complementary increase in Pu/U resulting from recrystallization could in principle offset this effect. This effect might be suspected when zircons with super-chondritic Pu/U show evidence for Xe loss, or when zircons with multiple Xe releases display release steps with simultaneously younger U-Xe ages and higher apparent Pu/U.

5.3.3. Hypotheses

There are multiple competing hypotheses for the origin(s) of apparent $(Pu/U)_O$ variations in Hadean zircons. These effects might be identifiable by correlations between apparent $(Pu/U)_O$ and other geochemical indicators for various geologic processes. Effects we search for include:

1) Xe loss: as explained in section 2.3.2., this may be either due to heating-induced Xe diffusion or, more likely, recrystallization of the zircon. In most cases this will yield an artificial lowering of Pu/U, along with a lowering of the U-Xe age. An exception is that for certain types of recrystallization, Pu/U may be enhanced within recrystallized regions of zircon and if this occurs early enough it may be evident in the Xe. The U-Xe age will nonetheless be anomalously young. Thus later Xe loss can be explored by looking for mismatches between $(Pu/U)_O$ estimates using ^{238}U vs. ^{235}U and by looking for correlations between $(Pu/U)_O$, relative U-Xe age, and indicators for aqueous (e.g., lowered $\delta^{18}O$) and other types of alteration.

2) Magmatic processes: the Pu/U of a magma, like other trace element ratios, should change over time in response to progressive crystallization, yielding correlations between zircon $(Pu/U)_O$, T^{xlln}, and other indicators for compositional evolution (e.g., Hf, Yb/Gd, Th/U; see section 2.3.2).

3) Aqueous alteration of magma precursors: From their inclusion mineralogy and high $\delta^{18}O$ observed in some zircons, the sources of Jack Hills magmas have been inferred to contain meta-sedimentary materials (e.g., Peck et al., 2001; Mojzsis et al., 2001; Trail et al., 2007b) due to. If $(Pu/U)_O$ variations derive from these processes, there should be a relationship between $(Pu/U)_O$ and other indicators of aqueous alteration (e.g., $\delta^{18}O$ divergence from the mantle value, Th/U).

5.4. Methods

Zircons were chosen for analysis from the sample set of Trail et al. (2007b). They have been previously analyzed for U-Pb age (Holden et al., 2009) and $\delta^{18}O$ (Trail et al., 2007b), and details of those analyses are available in their respective papers. We have carried out both trace element measurements via ion microprobe for 23 Hadean zircons from the Trail et al. (2007b) dataset and, subsequently, Xe isotope measurements on 11. An additional 31 >4 Ga zircons were also analyzed for $\delta^{18}O$ and trace elements at UCLA, and results from 4.0-3.8 Ga zircons falling into the Hadean-like Group I (see chapter 3) are also included for comparison.

5.4.1. Trace elements

Zircons had been previously mounted in 1” epoxy rounds and polished to expose the grain interiors (see Holden et al., 2009; Trail et al., 2007b). Trace element analyses were carried out on the CAMECA *ims*1270 ion microprobe at the University of Edinburgh in 2006. Energy offsets of -100 eV were applied to reduce molecular interferences. An additional 31 zircons

were analyzed on the CAMECA *ims*1270 ion microprobe at UCLA using similar conditions, with a ~15 nA primary beam focused to a 30 µm spot. All trace element and oxygen isotope data are tabulated in Appendix G.

5.4.2. Xe isotope analysis

Following the protocol of Turner et al. (2007), 11 zircons were plucked from their epoxy mounts and irradiated with thermal neutrons at Imperial College's CONSORT research reactor in order to induce fission of ^{235}U (see section 4.1. for explanation). Neutron fluence is estimated at ~6x10^{18} n/cm^2. A ^{134}Xe/U conversion factor of 1.26 x 10^{-8} atoms ^{134}Xe/atom ^{235}U was calculated from NIST 610 standard glass on the basis of 6.32 x 10^5 atoms fission ^{136}Xe measured by RELAX and a calculated 4.439 x 10^{11} atoms ^{235}U in the glass fragment. This represents ca. 60% of the expected value based on the estimated reactor neutron fluence (~6.15 x 10^{16} n/cm^2). This conversion factor is ~1.5x that calculated for the previous Hadean zircon study (Turner et al., 2007) and the data's position on the Xe ternary diagram (see Fig. 5.4) agrees fairly well with this calculation (see Fig. 5.2 for expected positions based on differing fluence).

The zircons were then analyzed for Xe isotopes using the Refrigerator-Enhanced Laser Analyzer for Xe (RELAX) resonant ionization time-of-flight mass spectrometer at the University of Manchester (Gilmour et al., 1994; Crowther et al., 2008). Briefly, individual zircons were heated with an infrared laser in successive heating steps to release Xe. This gas was captured by a cold finger, evaporated by another infrared laser pulse, and the Xe was selectively ionized by a Sirah dye laser with 249.6 nm wavelength (UV). The resultant ions were analyzed by time-of-flight mass spectrometry. All zircons produced multiple Xe releases at different heating steps, ranging from purely fission Xe to purely atmospheric Xe. We accept only steps that produced a relatively large signal (>5 mV total in the RELAX detector) and contained negligible ^{130}Xe (a

proxy for atmospheric Xe contamination). We also apply a small correction for the minor amounts of atmospheric Xe still present in each accepted release step. Isotopic data for all Xe release steps are given in Appendix H.

5.5. Results

We present Xe isotope measurements on 11 zircons that have also been characterized for trace elements, U-Pb ages, and $\delta^{18}O$. We also report these quantities for a larger Hadean dataset (N=54), Because the difficulty of the Xe isotopic measurement significantly limits our Xe-in-zircon sample set, this expanded geochemical dataset helps to put the Pu-U-Xe results into context.

5.5.1. Fission Xe Results

Data for all heating steps that produced fission Xe releases are shown in Table 1, and graphed in Figures 5.4 (classified into trace element groups) and 5.5 (classified according to $^{207}Pb/^{206}Pb$ age). $(Pu/U)_o$ for these 14 heating steps from 11 zircons range from below 0 to 0.0056. Three of our eleven studied zircons produced multiple fission Xe release steps; the other eight produced only a single usable fission Xe release. U-Xe ages and apparent Pu/U ratios are calculated for each step separately. U-Pb ages range from 4.2 to 4.0 Ga and U-Xe ages range from 4.3 to 1.8 Ma (see Fig. 5.6). Zircons analyzed in this study reproduce the low apparent $(Pu/U)_O$ group observed by Turner et al. (2004, 2007) but, unlike the earlier study, values at or above the chondritic estimate of ~0.007 (Hudson et al., 1989) are not seen. Also consistent with the Turner et al. (2007) results, the majority of U-Xe ages in this study are less than 4 Ga. However, 7 out of 14 releases yield U-Xe ages <2.5 Ga, whereas all U-Xe ages reported by Turner et al. (2007) are Archean, with the youngest ca. 2.8 Ga. All but one of the Xe gas release steps fall within the ternary plot (Fig. 5.4) consisting of the two radiogenic end-members (i.e.,

^{238}U and ^{244}Pu fission) and nucleogenic Xe from ^{235}U. The single fission Xe release from ANU 31-8.4 (in the older, high-Nd/U_t High-Nd/U group) falls significantly outside the ternary, perhaps reflecting problems with our correction procedure. This datum will not be further considered here.

5.5.2. Comparing Xe Results to Other Geochemical Indicators

As shown in Fig. 5.7B, the zircons' $(Pu/U)_O$ show only a weak correlation with $\delta^{18}O$ (when only the highest Pu/U release step from each zircon is considered, R^2~0.4). $(Pu/U)_O$ show no obvious correlations with indicators for melt cooling and crystallization such as Ti-in-zircon crystallization temperature (T^{xlln}), $(Th/U)_t$, Hf, or Yb/Gd (Fig. 5.8). However, $(Pu/U)_O$ does have a rough inverse relationship with several LREE/actinide ratios, seen most clearly with Nd/U_t (Fig. 5.7A). Zircons with low values for Nd/U and Pr/U show high variability in $(Pu/U)_o$, including the full range of Pu/U variability in this dataset. Grains with higher Nd/U and Pr/U have less variable $(Pu/U)_o$ and uniformly lower values. Nd/Th and Pr/Th produce similar graphs (not shown). Cerium shows somewhat different behavior, likely due to its multivalent nature in zircon (as opposed to the other LREE, which occur in zircon only in the trivalent oxidation state). This inverse relationship contrasts with the similar Pu and LREE chemistry seen in many meteorites and under reducing igneous conditions (e.g., Jones and Burnett, 1987).

U-Xe ages, $(Pu/U)_O$, and $^{207}Pb/^{206}Pb$ crystallization ages for all samples can be seen in Fig. 5.6, grouped by elemental geochemistry. The zircons are shown classified by group in several other geochemical variables in Fig. 5.8. High-Nd/U zircons (Group A) are defined as having $Nd/U_t > 0.01$ and have generally higher $(Th/U)_t$ and Yb/Gd, although there is a large degree of overlap between the groups. There is no appreciable difference in U_t or $\delta^{18}O$ between the groups. The low-Nd/U Group B contains all of the zircons with multiple Xe release steps as

well as all of the zircons with (Pu/U)o > 0.001 in this dataset. Four of our eleven studied zircons fall into the older, high-Nd/U_t Group A, displaying low $(Pu/U)_O$. Group A is generally characterized by older crystallization ages, with two of these zircons (ANU 31-15.8, ANU 31-14.3) having among the younger U-Xe ages in the dataset at 2.39 and 2.269 Ga, respectively. All other zircons fell into the low-Nd/U Group B, including the three grains with multiple Xe release steps and all samples with $(Pu/U)_O$> 0.001.

5.6. Discussion

An earlier investigation of Jack Hills zircon Xe revealed higher Pu/U generally falling among zircons with younger crystallization ages (Turner et al., 2007; see this study, Fig. 5.6). Similarly, in this study only the younger zircons display apparent $(Pu/U)_O$ > 0.001. The younger zircons, along with the lower-Nd/U zircons, appear to derive from later-stage melts or more felsic magmas in general based on trace element concentrations. However, we do not observe direct correlations between $(Pu/U)_O$ and indicators for melt compositional evolution within either group or among the zircon sample set as a whole.

Some caution is in order when interpreting the various relationships (and lack thereof) between $(Pu/U)_O$ and other geochemical indicators. The lack of many $(Pu/U)_O$ correlations with other variables in this dataset may well be due to the small sample size. With that caveat, the lack of a strong correlation between $(Pu/U)_o$ and $\delta^{18}O$ may be evidence against a direct link between aqueous alteration and $(Pu/U)_o$ variations in the source materials of the Jack Hills magmas (although fluids with a range of $\delta^{18}O$ could also explain the data). Similarly, the lack of correlations between $(Pu/U)_o$ and various indicators for magmatic differentiation seems to argue against the observed Pu/U variations being primary magmatic signals. A more likely scenario for the generation of the Hadean zircons' apparent $(Pu/U)_O$ variations involves a) the generation of

apparent (and/or actual) Pu/U variations by secondary alteration of the zircons, and also probably b) the formation of these zircons and their $(Pu/U)_o$ ratios by a multitude of processes. This heterogeneity of origins is consistent with the detrital nature of our sampled population.

5.6.1. Secondary Alteration

Xenon loss, as indicated by discordance between $^{207}Pb/^{206}Pb$ crystallization age and U-Xe age, appears ubiquitous among Hadean Jack Hills zircons (Turner et al., 2007; this study). Turner et al. (2007) found that Pu/U divergence from the chondritic estimate increases in Jack Hills zircons for increasing discordance between crystallization and U-Xe ages, indicating Xe loss as a method for generating Pu/U diversity. The variable but generally low estimates for Xe diffusivity in zircon (see Shukolyukov et al., 2009) indicate that this is unlikely to occur through simple volume diffusion in response to heating at normal crustal temperatures in pristine zircon. However, although zircon is a remarkably robust mineral in virtually all crustal environments, the accrual of sufficient radiation damage can lead to its chemical and physical alteration. In particular, ^{238}U spontaneous fission can significantly damage the zircon crystal lattice in regions of high U concentration that are below the annealing temperature of radiation damage in zircon (ca. 200°C; Tagami et al., 1998). When the degree of damage accrued results in loss of long range ordering, the crystal is said to be "metamict," and these zones are susceptible to recrystallization and chemical reaction with geologic fluids. Both of these processes are candidates for changing the apparent Pu/U of Xe releases from Hadean zircons. Fortuitously, both should also leave other geochemical clues behind in the zircons they affect.

5.6.1.1 Recrystallization

Since Xe is highly incompatible in the zircon lattice it is almost certainly lost from regions during recrystallization. Low diffusion rates (although estimates do vary considerably;

see Shukolyokov et al., 2009) may, however, mean that adjacent unrecrystallized regions of the crystal might retain Xe during such an event. This would lead to a zircon with Xe of various age and apparent Pu/U residing in different regions of the same zircon. Xe gas releases with younger U-Xe ages (assuming the same time of Xe loss) would show lower Pu/U due to the rapid decay loss of ^{244}Pu in the early solar system, but preferential retention of Pu over U in regions transgressively recrystallized by the mechanism proposed by Hoskin and Black (2000), similar to the preferential retention of U over Th, could lead to younger apparent U-Xe steps that could also preserve higher Pu/U if Xe loss occurred prior to ^{244}Pu extinction. Although we observe two zircons (ANU 33-12.14 and 33-13.6) with multiple fission Xe releases of different U-Xe age and $(Pu/U)_O$, their U-Xe ages are all post-Hadean and thus recrystallization should only be expected to lower the apparent $(Pu/U)_O$. There are no obviously transgressively recrystallized regions found during cathodoluminescence imaging of the zircons, although 33-13.6 shows some areas of originally magmatic oscillatory zonation that may have undergone some degree of alteration, if not the transgressive recrystallization of Hoskin and Black (2000).

5.6.1.2 Metamictization and Secondary Aqueous Alteration

Metamictization, which makes zircon more prone to aqueous and other chemical alteration and Pb loss, also certainly renders zircon more susceptible to Xe loss. One explanation for the weak trend (R^2~0.4) between the highest-$(Pu/U)_o$ releases and the $\delta^{18}O$ of their respective zircons (see Fig. 5.7B) may be the production of both low-Pu/U and low-$\delta^{18}O$ regions in the zircons by later reaction with a hydrous fluid. Alteration by hydrous fluids has been suggested as a mechanism responsible for some zircon chemistries and internal structures (e.g., Hoskin, 2005; Pidgeon et al., 1998; Vavra et al., 1996, 1999). Aqueous interactions do not generally alter the oxygen isotope composition of non-metamict zircon, but radiation-damaged zircon can

experience a downward shift in $\delta^{18}O$ through exchange with meteoric waters (Valley, 2003). Such altered regions also typically show higher contents of U and Th (Valley, 2003), although in the author's opinion it is not entirely clear whether this is the cause (higher U leads to more radiation damage leaving the area susceptible to alteration) or the effect (addition during alteration). Hoskin and Schaltegger (2003) report high, flat LREE patterns associated with aqueous alteration in zircons. A minority of Jack Hills zircons show similar patterns (e.g., Peck et al., 2001; Hoskin, 2005). Our high-Nd/U zircons display elevated LREE, along with muted Ce and Eu anomalies (see Fig. 5.9), although not to the extent noted by most published examples of alteration signatures (Hoskin and Schaltegger, 2003; Hoskin, 2005). It is possible that the high-Nd/U grains have been somewhat altered by fluid interactions, although they lack significant differences in U and Th contents or degree of U-Pb discordancy relative to the low-Nd/U group. Although across the Hadean population there is no difference between the $\delta^{18}O$ of high- and low-Nd/U zircons, among the high-Nd/U zircons analyzed for Xe average $\delta^{18}O$ is 5.2±0.7 vs. 6.1±0.7 (1σ) for low-Nd/U grains – slightly lower.

It is thus possible that the association of lower $\delta^{18}O$ and $Nd/U_t > 0.01$ exclusively with low-Pu/U zircons (see Fig. 5.7) may indicate that the low-Pu/U signature in these zircons is due to later aqueous alteration. The Proterozoic apparent U-Xe ages, resulting from substantial Xe loss in two high-Nd/U zircons, provides further support for this interpretation (although the other high Nd/U grain yields a Hadean age). It remains possible, however, that heterogeneous $\delta^{18}O$ is simply due to a spectrum of origins of the detrital Jack Hills zircon population and thus an absolute lowering of $\delta^{18}O$ relative the original composition is not knowable.

There are no obvious alteration-related REE patterns, higher U-Pb discordancies, nor higher U contents for the low-Nd/U grains with Proterozoic U-Xe ages, so it is not clear that

either aqueous alteration or other metamictization-induced alteration can be definitively identified. Whatever the mechanism, loss of xenon for the zircons with Proterozoic ages would have occurred at some point after ca. 1.8 Ga if loss occurred in one event, or possibly earlier for some of the individual zircons with older U-Xe ages. As discussed in section 5.3.3, an additional constraint on Xe loss is a comparison between separate estimates for $(Pu/U)_O$ derived using either the ^{238}U or the ^{235}U isotope. Agreement between the estimates will occur in the cases of minimal Xe loss or very recent Xe loss. Fig. 5.10 shows U-Xe age vs. the disagreement between $(Pu/U)_O$ estimates for our zircons. The majority of zircons throughout the range of U-Xe ages show large disagreement between estimates, which increases with decreasing U-Xe age as expected. However, the exact timing is not uniquely determined.

5.6.2. Sources of Primary Variations

Given our relatively small sample set and the apparent ubiquity of Xe loss among Jack Hills zircons (this study; Turner et al., 2004, 2007), it is difficult to constrain the extent and causes of primary Pu/U variations with any kind of certainty. Nevertheless we compare several candidate scenarios for Pu/U alteration among the precursors to Jack Hills magmas and discuss their likelihood in the petrogenesis of the Jack Hills zircons.

5.6.2.1. Aqueous alteration of magmatic precursors

The difference in solubility between Pu^{4+} and the uranyl ion UO_2^{2+} permits fractionation of U from Pu in aqueous systems (Langmuir, 1978). The higher-than-mantle $\delta^{18}O$ in some Hadean zircons is interpretted as evidence for the inclusion of hydrated metasediments in the Jack Hills Hadean magmas (*e.g.*, Mojzsis et al., 2001; Peck et al., 2001; Cavosie et al., 2005; Trail et al., 2007b; *cf.* Hoskin, 2005). As an end-member model, apparent primary Pu/U variations may have originated in low-temperature, sediment-forming weathering reactions of

rock that contained chondritic Pu/U (*i.e.*, $(Pu/U)_o \sim 0.007$; Hudson et al., 1989). On the other hand, magmatic rocks have been identified that are melting products of previously hydrothermally altered protoliths. Hydrothermal alteration in meteoric waters tends to lower the $\delta^{18}O$ of the altered rocks (Valley, 2003), and magmas derived from melting of these materials likewise often display $\delta^{18}O$ below the mantle value. However, hydrothermal alteration of oceanic crust by seawater can have more varied impacts on various lithologies'$\delta^{18}O$, as shown for the Samail Ophiolite (Gregory and Taylor, 1981). They demonstrate that various regions display $\delta^{18}O$ signatures altered to both above (pillow basalts, sheeted dikes) and below (lower gabbros, peridotites) the mantle value. Water-rock reactions in oceanic crust results in substantial addition of U relative to Th (Staudigel et al., 1996). Similar processes during the Hadean would have led to a low-Pu/U upper oceanic crust as well as the relatively low-Th/U crust seen today. We expect magmas formed by remelting of aqueous alteration products to show correlations among $\delta^{18}O$, Th/U, and Pu/U reflecting the redistribution of these elements and isotopes during aqueous alteration. Zircons from the Southwest Nevada Volcanic Field (SWNVF), for instance, derive partly from the remelting of hydrothermally altered materials and display both low $\delta^{18}O$ and Th/U well above the normal values for igneous zircon (Bindeman et al., 2006). Bindeman et al. (2006) interpret this to show loss of U from the protoliths during hydrothermal alteration. Claiborne et al. (2010), however, attribute the high Th/U in their southern Nevada granitic zircons to a regional trend toward unusually high Th/U making ambiguous identification of hydrothermal alteration of the high SWNVF as the source of the Th/U distribution. The loss of U by dissolution should create a positive correlation between Th/U and Pu/U as opposed to the negative correlation resulting from magmatic processes (see Fig. 5.11). Although we do not see

such trends in our dataset, this may well be an effect that would emerge from a larger population of zircon trace element, $\delta^{18}O$, and apparent Pu/U among undegassed zircons.

The rare zircons shown to have grown directly from hydrothermal fluids are varied in trace element behavior, but often include higher than average amounts of LREE, Fe, and common Pb (Hoskin and Schaltegger, 2003) and host hydrothermal mineral and fluid inclusions. One zircon in the high-Nd/U group (ANU 31-15.8) does display an unusually high LREE pattern, but this is probably equally common among hydrothermally altered zircons (Hoskin, 2005) and this grain looks otherwise magmatic or only slightly altered (T^{xlln}, $\delta^{18}O$, trace elements). Most likely, direct hydrothermal precipitation is not a major source of Jack Hills zircons or their Pu/U variations.

5.6.2.2. Magmatic processes

The quantities Th/U, Yb/Gd, and Hf (Claiborne et al., 2010; by Zr/Hf in Linnen and Kepler, 2002) correlate usefully with zircon crystallization temperature and magma cooling and progressive crystallization. In our sample set, zircons <4.1 Ga have somewhat higher Hf and Yb/Gd than those older than 4.1 Ga, suggesting that later zircons on average crystallized in more evolved or cooler liquids (or recrystallized; Bell and Harrison, 2013). These trends are reflected in the significant differences between the largely older (in crystallization age) high-Nd/U group and the mostly younger low-Nd/U Group B in these variables. The two time periods are more similar in $(Th/U)_t$ and T^{xlln}. Interestingly, U_t > 300 ppm occurs only in >4.05 Ga zircons, although higher U is usually associated with more evolved or felsic melts. Given the overall indicators for granitic origins of the zircons, the general lack of samples with >500 ppm U, usually a significant proportion of granitic zircons, indicates that our population is biased toward low-U grains. Given the detrital nature of the zircon population, this may reflect preferential

destruction (perhaps of metamict grains) during sedimentary transport. This bias may cause additional complexities in the zircon record and help to obscure possible $(Pu/U)_O$ trends with other indicators for magmatic evolution. We would normally expect $(Pu/U)_O$ to increase with progressive melt crystallization similarly to the decrease in Th/U, for instance.

5.6.3 Implications for Hadean Processes and Areas for Future Study

The ubiquity of Xe loss seen in Hadean Jack Hills zircons (Turner et al., 2004, 2007) highlights their long post-Hadean history. Although deposited in a deltaic conglomerate (since metamorphosed to greenschist facies) at ca. 3 Ga (Maas and McCulloch, 1992; Spaggiari et al., 2007), their whereabouts in the crust between the Hadean and that time are unknown. Extant crust of the Narryer Gneiss Complex records several magmatic episodes from ca. 3.75 to 1.8 Ga (Bennett et al., 1990; Myers, 1988; Nutman et al., 1991; Wilde, 2010), which may have affected the zircons if they resided in the Narryer crust. Indeed, 3.8-3.4 Ga overgrowths are widely seen on Hadean Jack Hills zircon cores which may record entrainment in later magmas or a response to metamorphism (Cavosie et al.,2004; Trail et al., 2007a; Abbott et al., 2012). Given the likelihood of thermal events that could have affected the zircons before and after deposition, it is remarkable the extent to which they preserve temporal geochemical variations not only in the Lu-Hf isotopic system (Harrison et al., 2005, 2008; Kemp et al., 2010; Bell et al., 2011) but also, as shown here, both trace element ratios and Xe compositions.

We interpret our high-Nd/U zircons' chemistry (higher, somewhat flat LREE patterns and slightly lowered $\delta^{18}O$) as likely indicative of post-crystallization exchange with an aqueous fluid, although the extent of Xe loss is quite heterogeneous in this group, with both Hadean and Proterozoic U-Xe ages. Other samples may have lost Xe by this or other mechanisms (e.g., metamictization, or recrystallization of part of the zircon grain), although the timing is less

certain. If the Xe loss which caused Proterozoic U-Xe ages happened in one event it must have occurred since ca. 1.8 Ga. The coincidence of this constraint with the last known volcanism in the Jack Hills (Wilde, 2010) is intriguing but inconclusive.

Primary Pu/U variations among Jack Hills zircons remain possible but cannot be resolved with the present dataset. They may however complicate the interpretation of Xe loss histories with respect to zircon chemistry. A larger dataset would allow greater scrutiny of the geochemistry of the few zircons with relatively pristine Xe, but generation of a much larger dataset is hampered by the difficulty of making the Xe-in-zircon measurement (see 5.4). Trends between apparent $(Pu/U)_O$ and indicators for magmatic processes and aqueous alteration, and more specifically by comparing any Th/U-$(Pu/U)_O$ trends with the predicted behavior of the actinides for aqueous alteration of precursor materials versus magmatic processes (see Fig. 5.11), might then more definitively show primary $(Pu/U)_O$ variations. Aqueous alteration should deplete or enhance U relative to both Th and Pu, leading to positive Th/U vs. Pu/U trends, while magmatic differentiation should impose a positive trend.

Other trace elements in the zircons do show trends in time which suggest that later zircons derived from more evolved magmatic liquids or more felsic granitoids than the >4.1 Ga samples. Although all zircons here and in the previous study of Turner et al. (2007) exhibit some degree of Xe loss, the presence of near- to super-chondritic apparent $(Pu/U)_O$ only among this younger zircon population may suggest an overall effect of magmatic differentiation. Although that cannot be confirmed with the present data, this potential signal merits further study.

5.7. Conclusions

Jack Hills zircons exhibit extensive Xe loss (with U-Xe ages ranging from ca. 4.3 to 1.8 Ga) and dominantly subchondritic $(Pu/U)_O$. Several zircons exhibit relative LREE enrichment

and may have undergone post-crystallization aqueous alteration; in addition, multiple fission Xe releases from several single zircons, of differing U-Xe relative age and apparent $(Pu/U)_O$ are probably the result of metamictization or recrystallization affecting smaller domains within the grains. Our zircons lack correlations among $(Pu/U)_O$ and geochemical indicators for both aqueous alteration and magmatic differentiation. This may be partly due to the small Xe-in-zircon sample size (N=11). Due to both the small sample size and the ubiquity of Xe loss we cannot definitively resolve primary Pu/U variations among our zircons. We identify several useful tests that could be performed with a larger dataset of our same variables to search for primary Pu/U variations and their causes, specifically involving the signs of Th/U-$(Pu/U)_O$ trends. The ca. 1.8 Ga U-Xe age requires Xe loss since at least that time at the earliest, but the data do not preclude earlier heating events causing Xe loss as well. Although the origins of $(Pu/U)_O$ variations remain somewhat uncertain, our results do underscore the long post-Hadean thermal history of the Jack Hills zircons.

Chapter Five Figures

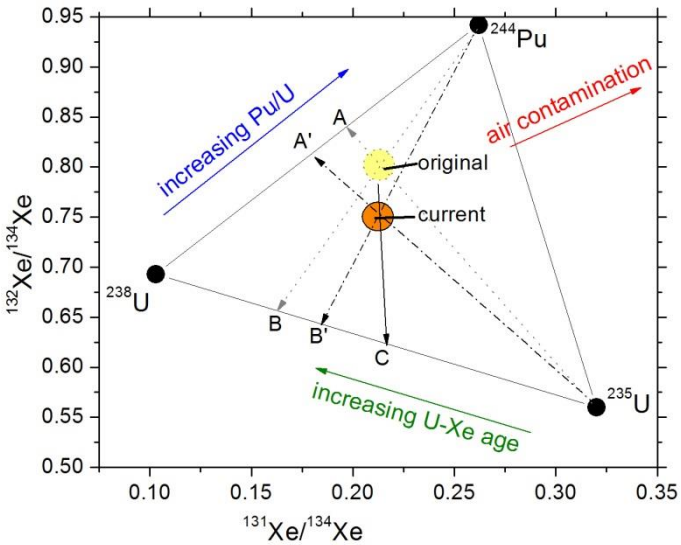

Fig. 5.1: Cartoon of the fission xenon ternary in ^{132}Xe/^{134}Xe vs. ^{131}Xe/^{134}Xe space with the effects of Xe loss on the interpretation of U-Xe age and $(Pu/U)_O$ illustrated, adapted from the discussion of Turner et al. (2007). $(Pu/U)_O$ is along the ^{238}U-^{244}Pu join, and U-Xe age is along the ^{238}U-^{235}U join. In this example Xe-loss history, our hypothetical zircon would without any Xe loss have been found with a Xe isotope composition at "original." The $(Pu/U)_O$ of "original" corresponds to point A, and its U-Xe age corresponds to its crystallization age at point B. The zircon has, however, undergone partial Xe loss at a time corresponding to point C, such that instead we measure a lower $(Pu/U)_O$ (A') and a U-Xe age intermediate between the crystallization and Xe loss ages at point B'.

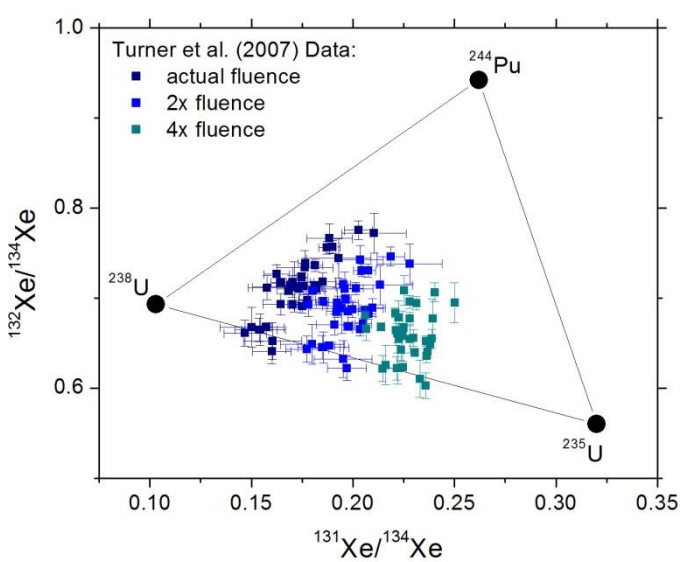

Fig. 5.2: The Xe isotope data of Turner et al. (2007) shown for the actual neutron fluence received, along with projections of the Xe isotope ratios for 2x and 4x the neutron fluence. Error bars from the measured samples are applied also to the modeled compositions. Higher neutron doses move Xe isotope ratios closer to the ^{235}U end-member and cause more spread along the ^{238}U-^{235}U join. Because the U-Xe ages calculated from the isotope ratios will depend on the rate of $^{235}U \rightarrow$ Xe conversion, this quantity varies for each irradiation session and Xe isotope ratios from different irradiations cannot be directly compared.

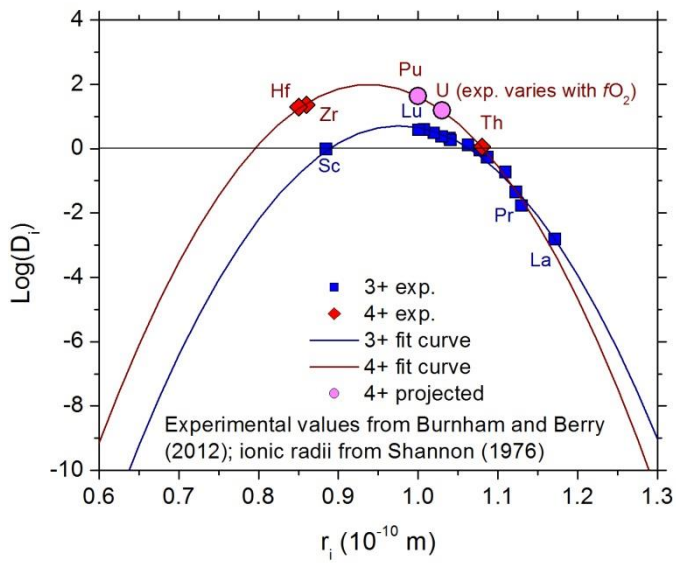

Fig. 5.3: Natural logarithm of zircon/melt partition coefficients plotted vs. ionic radius for several trivalent and tetravalent trace elements that substitute for Zr^{4+} in the zircon lattice. The greater compatibility of the HREE over the LREE and projected compatibilities of the heavier actinides over the lighter actinides are shown. R_i are taken from the crystal radii values of Shannon (1976). Experimental partition coefficient values are taken from Burnham and Berry (2012). Curves are the best-fit parabolas to the experimental data (for trivalent curve, R^2 = 0.983, for tetravalent curve, R^2 = 0.999). We project D_{Pu} and D_U based on their r_i. Burnham and Berry (2012) found that D_U varies with the fO_2 of the system, which may cast doubt on the projected D_U's applicability to Hadean magmas given their unknown fO_2.

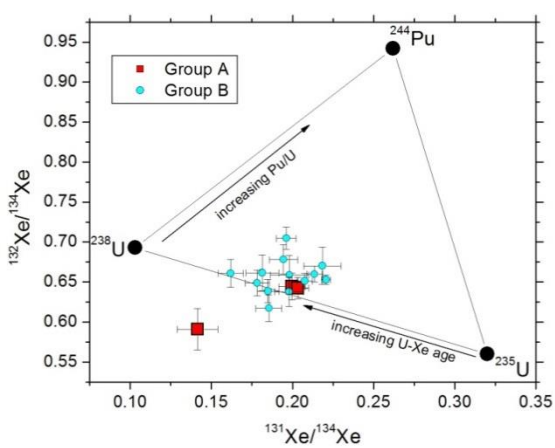

Fig. 5.4: Our data plotted on the fission xenon ternary and classified by trace element groups defined in 5.4.3. Group A has $Nd/U_t > 0.01$, and Group B has $Nd/U_t < 0.01$.

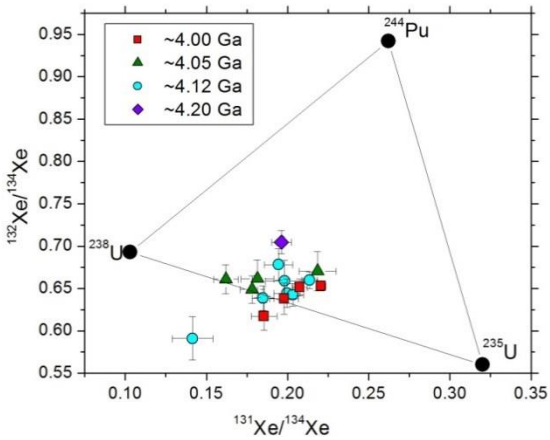

Fig. 5.5: Our data plotted on the fission xenon ternary and classified by $^{207}Pb/^{206}Pb$ age group.

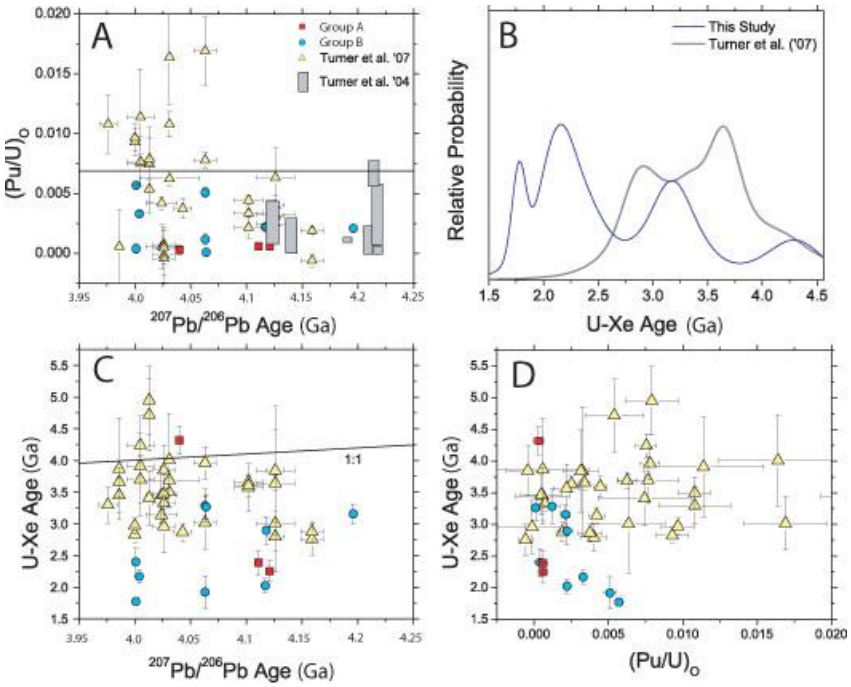

Fig. 5.6: Our U-Xe ages and $(Pu/U)_O$ vs. data from other studies of Jack Hills zircons. Our data are classified by trace element group. A) $(Pu/U)_O$ vs. $^{207}Pb/^{206}Pb$ age. All $(Pu/U)_O$ shown here are calculated using the ^{238}U Xe component. B) Probability density functions for our U-Xe ages compared to Turner et al. (2007). Although there is a large degree of overlap in the U-Xe age ranges, our study yielded previously unseen Proterozoic ages. C) U-Xe vs. crystallization age, showing a slightly larger spread in U-Xe ages among younger zircons but no other obvious patterns. D) U-Xe age vs. $(Pu/U)_O$. Unlike a previous study our data show a slight negative trend between the two parameters.

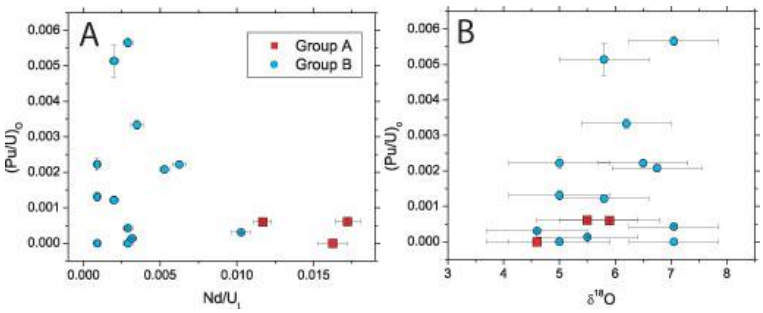

Fig. 5.7: Our zircons analyzed for xenon isotopes (N=11) in xenon-derived and other geochemical variables. The zircons are sorted into their Group A vs. Group B classifications. A) apparent $(Pu/U)_O$ versus Nd/U_t, B) apparent $(Pu/U)_O$ versus $\delta^{18}O$.

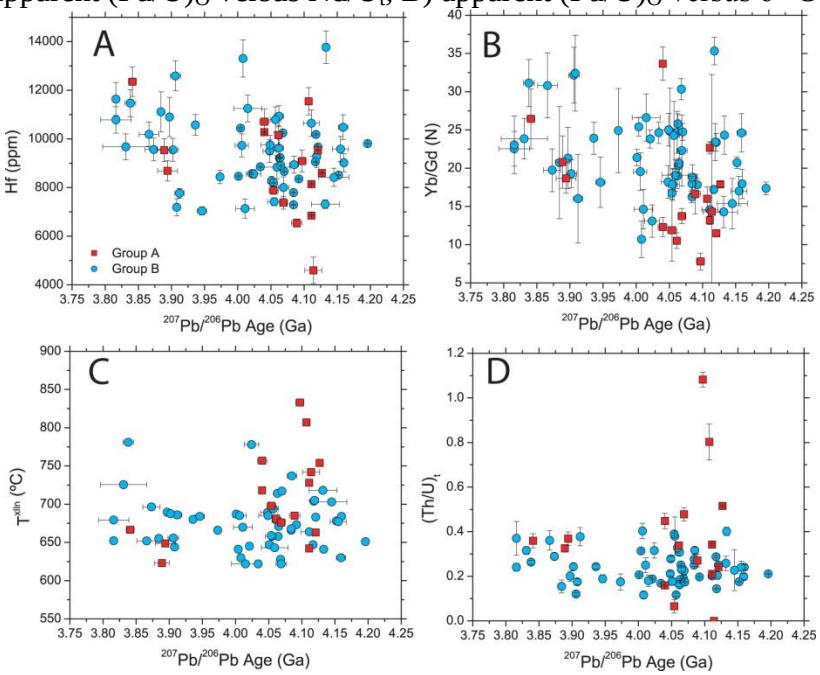

Fig. 5.8:High- and low-Nd/U zircons plotted in crystallization age and various trace elements vs. $^{207}Pb/^{206}Pb$ age. A) Hf; B) Yb/Gd normalized to the chondritic Yb/Gd ratio; C) T^{xlln}; D) Th/U_t.

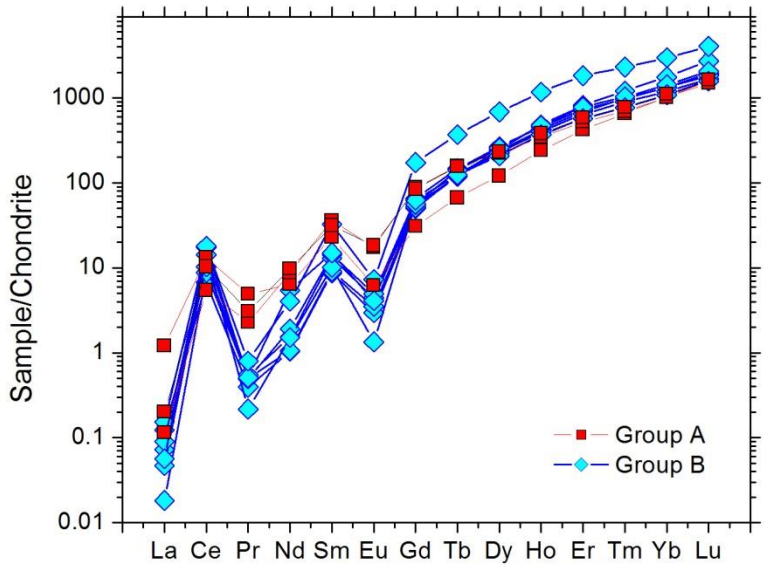

Fig. 5.9: REE diagram for 11 zircons analyzed for Xe isotopes, grouped by Nd/U. Among zircons analyzed for Xe, the high-Nd/U group also shows flatter LREE (lower Ce/Ce* and higher Eu/Eu* than low-Nd/U group) and elevated LREE in general, possibly indicative of aqueous alteration. $\delta^{18}O$ is also somewhat lower in the high Nd/U group (5.15±0.66 vs. 6.11±0.72 ‰), although the groups do not differ in degree of U-Pb discordance.

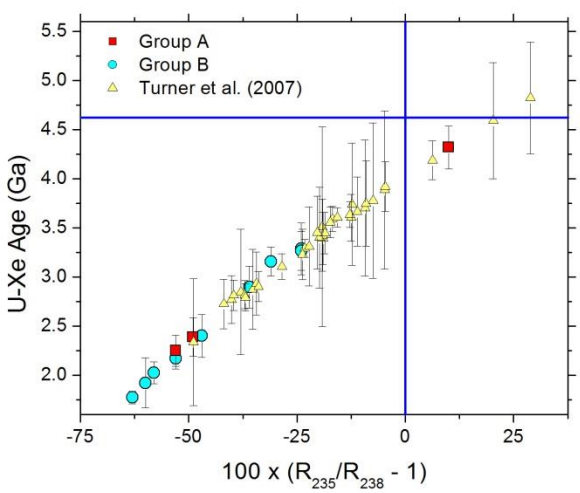

Fig. 5.10: U-Xe age vs. % disagreement between two estimates for $(Pu/U)_O$. The disagreement is computed as 100 x (R_{235}/R_{238} – 1), where R_x is the $(Pu/U)_O$ estimate based on the ^{x}U isotope. Agreement should occur between the two estimates only for very small Xe loss. Very recent Xe loss, while causing no change in the ^{238}U-derived $(Pu/U)_O$ estimate, should nonetheless still show as a much lower ^{235}U-derived estimate.

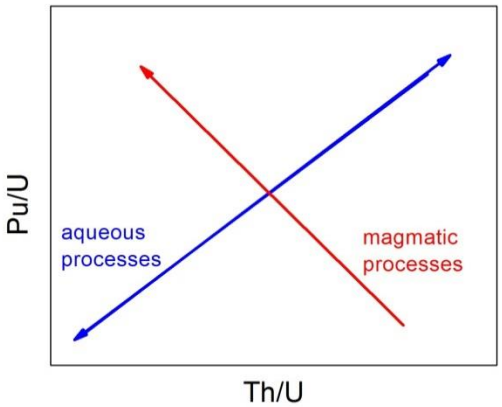

Fig. 5.11: Cartoon of predicted trends in apparent $(Pu/U)_O$ vs. $(U/Th)_t$ for various formation scenarios in zircons without secondary xenon loss.

Chapter Six: Modeling Subduction and Upper Plate Processes in a Warmer Mantle

Abstract:

Hadean and Archean geodynamics are highly controversial. When and how plate tectonics came to define lithospheric dynamics is uncertain, with estimates ranging from ca. 1 to >4 Ga. Different expected manifestations of plate tectonics on a much warmer early Earth make the use of Phanerozoic markers (e.g., blueschist; Stern, 2007) to establish plate tectonics in the geologic record, such as the low-temperature, high-pressure metamorphism unique to subduction zones on the modern Earth, of dubious value. We present preliminary models for intra-oceanic subduction into the warmer mantle expected on early Earth, without prescribed convergent plate motion. Mantle temperatures used range from close to the present value (ca. 1650 K) to the maximum value inferred from petrologic investigations of Archean mantle melts (ca. 1900 K). Mantle temperatures above 1900 K in some models simulate higher Rayleigh numbers for similar mantle viscosity in a 1900 K mantle. Most of our models display a two-sided subduction geometry in which the upper plate is pulled down with the downgoing plate, unlike natural subduction and not allowing for mantle wedge metasomatism and/or island arc development. Some models at very high mantle temperatures do display true one-sided subduction briefly before transitioning to two-sided. In addition, a variety of slab geometries develop, resulting in trench retreat, advance, or sequential combination of the two, and vary by the mantle temperatures and maximum lithospheric viscosities employed in the model. Despite many of the unrealistic aspects of the model, we have identified subduction-like versus non-subduction-like regimes among plates and outline some of their consequences for the upper plate thermal structure and mechanical evolution. Thermodynamic modeling with Perple_x can help identify

petrologic consequences for upper plate forearc lithologies, including the preservation of the low-T/high-P materials that are often sought in the geologic record as evidence for subduction.

6.1. Introduction: When did plate tectonics begin?

One of the notable ways in which Earth differs from other planets in our solar system is that its lithosphere is broken into rigid plates that move relative to each other. Plate tectonics is the surface expression of the mantle convection by which our planet loses heat to space; other terrestrial bodies in the solar system appear to instead lose heat by way of stagnant lid mantle convection, with effectively one lithosphere-wide plate (Sleep, 2007), or pure conduction (i.e., the Moon). The thermal history of the mantle is tied to its convection regime, with differing scaling relationships resulting in vastly different heat loss efficiencies (Sleep, 2007; Korenaga, 2013). Thus understanding when plate tectonics began on Earth is key to understanding the early history, not only of the crust, but also of the deep mantle.

Broadly speaking, the onset of plate tectonics is generally linked to the beginning of subduction (*e.g.*, Stern, 2007). Accordingly, searching for early evidence of plate tectonics involves the specific identification of what are presumed to be markers of ancient subduction zones, including ophiolites and low-temperature, high-pressure facies such as blueschist and eclogite (Stern, 2007). Recently, Shirey and Richardson (2011) surveyed diamond inclusion assemblages in kimberlites and found that whereas peridotitic and eclogitic assemblages occur since ca. 3 Ga, only the former are preserved in older diamonds. Thus they inferred that the Wilson Cycle and subduction became a prominent tectonic process at ca. 3 Ga such that metabasaltic and -sedimentary rocks could be brought to, and incorporated within, continental lithosphere. However, it remains possible that in a warmer early mantle, the requisite low-

temperature, high-pressure conditions did not exist in the upper plate such that captured subduction-related eclogites were not preserved – biasing the eclogite record of subduction towards a later onset of subduction in the cooling mantle.

Subduction zones also contribute to continental evolution in several ways. They produce magmas with characteristic chemical compositions similar in many aspects to the continental crust, and so are thought to be major loci of crustal growth (*e.g.* Rudnick and Gao, 2003). They also contribute to continental recycling, as continental-derived sediments are carried atop the subducting slab and into the mantle. However, the question of whether subduction can occur in the warmer mantle expected for the Archean and Hadean has been controversial (*e.g.*, Davies, 1992; cf. Davies, 2006) with at least one workers even point to the Neoproterozoic as the onset of the modern plate tectonic regime (Stern, 2007).

In this chapter, I present the results of a computational study modeling the behavior of oceanic slabs under thermal conditions thought appropriate for the Hadean and early Archean eons. We evaluate the likelihood of Hadean-Archean subduction based both on whether subduction can be maintained under mantle potential temperatures of 1800-3200K and whether the modeled thermal effects in the upper plate and slab/mantle wedge interface are consistent with the lithologies and apparent heat flows inferred from Hadean and Archean samples. We additionally look for possible regimes intermediate between subduction and non-subduction tectonics.

6.1.2 Subduction versus subduction-like regimes

It is likely that regimes may exist that are intermediate between stagnant-lid, one-plate mantle convection and modern subduction. Underthrusting environments that resemble modern

subduction in only some ways may well have made up convergent plate boundaries in the early Earth, owing to higher heat flows from a warmer mantle. Sizova et al. (2010), for instance, model the forced subduction of an oceanic slab underneath a continental margin under higher heat flows and find a "pre-subduction" style of underthrusting tectonics. This occurs, in their models, at ~160-250 K above the present mantle potential temperature. Above ~250 K over the present temperatures, no subduction-like processes occur. Sizova et al. (2010) attribute the differing tectonic behaviors to the weakening of plates by sub-lithospheric melts in the warmer mantle. Owing to this plate weakening, the pre-subduction regime does not support the development of high topography; mountain belts and plateaus >1500 m in height occur only in the modern subduction regime. This is a similar result to that of Rey and Coltice (2008) for Archean lithospheric strength under higher mantle heating and its inhibitory effects on the development of mountain belts and orogenic plateaus. The effects on intra-oceanic arcs have not been studied, and the existence of similar "pre-subduction" and "no-subduction" regimes would be useful to compare to the forced, ocean-continent subduction zone of Sizova et al. (2010).

6.1.2. Surface expressions of various plate regimes

In considering the sparse early Archean rock record and the Hadean mineral record, identifying subduction versus other regimes is difficult but may be possible. Several of the lines of evidence for subduction, presented in section 1.1 above, can be applied. Given the highly metamorphosed nature of much of the Archean rock record and the *ex situ* nature of detrital mineral records, aspects of geochemistry that survive alteration are most likely to be helpful. Helpfully, the mineral zircon is largely resistant to alteration and forms the bulk of our early detrital mineral record.

The applicability of inclusion assemblages in detrital zircons to diagnosing subduction versus other tectonic environments is somewhat precarious. Geothermobarometry on zircon and hosted mineral inclusions has been used to argue for a low heat flow (and therefore underthrust) environment for the >4 Ga Jack Hills zircon source terrane(s) (Hopkins et al., 2008, 2010). However, this implies knowledge of the global Hadean heat flow, of which estimates range over a factor of four (Sleep, 2000; Korenaga, 2008).

Zircon is ubiquitous in granitoids of virtually all tectonic settings (Dickinson, 2008). Assessing zircon provenance by trace element chemistry (e.g., Belousova et al., 2002; Grimes et al., 2007; Trail et al., 2007b) is mostly useful for discriminating felsic from mafic and ultramafic sources (Grimes et al., 2007), with discrimination among the various granitoids less certain (Hoskins et al., 2000). Although it would be useful to have a diagnostic test with which to distinguish, say, calc-alkaline versus TTG granitoids, such a tool does not presently exist.

The most salient difference between geodynamic models for a warmer mantle and that of the modern Earth is the inability of the former to create significant topography (Sizova et al., 2010). This feature will be investigated in this study and compared to preserved environmental features in the Archean rock record and Hadean mineral record, particularly P-T indicators. Unlike the study of metamorphic rocks in which petrography and chemistry can elucidate prograde or retrograde P-T-t paths , *ex situ* zircons with the proper (primary) mineral inclusions can only record a snapshot in P-T space, which is generally assumed to correspond to crystallization. However, the aggregate of many such snapshots can still be useful in shedding light on the source terrane geotherm(s) (Hopkins et al., 2008, 2010).

The style of subduction also has implications for the availability of protolith(s) to form zircon-bearing magmas. The highly variable geometry and character of subduction zones, lead to numerous ways for the upper plate to deform or host magmatism (Stegman, 2010). Subduction in an advancing arc can recycle old crust from the upper plate into the mantle, a process called *subduction erosion*. Subduction zones are accompanied by magmatic arcs, which manifest juvenile radiogenic isotope signatures when in retreat or not involving continent-continent collision. Although there are multiple mechanisms for producing juvenile crust outside of subduction zones, mantle-like isotopic signatures (e.g., Lu-Hf) clearly distinguish juvenile from ancient recycled crust and Phanerozoic subduction-related orogens tend to produce characteristic temporal patterns of Hf isotope evolution (Collins et al., 2011; see also this study, ch. 4).

6.2. Modeling Subduction and Mantle Circulation

Numerical modeling of subduction mechanics and its relation to arc magmatism have had varying degrees of success in simulating known aspects of Earth's behavior. Some models can replicate the geometry of slabs in natural subduction zones and its relation to relative trench motions (*e.g.*, Stegman et al., 2010), while others have shown the melting behavior and resulting crustal growth in continental arc settings with great detail (Vogt et al., 2012). Questions remain regarding how to generate consistent Earth-like asymmetric subduction, initiate subduction, and even whether subduction on the Hadean and Archean Earth is feasible. Global geochemical models for mantle circulation have yielded insights into the development of mantle geochemical signatures, but are unable to replicate all observed isotopic anomalies (e.g., Xie and Tackley, 2004) and usually do not include realistic earth-like subduction (Gerya, 2011). Challenges

remain in implementing realistic subduction zones to usefully model geochemistry in terrestrial mantle circulation.

6.2.1 One-Sided Subduction

An important and unique feature of subduction is its asymmetric nature – the overriding and downgoing plates move independently, with only one slab sinking. Only models emphasizing very low friction between the plates have been successful in replicating this feature (*e.g.*, Gerya et al., 2008). Except in such specialized scenarios, numerical models of subduction tend to evolve towards two-sided scenarios. Gerya et al. (2008) find that in order to sustain one-sided subduction, numerical models require a weak interface between the downgoing and overriding plates, building off earlier studies (e.g., Hassani et al., 1997; Hall et al., 2003; Sobolev and Babeyko, 2005) that showed the need for an effective friction coefficient of <0.1. Gerya et al. (2008) also find that strong plates are necessary, as weak plates will tend toward two-sided subduction. "Strong" plates are here defined as those for which $\sin(\phi) > 0.15$ (ϕ is the effective angle of internal friction and varies both with brittle strength and with pore fluid pressure λ as $\sin(\phi) = \sin[\phi_{dry}]\ [1 - \lambda]$). The weak interface between plates requires $\sin(\phi)$ approaching zero. Most models of global mantle circulation include "subduction" in which the two lithospheric plates sink into the mantle together either as a symmetrical or asymmetrical downwelling (Gerya, 2011). Such two-plate subduction zones do not replicate many of the salient features of terrestrial subduction, including the ability of the slab to dewater and hydrate the mantle wedge. For models that realistically take into account subduction zones in the context of crustal growth, then, modeling of Earth-like one-sided subduction is necessary.

6.2.2 Slab Geometry and Subduction Regimes

Various subduction styles exist both on Earth and in numerical simulations, and are often classified by the velocity of the trench relative to the downgoing slab. Most presently active subduction zones exhibit trench retreat, in which the trench moves horizontally in the direction opposite to the downgoing slab. This exerts tensile stress on the overriding plate and often leads to rifting or seafloor spreading in the backarc region. Relatively few subduction zones on Earth today exhibit trench advance, in which the trench moves horizontally in the same direction as the downgoing slab (e.g., Andes), exerting compression on the overriding plate. Trench velocity is the surface manifestation of various processes affecting slab geometry during subduction. Various slab geometries are possible. For example, Stegman et al. (2010) carried out 3D simulations of free subduction to determine systematically the conditions under which these various subduction regimes will operate. They find that the two most important factors controlling subduction regime are the Stokes buoyancy of the slab and the slab's effective flexural stiffness. Stokes buoyancy (B_S) is defined as the ratio of the slab's volumetric potential energy to the viscosity of the upper mantle:

$$B_S = \Delta\rho \cdot g \cdot h_{plate}/\eta_{um} \tag{6.1}$$

Where h_{plate} is the thickness of the slab, η_{um} is the viscosity of the upper mantle, g is the gravitational acceleration, and $\Delta\rho$ is the density contrast between plate and upper mantle. Effective flexural stiffness (D_{vis}^*) is the strength of the plate relative to the upper mantle:

$$D_{vis}^* = (\eta_{plate}/\eta_{um}) \cdot (h_{plate}/H)^3 \tag{6.2}$$

where η_{plate} is the slab viscosity and H is the depth of the upper mantle. Stegman et al. (2010) find that a continuously retreating trench, where the plate drapes across the top of the lower mantle as it subducts, occurs for weak (low effective flexural stiffness) plates with a relatively

high B_S. Advance-fold-retreat mode occurs at somewhat lower D_{vis}^* and B_S and involves an initial stage of trench advancement. The slab then forms a recumbent fold atop the lower mantle, continuing in retreating-trench mode. Stiff plates with low B_S are alone characterized by continuous trench advance, which occurs because the slab comes to rest upside-down on top of the lower mantle and continues to subduct this way, pulling the trench forward. Weak plates with low B_S show continuous folding, forming a slab pile atop the lower mantle. This manifests at the surface in sequential cycles of trench retreat and advance.

6.3. Questions

Much of what we can model geodynamically for the early Earth will not be preserved in rock and mineral records, so testability will limited to those few cases associated with rock forming events. However, use of isotopic tracers and attention to geotherms in the upper plate does give us an opportunity to test scenarios using mineral and rock records (e.g., Hopkins et al., 2010). Accordingly, although most of the questions addressed in this study will be theoretical implications on Hadean-Archean tectonic regimes, some may be testable against the Hadean and early Archean zircon record. Specific questions include:

1. Do models which lead to subduction of oceanic crust under today's conditions also lead to subduction under likely Hadean-Archean mantle temperatures? What about no-subduction and subduction-like regimes?
2. Are there thermal transitions among different styles of geodynamics and plate interactions, or instead smooth variations among styles with changing temperature?
3. Is the Jack Hills zircon record (granitic melting conditions with apparently low heat flows) compatible with any of these regimes?

4. Can the observation of eclogitic inclusions in continental mantle xenoliths after, but not before, ca. 3 Ga be explained by subduction in a warmer mantle?

6.4. Methods: Subduction and Mantle Modeling with StagYY

StagYY is a finite difference code for mantle convection developed by Paul Tackley (Tackley, 2008), and was previously used by Xie and Tackley (2004) to create forward models for mantle convection that incorporate various isotopic tracers. We undertook preliminary modeling for subduction under a warmer mantle, focusing on exploring various parameters' (slab thickness, overriding plate thickness, η_{max}, T_m) influence on subduction occurrence and style in this fairly simple model. We do not prescribe convergent plate motion but allow downwelling to develop following an initially prescribed downward flexure of one plate. We use a subduction zone geometry most appropriate to ocean-ocean convergence: a downgoing plate with an initial perturbation beneath the surface of 200 km and a radius of curvature of 400 km. A horizontal gap between our upper and lower plates of 50 km is prescribed. Downgoing and overriding plate thicknesses were prescribed for each model run, with downgoing slab thicknesses of 50, 100, or 200 km (corresponding to various modeled plate thicknesses for the early Earth). Most runs included a 50 km-thick upper plate, although several model runs with 25 and 100 km upper plate thicknesses were also included. Although the viscosity of the lithosphere would be quite high if it were determined only by its temperature, what is relevant for subduction is an effective viscosity that represents the finite strength of the lithosphere. We vary the maximum viscosity (η_{max}) of each model, which allows for variations of the viscosity contrast between the lithosphere and asthenosphere. For the modern Earth, η_{max} is estimated to be about 5×10^{21} Pa·s (Liu and Stegman, 2011), giving a viscosity contrast of 100. The asthenospheric upper mantle has a uniformly lower viscosity (η_{um}) set by its temperature that is limited by a minimum value

of 10^{19} Pa·s for all models. The reference viscosity for all models is set to 2 x 10^{20} Pa·s, which is anchored at a temperature of 1650 K (and will decrease with T_m down to the minimum value). Downgoing and overriding plate thicknesses were prescribed for each model run. We undertake this thermal model in a Cartesian, 2-dimensional 2000 x 600 km box, which represents the upper mantle. We did not consider the effects of partial melting. The model ran for ~15-30 Ma of modeled time. Table 6.1 lists the plate configurations used in the Cartesian models and Fig. 6.1 shows several of the initial geometries employed (T_m = 1650 K; temperature is contoured). Further information on the parameters employed in our models can be found in Appendix I.

We also use Perple_x, a collection of Fortran 77 codes for petrologic thermodynamic calculations, to predict the phase relationships, melting behavior, and densities of various lithologies for higher T_m conditions. We carry out these calculations for a MORB bulk composition (based on the average of GeoROC MORB compositions) to search for the stability region of eclogitic materials formed from a variety of lithologies relevant to hypothetical Archean-Hadean subduction zones.

6.5. Results

We ran Cartesian models with η_{max} ranging from 1 x 10^{21} to 2 x 10^{23} Pa·s. Mantle temperature T_m ranges from the approximate modern value of 1650 K to 3200 K. Based on petrological estimates of past mantle temperature (Abbott et al., 1994; Herzberg et al., 2010), we divide the models into those with observed Phanerozoic-Archean T_m 1650-1900 K and those which use T_m well above Archean estimates (1950-3200 K) in order to observe the effects of higher Rayleigh numbers (independent of viscosity changes) in a 1900 K mantle. Since the minimum allowed viscosity is 10^{19} Pa·s, which in this setup corresponds to a mantle temperature

of 1900 K, models with T_m > 1900 K do not account for further reduction in mantle viscosity. Thus, increasing mantle temperatures above 1900 K only influence the dynamics through increasing the negative buoyancy of the plate/slab due to the larger temperature contrasts between the lithosphere and asthenosphere. The thickness of the downgoing and upper plates were both important factors in model evolution, and each plate configuration is also considered separately. Models evolve to a variety of slab geometries, examples of which are shown in Fig. 6.2.

6.5.1 Cartesian Model Results, T_m = 1650 – 2000 K

Figure 6.3 presents results for those models with a downgoing slab 100 km thick, similar to modern oceanic lithosphere, and a 50 km overriding plate over a range of η_{max} of $1x10^{21}$ to $2x10^{23}$ Pa·s. Figure 6.4 similarly shows results for the four 100 km/100km model runs. We identified a variety of slab behaviors. All models in this T_m, η_{max} range result in subduction of material dominantly from the lower plate but also from the upper plate, such that truly one-sided subduction is not attained within our studied parameter space (although some models do not result in subduction at all). "Non-subduction behavior" noticed in some model runs includes two-sided amorphous downwellings, loss of slab cohesion resulting in spreading across the lower interface of the box, and development of secondary downwellings (the latter being most common at higher T_m and lower η_{max}). In many models the downgoing slab subducted but did not reach the lower interface within the 15-30 Ma represented in the model runtime. In the majority of models at intermediate η_{max}, the downgoing slab reached the lower interface and lay upon it rightside up, inducing a retreating motion of the trench relative to the upper plate. In the η_{max} = $1x10^{21}$ Pa·s, $T_m \geq$ 1900 K model runs, these conditions co-occur. At higher η_{max} and higher T_m,

the downgoing slab often lay upside down on the lower interface, causing the trench to advance relative to the upper plate.

Figures 6.5 and 6.6 contrast the behavior of a 50 km downgoing slab with upper plate thicknesses of 50 km and 25 km, respectively. Although non-subduction behavior dominates for the 50 km-50 km models at $\eta_{max} \leq 3x10^{22}$ Pa·s, models with the thinner upper plate show an increased field of rightside-up subduction at higher T_m. $3x10^{22}$ Pa·s models at lower T_m also display slab breakoff rather than continuous subduction. We did not undertake model runs with this plate configuration at higher η_{max}. Similarly, Figures 6.7-6.8 show the behavior of a 200 km slab with upper plate thicknesses of 50 km and 100 km, respectively. Most 200/50 models display simultaneous non-subduction behavior and slabs that lay rightside up on the lower interface. Model runs with high η_{max} display straightforward subduction behavior, mostly with rightside-up subduction. Intermediate T_m, high η_{max} model runs display upside-down subduction. Similar behavior occurs in the 200/100 models, but with upside-down slab behavior occuring even at lower η_{max}. These results show that not only slab thickness but also the interaction between the upper and lower plates is important for setting slab behavior in the Cartesian model.

For all Cartesian model plate configurations, subduction-like behavior is most common at high T_m and higher η_{max}. Models at lower η_{max} tend toward non-subduction behaviors. Overall, a thicker downgoing slab promotes subduction-like behavior in the models. Runs with 50 km downgoing slabs display an increased field of non-subduction behaviors that ranges to higher η_{max}, while 200 km slabs display subduction-like behavior throughout the studied model η_{max}, T_m space (although at lower η_{max} it co-occurs with non-subduction-like processes). However, the effects of slab thickness are also mediated somewhat by the thickness of the overriding plate,

suggesting that interactions between the two plates are important: a thinner overriding plate widens the field of subduction-like behavior for a 50km lower plate. Due to the truncated parameter space over which we ran 200/100 models, it is not clear whether the same holds for 200 km lower plates.

Four models with 100 km lithosphere for both the downgoing and upper plates show somewhat different results (Fig. 6.4) and hint at a shrinking of the η_{max} range where subduction can occur, but this is inconclusive at present given the small number of models run with this geometry.

6.5.2 Cartesian Model Results, Higher Rayleigh Numbers

Petrologic estimates of Archean mantle temperatures (Abbott et al., 1994; Herzberg et al., 2010) show a maximum of ca. 1900 K, although several theoretical models – mostly those including a "thermal catastrophe" – suggest Archean temperatures in excess of this range. This is also the T_m corresponding to η_{min} (see fig. 6.9). For several models, we set "T_m" values of 1950 – 3200 K, but since the viscosity of the mantle does not decrease accordingly, these models do not test the effects of higher mantle temperatures in a self-consistent manner. Instead we use these as test of higher Rayleigh number mantle convection at T_m = 1900 K – the higher ΔT creating this effect. Given that such temperatures will be in excess of the peridotite solidus for much of the upper mantle, effects of partial melting for models with these temperatures would be important. Our model does not deal with partial melt, focusing instead on the effects of higher-Ra mantle convection.

Several of these models yielded temporary one-sided subduction (see Fig. 6.10). Models with the 100 km subducting plate/50 km upper plate geometry cover the largest T_m-η_{max}

parameter space, with 50 km/50 km and 200 km/50 km having nearly as complete coverage up to 2800 K. The 50 km/25 km and 200 km/100 km models cover parameter space more sparsely but also show many effects of the increased T_m. Slab breakoff begins to become important for 50 km slabs at these T_m, and most 100-200 km (subducting plate) models show one-sided subduction for a substantial portion of the model time before the plates eventually couple such that the overriding plate is also carried downward.

6.5.3 Perple_x Results

Fig. 6.11 shows phase stabilities for a dry MORB (average of MORB from GeoROC database) as calculated using Perple_x. Contours are for volume % of various phases in the rock (black=melt, orange=plagioclase, blue=garnet; see figure caption for more information). Eclogite facies is rich in garnet, and plagioclase is absent. Garnet is stable in most of the higher-pressure portions of this slice of P-T space, although it lessens in abundance at higher temperatures and becomes zero at ca. 2000 K. This likely represents a maximum temperature of eclogite stability in a 100 km thick lithosphere. The quantitative P-T structure of the arc and forearc region for each model will be needed to determine eclogite stability more directly.

6.6. Discussion

The speed and geometry of subduction/downwelling in the Cartesian, melt-free model appears to be mainly controlled by the viscosity contrast between the slab and ambient upper mantle and the thickness (probably – weight) of the slab. Although most models yield two-sided downwellings rather than true one-sided subduction, the interaction of the downwelling slab with the lower interface mimics many aspects of the slab/lower mantle interactions noticed by Stegman et al. (2010). Minimum viscosity contrasts for slab cohesion may also be seen.

The models run with T_m > 1900 K do not model these mantle temperatures self-consistently, since mantle viscosity reaches a minimum at 1900 K. Instead, by increasing the ΔT ($T_m - T_{surface}$), these models increase the Rayleigh number

$$Ra = (\rho \cdot \alpha \cdot \Delta T \cdot g \cdot H^3)/(\eta_{um} \cdot \kappa) \quad (6.3)$$

(where ρ is density of the modeled material, α is thermal expansivity, H is mantle thickness, and κ is thermal diffusivity) to yield higher convective vigor in effectively a 1900 K mantle (based on the viscosity). The relationship between Rayleigh number and T_m in our models is shown in Fig. 6.9B.

In terms of Rayleigh number consequences, this would be mathematically equivalent to, for example, increasing ρ. Higher ΔT in these models will also increase the density contrast between the slab and mantle, increasing slab negative buoyancy and also promoting faster subduction. Higher subduction speeds allow some models to remain one-sided for substantial portions of model time (see Fig. 6.10 D, E).

6.6.1 One-sided subduction

Two-sided subduction dominates in our Cartesian models, unlike subduction on the modern Earth (see Fig. 6.10). With lower T_m and lower η_{max} the slabs tend to form symmetrical downwellings. However, at higher T_m and higher η_{max}, the downwellings tend to be more asymmetrical and the slabs to remain cohesive within the mantle, interacting with the lower interface in a similar manner to subducting plates. This effect is strongest with thicker slabs and weaker for the thinner, 50 km downgoing plates. In the T_m > 1900 K (high Rayleigh number) models, true one-sided subduction with independently moving plates occurs for a time, although eventually the downgoing and upper plates couple. The dependence on higher Rayleigh number

suggests that this is probably largely due to the faster plate motion this allows – fusion by thermal coupling does not occur until much of the original slab is already subducted, but fusion leading to subduction of the upper plate occurs eventually in all models.

In order to produce truly one-sided subduction, the model will require modifications. The designation of a very low-friction zone between the two plates may be necessary (as in the solution of Gerya et al., 2008). The likely source of this low-friction interface in subduction zones is water-rock chemical reactions, which are not included in our model. If, however, the subduction-like behavior of the cohesive slabs at higher η_{max} can be compared to real-world subduction zones and the previous models of Stegman et al. (2010), then we can argue that subduction is indeed not only possible but quite stable in a warmer mantle given a thick enough subducting slab. Thinner slabs exhibit subduction-like behavior only when the Rayleigh number is also increased (T_m = 1900 K). Given the Rayleigh number dependency, theoretically, thin but unusually dense slabs could subduct readily as well. However, we have not modeled the effects of specific densities on model evolution.

6.6.2 Subduction styles in a warmer mantle

For a slab similar in thickness to modern oceanic lithosphere, subduction-like behavior (albeit 2-sided) is possible in the Cartesian model under warmer mantle temperatures, and its field of stability in lithospheric η_{max} is in fact increased by higher T_m. This probably points to the viscosity contrast between lithosphere and asthenosphere as a crucial parameter in the formation of a subduction zone and determination of its geometry (as also found by Stegman et al., 2010, for a 3-d model of free subduction using a different code). Higher T_m lowers the viscosity of the ambient mantle, allowing less viscous lithosphere to still behave in a subduction-like manner.

Thicker slabs (200 km) show an expansion of the field of subduction stability into lower η_{max}, although this is accompanied by non-subduction-like downwellings elsewhere in the modeled space. Thinner slabs (50 km), however, only show subduction-like behavior at $\eta_{max} \geq 3 \times 10^{22}$ Pa·s except for the high-Ra models. Most models of Archean oceanic lithosphere posit a thicker crust, arguing that higher mantle temperature leads to a thicker melting column and ultimately more melt produced (cf. Davies, 2006, which postulated a highly depleted early upper mantle and thus a thinner oceanic crust). The mantle lithosphere may be thicker or thinner based on whether its thickness is controlled only by temperature (thinner, then, for higher T_m) or by the thickness of the melt-depleted mantle left behind by partial melting (thicker). It is likely that strong lithosphere of 200 km thickness could not exist in a mantle several hundred degrees warmer than the present day, so the 200 km downgoing slab models may be useful mainly for comparison of model behavior rather than applicable to the early Earth.

Our model does not differentiate mechanically between the crust and mantle lithosphere, but considers only the plate's thickness. For the Cartesian model, subduction is favored for thicker plates at all studied T_m (as defined by the range in η_{max} over which subduction is observed). Notably, though, we begin each model with the downgoing plate already deflected below the surface, overcoming some of the difficulty of initiating subduction with thicker plates.

Subduction geometries observed include slabs which lay rightside up on the lower boundary (corresponding to a retreating trench), slabs which lay upside down (corresponding to an advancing trench), and slabs which fold but may favor either advancing or retreating mode. For the 100 km downgoing slab, retreating mode appears to be the dominant slab behavior, although there is a field of advancing mode at intermediate T_m and high η_{max}. Advancing and folding behaviors appear to dominate for 50 km slabs when they achieve subduction-like

behavior at all (only in the 1900 K, high-Ra models), while advancing trenches are rare for 200 km slabs (possibly due to the difficulty of bending them sufficiently at the lower interface).

6.6.3 Eclogite production and preservation in a warmer mantle

Eclogite production occurs in subduction zones but must be preserved in the upper plate in order to be sampled via explosive volcanism. Most likely this requires a trench in the retreating mode. Such subduction zones are less likely to undergo subduction erosion of the forearc region and thus are more likely to preserve products of the low heat flow subduction environment. P-T conditions for garnet stability in metabasalts are shown in Fig. 6.11 based on average MORB and can be found in the forearc and slab regions at lithospheric temperatures up to ca. 2000 K. Defining eclogite (somewhat arbitrarily) as >20 volume % garnet (based on minimum garnet contents of eclogites from Sierra Leone by Fung and Haggerty, 1995), this makes eclogite stable up to ca. 1700 K. Given our present uncertainty as to the thermal structure of the trench and forearc, the maximum T_m remains uncertain, but will be higher than ca. 1700 K (since the forearc region is refrigerated by the downgoing slab). Determination of a high-T_m limit for eclogite preservation, combined with information on the likely slab geometries at this T_m, will help to determine if the eclogite is likely to be preserved or to be destroyed by subduction erosion. Given that with higher temperatures the field of advancing slab geometry increases, several factors will favor low T_m for eclogite preservation.

6.7. Conclusions

We have explored much of the η_{max}-T_m parameter space in our preliminary 2-D Cartesian model of free subduction with several initial slab geometries. For subducting slabs of modern thickness (ca. 100 km), warmer mantle temperatures expand the field of lithospheric viscosity in

which subduction is possible, although for the range of temperatures inferred from petrologic investigations of Archean mantle melts all of the model runs produced two-sided rather than Earthlike one-sided subduction. The majority of runs displayed trench retreat, with the exception being some advancing-trench runs at intermediate T_m (1850-1900 K and in the higher-Ra models) and high η_{max}. Thinner plates (here, 50 km) were less likely to subduct at all T_m, but also displayed an increased range of subduction stability in η_{max} with increasing T_m. None of our 50 km models displayed one-sided subduction, and many displayed slab breakoff events that effectively ended subduction. They were also more likely to display folding geometry (trench advance-retreat cycles). Thicker plates (200 km) were more likely to subduct at all T_m and to show retreating trenches. The preservation of subduction-related lithologies such as eclogite on the upper plate is tied both to the thermal structure of the forearc region – whether the eclogite will remain eclogite over geologic time – and whether the downgoing slab is eroding material from the forearc, which is more likely with an advancing trench. Perple_x results for MORB indicate that for many observed Phanerozoic-Archean mantle temperatures a chilled forearc will likely be in the eclogite facies (more certain results await a more certain determination of forearc thermal structure). Since lower η_{max} tends to lend itself to trench retreat with modern slab thicknesses, less viscous slabs for a given T_m may be preferred to preserve eclogite.

Chapter Six Tables and Figures

η_{max}, T_m Range (Pa·s, K)	Slab Thickness (km)	Upper Plate Thickness (km)
$1x10^{22}$-$3x10^{22}$, 1650-2800	50	25
$1x10^{21}$-$1x10^{23}$, 1650-2800	50	50
$1x10^{21}$-$2x10^{23}$, 1650-3200	100	50
$3x10^{22}$, 1650-1950	100	100
$1x10^{21}$-$1x10^{23}$, 1650-2800	200	50
$1x10^{22}$-$3x10^{22}$, 1650-2800	200	100

Table 6.1: Plate geometries used in Cartesian models.

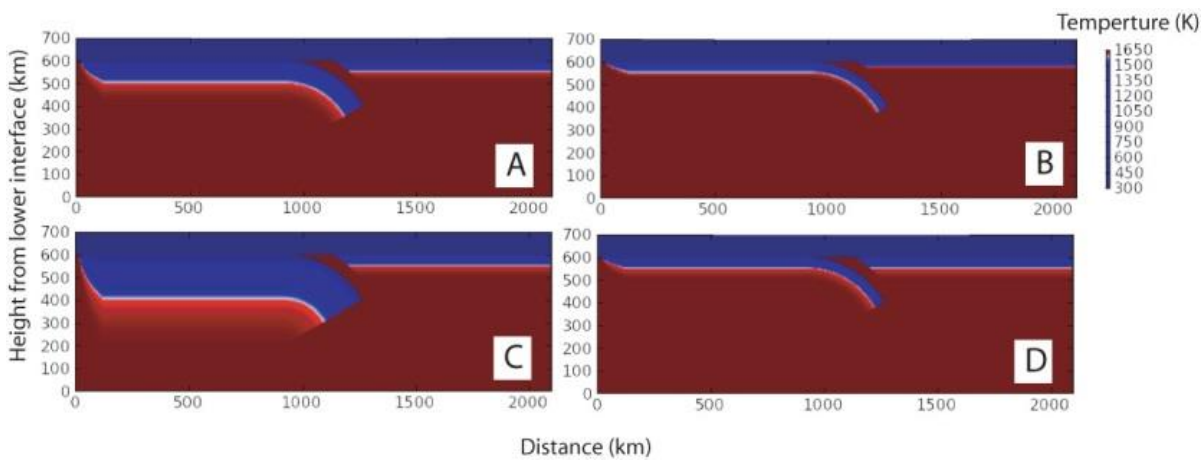

Fig. 6.1: Initial plate geometries for models with 1650 K background T_m. Temperature is contoured. Surface is at 600 km; above is 100 km of "sticky air" to form a free surface. Image output by StagYY. A) 100 km slab thickness, 50 km upper plate thickness; B) 50 km slab, 25 km upper plate; C) 200 km slab, 50 km upper plate; D) 50 km slab, 50 km upper plate. Models with 100 km slab/100 km upper plate and 200 km slab/100 km upper plate are not shown.

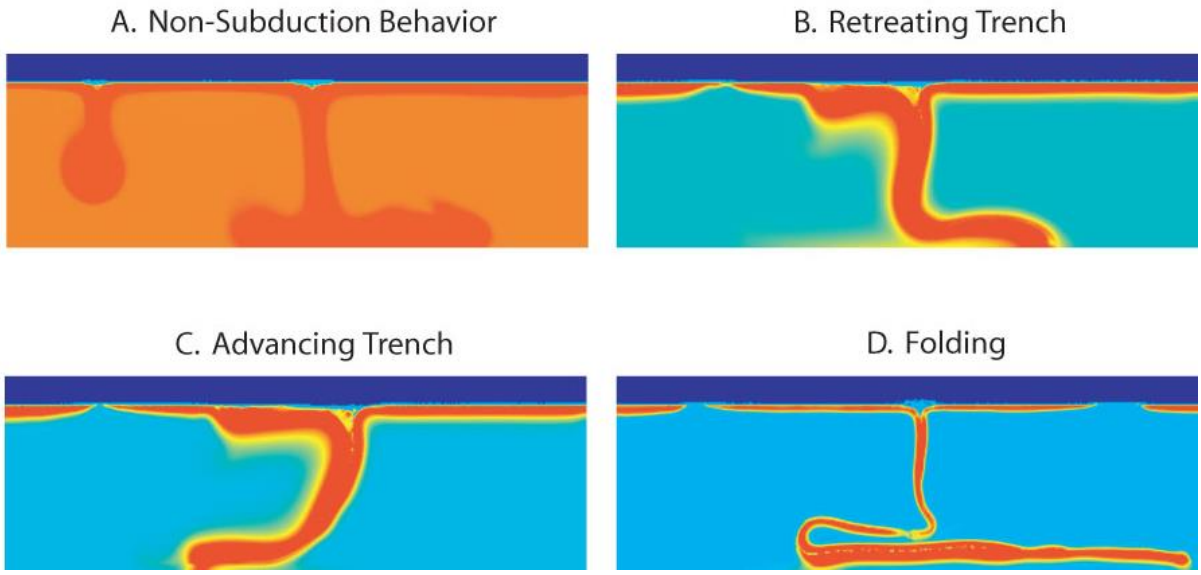

Fig. 6.2: Different slab geometries resulting from the various model conditions. Images are StagYY output with viscosity contoured (red=high, blue=low). A) non-subduction-type downwellings, 100 km slab/50 km upper plate model with T_m = 1700 K and η_{max} = 1 x 10^{21}Pa·s. B) Retreating-trench subduction, with slab lying rightside up on lower boundary. 100 km/50 km model; T_m = 1850 K, η_{max} = 2 x 10^{22}Pa·s. C) Advancing-trench subduction; slab lies upside down on lower boundary. 100 km/50 km model; T_m = 2000 K, η_{max} = 3 x 10^{22}Pa·s. D) Folding-slab subduction. 50 km/25 km model; T_m = 2800 K, η_{max} = 2 x 10^{22}Pa·s.

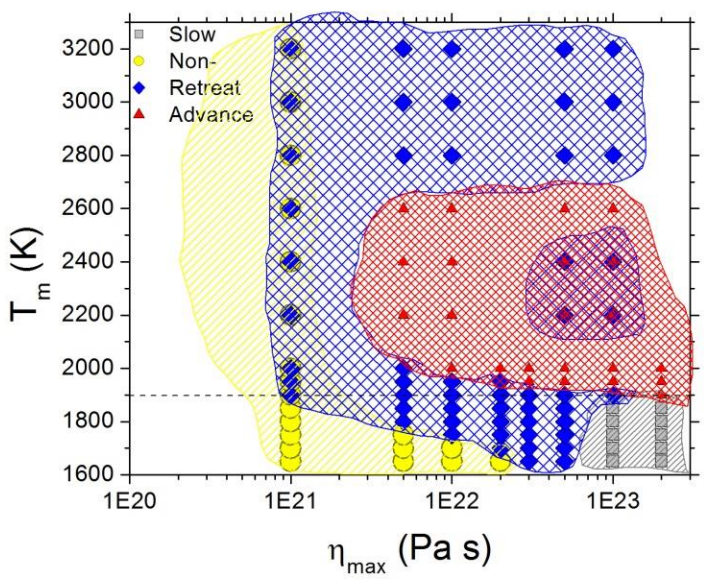

Fig. 6.3: Slab geometries for models with 100 km slab thickness and 50 km upper plate thickness, plotted by T_m and η_{max}. Two geometries on the same T_m, η_{max} represent separate histories for the original downgoing slab and the upper plate. Below the dashed line (ca. 1900

K), η_{um} varies self-consistently with T_m. Above, η_{um} remains at its 1900 K value and the effect of increasing temperature is to decrease the Rayleigh number (Ra) of a 1900 K model.

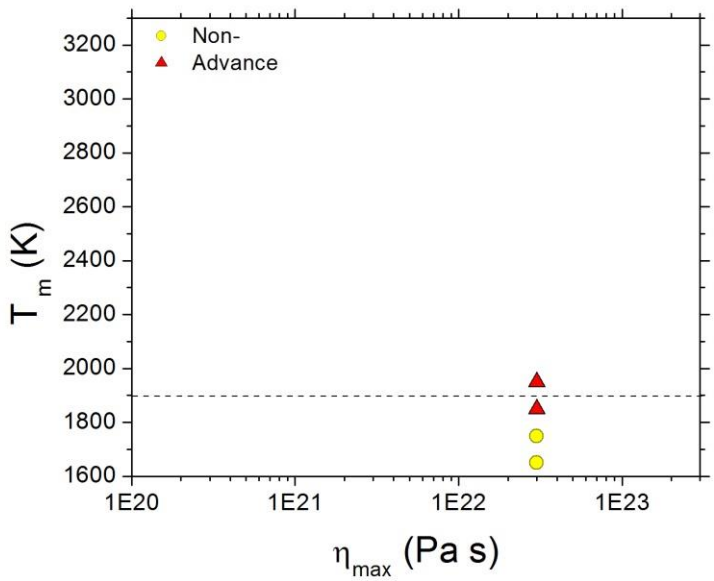

Fig. 6.4: Slab geometries for models with 100 km slab thickness and 100 km upper plate thickness, plotted by T_m and η_{max}. Dashed line as for Fig. 6.3.

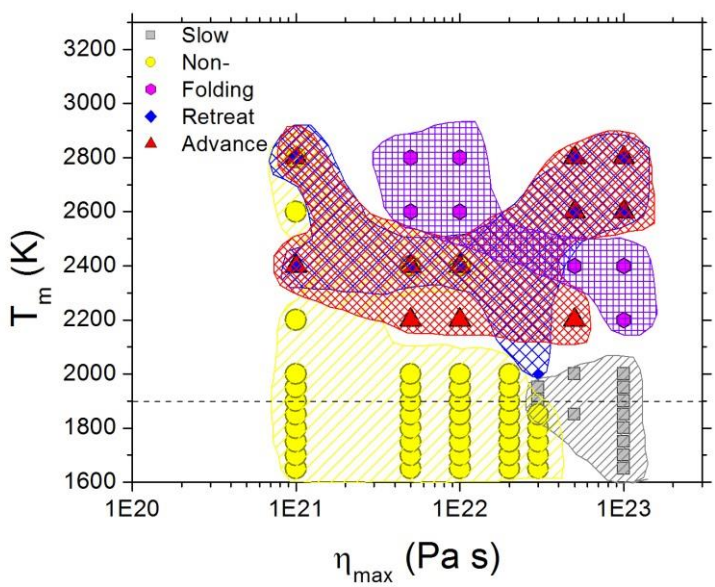

Fig. 6.5: Slab geometries for models with 50 km slab thickness and 50 km upper plate thickness, plotted by T_m and η_{max}. Dashed line as for Fig. 6.3.

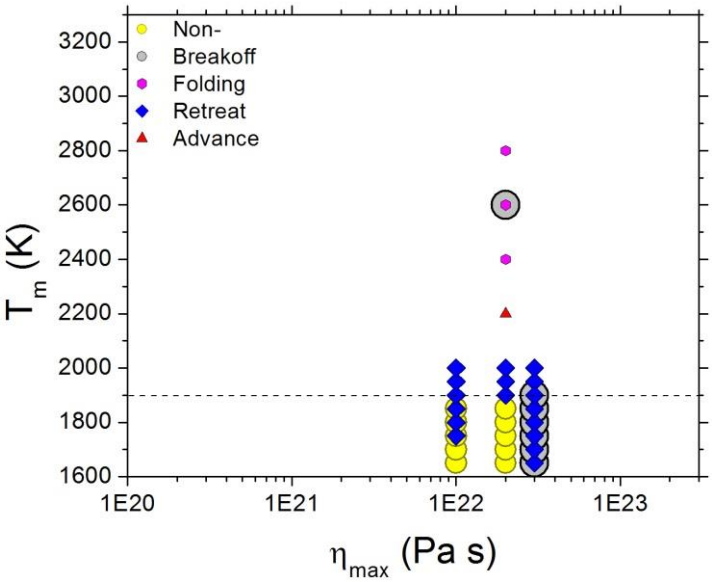

Fig. 6.6: Slab geometries for models with 50 km slab thickness and 25 km upper plate thickness, plotted by T_m and $\eta_{max.}$ Dashed line as for Fig. 6.3.

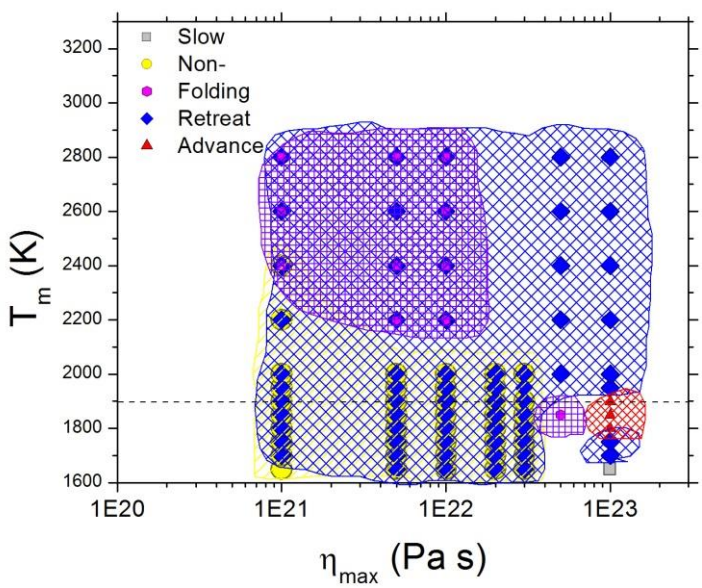

Fig. 6.7: Slab geometries for models with 200 km slab thickness and 50 km upper plate thickness, plotted by T_m and $\eta_{max.}$ Dashed line as for Fig. 6.3.

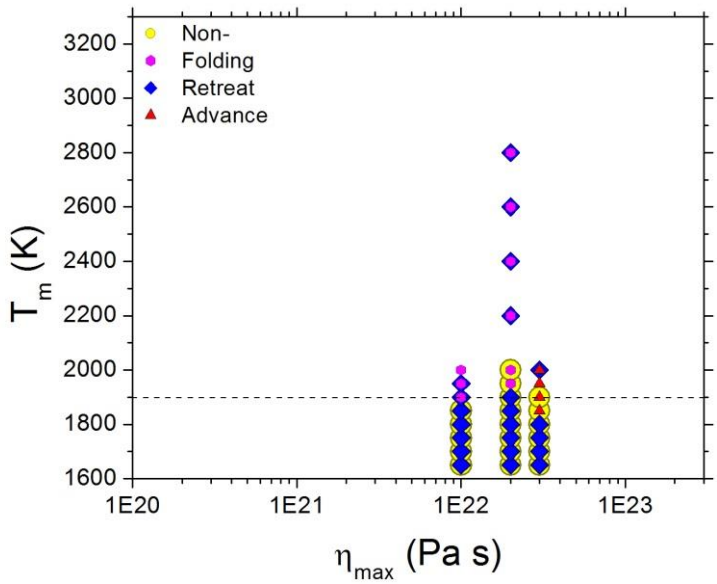

Fig. 6.8: Slab geometries for models with 200 km slab thickness and 100 km upper plate thickness, plotted by T_m and η_{max}. Dashed line as for Fig. 6.3.

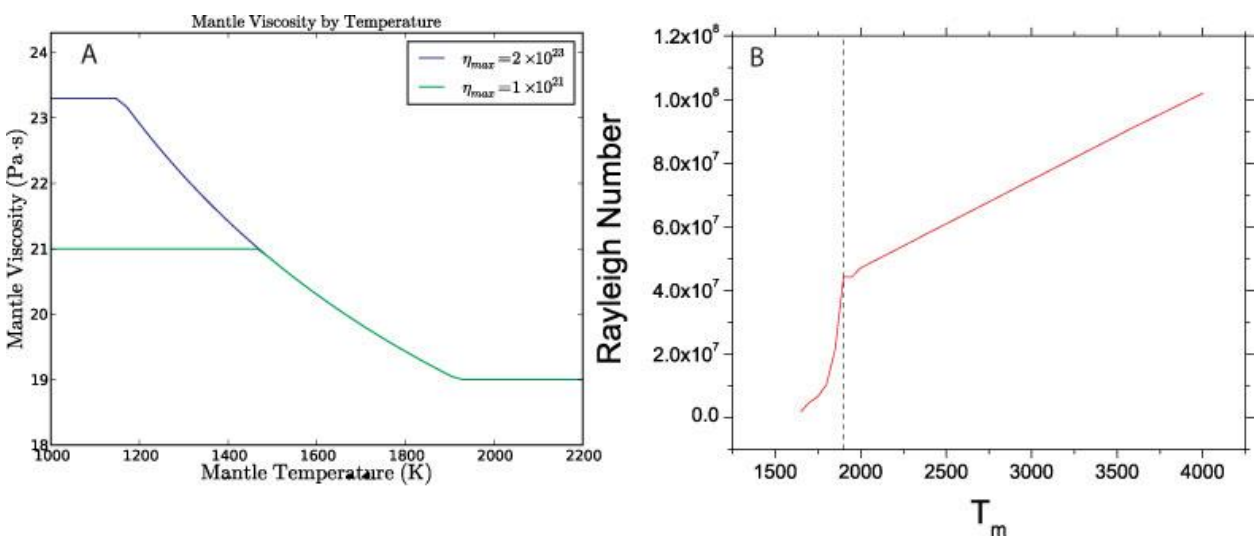

6.9: Viscosity and Rayleigh number variations with T_m in our models. A) variation of mantle viscosity η_{um} with T_m in the models, accounting for η_{max} and η_{min}. Figure courtesy of Dave Stegman and Robert Petersen. B) Rayleigh number versus T_m in our models. The dashed line shows the changeover from self-consistent T_m-η_{um} scaling to constant-η_{um} models.

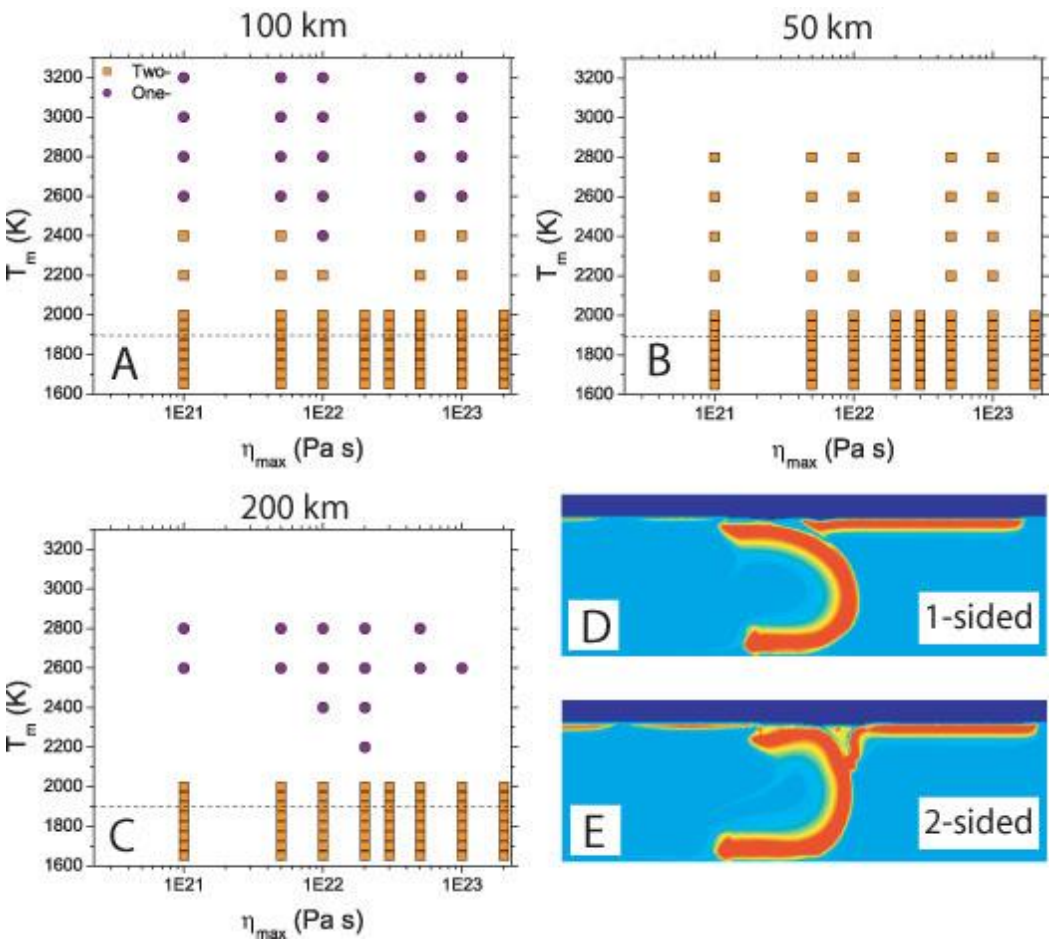

Fig. 6.10: 2-sided and 1-sided subduction observed for models with slab thicknesses of A) 100 km, B) 50 km, C) 200 km, tabulated by T_m and η_{max}. Variations with upper plate thickness were not resolved. D) 100 km slab (50 km upper plate; $\eta_{max} = 5x10^{22}$Pa·s, T_m = 2600 K) showing 1-sided subduction. StagYY output image. E)100 km slab (50 km upper plate; $\eta_{max} = 5x10^{22}$Pa·s, T_m = 2400 K) showing 2-sided subduction. StagYY output image. In almost all cases, models which displayed 1-sided subduction eventually transitioned to 2-sided subduction. Dashed lines in A-C as for Fig. 6.3.

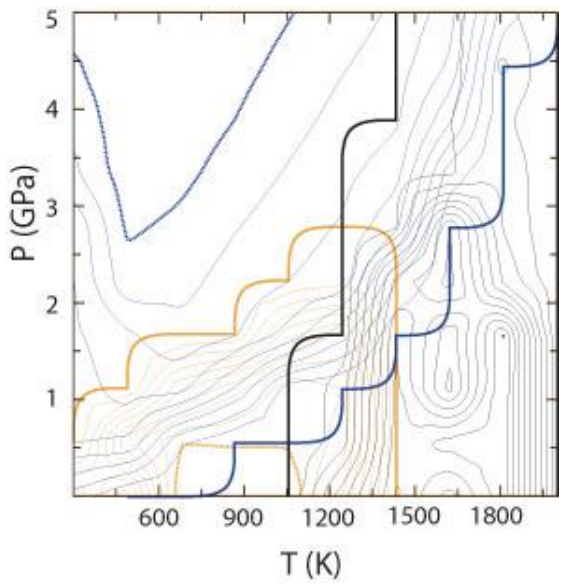

Fig. 6.11: Contoured volume % of melt (black), plagioclase (orange), and garnet (blue) in MORB for a specified portion of P-T space, based on calculations by Perple_x on a major element bulk composition from average MORB (GeoROC database). Thick contours are the minimum contoured value, dotted contours the maximum. Melt ranges 0-83 vol %, with contour intervals at 8.3%. Plagioclase ranges from 0-45 vol %, with intervals at 5%. Garnet ranges 0-37%, with intervals at 4.1%.Pressures at the base of the modeled 100 km upper plate lithosphere will be approximately 5 GPa. For increasing mantle temperatures, this corresponds to metabasalt with decreasing amounts of garnet (non-eclogitic). More detailed determinations of the trench and forearc thermal structure will help to determine if eclogite would be stable in the lower continental lithosphere in the warm mantle.

Chapter Seven: Conclusions and Future Work

In these studies we have considered detrital zircons from the Jack Hills population ranging 4.2-3.2 Ga, with an eye toward discerning any changing conditions during these billion years of zircon formation in what is now the Yilgarn Craton. The composition of the zircons in various isotopic systems and elemental abundances shows various differences among time periods, with the most dramatic difference between the >3.8 Ga and the dominant <3.6 Ga populations. Within these populations, however, various changes can also be noted. The Lu-Hf system shows a transition within the older population: >4 Ga zircons range between the solar system initial $^{176}Hf/^{177}Hf$ and the depleted mantle evolution line (with several highly depleted signatures seen by Harrison et al., 2005), but between 4 and 3.8 Ga the more extreme members of the population are no longer expressed (at least to our level of sampling). The crust represented by the zircons appears to evolve only by internal processing with no discernible juvenile input. Although the geochemistry of most >3.8 Ga zircons is broadly similar, trace element compositions appear to reflect a progression toward more evolved magmatic provenances from 4.2 to 3.8 Ga. The co-occurrence of this trace chemistry change with the increasing probability of Xe isotope compositions to record chondritic or super-chondritic $(Pu/U)_O$ may be related to this, but ubiquitous post-Hadean Xe loss complicates the interpretation of the Xe system. The $\delta^{18}O$ and T^{xlln} distributions (except for the anomalous Group II's T^{xlln}) does not change noticeably during this time. Several geochemical systems, then, record changing conditions in the ancestral Jack Hills crust over several hundred million years.

The principal result of these investigations, however, has been the identification of a period of relatively sudden change in zircon chemistry at ca. 3.9-3.7 Ga, consisting of two apparent events. Zircons older than this period display a range in both Hf and O isotopes

suggestive of mixing of ancient with more recent mantle-derived crust, with some amount of meta-sedimentary sources. Although the dominance of granitic crystallization temperatures throughout the time of Jack Hills zircon formation suggests dominantly felsic magma origins despite the differences pre- and post-3.8-3.7 Ga, the character of the granites changes and after 3.8 Ga. Zircons after this period show more truncated O isotope compositions suggestive of less input from aqueously altered materials. The Hf isotope record during this period takes a "sawtooth" shape, where ancient felsic crust is lost after ca. 3.7 Ga and juvenile addition to the crust occurs ca. 3.8 Ga. By analogy to the Phanerozoic, this pattern is reminiscent of a subduction-related orogen (Collins et al., 2011), and we interpret the Hf isotope record as evidence for some form of plate tectonic processes operating by at least the Eoarchean.

Zircons with a distinctive trace element geochemistry appear between 3.91 and 3.84 Ga. Their higher U concentrations despite their generally higher degree of U-Pb concordance suggests an unusual origins. The predominance of patchy or CL-homogeneous internal structures and the other distinctive aspects of their chemistry – high Hf along with low Th/U, P, and LREE compared to the prevailing >3.8 Ga population – are consistent with transgressive solid-state recrystallization (Hoskin and Black, 2000). We interpret them as evidence for a heating event in the Jack Hills zircon source ca. 3.9-3.8 Ga. One factor which may cast doubt on their origins from the prevailing Hadean population by recrystallization is that for the most part Group II zircons are genetically distinct from their contemporaneous Group I counterparts, being somewhat more radiogenic. This brings up the possibilities that either this group merely represents a genetically distinct magma(s) with an unusual chemistry or that the more radiogenic regions of the ancestral Jack Hills crust were more likely to have undergone this proposed heating event. The coincidence of this event's timing with the hypothesized Late Heavy

Bombardment was remarked upon in ch. 3; alternatively, its coincidence with the beginning of the "sawtooth" event of crustal loss and addition at ca. 3.8-3.7 Ga may record a crustal thermal response to this event.

Further investigations of these ca. 3.9-3.7 Ga events will be needed to determine their nature, as the reliance on a detrital zircon record omits a lot of important information about the context of the zircons' protoliths. However, investigation of our proposed subduction event is likely to be stymied by the relative paucity of 3.8-3.6 Ga zircons in the Jack Hills record. The nearby Mt. Narryer location (ca. 50 km from Jack Hills) also contains an early Archean-Hadean detrital zircon record but with more numerous 3.8-3.6 Ga zircons (Crowley et al., 2005), and so it may be the best option for future geochemical studies of the Narryer Gneiss Complex crust during this time period. >3.6 Ga zircons are found in several Archean quartzites around the Yilgarn Craton (Thern and Nelson, 2012). Although their identification with the Narryer Gneiss Complex is more uncertain given the lack of geochemical information, principal component analysis of the detrital zircon age record of these Archean quartzites may suggest their derivation from at least two Hadean terranes joined in the Eoarchean (Thern and Nelson, 2012). A few other sites on the planet yield Eoarchean zircons in usable quantities. The zircon Hf records of the Acasta Gneiss (Iiizuka et al., 2009), southwest Greenland (Naeraa et al., 2012), and the Nuvvuagittuq Greenstone Belt (O'Neil et al., 2013) show different histories of Eoarchean juvenile input, but require at least some mixing in of Hadean crust. Further investigation of these zircons' geochemistry may help determine if either of the event(s) identified in the Jack Hills source reflect global transitions or merely local changes in geologic environment.

Although we have explored much of the parameter space in our Cartesian model of subduction in a warmer mantle, the applicability of the model to the Earth is still somewhat

uncertain given the model's propensity for two-sided rather than 1-sided subduction. If it is applicable, however, it may point toward higher mantle temperatures enhancing the stability of subduction for oceanic plates with the same thickness as today. In the model, thinner plates are less likely to subduct but rather form other styles of downwelling, and are also more likely to show slab breakoff. Refining the model by switching to a cylindrical geometry and adding isotopic tracers will help to determine the effects of the modeled subduction on mantle circulation and the material reservoirs thus formed. With little information on mantle temperatures in the Eoarchean and Hadean, it is difficult to determine the regime of the model in which we would predict to find our purported 3.8-3.7 Ga subduction event or the earlier proposed subduction events of Hopkins et al. (2008, 2010).

Although many questions remain, we have established that the Eoarchean was an important period of change in the ancestral Jack Hills crust. Not only is much of the ancient felsic crust lost from the area during this time through a likely subduction event, but this event coincides with a significant restriction in the $\delta^{18}O$ distribution and occurs just after the appearance of a group of zircons ("Group II" of ch. 3) with a distinctive elemental geochemistry and internal textures consistent with metamorphic recrystallization. This period from 3.9-3.7 Ga represents the most dramatic yet identified period of change in the Jack Hills record. Given the antiquity of the zircons, it is also invaluable for determining whether this is merely a local event or reflects more global transitions on the Eoarchean Earth.

Appendix A: O and Hf-Pb Isotope Standards from Chapter Two

Sample	16O (cps)	18O (cps)	18O/16O raw	18/16 err	d18O raw	d18O err	#	corr. 18/16	2 s.d.	corr. d18O	2 s.d.
AS3@10	1.726E+09	3.513E+06	0.0020	0.0000	15.0037	0.1342	24	2.016E-03	1.117E-06	5.5	0.6
AS3@11	1.713E+09	3.485E+06	0.0020	0.0000	14.5538	0.1803	31	2.015E-03	1.142E-06	5.1	0.6
AS3@11a	1.771E+09	3.605E+06	0.0020	0.0000	15.2775	0.1873	32	2.017E-03	1.147E-06	5.8	0.6
AS3@12	1.845E+09	3.756E+06	0.0020	0.0000	15.2522	0.1516	38	2.017E-03	1.126E-06	5.8	0.6
AS3@13a	1.884E+09	3.834E+06	0.0020	0.0000	14.8301	0.1785	51	2.016E-03	1.141E-06	5.4	0.6
AS3@13b	1.859E+09	3.785E+06	0.0020	0.0000	15.2332	0.1596	54	2.017E-03	1.130E-06	5.8	0.6
AS3@14a	1.876E+09	3.816E+06	0.0020	0.0000	14.6786	0.0989	58	2.016E-03	1.102E-06	5.2	0.5
AS3@15a	1.771E+09	3.603E+06	0.0020	0.0000	14.7272	0.1611	64	2.016E-03	1.131E-06	5.3	0.6
AS3@16	1.762E+09	3.584E+06	0.0020	0.0000	14.6204	0.1868	65	2.016E-03	1.146E-06	5.2	0.6
AS3@17	1.761E+09	3.584E+06	0.0020	0.0000	14.9784	0.2387	72	2.016E-03	1.184E-06	5.5	0.6
AS3@17b	1.785E+09	3.632E+06	0.0020	0.0000	14.9181	0.1412	74	2.016E-03	1.120E-06	5.5	0.6
AS3@18	1.762E+09	3.585E+06	0.0020	0.0000	14.7363	0.2819	81	2.016E-03	1.221E-06	5.3	0.6
AS3@19	1.784E+09	3.629E+06	0.0020	0.0000	14.5148	0.2435	84	2.015E-03	1.187E-06	5.1	0.6
AS3@20	1.763E+09	3.588E+06	0.0020	0.0000	14.7219	0.1295	85	2.016E-03	1.115E-06	5.3	0.6
AS3@21	1.758E+09	3.575E+06	0.0020	0.0000	14.3908	0.0756	86	2.015E-03	1.094E-06	4.9	0.5
AS3@22	1.769E+09	3.599E+06	0.0020	0.0000	14.7040	0.1020	90	2.016E-03	1.103E-06	5.2	0.5
AS3@23	1.772E+09	3.604E+06	0.0020	0.0000	14.4797	0.2376	93	2.015E-03	1.182E-06	5.0	0.6
		Average	0.0020								
		2 stdev	0.0000								
		AS3	0.0020								
		alpha	1.0094								
		d.f. 2 stdev	0.0005								
AS3_RSES51@1	1.895E+09	3.825E+06	0.0020	0.0000	6.4216	0.1190	45	2.017E-03	6.173E-07	5.6	0.3
AS3_RSES51@2	1.896E+09	3.826E+06	0.0020	0.0000	6.4172	0.0578	46	2.017E-03	5.811E-07	5.6	0.3
AS3_RSES51@3	1.899E+09	3.830E+06	0.0020	0.0000	6.0476	0.0980	47	2.016E-03	6.022E-07	5.3	0.3

AS3_RSES51@4	1.861E+09	3.756E+06	0.0020	0.0000	6.3252	0.1072	48	2.016E-03	6.086E-07	5.6	0.3
AS3_RSES51@5	1.889E+09	3.810E+06	0.0020	0.0000	5.7040	0.1757	51	2.015E-03	6.691E-07	4.9	0.3
AS3_RSES51@6	1.858E+09	3.749E+06	0.0020	0.0000	6.3245	0.0823	58	2.016E-03	5.928E-07	5.5	0.3
AS3_RSES51@7	1.885E+09	3.803E+06	0.0020	0.0000	6.1021	0.0545	64	2.016E-03	5.797E-07	5.3	0.3
AS3_RSES51@8	1.854E+09	3.740E+06	0.0020	0.0000	6.1269	0.0550	70	2.016E-03	5.799E-07	5.4	0.3
AS3_RSES51@9	1.837E+09	3.706E+06	0.0020	0.0000	6.1835	0.0751	77	2.016E-03	5.889E-07	5.4	0.3
AS3_RSES51@10	1.821E+09	3.676E+06	0.0020	0.0000	6.4115	0.0509	83	2.017E-03	5.785E-07	5.6	0.3
AS3_RSES51@11	1.817E+09	3.666E+06	0.0020	0.0000	5.9699	0.1025	89	2.016E-03	6.051E-07	5.2	0.3
AS3_RSES51@12	1.825E+09	3.682E+06	0.0020	0.0000	6.0608	0.1181	93	2.016E-03	6.165E-07	5.3	0.3
AS3_RSES51@13	1.826E+09	3.684E+06	0.0020	0.0000	5.7929	0.1390	100	2.015E-03	6.336E-07	5.0	0.3
AS3_RSES51@14	1.824E+09	3.678E+06	0.0020	0.0000	5.5912	0.2168	106	2.015E-03	7.158E-07	4.8	0.4
AS3_RSES51@15	1.803E+09	3.638E+06	0.0020	0.0000	6.0033	0.0842	112	2.016E-03	5.937E-07	5.2	0.3
AS3_RSES51@16	1.732E+09	3.496E+06	0.0020	0.0000	6.6527	0.2373	118	2.017E-03	7.420E-07	5.9	0.4
AS3_RSES51@17	1.769E+09	3.567E+06	0.0020	0.0000	5.6634	0.2260	123	2.015E-03	7.272E-07	4.9	0.4
AS3_RSES51@18	1.761E+09	3.551E+06	0.0020	0.0000	5.6475	0.0689	129	2.015E-03	5.855E-07	4.9	0.3
AS3_RSES51@19	1.756E+09	3.543E+06	0.0020	0.0000	6.1373	0.1650	135	2.016E-03	6.584E-07	5.4	0.3
AS3_RSES51@20	1.766E+09	3.562E+06	0.0020	0.0000	6.1379	0.1325	140	2.016E-03	6.282E-07	5.4	0.3
AS3_RSES51@21	1.731E+09	3.494E+06	0.0020	0.0000	6.5925	0.1682	146	2.017E-03	6.619E-07	5.8	0.3
AS3_RSES51@22	1.730E+09	3.492E+06	0.0020	0.0000	6.2535	0.1727	153	2.016E-03	6.663E-07	5.5	0.3
AS3_RSES51@23	1.721E+09	3.473E+06	0.0020	0.0000	6.2114	0.1230	163	2.016E-03	6.204E-07	5.4	0.3
AS3_RSES51@24	1.722E+09	3.475E+06	0.0020	0.0000	6.0856	0.1714	169	2.016E-03	6.648E-07	5.3	0.3
AS3_RSES51@25	1.720E+09	3.469E+06	0.0020	0.0000	5.9987	0.1832	173	2.016E-03	6.773E-07	5.2	0.3
		Average	0.0020								
		2 stdev	0.0000								
		AS3	0.0020								
		alpha	1.0008								
		d.f. 2 stdev	0.0006								

Table A.1: Oxygen isotope standards (AS3) for ch. 2 oxygen isotope analyses.

Session	Standard Set	Analysis	178/177	2 se	176Lu/177Hf	2 se	176Hf/177Hf	2 se	176Hf/177Hf mass		207/206	2 se	
and day									**fractionation factor**				
Session 1 Day 1	Standard Set 1	Mudtank#1	1.4673	0.0000	0.0000	0.0000	0.2825	0.0000	0.9999		0.0606	0.0032	
Session 1 Day 1	Standard Set 1	Mudtank#2	1.4672	0.0000	0.0000	0.0000	0.2825	0.0000	0.9999		0.0625	0.0036	
Session 1 Day 1	Standard Set 1	Mudtank#3	1.4672	0.0000	0.0000	0.0000	0.2825	0.0000	0.9999		0.0634	0.0037	
Session 1 Day 1	Standard Set 1	Temora#1	1.4672	0.0001	0.0008	0.0000	0.2826	0.0000			0.0545	0.0030	
Session 1 Day 1	Standard Set 1	Temora#2	1.4672	0.0001	0.0017	0.0001	0.2826	0.0000			0.0570	0.0020	
Session 1 Day 1	Standard Set 1	AS3#1	1.4672	0.0000	0.0011	0.0000	0.2822	0.0000	0.9999		0.0762	0.0003	
Session 1 Day 1	Standard Sets 1&2	Mudtank#4	1.4672	0.0000	0.0000	0.0000	0.2825	0.0000	0.9999		0.0610	0.0031	
Session 1 Day 1	Standard Sets 1&2	Mudtank#5	1.4672	0.0000	0.0000	0.0000	0.2825	0.0000	0.9999		0.0570	0.0028	
Session 1 Day 1	Standard Sets 1&2	Temora#3	1.4672	0.0001	0.0011	0.0000	0.2827	0.0000			0.0565	0.0031	
Session 1 Day 1	Standard Set 2	Mudtank#6	1.4672	0.0000	0.0000	0.0000	0.2825	0.0000	0.9999		0.0611	0.0034	
Session 1 Day 1	Standard Set 2	Mudtank#7	1.4672	0.0000	0.0001	0.0000	0.2825	0.0000	0.9999		0.0633	0.0036	
Session 1 Day 1	Standard Set 2	Temora#4	1.4672	0.0000	0.0008	0.0000	0.2827	0.0000			0.0564	0.0353	
Session 1 Day 1	Standard Set 2	Temora#5	1.4671	0.0002	0.0009	0.0000	0.2827	0.0000			0.0775	0.0301	
Session 1 Day 1	Standard Set 2	AS3#3	1.4672	0.0000	0.0009	0.0000	0.2821	0.0000	0.9999		0.0759	0.0003	
Session 1 Day 1	Standard Set 2	Mudtank#8	1.4673	0.0000	0.0001	0.0000	0.2825	0.0000	1.0000		0.0627	0.0043	
Session 1 Day 1	Standard Set 2	Mudtank#9	1.4672	0.0000	0.0001	0.0000	0.2825	0.0000	0.9999		0.0655	0.0031	
Session 1 Day 1	Standard Set 2	AS3#4	1.4671	0.0001	0.0011	0.0000	0.2822	0.0000	1.0000		0.0773	0.0009	
Session 1 Day 1	Standard Set 2	AS3#5	1.4672	0.0000	0.0009	0.0000	0.2822	0.0000	0.9999		0.0762	0.0003	
Session 1 Day 1	Standard Set 2	Mudtank#11	1.4672	0.0000	0.0001	0.0000	0.2825	0.0000	0.9999		0.0647	0.0040	
Session 1 Day 1	Standard Set 2	Mudtank#12	1.4672	0.0000	0.0000	0.0000	0.2825	0.0000	0.9999		0.0605	0.0037	
Session 1 Day 1	Standard Set 2	AS3#6	1.4671	0.0001	0.0011	0.0000	0.2822	0.0000	1.0001		0.0766	0.0009	
Session 1 Day 1	Standard Set 2	AS3#7	1.4673	0.0002	0.0017	0.0000	0.2822	0.0002	1.0000		0.0819	0.0078	
Session 1 Day 1	Standard Set 2	AS3#8	1.4672	0.0000	0.0013	0.0000	0.2822	0.0000	0.9999		0.0760	0.0002	
Session 1 Day 1	Standard Set 2	Mudtank#13	1.4672	0.0000	0.0000	0.0000	0.2825	0.0000	1.0000		0.0636	0.0033	
Session 1 Day 1	Standard Set 2	Mudtank#14	1.4672	0.0000	0.0000	0.0000	0.2825	0.0000	1.0000		0.0640	0.0035	
Session 1 Day 1	Standard Set 2	Mudtank#15	1.4672	0.0000	0.0000	0.0000	0.2825	0.0000	1.0000		0.0591	0.0033	
									avg m.f.f.	**2stdev m.f.f.**			
							CORRECTION 1		**0.9999**	**0.0001**			
							CORRECTION 2		**0.9999**	**0.0001**			
Session 2 Day 1	Standard Set 1	glass_u001	1.4632	0.0004	NIST610 glass	0.1435	0.0002			0.2818	0.0003		
Session 2 Day 1	Standard Set 1	glass_u002	1.4636	0.0005	NIST610 glass	0.1433	0.0001			0.2812	0.0004		
Session 2 Day 1	Standard Set 1	Mudtank_u001	1.4671	0.0000	Mudtank zircon	0.0000	0.0000			0.2825	0.0000	0.9999	
Session 2 Day 1	Standard Set 1	Mudtank_u002	1.4672	0.0000	Mudtank zircon	0.0000	0.0000			0.2825	0.0000	0.9999	

Session 2 Day 1	Standard Set 1	AS3_u001	1.4671	0.0002	AS3 zircon	0.0009	0.0000	0.7900		0.2821	0.0000	0.9997	
Session 2 Day 1	Standard Set 1	AS3_u002	1.4671	0.0001	AS3 zircon	0.0009	0.0000	0.7632		0.2821	0.0000	0.9999	
Session 2 Day 1	Standard Set 1	glass_u003	1.4638	0.0004	NIST610 glass	0.1435	0.0002			0.2820	0.0004		
Session 2 Day 1	Standard Set 1	Mudtank_u003	1.4672	0.0000	Mudtank zircon	0.0000	0.0000			0.2825	0.0000	0.9999	
Session 2 Day 1	Standard Set 1	Temora_u001	1.4672	0.0001	Temora 2 zircon	0.0008	0.0000	0.7485		0.2826	0.0000		
Session 2 Day 1	Standard Set 1	AS3_u003	1.4671	0.0001	AS3 zircon	0.0009	0.0000	0.7592		0.2821	0.0000	0.9999	
Session 2 Day 1	Standard Set 1	AS3_u004	1.4671	0.0001	AS3 zircon	0.0009	0.0000	0.7566		0.2821	0.0000	0.9999	
Session 2 Day 1	Standard Set 1	glass_u004	1.4637	0.0004	NIST610 glass	0.1431	0.0002			0.2813	0.0003		
Session 2 Day 1	Standard Sets 1&2	glass_u005	1.4639	0.0004	NIST610 glass	0.1434	0.0001			0.2815	0.0003		
Session 2 Day 1	Standard Sets 1&2	Mudtank_u004	1.4672	0.0001	Mudtank zircon	0.0000	0.0000			0.2825	0.0000	0.9999	
Session 2 Day 1	Standard Sets 1&2	Mudtank_u005	1.4672	0.0001	Mudtank zircon	0.0000	0.0000			0.2825	0.0000	0.9999	
Session 2 Day 1	Standard Sets 1&2	AS3_u005	1.4671	0.0002	AS3 zircon	0.0009	0.0001	0.7500		0.2821	0.0000	0.9998	
Session 2 Day 1	Standard Sets 1&2	Temora_u002	1.4672	0.0001	Temora 2 zircon	0.0013	0.0000	1.1870		0.2826	0.0000		
Session 2 Day 1	Standard Set 2	glass_u006	1.4631	0.0005	NIST610 glass	0.1433	0.0002			0.2818	0.0004		
Session 2 Day 1	Standard Set 2	Mudtank_u006	1.4671	0.0000	Mudtank zircon	0.0000	0.0000			0.2825	0.0000	1.0000	
Session 2 Day 1	Standard Set 2	AS3_u006	1.4671	0.0001	AS3 zircon	0.0011	0.0001	0.9570		0.2821	0.0000	0.9999	
Session 2 Day 1	Standard Set 2	Mudtank_u007	1.4671	0.0001	Mudtank zircon	0.0000	0.0000			0.2825	0.0000	1.0000	
Session 2 Day 1					**SESSION 2 DAY 1**			**avg m.f.f.**	**2stdev m.f.f.**			**avg m.f.f.**	**2stdev m.f.f.**
						CORRECTION 1		**0.8221**	**0.3230**	**CORRECTION 1**		**0.9999**	**0.00016**
						CORRECTION 2		**0.9647**	**0.4371**	**CORRECTION 2**		**0.9999**	**0.00019**
Session 2 Day 2	Standard Set 1	NIST610_v004	1.4670	0.0002	NIST610 glass	0.1420	0.0002			0.2815	0.0004		
Session 2 Day 2	Standard Set 1	AS3_v001	1.4673	0.0001	AS3 zircon	0.0017	0.0001			0.2822	0.0000	1.0000	
Session 2 Day 2	Standard Set 1	Mudtank_v004	1.4673	0.0000	Mudtank zircon	0.0000	0.0000			0.2825	0.0000	0.9998	
Session 2 Day 2	Standard Set 1	Mudtank_v005	1.4673	0.0000	Mudtank zircon	0.0000	0.0000			0.2825	0.0000	0.9998	
Session 2 Day 2	Standard Set 1	AS3_v002	1.4673	0.0001	AS3 zircon	0.0012	0.0001			0.2822	0.0000	1.0000	
Session 2 Day 2	Standard Set 1	NIST610_v005	1.4673	0.0002	NIST610 glass	0.1424	0.0001			0.2816	0.0003		
Session 2 Day 2	Standard Set 1	NIST610_v006	1.4671	0.0002	NIST610 glass	0.1423	0.0002			0.2816	0.0003		
Session 2 Day 2	Standard Set 1	Mudtank_v006	1.4673	0.0000	Mudtank zircon	0.0000	0.0000			0.2825	0.0000	0.9999	
Session 2 Day 2	Standard Set 1	AS3_v003	1.4672	0.0001	AS3 zircon	0.0011	0.0000			0.2822	0.0000	1.0000	
Session 2 Day 2	Standard Set 1	Temora_v001	1.4673	0.0001	Temora 2 zircon	0.0010	0.0000			0.2827	0.0000		
Session 2 Day 2	Standard Set 1	Temora_v002	1.4673	0.0001	Temora 2 zircon	0.0010	0.0000			0.2826	0.0000		
Session 2 Day 2	Standard Set 1	AS3_v004	1.4673	0.0001	AS3 zircon	0.0011	0.0001			0.2822	0.0000	0.9999	
Session 2 Day 2	Standard Set 1	Mudtank_v007	1.4673	0.0001	Mudtank zircon	0.0000	0.0000			0.2825	0.0000	0.9998	
Session 2 Day 2	Standard Sets 1&2	NIST610_v007	1.4673	0.0002	NIST610 glass	0.1421	0.0001			0.2818	0.0006		
Session 2 Day 2	Standard Sets 1&2	Mudtank_v008	1.4673	0.0000	Mudtank zircon	0.0000	0.0000			0.2825	0.0000	0.9999	
Session 2 Day 2	Standard Sets 1&2	Mudtank_v009	1.4673	0.0001	Mudtank zircon	0.0000	0.0000			0.2825	0.0000	0.9999	
Session 2 Day 2	Standard Sets 1&2	AS3_v005	1.4673	0.0001	AS3 zircon	0.0017	0.0001			0.2822	0.0000	1.0000	
Session 2 Day 2	Standard Sets 1&2	Temora_v003	1.4673	0.0001	Temora 2 zircon	0.0006	0.0000			0.2827	0.0000		

Session 2 Day 2	Standard Sets 1&2	AS3_v006	1.4673	0.0001	AS3 zircon	0.0011	0.0001			0.2821	0.0000	0.9998	
Session 2 Day 2	Standard Sets 2&3	NIST610_v008	1.4674	0.0002	NIST610 glass	0.1423	0.0001			0.2818	0.0002		
Session 2 Day 2	Standard Sets 2&3	Mudtank_v010	1.4673	0.0001	Mudtank zircon	0.0000	0.0000			0.2825	0.0000	0.9999	
Session 2 Day 2	Standard Sets 2&3	AS3_v007	1.4674	0.0001	AS3 zircon	0.0019	0.0003			0.2821	0.0001	0.9999	
Session 2 Day 2	Standard Sets 2&3	Temora_v004	1.4674	0.0001	Temora 2 zircon	0.0011	0.0000			0.2826	0.0000		
Session 2 Day 2	Standard Set 3	NIST610_v009	1.4672	0.0003	NIST610 glass	0.1422	0.0002			0.2817	0.0003		
Session 2 Day 2		NIST614_v001	1.4758	0.0403	NIST614 glass	0.0382	0.0032			0.2750	0.0301		
Session 2 Day 2	Standard Set 3	Mudtank_v011	1.4673	0.0001	Mudtank zircon	0.0000	0.0000			0.2824	0.0000	0.9998	
Session 2 Day 2		NIST614_v002	1.6037	0.1091	NIST614 glass	0.1069	0.0087			0.3414	0.0864		
Session 2 Day 2	Standard Set 3	Mudtank_v012	1.4673	0.0001	Mudtank zircon	0.0000	0.0000			0.2824	0.0000	0.9998	
Session 2 Day 2	Standard Set 3	AS3_v009	1.4674	0.0001	AS3 zircon	0.0008	0.0001			0.2821	0.0000	0.9999	
Session 2 Day 2	Standard Set 3	AS3_v010	1.4675	0.0002	AS3 zircon	0.0011	0.0001			0.2821	0.0000	0.9996	
Session 2 Day 2	Standard Set 3	Mudtank_v013	1.4673	0.0001	Mudtank zircon	0.0000	0.0000			0.2824	0.0000	0.9998	
Session 2 Day 2	Standard Set 3	AS3_v011	1.4673	0.0001	AS3 zircon	0.0011	0.0001			0.2821	0.0000	0.9999	
Session 2 Day 2	Standard Set 3	NIST610_v010	1.4680	0.0003	NIST610 glass	0.1422	0.0002			0.2815	0.0003		
Session 2 Day 2									**SESSION 2 DAY 2**			**avg m.f.f.**	**2stdev m.f.f.**
										CORRECTION 1		**0.9999**	**0.00016**
										CORRECTION 2		**0.9999**	**0.00009**
										CORRECTION 3		**0.9998**	**0.00018**
Session 2 Day 3	Standard Set 1	NIST610_w001	1.4677	0.0003	NIST610 glass	0.1423	0.0001			0.2818	0.0002		
Session 2 Day 3	Standard Set 1	NIST610_w002	1.4679	0.0003	NIST610 glass	0.1419	0.0001			0.2818	0.0002		
Session 2 Day 3	Standard Set 1	AS3_w001	1.4673	0.0001	AS3 zircon	0.0018	0.0001			0.2822	0.0000	1.0000	
Session 2 Day 3	Standard Set 1	Mudtank_w001	1.4673	0.0001	Mudtank zircon	0.0000	0.0000			0.2825	0.0000	0.9999	
Session 2 Day 3	Standard Set 1	Mudtank_w002	1.4673	0.0001	Mudtank zircon	0.0000	0.0000			0.2825	0.0000	0.9998	
Session 2 Day 3	Standard Set 1	AS3_w002	1.4673	0.0001	AS3 zircon	0.0011	0.0001			0.2822	0.0000	0.9999	
Session 2 Day 3	Standard Set 1	Temora_w001	1.4674	0.0001	Temora 2 zircon	0.0009	0.0000			0.2826	0.0000		
Session 2 Day 3	Standard Set 1	NIST610_w003	1.4675	0.0002	NIST610 glass	0.1417	0.0001			0.2819	0.0003		
Session 2 Day 3	Standard Set 1	Mudtank_w003	1.4673	0.0001	Mudtank zircon	0.0000	0.0000			0.2825	0.0000	0.9999	
Session 2 Day 3	Standard Set 1	AS3_w003	1.4673	0.0001	AS3 zircon	0.0018	0.0001			0.2822	0.0000	1.0000	
Session 2 Day 3	Standard Set 1	Mudtank_w004	1.4673	0.0001	Mudtank zircon	0.0000	0.0000			0.2825	0.0000	0.9999	
Session 2 Day 3	Standard Set 1	AS3_w004	1.4672	0.0001	AS3 zircon	0.0015	0.0001			0.2822	0.0000	1.0000	
Session 2 Day 3	Standard Set 1	NIST610_w004	1.4674	0.0002	NIST610 glass	0.1420	0.0001			0.2818	0.0002		
Session 2 Day 3	Standard Set 1	Mudtank_w005	1.4673	0.0001	Mudtank zircon	0.0000	0.0000			0.2825	0.0000	0.9998	
Session 2 Day 3	Standard Set 1	AS3_w006	1.4674	0.0002	AS3 zircon	0.0011	0.0001			0.2822	0.0000	1.0000	
Session 2 Day 3	Standard Set 1	Mudtank_w006	1.4672	0.0001	Mudtank zircon	0.0000	0.0000			0.2825	0.0001	1.0000	
Session 2 Day 3	Standard Set 1	AS3_w007	1.4674	0.0002	AS3 zircon	0.0009	0.0001			0.2821	0.0000	0.9998	
Session 2 Day 3	Standard Set 1	Temora_w002	1.4673	0.0001	Temora 2 zircon	0.0008	0.0000			0.2826	0.0000		

Session 2 Day 3	Standard Sets 1&2	NIST610_w005	1.4674	0.0003	NIST610 glass	0.1421	0.0002			0.2813	0.0011		
Session 2 Day 3		NIST614_v001	1.5546	0.0835	NIST614 glass	0.0828	0.0152			0.2978	0.0846		
Session 2 Day 3	Standard Sets 1&2	Temora_w003	1.4672	0.0002	Temora 2 zircon	0.0016	0.0001			0.2827	0.0000		
Session 2 Day 3	Standard Sets 1&2	Mudtank_w007	1.4673	0.0000	Mudtank zircon	0.0000	0.0000			0.2825	0.0000	0.9998	
Session 2 Day 3	Standard Sets 1&2	AS3_w008	1.4673	0.0001	AS3 zircon	0.0013	0.0001			0.2822	0.0000	0.9999	
Session 2 Day 3	Standard Sets 1&2	AS3_w009	1.4673	0.0001	AS3 zircon	0.0012	0.0001			0.2822	0.0000	0.9999	
Session 2 Day 3	Standard Sets 1&2	Mudtank_w008	1.4673	0.0001	Mudtank zircon	0.0000	0.0000			0.2825	0.0000	0.9999	
Session 2 Day 3	Standard Sets 1&2	NIST610_w006	1.4676	0.0003	NIST610 glass	0.1418	0.0002			0.2813	0.0003		
Session 2 Day 3	Standard Set 2	NIST610_w007	1.4671	0.0002	NIST610 glass	0.1417	0.0002			0.2818	0.0002		
Session 2 Day 3	Standard Set 2	Mudtank_w009	1.4673	0.0001	Mudtank zircon	0.0000	0.0000			0.2824	0.0000	0.9998	
Session 2 Day 3	Standard Set 2	AS3_w010	1.4674	0.0002	AS3 zircon	0.0014	0.0001			0.2821	0.0000	0.9999	
Session 2 Day 3	Standard Set 2	Temora_w004	1.4674	0.0001	Temora 2 zircon	0.0011	0.0000			0.2825	0.0000		
Session 2 Day 3	Standard Set 2	AS3_w011	1.4674	0.0002	AS3 zircon	0.0012	0.0001			0.2821	0.0000	0.9999	
Session 2 Day 3	Standard Set 2	Mudtank_w010	1.4673	0.0001	Mudtank zircon	0.0000	0.0000			0.2825	0.0000	0.9999	
Session 2 Day 3	Standard Set 2	Mudtank_w011	1.4673	0.0001	Mudtank zircon	0.0000	0.0000			0.2825	0.0000	0.9999	
Session 2 Day 3	Standard Set 2	AS3_w012	1.4674	0.0002	AS3 zircon	0.0009	0.0001			0.2820	0.0001	0.9993	
Session 2 Day 3	Standard Set 2	Temora_w005	1.4674	0.0002	Temora 2 zircon	0.0008	0.0000			0.2826	0.0000		
Session 2 Day 3	Standard Set 2	NIST610_w008	1.4675	0.0003	NIST610 glass	0.1420	0.0001			0.2811	0.0010		
Session 2 Day 3									**SESSION 2 DAY 3**			**avg m.f.f.**	**2stdev m.f.f.**
										CORRECTION 1		**0.9999**	**0.00014**
										CORRECTION 2		**0.9998**	**0.00038**

Table A.2: Hf-Pb standard analyses (AS3, Mudtank, Temora 2, NIST 610 glass) for ch. 2.

Appendix B: All Data for Chapter Two Unknowns

Sample name	Session	Day	Age (Ga)	2 s.d.	176Hf/177 Hf	2 s.d.	176Lu/177 Hf	2 s.d.	Hf(T) CHUR	Hf (T)	eps Hf	2 s.d.	Hf(T) DMM	TDM .006	2 sigma	TDM .01	2 sigma	TDM .022	2 sigma
RSES51_10-1	2	1	3.982	0.005	0.2802	0.0001	0.0017	0.0000	0.2802	0.2800	-5.1	2.1	0.280	4.318	0.082	4.364	0.094	4.627	0.157
RSES51_10-10	2	1	3.463	0.001	0.2804	0.0001	0.0013	0.0000	0.2805	0.2803	-8.4	2.1	0.281	4.042	0.083	4.121	0.095	4.571	0.159
RSES51_10-11	2	2	3.395	0.001	0.2804	0.0000	0.0008	0.0000	0.2806	0.2803	-9.5	1.9	0.281	4.036	0.073	4.123	0.082	4.621	0.138
RSES51_10-12 blks 1-4	2	2	3.783	0.011	0.2800	0.0001	0.0008	0.0000	0.2803	0.2800	-13.1	2.1	0.280	4.513	0.082	4.612	0.093	5.179	0.154
RSES51_10-12 blks 5-10	2	2	3.615	0.014	0.2800	0.0001	0.0008	0.0000	0.2804	0.2800	-17.4	2.1	0.281	4.567	0.084	4.696	0.095	5.432	0.157
RSES51_10-14	2	2	3.380	0.001	0.2804	0.0000	0.0007	0.0000	0.2806	0.2803	-9.1	1.9	0.281	4.004	0.073	4.088	0.083	4.574	0.140
RSES51_10-4 blks 8-10	2	1	2.912	0.010	0.2805	0.0001	0.0071	0.0002	0.2809	0.2801	-29.0	4.0	0.281	4.500	0.171	4.713	0.193	5.925	0.320
RSES51_10-6	2	1	3.456	0.002	0.2806	0.0001	0.0013	0.0000	0.2805	0.2805	-1.9	2.2	0.281	3.744	0.086	3.783	0.098	4.008	0.165
RSES51_1-10	1	1	3.390	0.003	0.2804	0.0000	0.0004	0.0000	0.2806	0.2804	-7.1	1.2	0.281	3.905	0.032	3.975	0.037	4.377	0.061
RSES51_1-11	1	1	3.371	0.003	0.2804	0.0000	0.0008	0.0000	0.2806	0.2803	-9.6	1.2	0.281	4.001	0.029	4.087	0.033	4.577	0.055
RSES51_11-1	2	2	3.408	0.003	0.2803	0.0000	0.0009	0.0000	0.2806	0.2803	-10.4	1.9	0.281	4.086	0.074	4.177	0.084	4.704	0.140
RSES51_11-10	2	2	3.389	0.001	0.2804	0.0000	0.0007	0.0000	0.2806	0.2803	-9.4	1.9	0.281	4.026	0.073	4.112	0.083	4.608	0.140
RSES51_11-3	2	2	3.399	0.022	0.2804	0.0000	0.0005	0.0000	0.2806	0.2804	-8.3	1.9	0.281	3.983	0.076	4.062	0.085	4.516	0.140
RSES51_11-6	2	2	3.402	0.002	0.2803	0.0000	0.0007	0.0000	0.2806	0.2802	-12.1	1.9	0.281	4.155	0.072	4.257	0.082	4.842	0.138
RSES51_11-9	2	2	3.395	0.001	0.2804	0.0000	0.0006	0.0000	0.2806	0.2803	-9.6	1.9	0.281	4.039	0.075	4.126	0.085	4.627	0.142
RSES51_12-1	2	2	3.455	0.001	0.2803	0.0000	0.0011	0.0000	0.2805	0.2803	-9.9	1.9	0.281	4.101	0.074	4.188	0.084	4.690	0.140
RSES51_12-12	2	2	3.898	0.001	0.2802	0.0000	0.0003	0.0000	0.2802	0.2801	-4.1	1.4	0.280	4.205	0.047	4.247	0.054	4.487	0.091
RSES51_12-13	2	2	3.394	0.002	0.2803	0.0000	0.0007	0.0000	0.2806	0.2803	-12.0	1.5	0.281	4.145	0.051	4.247	0.057	4.829	0.096
RSES51_12-15	2	2	3.392	0.002	0.2804	0.0000	0.0009	0.0000	0.2806	0.2803	-10.2	1.6	0.281	4.065	0.056	4.156	0.064	4.678	0.107
RSES51_12-3 blks1-5	2	2	3.545	0.003	0.2804	0.0000	0.0006	0.0000	0.2805	0.2804	-3.5	2.0	0.281	3.892	0.079	3.939	0.089	4.210	0.151
RSES51_12-3 blks6-10	2	2																	
RSES51_12-8	2	2	3.403	0.004	0.2805	0.0000	0.0012	0.0001	0.2806	0.2804	-6.3	1.6	0.281	3.897	0.057	3.964	0.065	4.350	0.109
RSES51_12-9	2	2	3.405	0.002	0.2803	0.0000	0.0007	0.0000	0.2806	0.2803	-11.4	1.4	0.281	4.126	0.045	4.224	0.051	4.783	0.085
RSES51_13-11	2	2	3.388	0.002	0.2805	0.0001	0.0011	0.0000	0.2806	0.2804	-5.1	2.2	0.281	3.833	0.089	3.893	0.101	4.241	0.170
RSES51_13-13 blks8-10	2	2	3.561	0.042	0.2804	0.0001	0.0009	0.0000	0.2805	0.2803	-5.4	2.6	0.281	3.990	0.115	4.048	0.129	4.382	0.209
RSES51_13-14	2	2	3.460	0.001	0.2804	0.0001	0.0005	0.0000	0.2805	0.2804	-5.8	2.2	0.281	3.925	0.087	3.988	0.099	4.351	0.166
RSES51_13-15	2	2	3.394	0.002	0.2804	0.0001	0.0006	0.0000	0.2806	0.2803	-9.4	2.2	0.281	4.032	0.088	4.118	0.100	4.614	0.168
RSES51_13-2	2	2	3.638	0.001	0.2803	0.0000	0.0004	0.0000	0.2804	0.2802	-7.1	1.4	0.281	4.127	0.047	4.194	0.054	4.575	0.091
RSES51_13-3	2	2	3.460	0.001	0.2805	0.0001	0.0013	0.0000	0.2805	0.2804	-6.2	2.1	0.281	3.939	0.085	4.004	0.096	4.378	0.161
RSES51_13-5	2	2	3.456	0.001	0.2804	0.0001	0.0008	0.0000	0.2805	0.2803	-7.1	2.1	0.281	3.976	0.085	4.046	0.096	4.452	0.162
RSES51_13-8	2	2	3.562	0.002	0.2804	0.0001	0.0003	0.0000	0.2805	0.2804	-3.9	2.3	0.281	3.920	0.091	3.968	0.104	4.248	0.175

RSES51_14-1	2	3	3.631	0.003	0.2804	0.0000	0.0013	0.0000	0.2804	0.2803	-4.4	1.8	0.281	4.000	0.068	4.050	0.077	4.338	0.129
RSES51_14-11	2	3	3.390	0.005	0.2804	0.0000	0.0005	0.0000	0.2806	0.2803	-9.1	1.9	0.281	4.011	0.071	4.095	0.080	4.578	0.134
RSES51_14-13	2	3	3.762	0.002	0.2804	0.0000	0.0016	0.0001	0.2803	0.2803	-2.5	1.8	0.280	4.022	0.069	4.057	0.078	4.261	0.131
RSES51_14-15	2	3	3.541	0.005	0.2805	0.0000	0.0006	0.0000	0.2805	0.2805	-1.3	1.8	0.281	3.789	0.069	3.822	0.079	4.016	0.133
RSES51_14-3	2	3	3.560	0.003	0.2804	0.0000	0.0004	0.0000	0.2805	0.2803	-4.8	1.8	0.281	3.960	0.069	4.014	0.078	4.327	0.132
RSES51_14-8	2	3	3.385	0.005	0.2803	0.0000	0.0005	0.0000	0.2806	0.2803	-10.4	1.8	0.281	4.066	0.068	4.159	0.078	4.688	0.130
RSES51_14-9	2	3	3.395	0.004	0.2803	0.0000	0.0005	0.0000	0.2806	0.2803	-11.8	1.8	0.281	4.138	0.068	4.239	0.077	4.816	0.130
RSES51_1-5	1	1	3.402	0.006	0.2803	0.0000	0.0007	0.0000	0.2806	0.2803	-11.7	1.2	0.281	4.118	0.036	4.214	0.040	4.770	0.067
RSES51_15-10	2	3	3.575	0.001	0.2804	0.0000	0.0004	0.0000	0.2805	0.2803	-4.9	1.8	0.281	3.977	0.069	4.032	0.078	4.346	0.131
RSES51_15-11	2	3	3.463	0.001	0.2803	0.0000	0.0008	0.0000	0.2805	0.2803	-10.1	1.8	0.281	4.119	0.069	4.208	0.078	4.718	0.131
RSES51_15-14	2	3	3.400	0.001	0.2803	0.0000	0.0006	0.0000	0.2806	0.2803	-10.3	1.9	0.281	4.076	0.071	4.167	0.081	4.692	0.135
RSES51_15-2	2	3	3.527	0.002	0.2804	0.0000	0.0006	0.0000	0.2805	0.2804	-3.4	1.8	0.281	3.870	0.067	3.917	0.076	4.185	0.128
RSES51_15-3	2	3	3.410	0.005	0.2803	0.0000	0.0012	0.0001	0.2806	0.2802	-13.3	1.9	0.281	4.216	0.071	4.325	0.081	4.949	0.135
RSES51_1-6	1	1	3.864	0.011	0.2803	0.0000	0.0032	0.0002	0.2803	0.2800	-9.3	1.9	0.280	4.383	0.075	4.454	0.085	4.858	0.141
RSES51_16-1	2	3	3.397	0.002	0.2803	0.0000	0.0008	0.0000	0.2806	0.2803	-11.9	1.8	0.281	4.145	0.068	4.246	0.077	4.826	0.128
RSES51_16-10	2	3	3.396	0.002	0.2804	0.0000	0.0008	0.0000	0.2806	0.2803	-9.3	1.8	0.281	4.029	0.069	4.114	0.078	4.606	0.131
RSES51_16-13	2	3	3.397	0.001	0.2803	0.0000	0.0004	0.0000	0.2806	0.2803	-9.6	1.9	0.281	4.040	0.073	4.127	0.083	4.626	0.139
RSES51_16-14	2	3	3.392	0.001	0.2803	0.0000	0.0005	0.0000	0.2806	0.2803	-10.4	1.9	0.281	4.071	0.072	4.163	0.082	4.691	0.137
RSES51_16-15	2	3	3.391	0.002	0.2803	0.0000	0.0003	0.0000	0.2806	0.2803	-10.8	1.9	0.281	4.091	0.072	4.186	0.082	4.730	0.137
RSES51_16-2	2	3	3.408	0.003	0.2803	0.0000	0.0006	0.0000	0.2806	0.2803	-10.3	1.8	0.281	4.081	0.069	4.172	0.079	4.695	0.132
RSES51_16-3	2	3	3.396	0.003	0.2804	0.0000	0.0003	0.0000	0.2806	0.2804	-7.1	1.9	0.281	3.929	0.071	4.001	0.081	4.416	0.135
RSES51_1-7	1	1	3.396	0.006	0.2804	0.0000	0.0009	0.0000	0.2806	0.2804	-8.5	1.2	0.281	3.971	0.030	4.048	0.034	4.496	0.056
RSES51_17-1	2	3	3.950	0.003	0.2801	0.0001	0.0009	0.0000	0.2802	0.2801	-5.3	4.0	0.280	4.302	0.172	4.350	0.196	4.626	0.330
RSES51_17-11	2	3	3.764	0.001	0.2803	0.0001	0.0012	0.0000	0.2803	0.2803	-2.8	4.0	0.280	4.036	0.173	4.073	0.196	4.287	0.331
RSES51_17-12	2	3	3.543	0.003	0.2803	0.0001	0.0002	0.0000	0.2805	0.2803	-8.1	4.0	0.281	4.093	0.174	4.168	0.197	4.597	0.331
RSES51_17-2	2	3	3.976	0.005	0.2800	0.0001	0.0005	0.0000	0.2802	0.2800	-7.5	4.1	0.280	4.422	0.176	4.482	0.200	4.830	0.336
RSES51_17-3	2	3	3.401	0.002	0.2803	0.0001	0.0005	0.0000	0.2806	0.2803	-9.6	4.0	0.281	4.045	0.171	4.133	0.194	4.633	0.326
RSES51_17-6 blks2-3,7-10	2	3	3.410	0.036	0.2803	0.0001	0.0007	0.0000	0.2806	0.2803	-10.1	4.0	0.281	4.072	0.178	4.162	0.201	4.677	0.334
RSES51_17-7	2	3	3.387	0.001	0.2805	0.0001	0.0006	0.0000	0.2806	0.2804	-5.2	4.0	0.281	3.836	0.174	3.897	0.197	4.248	0.332
RSES51_17-9 blks1-6	2	3	3.461	0.001	0.2804	0.0001	0.0008	0.0000	0.2805	0.2803	-7.9	4.0	0.281	4.018	0.172	4.093	0.195	4.526	0.327
RSES51_17-9 blks7-10	2	3	3.493	0.002	0.2804	0.0001	0.0011	0.0000	0.2805	0.2803	-7.5	4.1	0.281	4.028	0.179	4.100	0.203	4.517	0.342
RSES51_1-9 blks 1-4	1	1	3.515	0.006	0.2805	0.0001	0.0048	0.0002	0.2805	0.2801	-13.5	3.7	0.281	4.291	0.159	4.396	0.181	4.997	0.302
RSES51_1-9 blks 9-10	1	1									-10.0								
RSES51_2-10	1	1	3.534	0.003	0.2805	0.0000	0.0010	0.0000	0.2805	0.2805	-1.7	1.8	0.281	3.775	0.060	3.808	0.068	3.997	0.115
RSES51_2-10	1	1	3.534	0.003	0.2805	0.0000	0.0010	0.0000	0.2805	0.2805	-1.7	1.8	0.281	3.775	0.060	3.808	0.068	3.997	0.115
RSES51_2-11	1	1	3.386	0.001	0.2804	0.0000	0.0007	0.0000	0.2806	0.2803	-9.7	1.7	0.281	4.016	0.056	4.101	0.064	4.591	0.107
RSES51_2-12 blks1-3	1	1	3.407	0.010	0.2803	0.0001	0.0012	0.0002	0.2806	0.2803	-11.7	2.3	0.281	4.123	0.083	4.220	0.094	4.775	0.157
RSES51_2-14	1	1	3.388	0.002	0.2804	0.0000	0.0005	0.0000	0.2806	0.2804	-8.7	1.6	0.281	3.972	0.057	4.051	0.065	4.506	0.109

RSES51_2-3	1	1	3.384	0.001	0.2804	0.0000	0.0010	0.0000	0.2806	0.2803	-11.0	1.8	0.281	4.072	0.057	4.165	0.065	4.700	0.109
RSES51_2-4	1	1	3.463	0.038	0.2804	0.0000	0.0012	0.0001	0.2806	0.2803	-9.4	2.2	0.281	4.064	0.087	4.145	0.096	4.613	0.153
RSES51_2-5	1	1	3.546	0.005	0.2804	0.0000	0.0004	0.0000	0.2805	0.2804	-4.7	1.6	0.281	3.920	0.058	3.970	0.066	4.262	0.111
RSES51_2-6	1	1	3.394	0.001	0.2803	0.0000	0.0005	0.0000	0.2806	0.2803	-10.3	1.6	0.281	4.051	0.056	4.140	0.064	4.650	0.107
RSES51_2-7	1	1	3.384	0.002	0.2804	0.0000	0.0004	0.0000	0.2806	0.2803	-9.2	1.6	0.281	3.993	0.058	4.076	0.065	4.549	0.110
RSES51_2-8	1	1	3.379	0.002	0.2804	0.0000	0.0009	0.0000	0.2806	0.2803	-11.0	1.8	0.281	4.067	0.059	4.160	0.066	4.695	0.111
RSES51_2-9	1	1	3.387	0.002	0.2804	0.0000	0.0008	0.0001	0.2806	0.2803	-9.6	1.7	0.281	4.012	0.059	4.096	0.067	4.582	0.112
RSES51_3-1	1	1	3.547	0.002	0.2804	0.0000	0.0007	0.0000	0.2805	0.2804	-3.9	2.1	0.281	3.887	0.079	3.933	0.089	4.198	0.150
RSES51_3-10 core	1	1	3.363	0.002	0.2805	0.0000	0.0020	0.0000	0.2806	0.2804	-7.6	2.3	0.281	3.905	0.061	3.979	0.069	4.401	0.116
RSES51_3-10 rim	1	1									2.9								
RSES51_3-11	1	1	3.379	0.001	0.2804	0.0000	0.0009	0.0000	0.2806	0.2803	-10.5	1.7	0.281	4.046	0.058	4.137	0.066	4.656	0.111
RSES51_3-12	1	1	3.704	0.003	0.2804	0.0000	0.0017	0.0001	0.2804	0.2802	-5.4	2.2	0.280	4.081	0.062	4.133	0.071	4.428	0.119
RSES51_3-13 blks 1-2	1	1																	
RSES51_3-13 blks 6-9	1	1	3.530	0.038	0.2804	0.0001	0.0019	0.0000	0.2805	0.2803	-7.0	2.7	0.281	4.013	0.099	4.078	0.110	4.455	0.178
RSES51_3-14	1	1	3.383	0.001	0.2803	0.0000	0.0010	0.0000	0.2806	0.2803	-11.6	1.8	0.281	4.100	0.058	4.197	0.066	4.753	0.110
RSES51_3-2	1	1	3.399	0.004	0.2804	0.0000	0.0008	0.0000	0.2806	0.2803	-9.4	1.7	0.281	4.015	0.058	4.098	0.065	4.577	0.110
RSES51_3-3 blks 1-3	1	1	3.512	0.003	0.2804	0.0000	0.0006	0.0000	0.2805	0.2804	-5.3	1.8	0.281	3.920	0.063	3.975	0.072	4.294	0.120
RSES51_3-3 blks 5-7	1	1	3.467	0.002	0.2804	0.0000	0.0007	0.0000	0.2806	0.2804	-5.6	1.9	0.281	3.898	0.070	3.957	0.080	4.293	0.134
RSES51_3-4	1	1	3.529	0.002	0.2804	0.0000	0.0005	0.0000	0.2805	0.2803	-6.3	1.7	0.281	3.979	0.063	4.041	0.071	4.392	0.119
RSES51_3-5	1	1	3.538	0.003	0.2802	0.0000	0.0003	0.0000	0.2805	0.2802	-10.3	1.6	0.281	4.165	0.057	4.250	0.064	4.737	0.108
RSES51_3-6 blks 1-2	1	1																	
RSES51_3-6 blks 3-5	1	1																	
RSES51_3-6 blks 7-8	1	1																	
RSES51_3-7	1	1	3.633	0.001	0.2803	0.0000	0.0008	0.0000	0.2804	0.2802	-7.3	1.7	0.281	4.108	0.057	4.173	0.065	4.543	0.109
RSES51_3-8	1	1	3.392	0.007	0.2803	0.0000	0.0011	0.0000	0.2806	0.2803	-12.4	1.8	0.281	4.142	0.058	4.243	0.065	4.825	0.109
RSES51_3-9	1	1	3.411	0.003	0.2804	0.0000	0.0011	0.0000	0.2806	0.2803	-10.4	1.8	0.281	4.069	0.057	4.158	0.065	4.670	0.108
RSES51_4-1	1	1	3.395	0.002	0.2805	0.0000	0.0008	0.0000	0.2806	0.2804	-6.4	1.7	0.281	3.877	0.060	3.943	0.068	4.319	0.114
RSES51_4-2	1	1	3.686	0.034	0.2803	0.0000	0.0006	0.0000	0.2804	0.2803	-4.7	1.7	0.280	4.032	0.067	4.079	0.074	4.350	0.116
RSES51_4-3 blks 3-10	1	1																	
RSES51_4-3 rim	1	1																	
RSES51_4-4	1	1																	
RSES51_4-4 blks 6-7	1	1																	
RSES51_4-5	1	1	3.829	0.004	0.2800	0.0000	0.0005	0.0000	0.2803	0.2800	-11.4	1.7	0.280	4.446	0.059	4.530	0.067	5.010	0.112
RSES51_4-6	1	1	3.369	0.005	0.2804	0.0000	0.0007	0.0000	0.2806	0.2804	-9.1	1.7	0.281	3.976	0.057	4.059	0.065	4.531	0.109
RSES51_4-7	1	1	3.754	0.002	0.2803	0.0000	0.0009	0.0000	0.2804	0.2802	-5.0	1.8	0.280	4.104	0.057	4.151	0.065	4.424	0.110
RSES51_4-8	1	1	3.384	0.002	0.2804	0.0000	0.0006	0.0000	0.2806	0.2803	-9.8	1.7	0.281	4.017	0.058	4.103	0.065	4.595	0.109
RSES51_4-9	1	1	4.061	0.002	0.2801	0.0000	0.0005	0.0000	0.2802	0.2800	-4.4	1.7	0.280	4.322	0.058	4.357	0.065	4.562	0.110
RSES51_5-1 blks1-5	1	1	3.850	0.002	0.2802	0.0000	0.0003	0.0000	0.2803	0.2802	-4.9	1.7	0.280	*4.176*	*0.061*	*4.220*	*0.069*	*4.475*	*0.116*
RSES51_5-1 blks1-5	1	1	3.850	0.002	0.2802	0.0000	0.0003	0.0000	0.2803	0.2802	-4.9	1.7	0.280	*4.176*	*0.061*	*4.220*	*0.069*	*4.475*	*0.116*

RSES51_5-1 blks6-10	1	1	3.822	0.005	0.2802	0.0000	0.0004	0.0000	0.2803	0.2801	-6.2	1.8	0.280	4.210	0.065	4.263	0.074	4.566	0.124
RSES51_5-2	1	1	3.547	0.003	0.2804	0.0000	0.0003	0.0000	0.2805	0.2804	-3.4	1.6	0.281	3.865	0.059	3.908	0.067	4.157	0.112
RSES51_5-3 blks1-7	1	1	3.379	0.003	0.2804	0.0000	0.0008	0.0000	0.2806	0.2803	-10.4	1.7	0.281	4.041	0.057	4.131	0.065	4.646	0.109
RSES51_5-4 blks1-7	1	1	3.459	0.001	0.2804	0.0000	0.0010	0.0000	0.2806	0.2804	-6.2	1.8	0.281	3.921	0.060	3.983	0.068	4.343	0.114
RSES51_5-5	1	1	3.378	0.002	0.2804	0.0000	0.0005	0.0000	0.2806	0.2803	-9.3	1.7	0.281	3.991	0.058	4.075	0.066	4.552	0.111
RSES51_5-6	1	1	3.374	0.004	0.2804	0.0000	0.0010	0.0000	0.2806	0.2803	-9.7	2.0	0.281	4.007	0.070	4.093	0.080	4.585	0.133
RSES51_5-7	1	1	3.396	0.003	0.2803	0.0000	0.0007	0.0000	0.2806	0.2803	-10.8	1.7	0.281	4.071	0.058	4.163	0.066	4.687	0.111
RSES51_5-8 blks1-6	1	1																	
RSES51_5-8 blks7-10	1	1																	
RSES51_5-9	1	1	3.380	0.001	0.2804	0.0000	0.0009	0.0000	0.2806	0.2803	-10.2	1.7	0.281	4.034	0.056	4.122	0.064	4.630	0.107
RSES51_6-1	1	1	3.450	0.003	0.2803	0.0000	0.0005	0.0000	0.2806	0.2803	-10.5	1.6	0.281	4.105	0.057	4.193	0.065	4.702	0.108
RSES51_6-1	1	1	3.450	0.003	0.2803	0.0000	0.0005	0.0000	0.2806	0.2803	-10.5	1.6	0.281	4.105	0.057	4.193	0.065	4.702	0.108
RSES51_6-10	1	1	3.563	0.008	0.2803	0.0000	0.0003	0.0000	0.2805	0.2803	-6.7	1.6	0.281	4.024	0.059	4.087	0.067	4.447	0.111
RSES51_6-10	1	1	3.563	0.008	0.2803	0.0000	0.0003	0.0000	0.2805	0.2803	-6.7	1.6	0.281	4.024	0.059	4.087	0.067	4.447	0.111
RSES51_6-11	1	1	3.580	0.002	0.2804	0.0000	0.0008	0.0000	0.2805	0.2803	-5.1	1.7	0.281	3.967	0.058	4.020	0.066	4.322	0.112
RSES51_6-2	1	1	3.445	0.001	0.2804	0.0000	0.0008	0.0000	0.2806	0.2803	-9.6	1.7	0.281	4.058	0.057	4.142	0.064	4.619	0.108
RSES51_6-3	1	1	3.438	0.003	0.2804	0.0000	0.0008	0.0000	0.2806	0.2804	-6.3	1.7	0.281	3.906	0.057	3.969	0.065	4.334	0.109
RSES51_6-4	1	1	3.378	0.001	0.2804	0.0000	0.0007	0.0000	0.2806	0.2803	-9.5	1.7	0.281	4.000	0.057	4.084	0.065	4.568	0.109
RSES51_6-5	1	1	3.384	0.003	0.2804	0.0000	0.0005	0.0000	0.2806	0.2803	-10.1	1.6	0.281	4.032	0.057	4.120	0.065	4.624	0.109
RSES51_6-6	1	1	3.380	0.002	0.2804	0.0000	0.0005	0.0000	0.2806	0.2803	-9.7	1.7	0.281	4.012	0.058	4.097	0.066	4.588	0.110
RSES51_6-7	1	1	3.383	0.001	0.2804	0.0000	0.0007	0.0000	0.2806	0.2804	-9.0	1.7	0.281	3.982	0.057	4.063	0.065	4.529	0.108
RSES51_6-8 blks1-5	1	1	3.395	0.004	0.2804	0.0000	0.0008	0.0000	0.2806	0.2803	-9.6	1.8	0.281	4.019	0.061	4.103	0.069	4.589	0.115
RSES51_6-8 blks1-5	1	1	3.395	0.004	0.2804	0.0000	0.0008	0.0000	0.2806	0.2803	-9.6	1.8	0.281	4.019	0.061	4.103	0.069	4.589	0.115
RSES51_6-8 blks6-8	1	1	3.416	0.003	0.2805	0.0001	0.0013	0.0000	0.2806	0.2804	-7.4	2.5	0.281	3.938	0.093	4.008	0.105	4.415	0.176
RSES51_6-8 blks9-10	1	1																	
RSES51_6-9	1	1	3.393	0.002	0.2803	0.0000	0.0006	0.0000	0.2806	0.2803	-10.4	1.7	0.281	4.053	0.058	4.142	0.066	4.655	0.111
RSES51_7-1	1	1	3.459	0.072	0.2804	0.0002	0.0015	0.0005	0.2806	0.2803	-10.2	6.7	0.281	4.097	0.298	4.184	0.335	4.680	0.554
RSES51_7-10 blks2-4	2	1	3.536	0.002	0.2805	0.0001	0.0008	0.0000	0.2805	0.2804	-3.4	2.0	0.281	3.877	0.080	3.923	0.091	4.190	0.154
RSES51_7-10 blks7-10	2	1	3.519	0.002	0.2805	0.0001	0.0008	0.0000	0.2805	0.2804	-3.7	2.1	0.281	3.877	0.084	3.925	0.095	4.205	0.160
RSES51_7-2 blk10	1	1																	
RSES51_7-2 blks1-7	1	1	3.351	0.006	0.2803	0.0000	0.0009	0.0000	0.2806	0.2803	-12.2	1.8	0.281	4.100	0.060	4.201	0.068	4.781	0.113
RSES51_7-2 blks8-9	1	1																	
RSES51_7-5	2	1	3.532	0.003	0.2804	0.0000	0.0006	0.0000	0.2805	0.2803	-6.0	2.0	0.281	3.992	0.076	4.054	0.087	4.413	0.146
RSES51_7-6	2	1	3.408	0.001	0.2805	0.0000	0.0017	0.0001	0.2806	0.2804	-7.6	2.0	0.281	3.963	0.075	4.038	0.085	4.470	0.143
RSES51_7-8	2	1	3.405	0.001	0.2804	0.0000	0.0007	0.0000	0.2806	0.2803	-8.2	1.9	0.281	3.985	0.073	4.064	0.083	4.515	0.139
RSES51_7-9	2	1	3.399	0.001	0.2804	0.0000	0.0010	0.0000	0.2806	0.2803	-9.0	1.9	0.281	4.015	0.074	4.098	0.084	4.577	0.141
RSES51_8-11	2	1	3.402	0.002	0.2804	0.0000	0.0006	0.0000	0.2806	0.2804	-6.6	1.9	0.281	3.909	0.074	3.978	0.084	4.374	0.142
RSES51_8-15	2	1	3.521	0.010	0.2805	0.0001	0.0018	0.0001	0.2805	0.2804	-4.8	2.4	0.281	3.930	0.100	3.986	0.114	4.305	0.191

RSES51_9-1	2	1	3.463	0.002	0.2804	0.0000	0.0004	0.0000	0.2805	0.2804	-5.8	2.0	0.281	3.927	0.076	3.990	0.086	4.352	0.145
RSES51_9-11	2	1	3.461	0.002	0.2804	0.0001	0.0008	0.0000	0.2805	0.2803	-8.4	2.1	0.281	4.039	0.085	4.118	0.096	4.568	0.162
RSES51_9-2a	2	1	4.095	0.003	0.2802	0.0000	0.0020	0.0000	0.2801	0.2800	-3.9	1.9	0.280	4.356	0.077	4.392	0.087	4.596	0.147
RSES51_9-2b blks2-3	*2*	*1*																	
RSES51_9-2b blks4-8	2	1	4.102	0.005	0.2801	0.0001	0.0010	0.0000	0.2801	0.2800	-4.4	2.2	0.280	4.384	0.091	4.422	0.103	4.643	0.174
RSES51_9-2b blks9-10	*2*	*1*																	
RSES51_9-8	2	1	3.415	0.003	0.2803	0.0000	0.0005	0.0000	0.2806	0.2803	-10.3	1.9	0.281	4.086	0.074	4.177	0.084	4.698	0.141

Sample name	**d18O**	**1 s.d.**	**[Ti]**	**1 se [Ti]**	**Tc**	**1 sigma**	**CL Zone Type**	**CL Brightness**	**Size**	**Shape**
			ppm		**deg C**	**deg C**	**Osc, Sect, X**	**bright, med, dark**	**umxum**	
RSES51_10-1			10.24	0.07	743	52	spotty	dark	100x150	rounded prismatic
RSES51_10-10	5.9	0.3					patchy	dark	200x200	equant
RSES51_10-11	5.4	0.3					patchy	bright/med	150x175	equant
RSES51_10-12 blks 1-4	5.5	0.4					patchy	med	200x250	angular
RSES51_10-12 blks 5-10							patchy	med	200x250	angular
RSES51_10-14							chaotic	med	150x200	equant round
RSES51_10-4 blks 8-10							chaotic	bright	200x250	rough equant
RSES51_10-6	5.9	0.6					X	dark	150x150	equant
RSES51_1-10	5.9	0.3					X	med	150x150	subrounded
RSES51_1-11	5.4	0.3	8.60	0.03	728	29	osc & sector, xenocrystic core	bright	400x400	subrounded
RSES51_11-1	6.1	0.6					bright polygonal rim, med core	bright	200x200	octagonal
RSES51_11-10	5.7	0.5					osc, planar	bright	150x200	equant
RSES51_11-3							sector/patchy	bright/med	150x150	equant
RSES51_11-6							osc, offcenter concentric	bright	125x150	triangular
RSES51_11-9							pathcy, faint	med	150x250	triangular
RSES51_12-1							faint rim	med	250x350	rounded prismatic
RSES51_12-12			1.78	0.00	609	43	X	dark	150x250	rounded prismatic
RSES51_12-13	5.6	0.6					dark rim med core	med	150x250	rounded prismatic
RSES51_12-15							med rim in patches, dark core	dark/med	150x200	subangular
RSES51_12-3 blks1-5							osc conc offcenter??	med	125x125	equant
RSES51_12-3 blks6-10							osc conc offcenter??	med	125x125	equant
RSES51_12-8							probably sector; too small to tell	bright	125x125	round equant
RSES51_12-9	5.3	0.6					osc conc with dark rim in patches	bright	250x250	round equant
RSES51_13-11							X or faint	med-dark	150x200	rounded prismatic
RSES51_13-13 blks8-10							X or chaotic faint	dark	150x300	rounded prismatic
RSES51_13-14	5.9	0.3					osc conc	dark/med	200x200	round equant
RSES51_13-15	5.0	0.3					polygonal concentric bright zone	dark/bright	150x150	round equant
RSES51_13-2			3.94	0.01	665	47	bright rim, sect/chaotic core	med/bright	150x200	angular

RSES51_13-3							patchy? Faint	dark/med	150x150	angular
RSES51_13-5							osc	med-bright	200x200	round
RSES51_13-8							osc conc? Faint	med	250x250	angular
RSES51_14-1	4.9	0.4					chaotic? faint	med	150x175	subangular
RSES51_14-11							core/rim, both osc	bright	250x250	octagonal
RSES51_14-13							rim/core	med	125x125	round
RSES51_14-15	4.8	0.5					X or faint chaotic	med-dark	150x250	rounded prismatic
RSES51_14-3							concentric broad osc	med/bright	200x250	subrounded
RSES51_14-8	5.3	0.6					osc conc offcenter	bright	150x200	angular
RSES51_14-9	5.0	0.6					chaotic	bright	200x200	equant/chevron
RSES51_1-5	6.1	0.3	8.27	0.03	724	29	osc (disrupted?)	bright	175x200	subrounded broken
RSES51_15-10							patchy	med-bright	125x150	subrounded
RSES51_15-11							patchy?	med-bright	150x150	subrounded
RSES51_15-14	5.3	0.5					osc, possible disruption	bright	200x250	subangular
RSES51_15-2							osc with disruption	med-bright	200x300	subangular
RSES51_15-3	5.8	0.3					osc planar	med-bright	150x175	subrounded
RSES51_1-6	4.9	0.3					faint	med	200x300	subrounded broken
RSES51_16-1	5.5	0.3					X (possible dark rim)	bright	250x350	broken euhedral prism
RSES51_16-10	5.8	0.3					X to faint sect	med	125x200	subrounded
RSES51_16-13							osc planar	med	150x250	subangular
RSES51_16-14	5.2	0.4					patchy	bright	150x150	subangular
RSES51_16-15	4.9	0.3					osc conc	med/bright	125x125	subrounded
RSES51_16-2	5.3	0.3					patchy	bright	150x200	triangular
RSES51_16-3	5.3	0.3					patchy core, osc conc outside	bright/med	175x175	subrounded
RSES51_1-7							X	dark	150x150	broken; resorbed??
RSES51_17-1	5.8	0.3	5.45	0.02	690	49	X to uncertain	bright	175x200	subrounded
RSES51_17-11	4.2	0.3					X	dark	150x200	subangular
RSES51_17-12	5.9	0.3					osc planar?	med-bright	125x150	subrounded
RSES51_17-2	6.1	0.3	6.20	0.03	700	49	X	bright	150x200	subrounded
RSES51_17-3	5.5	0.3					X	bright	125x250	subrounded
RSES51_17-6 blks2-3,7-10	5.7	0.3					osc conc with chaotic core	bright/med	200x250	euhedral
RSES51_17-7							osc conc with sect in rim(?)	med	125x200	subrounded broken
RSES51_17-9 blks1-6							X (rim?)	med	100x125	subrounded
RSES51_17-9 blks7-10							X (rim?)	med	100x125	subrounded
RSES51_1-9 blks 1-4	5.9	0.3					stripes	bright, med, dark	150x200	subrounded; crack
RSES51_1-9 blks 9-10							stripes	bright, med, dark	150x200	subrounded; crack
RSES51_2-10	5.9	0.3	4.07	0.01	668	47	X or faint stripe	med	175x200	subrounded
RSES51_2-10	5.9	0.3	4.07	0.01	668	47	X or faint stripe	med	175x200	subrounded
RSES51_2-11	5.6	0.3	6.80	0.02	708	29	bright rim, uncertain core	med	150x150	subrounded

RSES51_2-12 blks1-3	5.1	0.3	3.36	0.00	653	27	X or faint patchy	med	150x200	subrounded
RSES51_2-14			4.67	0.01	678	28	rim/core	med	150x300	euhedral
RSES51_2-3	5.7	0.3	4.40	0.01	673	28	osc internal, truncated by rims; 2 grains	med-bright	lased: 175x250	lased: square; other: broken
RSES51_2-4	5.4	0.3	4.05	0.01	667	27	patchy	med-bright	200x250	subrounded
RSES51_2-5	5.8	0.3	6.01	0.01	698	28	X or faint broad stripe	med	200x250	subrounded
RSES51_2-6	5.3	0.3	5.51	0.01	691	28	patchy	med	200x300	subrounded triangular
RSES51_2-7	5.1	0.3	4.87	0.01	681	28	X or faint	med	175x250	subangular
RSES51_2-8	5.0	0.3	4.99	0.01	683	28	osc; core disrupted?	bright	175x250	subangular, broken
RSES51_2-9	6.1	0.3	3.68	0.01	660	27	thin bright rim	med	175x175	subangular broken
RSES51_3-1	5.8	0.3	12.56	0.11	761	54	X to faint	med	150x225	subrounded
RSES51_3-10 core	6.0	0.3					X to faint stripes (rim?)	dark	125x150	subrounded broken
RSES51_3-10 rim							X to faint stripes (rim?)	dark	125x150	subrounded broken
RSES51_3-11	5.4	0.3					osc faint	med	150x175	subangular
RSES51_3-12	4.5	0.3					stripes	bright, med, dark	150x200	subrounded
RSES51_3-13 blks 1-2	4.8	0.3	3.80	0.01	662	27	X	med	150x200	square
RSES51_3-13 blks 6-9							X	med	150x200	square
RSES51_3-14	5.4	0.3	2.13	0.00	621	26	X with cracks	med-bright	200x200	angular
RSES51_3-2							X to faint	med	125x200	subangular fragment
RSES51_3-3 blks 1-3	5.9	0.3					X	med	150x150	subrounded fragment
RSES51_3-3 blks 5-7							X	med	150x150	subrounded fragment
RSES51_3-4	4.6	0.3					faint truncated by rim?	med	150x200	square fragment
RSES51_3-5	5.8	0.3	2.68	0.00	637	26	faint stripes	med	250x250	subangular
RSES51_3-6 blks 1-2	5.0	0.3	3.34	0.00	653	27	faint with dark cracks, bright patch	med	175x250	subangular broken
RSES51_3-6 blks 3-5							faint with dark cracks, bright patch	med	175x250	subangular broken
RSES51_3-6 blks 7-8							faint with dark cracks, bright patch	med	175x250	subangular broken
RSES51_3-7	5.9	0.3	2.41	0.00	630	26	X	dark	175x175	subangular
RSES51_3-8	5.1	0.3					patchy	bright/cark	175x175	triangular
RSES51_3-9							faint patches?	med	150x175	broken
RSES51_4-1	5.9	0.3	2.43	0.00	630	26	stripes, some chaotic	bright, dark	200x300	subrounded triangular
RSES51_4-2	5.3	0.3					patchy, faint	med-bright	200x300	subrounded broken
RSES51_4-3 blks 3-10							X	med-dark	150x200	subrounded
RSES51_4-3 rim	4.8	0.3	3.93	0.01	665	27	X	med-dark	150x200	subrounded
RSES51_4-4	5.7	0.3	2.10	0.00	620	26	X or faint	med	175x175	square broken
RSES51_4-4 blks 6-7							X or faint	med	175x175	square broken
RSES51_4-5	6.0	0.3					patchy, irregular	med-bright	250x300	subangular
RSES51_4-6							faint chaotic/patchy	med	125x150	subrounded scrungy
RSES51_4-7	5.2	0.3					osc conc, homogeneous core	med	150x200	square broken
RSES51_4-8	6.4	0.3	4.04	0.01	667	27	patchy	med	175x250	subangular
RSES51_4-9	5.7	0.3	4.03	0.01	667	27	dark patches around edge? Or just holes?	med-bright	150x150	subangular

RSES51_5-1 blks1-5	5.3	0.3	0.91	0.00	567	24	X	med	125x200	subrounded broken
RSES51_5-1 blks1-5	5.3	0.3	3.84	0.01	663	47	X	med	125x200	subrounded broken
RSES51_5-1 blks6-10							X	med	125x200	subrounded broken
RSES51_5-2	5.9	0.3	2.63	0.00	636	26	osc, faint broad stripes	med	175x200	subrounded
RSES51_5-3 blks1-7	5.3	0.3	3.68	0.01	660	27	faint irregular	med	250x250	subangular
RSES51_5-4 blks1-7	5.6	0.3					X to faint patches	med	150x175	subrounded
RSES51_5-5	5.5	0.3	2.02	0.00	617	26	osc (some) & homogeneous center	med-bright	200x250	subangular
RSES51_5-6	5.2	0.3					patches, irregular	med/bright	150x175	subrounded broken
RSES51_5-7	5.9	0.3	3.13	0.00	648	27	patches, irregular	med-bright	150x200	subangular
RSES51_5-8 blks1-6	6.0	0.3					faint; patchy?	med-bright	250x300	subrounded
RSES51_5-8 blks7-10							faint; patchy?	med-bright	250x300	subrounded
RSES51_5-9	5.6	0.3	2.60	0.00	635	26	X	med	150x200	subangular
RSES51_6-1			54.25	2.04	915	64	X or faint sect	med	150x150	subangular
RSES51_6-1			63.68	2.80	935	65	X or faint sect	med	150x150	subangular
RSES51_6-10	5.7	0.3	4.93	0.02	682	48	X or faint	bright/dark	125x175	angular
RSES51_6-10	5.7	0.3	4.93	0.02	682	48	X or faint	bright/dark	125x175	angular
RSES51_6-11	5.8	0.3	4.41	0.01	674	48	X	med	125x175	subrounded
RSES51_6-2	5.5	0.3	3.63	0.01	659	47	X	med	150x150	angular
RSES51_6-3							osc conc??	med	200x200	subrounded
RSES51_6-4	4.8	0.3	4.37	0.01	673	48	X	med	150x200	subrounded
RSES51_6-5							faint patchy	med-bright	150x150	subrounded
RSES51_6-6							stripes; fragment -- can't tell	bright	150x200	subrounded
RSES51_6-7	5.5	0.3	3.94	0.01	665	47	osc + sect	med-bright	125x175	subangular
RSES51_6-8 blks1-5	5.2	0.3	5.23	0.02	687	49	X to faint	med-bright	??	??
RSES51_6-8 blks1-5	5.2	0.3	5.23	0.02	687	49	X to faint	med-bright	??	??
RSES51_6-8 blks6-8							X to faint	med-bright	??	??
RSES51_6-8 blks9-10							X to faint	med-bright	??	??
RSES51_6-9	5.6	0.3					X + rim	med-bright	125x200	angular
RSES51_7-1	5.3	0.3	6.45	0.03	704	50	stripes or patches; faint	bright/med	200x200	angular
RSES51_7-10 blks2-4							X	med	150x150	subrounded
RSES51_7-10 blks7-10							X	med	150x150	subrounded
RSES51_7-2 blk10							patchy/chaotic	bright	125x125	subangular
RSES51_7-2 blks1-7	5.6	0.3					patchy/chaotic	bright	125x125	subangular
RSES51_7-2 blks8-9							patchy/chaotic	bright	125x125	subangular
RSES51_7-5							X to faint	med	150x150	subrounded
RSES51_7-6							X to faint	med	125x200	subrounded
RSES51_7-8							X	med	150x175	angular
RSES51_7-9							osc conc?	med	150x200	subangular
RSES51_8-11							two zones; patchy? Fragment	med-bright	125x125	subangular

RSES51_8-15							X	dark	125x150	rounded
RSES51_9-1							osc + sect	bright/med	125x175	subrounded
RSES51_9-11	6.2	0.6					X (rim?)	med-bright	150x150	subangular
RSES51_9-2a							patchy	med	200x300	triangular
RSES51_9-2b blks2-3							patchy	med	200x300	triangular
RSES51_9-2b blks4-8							patchy	med	200x300	triangular
RSES51_9-2b blks9-10							patchy	med	200x300	triangular
RSES51_9-8							osc with disruption	bright	200x200	subangular

Sample name	**Inclusion**	**Inclusion**	**Inclusion**	**Inclusion**
	Qualitative Comp. (EDAX)	**Mineralogy**	**Size (um)**	**Notes**
RSES51_10-1				
RSES51_10-10				
RSES51_10-11				
RSES51_10-12 blks 1-4				
RSES51_10-12 blks 5-10				
RSES51_10-14				
RSES51_10-4 blks 8-10				
RSES51_10-6				
RSES51_1-10				
RSES51_1-11				
RSES51_11-1	1) Si+Al+Fe+K; 2) Si+Mg+Al; 3) Si+Al+Na+K	1) musc+qtz; 2) orthoclase+qtz+biotite; 3) orthoclase	1) 10; 2) 10; 3) 2	3) in outer CL zone
RSES51_11-10				
RSES51_11-3				
RSES51_11-6				
RSES51_11-9				
RSES51_12-1				
RSES51_12-12				
RSES51_12-13				
RSES51_12-15				
RSES51_12-3 blks1-5				
RSES51_12-3 blks6-10				
RSES51_12-8				
RSES51_12-9				
RSES51_13-11				
RSES51_13-13 blks8-10				
RSES51_13-14				
RSES51_13-15				

RSES51_13-2				
RSES51_13-3				
RSES51_13-5				
RSES51_13-8				
RSES51_14-1				
RSES51_14-11				
RSES51_14-13				
RSES51_14-15				
RSES51_14-3				
RSES51_14-8				
RSES51_14-9	Si, Al, K +/- Fe, Mg	orthoclase	10	on rim of laser pit
RSES51_1-5	Si	quartz	20x10	recessed
RSES51_15-10				
RSES51_15-11				
RSES51_15-14	Si	quartz	20	intersects a crack
RSES51_15-2				
RSES51_15-3				
RSES51_1-6	1) Al+Si+K; 2) Si	1) ??; 2) qtz	1) <10; 2) > and <10	some on cracks; some recessed
RSES51_16-1	1) Si; 2) Si+Na_Al_K	1) quartzes; 2) orthoclase, anorthoclase, albite	1) 10 & 20; 2) in a 10 um incl.	2) with quartz, Fe-phase
RSES51_16-10				
RSES51_16-13				
RSES51_16-14				
RSES51_16-15				
RSES51_16-2				
RSES51_16-3				
RSES51_1-7				
RSES51_17-1				
RSES51_17-11				
RSES51_17-12				
RSES51_17-2				
RSES51_17-3				
RSES51_17-6 blks2-3,7-10				
RSES51_17-7				
RSES51_17-9 blks1-6				
RSES51_17-9 blks7-10				
RSES51_1-9 blks 1-4				
RSES51_1-9 blks 9-10				
RSES51_2-10				
RSES51_2-10				

RSES51_2-11				
RSES51_2-12 blks1-3	1) Si; 2) Si+Al+K	1) quartz; 2) muscovites	1) 20; 2) 5	1) round; 2) in qtz, 2
RSES51_2-14				
RSES51_2-3	Si	quartz	20x20	flush
RSES51_2-4				
RSES51_2-5				
RSES51_2-6				
RSES51_2-7				
RSES51_2-8				
RSES51_2-9				
RSES51_3-1				
RSES51_3-10 core	1) Fe+REE; 2) Si	1) ??; 2) quartz	1) 5; 2) 5	1) near hole; 2) recessed
RSES51_3-10 rim				
RSES51_3-11				
RSES51_3-12				
RSES51_3-13 blks 1-2				
RSES51_3-13 blks 6-9				
RSES51_3-14	Na, K; +/- Al & Fe		"small"	
RSES51_3-2				
RSES51_3-3 blks 1-3	1) Ca; 2) Si	1) ??; 2) qtz	<10	recessed
RSES51_3-3 blks 5-7				
RSES51_3-4				
RSES51_3-5				
RSES51_3-6 blks 1-2	Si	quartz		recessed
RSES51_3-6 blks 3-5				
RSES51_3-6 blks 7-8				
RSES51_3-7				
RSES51_3-8				
RSES51_3-9				
RSES51_4-1				
RSES51_4-2	Fe, Ti	ilmenite	10	perhaps raised
RSES51_4-3 blks 3-10				
RSES51_4-3 rim				
RSES51_4-4				
RSES51_4-4 blks 6-7				
RSES51_4-5	Si	quartz	20x10	prismatic
RSES51_4-6				
RSES51_4-7	Si	quartz		near edge/crack
RSES51_4-8				

RSES51_4-9				
RSES51_5-1 blks1-5				
RSES51_5-1 blks1-5				
RSES51_5-1 blks6-10				
RSES51_5-2				
RSES51_5-3 blks1-7				
RSES51_5-4 blks1-7				
RSES51_5-5				
RSES51_5-6				
RSES51_5-7				
RSES51_5-8 blks1-6				
RSES51_5-8 blks7-10				
RSES51_5-9				
RSES51_6-1				
RSES51_6-1				
RSES51_6-10				
RSES51_6-10				
RSES51_6-11				
RSES51_6-2				
RSES51_6-3				
RSES51_6-4				
RSES51_6-5				
RSES51_6-6				
RSES51_6-7				
RSES51_6-8 blks1-5				
RSES51_6-8 blks1-5				
RSES51_6-8 blks6-8				
RSES51_6-8 blks9-10				
RSES51_6-9				
RSES51_7-1				
RSES51_7-10 blks2-4				
RSES51_7-10 blks7-10				
RSES51_7-2 blk10				
RSES51_7-2 blks1-7				
RSES51_7-2 blks8-9				
RSES51_7-5				
RSES51_7-6				
RSES51_7-8				
RSES51_7-9	1) Ca; 2) Na+Al; 3) Si	1) ??; 2) ??; 3) quartz	1&2) 5; 3) 10x30	

RSES51_8-11	Ca		2	
RSES51_8-15				
RSES51_9-1				
RSES51_9-11				
RSES51_9-2a				
RSES51_9-2b blks2-3				
RSES51_9-2b blks4-8				
RSES51_9-2b blks9-10				
RSES51_9-8		quartz with Fe-REE speckles	30 um; with 1-5 um speckles	round; on edge

Table B.1: Data for Chapter Two Unknowns.

Appendix C: Chapter Three

Age											Oxygen Isotopes			
Sample	**206Pb/238U Age (Ma)**	**207Pb/206Pb Age (Ma)**	**1 sd**	**% discordance**	**Age Data From…**	**207Pb*/235 U**	**1 s.e.**	**206Pb*/238 U**	**1 s.e.**		**d18 O**	**1 sd***	**Analysis Accepted?**	**When?**
												*internal + in-mount standards	n=0, y=1, poorly imaged=2	
RSES53-1.11	3598	3755	14	4	This study	37.23	0.9757	0.7473	0.02172		5.7	0.3	2	Summer 2010
RSES53-1.19	3604	3599	2	0	This study	33.67	0.8335	0.7491	0.01858					
RSES53-1.7	1700	3694	11	117	This study	14.44	0.3471	0.3018	0.006499		4.3	0.1	2	Summer 2010
RSES53-1.7	1700	3694	11	117	This study	14.44	0.3471	0.3018	0.006499		2.8	1.1	2	Summer 2010
RSES53-2.18	3165	3631	3	15	This study	29.1	0.843	0.6339	0.01768					
RSES53-3.1	3669	3686	4	0	This study	36.5	0.9265	0.7667	0.01994		5.8	0.3	2	Summer 2010
RSES53-3.1	3669	3686	4	0	This study	36.5	0.9265	0.7667	0.01994		5.8	1.0	2	Summer 2010
RSES53-3.12	2228	3819	12	71	This study	21.45	0.5412	0.4129	0.0106		4.5	0.2	2	Summer 2010
RSES53-3.12	2228	3819	12	71	This study	21.45	0.5412	0.4129	0.0106		5.8	0.2	2	Summer 2010
RSES53-3.4	3914	3839	5	-2	This study	43.97	1.099	0.8353	0.0212		3.4	0.3	2	Summer 2010
RSES53-3.4	3914	3839	5	-2	This study	43.97	1.099	0.8353	0.0212		6.8	1.5	2	Summer 2010
RSES53-3.5	3585	3878	3	8	This study	40.18	0.956	0.7438	0.01792		5.0	0.3	2	Summer 2010
RSES53-4.6	3539	3767	4	6	This study	36.71	0.9114	0.7315	0.01773		6.2	1.4	2	Summer 2010
RSES53-4.6	3539	3767	4	6	This study	36.71	0.9114	0.7315	0.01773		5.4	0.2	2	Summer 2010
RSES53-5.1	3037	3592	3	18	This study	26.93	0.5889	0.6018	0.0135					
RSES53-13.17	2193	3981	9	82	Holden et al. (2009)									
RSES53-13.19	4099	3908	8	-5	Holden et al. (2009)						5.9	0.4	2	Summer 2010
RSES53-15.5	3713	3912	5	5	Holden et al. (2009)									
RSES53-16.1	3336	3902	8	17	Holden et al. (2009)									
RSES53-16.11	3842	3911	5	2	Holden et al. (2009)						6.5	0.2	1	Summer 2010
RSES53-17.10	2128	3974	8	87	Holden et al. (2009)									
RSES53-19.3	3557	3984	6	12	Holden et al. (2009)									
RSES53-2.7	2305	3864	9	68	Holden et al. (2009)									
RSES53-4.7	3764	3884	6	3	Holden et al. (2009)									
RSES54-1.10	2856	3570	3	25	This study	24.61	2.475	0.5575	0.05608					
RSES54-1.19	3300	3610	6	9	This study	30.27	4.133	0.6685	0.09125					
RSES54-1.4	582	3769	10	548	This study	4.744	0.5266	0.09439	0.01051					

RSES54-1.5	3206	3997	5	25	This study	37.68	4.89	0.6444	0.08366					
RSES54-11.12	3640	3644	4	0	This study	22.07	6.47	0.4767	0.1401		4.8	0.3	1	Summer 2010
RSES54-12.10	2791	3611	4	29	This study	11.38	2.23	0.251	0.04927		5.9	0.3	2	Summer 2010
RSES54-12.11	-5494	3634	100	-166	This study	-0.02085	0.001286	-0.0004533	0.00001856					
RSES54-12.17	3144	3986	15	27	Holden et al. (2009)						6.0	0.1	2	Summer 2010
RSES54-12.2	2798	3931	126	40	Holden et al. (2009)						4.4	0.1	2	Summer 2010
RSES54-12.5	2378	3646	70	53	This study	5.872	2.195	0.1266	0.04866		5.0	0.1	2	Summer 2010
RSES54-13.14	2864	3648	3	27	This study	11.76	2.388	0.2534	0.05144					
RSES54-14.19	3016	3703	4	23	This study	10.18	1.618	0.2115	0.03372		5.9	0.1	2	Summer 2010
RSES54-14.6	3249	3914	8	20	Holden et al. (2009)						4.6	0.2	2	Summer 2010
RSES54-14.6	3249	3914	8	20	Holden et al. (2009)						5.1	0.4	2	Summer 2010
RSES54-15.11	3672	3897	4	6	This study	107.9	140.1	1.971	2.561		5.1	0.2	0	Summer 2010
RSES54-16.14	2760	3753	2	36	This study	9.509	1.369	0.1911	0.02757		4.8	0.2	2	Summer 2010
RSES54-16.20	4330	3946	8	-9	Holden et al. (2009)						4.8	0.3	0	Summer 2010
RSES54-17.1	3704	3754	9	1	This study	36.75	22.94	0.7383	0.4617		6.0	0.2	0	Summer 2010
RSES54-17.17	4202	3924	9	-7	Holden et al. (2009)						5.2	0.2	1	Summer 2010
RSES54-17.18	4099	3974	6	-3	Holden et al. (2009)						6.8	0.3	1	Summer 2010
RSES54-17.18	4099	3974	6	-3	Holden et al. (2009)						3.3	0.4	1	Summer 2010
RSES54-18.11	4077	3906	8	-4	Holden et al. (2009)						6.0	0.2	2	Summer 2010
RSES54-19.13	2222	3800	2	71	This study	13.21	3.383	0.2575	0.06594					
RSES54-19.5	4038	3869	8	-4	Holden et al. (2009)						6.0	0.2	2	Summer 2010
RSES54-2.16	3315	3597	5	9	This study	30.19	4.253	0.6723	0.09469					
RSES54-20.3	1960	3603	6	84	This study	4.33	0.4973	0.09606	0.01108		5.7	0.1	2	Summer 2010
RSES54-3.12	2457	3622	4	47	This study	21.17	2.449	0.4639	0.05364					
RSES54-3.9	3859	3997	8	4	Holden et al. (2009)						5.8	0.1	0	Summer 2010
RSES54-4.17	2371	3973	8	68	Holden et al. (2009)						5.7	0.1	2	Summer 2010
RSES54-4.9	1073	3757	6	250	This study	1.769	0.1261	0.03548	0.002557		5.7	0.2	2	Summer 2010
RSES54-5.17	2961	3624	4	22	This study	6.799	0.6843	0.1487	0.01502		4.9	0.3	2	Summer 2010
RSES54-5.20	2491	3916	15	57	Holden et al. (2009)									
RSES54-6.12	3297	3738	4	13	This study	-41.11	25.35	-0.835	0.5146		4.5	0.2	0	Summer 2010
RSES54-6.17	3419	3647	9	7	This study	14.12	2.937	0.3042	0.06293		5.6	0.4	0	Summer 2010
RSES54-6.4	2986	3983	7	33	Holden et al. (2009)						6.7	0.1	2	Summer 2010
RSES54-6.4	2986	3983	7	33	Holden et al. (2009)						6.5	0.1	2	Summer 2010

RSES54-7.5	3627	3674	3	1	This study	37.29	20	0.7896	0.4238		5.2	0.3	0	Summer 2010
RSES54-8.16	2813	3738	3	33	This study	8.739	1.109	0.1775	0.02251		5.6	0.1	2	Summer 2010
RSES54-9.4	3879	3984	13	3	Holden et al. (2009)						5.9	0.1	1	Summer 2010
RSES55-1.3	280	3665	6	1210	This study	2.149	0.07901	0.04576	0.001687					
RSES55-11.11	2390	3701	3	55	This study	21.58	1.197	0.4488	0.02479					
RSES55-11.19	1787	3854	7	116	This study	17.21	1.647	0.3235	0.03078					
RSES55-11.3	3816	3841	6	1	This study	41.83	2.949	0.7934	0.05622					
RSES55-12.1	4209	3831	7	-9	This study	45.55	5.016	0.8701	0.09448					
RSES55-12.13	4735	3882	4	-18	This study	53.81	6.124	0.9932	0.1129					
RSES55-12.7	125	3777	4	2917	This study	1.046	0.02466	0.02071	0.0004957					
RSES55-13.1	606	3896	31	543	Holden et al. (2009)									
RSES55-13.13	4006	3935	7	-2	This study	45.81	4.473	0.8163	0.08034		2.4	0.2	2	Summer 2010
RSES55-13.7	4145	3971	21	-4	Holden et al. (2009)									
RSES55-13.8	3408	3885	7	14	Holden et al. (2009)						4.8	0.3	2	Summer 2010
RSES55-14.20	3227	3599	2	12	This study	29.11	1.728	0.6475	0.03844					
RSES55-14.4	3157	3946	12	25	Holden et al. (2009)									
RSES55-14.6	1126	3613	8	221	This study	8.9	0.4804	0.1961	0.0108					
RSES55-15.11	2692	3894	15	45	Holden et al. (2009)									
RSES55-15.13	4137	3866	15	-7	Holden et al. (2009)									
RSES55-15.16	3587	3997	8	11	Holden et al. (2009)									
RSES55-15.8	1769	3736	5	111	This study	15.94	0.7178	0.3242	0.01468					
RSES55-15.9	4106	3934	11	-4	Holden et al. (2009)									
RSES55-19.19	3867	3990	8	3	Holden et al. (2009)									
RSES55-3.13	4027	3862	5	-4	This study	45.13	3.369	0.8442	0.06276		5.0	0.1	0	Summer 2010
RSES55-3.18	1447	3639	19	151	This study	12.22	0.4111	0.2646	0.008053					
RSES55-4.19	2771	3603	7	30	This study	24.05	1.975	0.5334	0.04368		6.3	0.2	2	Summer 2010
RSES55-4.6	3997	3940	8	-1	Holden et al. (2009)									
RSES55-5.13	4128	3816	5	-8	This study	44.7	4.558	0.8622	0.08761		5.0	0.3	1	Summer 2010
RSES55-5.16	1046	3785	10	262	This study	9.166	0.4098	0.1804	0.00806					
RSES55-5.20	3922	3974	7	1	Holden et al. (2009)									
RSES55-5.6	3726	3749	5	1	This study	37.91	2.699	0.7644	0.05413		3.6	0.1	0	Summer 2010
RSES55-6.12	3728	3913	7	5	Holden et al. (2009)						5.2	0.4	2	Summer 2010
RSES55-6.19	4052	3971	10	-2	Holden et al. (2009)									
RSES55-6.8	3592	3754	2	5	This study	36.26	2.512	0.7286	0.05047		4.3	0.3	0	Summer

														2010
RSES55-7.20	4264	3971	9	-7	Holden et al. (2009)									
RSES55-8.1	472	3608	5	665	This study	3.592	0.1284	0.07942	0.002754					
RSES55-8.14	3725	3631	4	-3	This study	35.09	2.461	0.7642	0.05386					
RSES55-9.15	3744	3599	4	-4	This study	34.17	2.662	0.76	0.0592		6.0	0.1	0	Summer 2010
RSES56-01.18	3885	3843	4	-1	This study	43.67	2.569	0.827	0.0489		6.5	0.6	1	Summer 2010
RSES56-02.09	3590	3890	5	8	This study	40.59	2.382	0.7453	0.04331		5.7	0.1	1	Summer 2010
RSES56-02.17	3099	3791	6	18	This study	31.47	1.923	0.6172	0.03718					
RSES56-02.18	3897	3938	6	1	This study	46.69	2.964	0.8305	0.05247					
RSES56-03.17	3674	3889	11	6	This study	41.8	2.455	0.7683	0.0446		5.9	0.2	1	Summer 2010
RSES56-03.17	3674	3889	11	6	This study	41.8	2.455	0.7683	0.0446		6.2	1.1	1	Summer 2010
RSES56-06.01B	467	3778	73	88	This study	3.801	0.3182	0.07516	0.00388					
RSES56-07.06	3951	3924	7	-1	This study	47.11	3.307	0.8458	0.05952		5.5	0.1	0	Summer 2010
RSES56-09.10	3179	3847	3	17	This study	33.75	1.787	0.6375	0.03367					
RSES56-1.17	2240	3910	17	75	Holden et al. (2009)									
RSES56-10.11	3705	3914	10	6	Holden et al. (2009)									
RSES56-10.15	3408	3995	11	17	Holden et al. (2009)									
RSES56-10.17	3924	3870	5	-1	This study	45.04	2.908	0.838	0.05447		6.2	0.4	0	Summer 2010
RSES56-10.17	3924	3870	5	-1	This study	45.04	2.908	0.838	0.05447		6.3	1.2	1	Summer 2010
RSES56-13.17	1453	3764	6	61	This study	12.67	0.541	0.2528	0.01069		5.3	0.1	2	Summer 2010
RSES56-14.09	3259	3760	4	13	This study	32.86	1.803	0.6578	0.03629		-2.8	1.9	2	Summer 2010
RSES56-14.10	2193	3995	3	45	This study	23.67	1.11	0.4052	0.01875					
RSES56-14.14	3843	3983	5	4	Holden et al. (2009)									
RSES56-14.19	2689	3838	6	30	This study	27.22	1.607	0.5176	0.03076					
RSES56-15.16	798	3882	81	386	Holden et al. (2009)									
RSES56-17.14	3648	3866	12	6	Holden et al. (2009)									
RSES56-18.15	707	3818	93	440	Holden et al. (2009)									
RSES56-3.3	2633	3915	13	49	Holden et al. (2009)									
RSES56-5.16	4091	4000	14	-2	Holden et al. (2009)									
RSES56-6.2	4115	3991	8	-3	Holden et al. (2009)									
RSES56-7.12	3940	3980	7	1	Holden et al. (2009)									
RSES58-1.18	3305	3729	10	13	This study	32.78	3.607	0.6698	0.07348		6.2	0.1	2	Summer 2010
RSES58-1.19	4025	3979	6	-1	This study	50.1	5.77	0.8672	0.0998		6.8	0.1	0	Summer 2010

RSES58-1.9	2945	3987	3	35	This study	33.65	3.704	0.5792	0.06375		5.9	0.1	2	Summer 2010
RSES58-10.15	4080	3941	11	-3	This study	49.74	5.963	0.8831	0.1058		6.0	0.1	1	Summer 2010
RSES58-11.3	3897	3815	3	-2	This study	43.04	5.135	0.8304	0.09907		6.0	0.1	2	Summer 2010
RSES58-12.3	4261	3926	18	-8	Holden et al. (2009)						6.2	0.2	1	Summer 2010
RSES58-13.14	3985	3892	7	-2	This study	46.66	5.508	0.8557	0.101		6.3	0.2	1	Summer 2010
RSES58-13.6	3554	3599	2	1	This study	33.07	3.846	0.7354	0.08555		5.1	0.3	0	Summer 2010
RSES58-13.6	3554	3599	2	1	This study	33.07	3.846	0.7354	0.08555		-0.4	0.4	0	Summer 2010
RSES58-13.9	3597	3951	22	10	Holden et al. (2009)									
RSES58-14.18	2345	3951	13	68	Holden et al. (2009)						5.9	0.1	2	Summer 2010
RSES58-14.4	3004	3621	4	21	This study	27.07	3.053	0.5935	0.06692		4.2	0.3	2	Summer 2010
RSES58-14.4	3004	3621	4	21	This study	27.07	3.053	0.5935	0.06692		-0.5	0.5	2	Summer 2010
RSES58-15.1	3783	3766	1	0	This study	40.06	4.84	0.7984	0.09648		5.3	0.2	2	Summer 2010
RSES58-15.12	3701	3605	7	-3	This study	35.01	4.158	0.7757	0.09213		5.0	0.1	0	Summer 2010
RSES58-15.13	3994	3893	4	-3	This study	46.82	5.587	0.8582	0.1024		6.2	0.1	1	Summer 2010
RSES58-15.13	3994	3893	4	-3	This study	46.82	5.587	0.8582	0.1024		2.0	0.3	1	Summer 2010
RSES58-15.9	2207	3988	6	81	This study	23.72	2.434	0.4082	0.0418		5.8	0.1	2	Summer 2010
RSES58-16.15	418	3964	48	848	Holden et al. (2009)						4.9	0.2	2	Summer 2010
RSES58-16.15.2	1452	3816	23	163	Holden et al. (2009)						4.9	0.2	2	Summer 2010
RSES58-16.17	3614	3635	3	1	This study	34.59	4.393	0.7516	0.09544		5.8	0.1	1	Summer 2010
RSES58-16.17	3614	3635	3	1	This study	34.59	4.393	0.7516	0.09544		-0.9	0.4	0	Summer 2010
RSES58-16.2	4020	3930	5	-2	This study	48.42	5.746	0.8657	0.1027		5.5	0.3	0	Summer 2010
RSES58-16.2	4020	3930	5	-2	This study	48.42	5.746	0.8657	0.1027		4.0	2.9	0	Summer 2010
RSES58-17.1	3954	3996	15	1	Holden et al. (2009)						5.6	0.1	1	Summer 2010
RSES58-17.2	4131	3970	14	-4	Holden et al. (2009)						6.1	0.1	0	Summer 2010
RSES58-17.7	3908	3910	6	0	Holden et al. (2009)						5.9	0.2	1	Summer 2010
RSES58-18.17	3670	3982	15	9	Holden et al. (2009)						6.4	0.1	0	Summer 2010
RSES58-18.3	3255	3627	6	11	This study	30.07	3.547	0.6568	0.07748					
RSES58-18.4	1733	3992	18	130	Holden et al. (2009)						6.0	0.3	2	Summer 2010
RSES58-19.19	3732	3956	17	6	Holden et al. (2009)						5.9	0.1	0	Summer 2010
RSES58-19.5	2383	3967	8	66	Holden et al. (2009)						6.2	0.1	2	Summer 2010
RSES58-19.7	1742	3992	71	129	Holden et al. (2009)						5.4	0.2	2	Summer 2010
RSES58-2.9	2470	3774	10	53	This study	23.54	2.335	0.467	0.04603		5.6	0.1	2	Summer 2010
RSES58-3.13	4030	3902	8	-3	Holden et al.						5.9	0.1	1	Summer

					(2009)									2010
RSES58-4.19	4251	3974	16	-7	Holden et al. (2009)						5.8	0.1	1	Summer 2010
RSES58-4.7	4259	3985	18	-6	Holden et al. (2009)						6.3	0.1	1	Summer 2010
RSES58-5.11	3989	3871	4	-3	This study	46.05	5.423	0.8566	0.1009		4.6	0.3	2	Summer 2010
RSES58-8.12	4030	4000	16	-1	Holden et al. (2009)									
RSES58-8.2	4134	3996	6	-3	Holden et al. (2009)						5.7	0.2	1	Summer 2010
RSES58-8.7	1146	3648	10	218	This study	9.029	0.86	0.1945	0.01851		-5.7	0.6	2	Summer 2010
RSES59-03.02	2806	3937	7	40	This study	31.15	1.425	0.5545	0.02565		5.6	0.2	2	Summer 2010
RSES59-03.03	772	3754	2	386	This study	6.469	0.4106	0.13	0.008388		4.5	0.3	2	Summer 2010
RSES59-03.15	3756	3685	8	-2	This study	37.99	3.135	0.7987	0.06528		5.5	0.2	1	Summer 2010
RSES59-04.07	3569	3702	8	4	This study	36.04	2.178	0.7491	0.04515		5.3	0.3	0	Summer 2010
RSES59-04.08	4033	3838	8	-5	This study	46.22	3.558	0.8785	0.06576		-5.7	0.9	2	Summer 2010
RSES59-04.17	3703	3753	4	1	This study	39.18	2.117	0.7876	0.04242		6.0	0.2	1	Summer 2010
RSES59-05.09	3638	3618	3	-1	This study	35	2.02	0.7687	0.04458		5.4	0.3	1	Summer 2010
RSES59-06.18	3810	3768	4	-1	This study	41.02	2.402	0.8168	0.04737		6.0	0.1	1	Summer 2010
RSES59-07.01	1812	3722	5	105	This study	16.07	0.9531	0.3297	0.01991		6.1	0.2	2	Summer 2010
RSES59-07.01	1812	3722	5	105	This study	16.07	0.9531	0.3297	0.01991		3.1	0.4	2	Summer 2010
RSES59-07.18	354	3660	30	933	This study	2.689	0.2175	0.05748	0.0045					
RSES59-08.07	804	3728	8	364	This study	6.631	0.2874	0.1355	0.005855		5.5	0.4	2	Summer 2010
RSES59-08.13	1280	3846	6	200	This study	11.82	0.4496	0.2236	0.008424		5.9	0.3	2	Summer 2010
RSES59-08.17	3624	3741	4	3	This study	37.75	2.071	0.765	0.04212		6.0	0.1	1	Summer 2010
RSES59-09.11	3733	3656	5	-2	This study	37.06	2.343	0.794	0.04974		5.6	0.1	0	Summer 2010
RSES59-10.08	3438	3859	3	12	This study	38.09	2.17	0.7139	0.04082					
RSES59-10.11	2387	3696	13	55	This study	21.79	1.335	0.4549	0.02728		5.8	0.2	2	Summer 2010
RSES59-10.12	1401	3995	12	185	Holden et al. (2009)						6.6	0.6	2	Winter 2010
RSES59-10.16	3444	3621	7	5	This study	32.68	1.929	0.7167	0.04154		5.5	0.2	2	Summer 2010
RSES59-10.19	4059	3961	11	-2	Holden et al. (2009)									
RSES59-11.8	1407	3946	13	180	Holden et al. (2009)						5.9	0.6	2	Winter 2010
RSES59-11.8	1407	3946	13	180	Holden et al. (2009)						6.2	0.6	2	Winter 2010
RSES59-12.04	3086	3778	7	22	This study	31.52	1.894	0.6235	0.03724		5.8	0.2	2	Summer 2010
RSES59-13.17	3708	3787	7	2	This study	40.1	2.5	0.7883	0.04957		6.0	0.2	1	Summer 2010
RSES59-14.04	3043	3674	88	21	This study	28.92	2.418	0.6126	0.03386		5.2	0.4	2	Summer 2010
RSES59-	2435	3715	5	53	This study	22.64	1.045	0.4668	0.02182		5.8	0.2	2	Summer

14.06														2010
RSES59-14.07	3547	3629	4	2	This study	34.12	1.804	0.7441	0.03954		6.0	0.1	1	Summer 2010
RSES59-14.11	3276	3691	11	13	This study	32.07	2.091	0.6716	0.04207		6.5	0.2	1	Summer 2010
RSES59-14.12	4154	3910	6	-6	Holden et al. (2009)									
RSES59-14.14	4059	3846	6	-5	Holden et al. (2009)						5.1	0.1	2	Summer 2010
RSES59-14.16	2720	3618	4	33	This study	24.31	1.295	0.534	0.02876		5.7	0.1	2	Summer 2010
RSES59-15.01	3626	3629	5	0	This study	35.1	2.232	0.7653	0.0481		6.0	0.1	2	Summer 2010
RSES59-15.13	1604	3925	13	145	Holden et al. (2009)									
RSES59-15.16	3663	3635	4	-1	This study	35.71	2.037	0.7755	0.04406		6.0	0.3	1	Summer 2010
RSES59-15.17	1384	3955	11	186	Holden et al. (2009)									
RSES59-15.9	4049	3860	4	-5	Holden et al. (2009)									
RSES59-16.01	3841	3860	7	0	This study	44.09	2.6	0.8257	0.04856		5.9	0.2	0	Summer 2010
RSES59-16.03	3773	3929	14	4	This study	45.06	2.868	0.8063	0.05005		5.7	0.1	2	Summer 2010
RSES59-16.05	3630	3655	4	1	This study	35.7	2.053	0.7653	0.04382		6.5	0.1	2	Summer 2010
RSES59-16.06	3537	3639	6	3	This study	34.23	2.078	0.7416	0.04458		6.0	0.2	2	Summer 2010
RSES59-16.12	3951	3912	14	-1	Holden et al. (2009)									
RSES59-16.14	4005	3939	14	-2	Holden et al. (2009)									
RSES59-16.2	2304	3936	6	71	Holden et al. (2009)									
RSES59-17.07	3585	3609	4	1	This study	34.13	2.155	0.7538	0.04721					
RSES59-17.13	3723	3801	22	2	Holden et al. (2009)									
RSES59-17.15	3862	3978	12	3	Holden et al. (2009)									
RSES59-17.16	3873	3873	13	0	This study	44.89	3.051	0.8337	0.05723					
RSES59-19.18	1268	3603	8	184	This study	10	0.3174	0.2219	0.007125					
RSES59-19.18	1268	3603	8	184	This study	10	0.3174	0.2219	0.007125					
RSES59-6.12	4053	3875	6	-4	Holden et al. (2009)									
RSES59-6.4	4213	3945	9	-6	Holden et al. (2009)						6.7	0.1	1	Summer 2010
RSES59-6.5	2230	3990	13	79	Holden et al. (2009)						6.0	0.2	2	Summer 2010
RSES59-8.11	3885	3964	7	2	Holden et al. (2009)									
RSES59-9.14	4203	3951	12	-6	Holden et al. (2009)						5.7	0.1	2	Summer 2010
RSES72-1.2	3509	3864	5	10	This study	38.45	2.15	0.7185	0.03966		5.1	1.1	1	Winter 2010
RSES72-1.3	3873	3601	7	-7	This study	33.7	2.861	0.7484	0.06315		7.2	1.1	1	Winter 2010
RSES72-12.9	3726	3897	3	4	This study	42.84	3.249	0.7833	0.05951		5.2	1.1	1	Winter 2010
RSES72-13.1	3867	3924	9	1	This study	41.31	3.514	0.7417	0.06313		6.9	1.2	1	Winter

														2010
RSES72-13.1	3867	3924	9	1	This study	41.31	3.514	0.7417	0.06313		8.9	1.1	1	Winter 2010
RSES72-14.9	3430	3848	7	11	This study	40.17	2.769	0.7586	0.05204		5.3	1.1	1	Winter 2010
RSES72-15.7	3624	3599	5	-1	This study	33.46	2.56	0.7439	0.0571		5.2	1.1	1	Winter 2010
RSES72-17.8	3653	3635	5	0	This study	34.82	2.7	0.7562	0.0587		1.1	1.2	2	Winter 2010
RSES72-17.8	3653	3635	5	0	This study	34.82	2.7	0.7562	0.0587		5.5	1.1	2	Winter 2010
RSES72-3.2	3362	3637	4	8	This study	29.86	1.674	0.6477	0.03624		5.7	1.1	1	Winter 2010
RSES72-4.2	3678	3957	6	7	This study	43.28	2.401	0.7603	0.04219		3.4	1.1	1	Winter 2010
RSES72-9.3	3351	3634	7	8	This study	31.65	1.647	0.6881	0.036		5.4	1.1	0	Winter 2010
RSES73-10.4b	2800	3888	3	39	This study	29.6	1.185	0.544	0.02188		5.3	0.9	1	Winter 2010
RSES73-12.8b	2006	3953	8	97	This study	20.73	1.028	0.365	0.0182		1.7	0.9	0	Winter 2010
RSES73-13.3b	2839	3598	4	27	This study	24.86	0.9776	0.5534	0.02155		5.3	0.9	1	Winter 2010
RSES73-13.7b	3939	3938	2	0	This study	47.36	2.088	0.8422	0.03715		5.5	0.9	1	Winter 2010
RSES73-14.3b	3962	3941	6	-1	This study	47.83	2.179	0.8491	0.03756		5.2	0.9	0	Winter 2010
RSES73-15.8b	1151	3717	5	223	This study	9.495	0.3567	0.1955	0.00728					
RSES73-17.10	3884	3905	6	1	This study	45.48	1.952	0.8267	0.03551		5.8	0.9	1	Winter 2010
RSES73-17.10	3884	3905	6	1	This study	45.48	1.952	0.8267	0.03551		7.4	0.9	1	Winter 2010
RSES73-2.3	3078	3863	4	26	This study	32.74	1.329	0.6119	0.02467		5.5	0.9	0	Winter 2010
RSES73-3.1	1562	3989	5	155	This study	15.95	0.5822	0.2742	0.01024		4.3	0.9	2	Winter 2010
RSES73-3.2	3689	3866	4	5	This study	41.41	1.777	0.7724	0.03317		5.7	0.9	1	Winter 2010
RSES73-3.7	2887	3831	35	33	This study	29.58	2.84	0.565	0.05077		4.9	0.9	1	Winter 2010
RSES73-4.7	3851	3894	5	1	This study	44.63	1.83	0.8174	0.03333		5.3	0.9	1	Winter 2010
RSES73-5.8	3682	3884	4	5	This study	41.79	1.786	0.7703	0.03288		4.4	0.9	1	Winter 2010
RSES73-7.2	1742	3647	4	109	This study	14.4	0.4241	0.3102	0.009152		3.9	0.9	0	Winter 2010
RSES73-7.6	3205	3846	2	20	This study	34.07	1.37	0.644	0.02584		4.5	0.9	0	Winter 2010
RSES73-9.4	3460	3884	3	12	This study	38.53	1.643	0.7103	0.03013					
RSES73-9.6	1589	3772	9	137	This study	14.08	0.5789	0.2796	0.01206		5.7	0.9	0	Winter 2010

	Ti Thermometry (MC)										**Structure and Morphology on Selected Zircons**		
Sample	**Ti, ppm**	**% error**	**Txlln, C**	**est. 1 sd**	**2nd ti**	**2nd ti % err**	**2nd Txlln**	**2nd T 1 sd**	**Analysis Accepted?**	**When?**	**CL texture**	**Morphology**	
									0=no, 1=yes, 2=poorly imaged				
RSES53-1.11	1.37	0.08	592	10					2	Spring 2010	faint patches	rounded	

RSES53-1.19													
RSES53-1.7	35.10	1.96	865	20					2	Spring 2010			
RSES53-1.7	35.10	1.96	865	20					2	Spring 2010			
RSES53-2.18													
RSES53-3.1	3.85	0.22	663	10					2	Spring 2010	patchy	subrounded broken	
RSES53-3.1	3.85	0.22	663	10					2	Spring 2010	patchy	subrounded broken	
RSES53-3.12	6.19	0.49	700	11					2	Fall 2009	patchy	angular	
RSES53-3.12	6.19	0.49	700	11					2	Fall 2009	patchy	angular	
RSES53-3.4	12.72	0.71	762	11					2	Spring 2010	homogeneous	angular	
RSES53-3.4	12.72	0.71	762	11					2	Spring 2010	homogeneous	angular	
RSES53-3.5	2.26	0.13	625	10					2	Spring 2010	broad osc or stripes	subangular	
RSES53-4.6	7.51	0.42	716	10					2	Spring 2010	oscillatory	subangular	
RSES53-4.6	7.51	0.42	716	10					2	Spring 2010	oscillatory	subangular	
RSES53-5.1													
RSES53-13.17													
RSES53-13.19	1.41	0.11	594	10					2	Fall 2009	concentric zones	round	
RSES53-15.5	2.61	0.20	635	10					2	Fall 2009	homogeneous	angular	misshapen
RSES53-16.1													
RSES53-16.11	8.71	0.68	729	11					2	Fall 2009	homogeneous	angular	
RSES53-17.10	4.95	0.39	683	10					2	Fall 2009	faint osc	subangular	
RSES53-19.3	10.32	0.81	744	12					2	Fall 2009	faintly patchy	angular	
RSES53-2.7													
RSES53-4.7	8.69	0.68	729	11					2	Fall 2009	ambiguous	subround	
RSES54-1.10													
RSES54-1.19													
RSES54-1.4													
RSES54-1.5													
RSES54-11.12	11.77	0.66	755	11					0	Spring 2010			
RSES54-12.10	8.39	0.47	726	11					2	Spring 2010			
RSES54-12.11													
RSES54-12.17	73.88	4.13	953	41					1	Spring 2010	patchy over osc	subround	
RSES54-12.2	16.31	0.91	786	12					1	Spring 2010	patchy	subangular	
RSES54-12.5	1.51	0.08	598	10					1	Spring 2010			
RSES54-13.14	59.34	3.31	926	32					0	Spring 2010			
RSES54-14.19	44.56	2.49	892	24					0	Spring 2010			
RSES54-14.6	14.73	0.82	776	12					1	Spring 2010	pathcy oscillatory	subangular	
RSES54-14.6	14.73	0.82	776	12					1	Spring 2010	pathcy oscillatory	subangular	

RSES54-15.11	3.39	0.19	654	10					2	Spring 2010	concentric zones	angular	
RSES54-16.14	54.87	3.06	916	30					1	Spring 2010	streaks; faint patches	angular	
RSES54-16.20	1.89	0.11	613	10					1	Spring 2010	faint osc		
RSES54-17.1	2.76	0.15	639	10					0	Spring 2010	patchy/cloudy	subrounded	
RSES54-17.17	1.85	0.10	611	10					1	Spring 2010	altered/cloudy osc		
RSES54-17.18	18.42	1.03	798	13					0	Spring 2010	patchy	angular	
RSES54-17.18	18.42	1.03	798	13					0	Spring 2010	patchy	angular	
RSES54-18.11	2.60	0.15	635	10					1	Spring 2010	ambiguous	subangular	
RSES54-19.13	51.20	2.86	908	28					2	Spring 2010			
RSES54-19.5	1.93	0.11	614	10					1	Spring 2010	oscillatory + sector	angular	concave
RSES54-2.16													
RSES54-20.3	2.19	0.12	623	10					1	Spring 2010			
RSES54-3.12													
RSES54-3.9	3.96	0.22	665	10					1	Spring 2010	patchy		
RSES54-4.17	9.88	0.55	740	11					2	Spring 2010	faint osc	angular	
RSES54-4.9	46.08	2.57	896	25					1	Spring 2010	patchy	subangular	
RSES54-5.17	3.55	0.20	657	10					2	Spring 2010			
RSES54-5.20	51.76	2.89	909	28					2	Spring 2010			
RSES54-6.12	6.86	0.38	709	10					1	Spring 2010			
RSES54-6.17	17.71	0.99	794	13					0	Spring 2010	patchy/cloudy	subangular	
RSES54-6.4	5.74	0.32	694	10					0	Spring 2010	patchy	subangular	
RSES54-6.4	5.74	0.32	694	10					0	Spring 2010	patchy	subangular	
RSES54-7.5	15.17	0.85	779	12					2	Spring 2010	homogeneous or very faint patches	angular	
RSES54-8.16	65.36	3.65	938	36					1	Spring 2010			
RSES54-9.4	4.16	0.23	669	10					1	Spring 2010	osc		
RSES55-1.3	51.74	2.89	909	28	49.74	2.78	905	51	0	Spring 2010			
RSES55-11.11	3.32	0.19	652	10					0	Spring 2010	patchy	angular	
RSES55-11.19	16.54	0.92	787	12					2	Spring 2010	patchy	subangular	
RSES55-11.3									1		patchy	angular	
RSES55-12.1	1668.44	110.04	1549	1705					2	Spring 2010			
RSES55-12.13	45.43	2.54	894	25	214.20	11.96	1108	62	2	Spring 2010			
RSES55-12.7	364.01	20.33	1200	244					2	Spring 2010			
RSES55-13.1													
RSES55-13.13	8.57	0.48	727	11					0	Spring 2010	patchy	subrounded	
RSES55-13.7	13.22	0.74	766	11					1	Spring 2010	patchy	subangular broken	
RSES55-13.8	33.07	1.85	858	19					1	Spring 2010	patchy	subangular	

RSES55-14.20	1181.32	66.25	1456	965					0	Spring 2010			
RSES55-14.4	560.22	31.32	1284	402					2	Spring 2010			
RSES55-14.6	82.26	4.59	967	46					2	Spring 2010			
RSES55-15.11	16.10	0.90	785	12					0	Spring 2010	oscillatory	angular	
RSES55-15.13	3.45	0.19	655	10					2	Spring 2010	oscillatory	subangular	
RSES55-15.16	1533.13	124.31	1525	1896	192.09	10.73	1090	61	a: 0, b: 1	Spring 2010	patchy	subrounded	
RSES55-15.8	28.95	1.62	844	17	77.31	4.32	959	54	0	Spring 2010			
RSES55-15.9	5.91	0.33	697	10					1	Spring 2010	swirly-patchy	angular; nealry euhedral	
RSES55-19.19	21.73	1.21	814	14	20.74	1.16	809	45	2	Spring 2010			
RSES55-3.13	12.81	0.72	763	11					0	Spring 2010	homogeneous	subangular	
RSES55-3.18													
RSES55-4.19	11.80	0.66	756	11					1	Spring 2010			
RSES55-4.6													
RSES55-5.13	4.72	0.26	679	10					1	Spring 2010	patchy	subround	
RSES55-5.16	57.28	3.20	922	31					2	Spring 2010			
RSES55-5.20													
RSES55-5.6	8.35	0.47	725	11					0	Spring 2010	faint patches	angular	
RSES55-6.12	9.55	0.53	737	11					2	Spring 2010	patches over osc	angular, concave	
RSES55-6.19													
RSES55-6.8	3.93	0.22	665	10					1	Spring 2010	faint patches	rounded	
RSES55-7.20													
RSES55-8.1	556.71	31.09	1283	399					0	Spring 2010			
RSES55-8.14													
RSES55-9.15	9.05	0.51	732	11					1	Spring 2010	patchy	subangular	
RSES56-01.18	0.96	0.05	570	10					2	Spring 2010	faint stripes	angular	
RSES56-02.09	0.94	0.05	568	10					1	Spring 2010	patchy	subround	
RSES56-02.17													
RSES56-02.18	3.38	0.19	654	10					2	Spring 2010			
RSES56-03.17	2.67	0.15	637	10					1	Spring 2010	broad osc? Conc. Zones?	subround	
RSES56-03.17	2.67	0.15	637	10					1	Spring 2010	broad osc? Conc. Zones?	subround	
RSES56-06.01B													
RSES56-07.06											homogeneous	angular anhedral	
RSES56-09.10													
RSES56-1.17													
RSES56-10.11													
RSES56-10.15													

RSES56-10.17	1.69	0.09	605	10					1	Spring 2010	broad concentric zones	angular	
RSES56-10.17	1.69	0.09	605	10					1	Spring 2010	broad concentric zones	angular	
RSES56-13.17	4.67	0.26	678	10					0	Spring 2010			
RSES56-14.09	51.18	2.86	908	28					2	Spring 2010			
RSES56-14.10													
RSES56-14.14													
RSES56-14.19													
RSES56-15.16													
RSES56-17.14													
RSES56-18.15													
RSES56-3.3													
RSES56-5.16													
RSES56-6.2													
RSES56-7.12													
RSES58-1.18	1.02	0.06	573	10					1	Spring 2010			
RSES58-1.19	7.81	0.44	720	10					2	Spring 2010	patchy		
RSES58-1.9	16.42	0.92	786	12					2	Spring 2010	faintly patchy	subangular	
RSES58-10.15	3.86	0.22	664	10					2	Spring 2010	osc, somewhat cloudy		
RSES58-11.3									1				
RSES58-12.3	4.03	0.22	667	10					2	Spring 2010	patchy		
RSES58-13.14	1.54	0.09	599	10					1	Spring 2010	homogeneous	rounded	
RSES58-13.6	4.27	0.24	671	10					2	Spring 2010	homogeneous	subangular	
RSES58-13.6	4.27	0.24	671	10					2	Spring 2010	homogeneous	subangular	
RSES58-13.9	325.35	18.17	1179	215					2	Spring 2010	cloudy over osc	subangular	
RSES58-14.18	5.80	0.32	695	10					2	Spring 2010	osc + sect	subangular and equant (eu/subhedral?)	
RSES58-14.4	68.34	3.82	944	37					0	Spring 2010			
RSES58-14.4	68.34	3.82	944	37					0	Spring 2010			
RSES58-15.1	2.79	0.16	640	10					2	Spring 2010			
RSES58-15.12	4.69	0.26	678	10					1	Spring 2010	patchy	subangular	
RSES58-15.13	1.51	0.08	598	10					1	Spring 2010	homogeneous	subangular	
RSES58-15.13	1.51	0.08	598	10					1	Spring 2010	homogeneous	subangular	
RSES58-15.9	3.04	0.17	646	10					2	Spring 2010			
RSES58-16.15	4.91	0.27	682	10					1	Spring 2010	patchy		
RSES58-16.15.2	4.91	0.27	682	10					1	Spring 2010			
RSES58-16.17	9.18	0.51	733	11					1	Spring 2010	homogeneous; some ghosting?	subangular	

RSES58-16.17	9.18	0.51	733	11					1	Spring 2010	homogeneous; some ghosting?	subangular	
RSES58-16.2	2.52	0.14	633	10					1	Spring 2010	very faint; streaks?	subrounded	
RSES58-16.2	2.52	0.14	633	10					1	Spring 2010	very faint; streaks?	subrounded	
RSES58-17.1	3.49	0.19	656	10					2	Spring 2010	osc		
RSES58-17.2	2.83	0.16	641	10					1	Spring 2010	patchy		
RSES58-17.7	0.64	0.04	546	10					1	Spring 2010	homogeneous	angular	
RSES58-18.17	3.31	0.19	652	10					1	Spring 2010	osc + patches		
RSES58-18.3	8.44	0.47	726	11					2	Spring 2010			
RSES58-18.4	3.44	0.19	655	10					1	Spring 2010	faint broad concentric zones	subangular; subhedral broken	
RSES58-19.19	3.35	0.19	653	10					1	Spring 2010	osc		
RSES58-19.5	18.18	1.02	796	13					2	Spring 2010	faint stripes	subangular	
RSES58-19.7	3.07	0.17	647	10					1	Spring 2010	faint; alteration areas?	subangular	
RSES58-2.9	2.33	0.13	627	10					1	Spring 2010			
RSES58-3.13	2.82	0.16	641	10					1	Spring 2010	oscillatory and patchy	subround	
RSES58-4.19	2.64	0.15	636	10					1	Spring 2010	cloudy		
RSES58-4.7	12.25	0.68	759	11					1	Spring 2010	osc (brilliant)		
RSES58-5.11	1.27	0.07	587	10					1	Spring 2010	homogeneous	angular	concave
RSES58-8.12													
RSES58-8.2	9.87	0.55	740	11					0	Spring 2010	osc		
RSES58-8.7	4.58	0.26	677	10					2	Spring 2010			
RSES59-03.02	11.78	0.66	755	11					2	Spring 2010	patchy	subangular	
RSES59-03.03	213.12	11.90	1107	132					2	Spring 2010			
RSES59-03.15	4.72	0.26	679	10					2	Spring 2010	patchy	subangular	
RSES59-04.07	15.98	0.89	784	12					1	Spring 2010	patchy	subangular	
RSES59-04.08	4.81	0.27	680	10					2	Spring 2010			
RSES59-04.17	3.93	0.22	665	10					1	Spring 2010			
RSES59-05.09	4.41	0.25	674	10					1	Spring 2010	homogeneous	subangular broken	
RSES59-06.18	5.98	0.33	698	10					1	Spring 2010	homogeneous; perhaps some ghosting?	subrounded	
RSES59-07.01	10.49	0.59	745	11					2	Spring 2010			
RSES59-07.01	10.49	0.59	745	11					2	Spring 2010			
RSES59-07.18	79.91	4.46	964	44					0	Spring 2010			
RSES59-08.07	22.57	1.26	818	14					0	Spring 2010			
RSES59-08.13	16.70	0.93	788	12					0	Spring 2010	ambiguous	subround	
RSES59-08.17	1.64	0.09	603	10					2	Spring 2010	patchy	angular	
RSES59-09.11	1.60	0.09	602	10					1	Spring 2010	patchy osc	subrounded	

RSES59-10.08	12.05	0.67	757	11					1	Spring 2010	blocky	angular	
RSES59-10.11	31.70	1.77	854	18					1	Spring 2010			
RSES59-10.12	2.40	0.13	629	10					2	Spring 2010	faint; part homogeneous + part osc?	angular concave	
RSES59-10.16	3.83	0.21	663	10					1	Spring 2010	patchy	angular	
RSES59-10.19	5.24	0.29	687	10					2	Spring 2010	osc; altered to homogeneous (one end)	rounded	
RSES59-11.8	5.06	0.28	684	10					2	Spring 2010	very faint; homogeneous?	subangular; broken subhedral?	
RSES59-11.8	5.06	0.28	684	10					2	Spring 2010	very faint; homogeneous?	subangular; broken subhedral?	
RSES59-12.04	5.23	0.29	687	10					2	Spring 2010			
RSES59-13.17	2.78	0.16	639	10					2	Spring 2010	patchy (away from analysis spots)	subangular	
RSES59-14.04	3.93	0.22	665	10					1	Spring 2010			
RSES59-14.06	1.43	0.08	595	10					0	Spring 2010			
RSES59-14.07	2.34	0.13	628	10					0	Spring 2010	patchy	angular	
RSES59-14.11	13.46	0.75	768	12					1	Spring 2010	patchy	angular	
RSES59-14.12	0.42	0.02	522	10					1	Spring 2010	homogeneous	subangular	
RSES59-14.14	2.49	0.14	632	10					2	Spring 2010			
RSES59-14.16	2.52	0.14	633	10					2	Spring 2010			
RSES59-15.01	0.58	0.03	540	10					2	Spring 2010			
RSES59-15.13	8.63	0.48	728	11					2	Spring 2010	dark + light regions; altered osc??	subangular anhedral	
RSES59-15.16	1.14	0.06	580	10					2	Spring 2010	homogeneous	subrounded	
RSES59-15.17													
RSES59-15.9	1.78	0.10	609	10					2	Spring 2010			
RSES59-16.01	0.67	0.04	549	10					1	Spring 2010	ambiguous	angular	
RSES59-16.03	5.13	0.29	685	10					2	Spring 2010	patchy?	subhedral broken subangular	
RSES59-16.05	13.01	0.73	765	11					0	Spring 2010			
RSES59-16.06	3.16	0.18	649	10					1	Spring 2010			
RSES59-16.12	32.09	1.79	855	18					1	Spring 2010	oscillatory and ambiguous	angular	
RSES59-16.14	2.87	0.16	642	10					2	Spring 2010	bright center; dark exterior layers	subrounded	
RSES59-16.2	4.82	0.27	680	10					2	Spring 2010	mostly homogeneous; edge osc	angular, concave	
RSES59-17.07	7.10	0.40	712	10					1	Spring 2010			
RSES59-17.13	4.10	0.23	668	10					2	Spring 2010			
RSES59-17.15	3.26	0.18	651	10					1	Spring 2010	dark core, light thick rim(s); altered?	rounded (subhedral broken?)	
RSES59-17.16	6.93	0.39	710	10					1	Spring 2010	oscillatory and patchy	subround	
RSES59-19.18	95.94	5.36	988	54					0	Spring 2010			

RSES59-19.18	125.16	6.99	1025	72					0	Spring 2010			
RSES59-6.12	1.15	0.06	580	10					1	Spring 2010	homogeneous	subround	
RSES59-6.4	3.46	0.19	655	10					2	Spring 2010	patchy	subangular	
RSES59-6.5	1.93	0.11	614	10					2	Spring 2010	patchy	subrounded broken	
RSES59-8.11	77.35	4.32	959	43					2	Spring 2010			
RSES59-9.14	5.53	0.31	691	10					2	Spring 2010	altered patches	angular	
RSES72-1.2	1.03	0.07	574	10					1	Summer 2009	patchy	subround	
RSES72-1.3													
RSES72-12.9	10.77	0.74	747	11					1	Summer 2009	oscillatory	subangular	
RSES72-13.1	4.93	0.34	682	10					1	Summer 2009	patchy	subrounded	
RSES72-13.1	4.93	0.34	682	10					1	Summer 2009	patchy	subrounded	
RSES72-14.9	7.29	0.50	714	11					1	Summer 2009	patchy	subangular	
RSES72-15.7													
RSES72-17.8	2.08	0.14	619	10					2	Summer 2009			
RSES72-17.8	2.08	0.14	619	10					2	Summer 2009			
RSES72-3.2													
RSES72-4.2	2.00	0.14	617	10					1	Summer 2009	osc	subrounded broken	
RSES72-9.3													
RSES73-10.4b	1.55	0.12	600	10					2	Summer 2009			
RSES73-12.8b	8.97	0.70	731	11					1	Summer 2009	faintly patchy	subangular	
RSES73-13.3b													
RSES73-13.7b	5.85	0.46	696	10					1	Summer 2009	faint patches	subangular	
RSES73-14.3b	0.82	0.06	560	10					2	Summer 2009	very faint, ambiguous	subrounded	
RSES73-15.8b													
RSES73-17.10	1.23	0.10	585	10					2	Summer 2009	homogeneous	subangular	
RSES73-17.10	1.23	0.10	585	10					2	Summer 2009	homogeneous	subangular	
RSES73-2.3	15.04	1.18	778	14					1	Summer 2009	oscillatory + some disruption	subangular	broken euhedral
RSES73-3.1	25.37	1.99	830	19					1	Summer 2009	faint wide stripe/ osc??	subangular	
RSES73-3.2			590	10					1		homogeneous	subround	broken
RSES73-3.7	7.44	0.58	716	11					1	Summer 2009	sector	subrounded	straight edge -- broken?
RSES73-4.7	1.76	0.14	608	10					1	Summer 2009	homogeneous	angular	concave/broken
RSES73-5.8	9.92	0.78	740	12					1	Summer 2009	oscillatory	subround/subangular?	
RSES73-7.2	8.64	0.68	728	11					2	Summer 2009			
RSES73-7.6	70.67	5.55	948	54					1	Summer 2009	ambiguous	rounded	

RSES73-9.4	12.32	0.97	760	12					1	Summer 2009	faint patches	subround	
RSES73-9.6											faint sector?	subangular	chunk missing

Table C.1: Age, oxygen isotope, crystallization temperature, and morphologies of surveyed 4.0-3.6 Ga zircons from chapter 3

Appendix D: Statistical Analyses for Chapter Three

D.1 Ti_{MC} Survey of 4.0-3.6 Ga Zircons (Section 4.1 of the Results)

The Wilcoxon Rank Sum Test (as described in McClave and Sincich, 2006) compares two samples of non-specified distribution in a particular variable and tests the hypothesis that their probability distributions are distinct. Data points from the two samples in a particular variable are arranged from smallest to largest and ranked 1 – n from smallest to largest. The test statistic is computed by summing these ranks for the group with the smaller number of data points. For samples in which the smaller population has $n \geq 10$, the test results can be approximated by a normal distribution; the test statistic (the rank sum of the smaller sample) yields a Z-score showing the probability that one sample has a larger value than the other.

D.1.1 Measurement Quality

Ion probe analysis pits were imaged to determine whether the pits overlap cracks, as this is a known risk for measuring artificially high Ti contents (Harrison and Schmitt, 2007). Indeed, analysis spots that overlap cracks as imaged by the Leo 1430VP Scanning Electron Microscope at UCLA display higher Ti_{MC} and thus T^{xlln}_{MC} than those imaged as being placed on a pristine area of the zircon surface (see table below). There was a third category of ion probe analysis pits which could not be definitively imaged for cracks, due usually to topography on the zircon surfaces or complications from later carbon coating for imaging. These poorly imaged points are not statistically different from the definitively clean pits (as seen in the table below). The effect of sampling over cracks is to artificially increase the Ti measurement (Harrison and Schmitt, 2007) and there is no known case of a crack artificially *lowering* the Ti measurement, so the ambiguous points can be considered to give a *maximum* T^{xlln}. Thus the lack of significant difference between the definitely clean and ambiguous measurements is good evidence that the poorly imaged points are not higher in T^{xlln} than the definitely clean points (it is possible, but unlikely given their good match, that the ambiguous points may under-sample *lower* T^{xlln}).

Groups included: definitely on cracks ("rej," consisting of 29 measurements), higher-confidence spots that are definitely not on cracks ("HC," 84 measurements), and lower-confidence spots with ambiguous images ("LC," 88 measurements). The "overall" tests use all data in the period 4.0-3.6 Ga. The "not ca. 3.9 Ga" tests specifically exclude zircons from the period 3.91-3.84 Ga due to the unusually low Ti contents in many accepted measurements during this period. Both sets of tests demonstrate the similarity of the high- and low-confidence measurements, unlike the high-confidence and rejected measurements.

Groups	**Overall: HC vs. rej**	**Overall: HC vs. LC**	**HC vs. rej, not ca. 3.9 Ga**	**HC vs. LC, not ca. 3.9 Ga**

Test Stat	1923	2729	1113	1678
Z Score	4.33	0.2	3.3	0.64
P-value	<0.001	0.842	0.001	0.522

Table D.1: Wilcoxon test scores for high- and low-confidence measurements in T^{xlln}.

We have elected to include the ambiguous measurements in our survey, given their lack of difference from the certainly clean points. Their inclusion does not change our conclusions but does augment our dataset considerably.

D.1.2 Ti_{MC} Survey Reveals Anomalous Period at 3.91-3.84 Ga

Data used for these analyses include the "accepted" and "uncertain" Ti_{MC} analyses in table S1 of the SOM.

Time Periods	**Ca. 3.9 Ga vs. Hadean**	**Ca. 3.9 Ga vs. post-3.84**	**Ca. 3.9 Ga vs. pre-3.91**	**Post-3.84 vs. Hadean**	**Pre-3.91 vs. Hadean**
Test Stat	2262	1997	1907	3943	3245
Z Score	-2.59	2.28	2.28	0.126	-0.53
P-value	0.010	0.023	0.023	0.900	0.596

Table D.2: Wilcoxon test scores for 3.84-3.91 Ga zircons and those outside that time period.

The Ti_{MC} distribution of zircons in the period 3.91-3.84 Ga ("ca. 3.9 Ga") is statistically distinct from the Hadean distribution of Harrison et al. (2008) as well as from the periods 3.84-3.6 ("post-3.84") and 4.0-3.91 Ga ("pre-3.91"), whereas the post-3.84 and pre-3.91 Ga time periods are not distinct from the Hadean.

D.2 Elemental Groups (Section 4.2 of the Results)

The period 3.91-3.84 Ga was targeted for more detailed trace element analysis based on the findings of the Ti_{MC} survey.

D.2.1 Wilcoxon Rank Sum Tests on Several Variables

Data used for these analyses include the accepted Hadean and ca. 3900 Ma trace element measurements in table S2 of the SOM. For zircons with more than one accepted analysis, we use the average value for the grain in computing our statistics. Because several of the geochemical variables we use in the discriminant analysis are non-normally distributed among our zircons, we used the Wilcoxon Rank Sum Test (see McClave and Sincich, 2006) to determine that the visually picked (from Fig. 2a) Group I and II zircons have statistically significant differences in their U_t, $(Th/U)_t$, Hf, Ce, and P compositions.

Group I and II zircons are distinct in all 5 variables at a significance level >95%, according to the 2-tailed normal approximation of the Wilcoxon test. Z-scores are shown below:

Grps. I & II	**U_t**	**$(Th/U)_t$**	**Hf**	**Ce**	**P**
Test Stat	96	289	115	299	273
Z Score	-4.42	3.66	-3.62	4.08	2.99
P-value	<0.001	<0.001	<0.001	<0.001	0.003

Table D.3: Wilcoxon test scores for Groups I and II in various trace elements.

Group II and Hadean zircons are distinct in all of the above variables except for Ce at the 95% significance level:

Grp. II & Hadean	**U_t**	**$(Th/U)_t$**	**Hf**	**Ce**	**P**
Test Stat	117	321	139	263	307
Z Score	-4.25	3.85	-3.37	1.55	3.29
P-value	<0.001	<0.001	<0.001	0.122	0.001

Table D.4: Wilcoxon test scores for Group II and Hadean zircons in various trace elements.

However, Group I zircons are not distinct from the Hadean population:

Grp. I & Hadean	**U_t**	**$(Th/U)_t$**	**Hf**	**Ce**	**P**
Test Stat	187	166	191	200	188
Z Score	0.24	-0.801	0.412	0.873	0.291
P-value	0.808	0.423	0.680	0.382	0.771

Table D.5: Wilcoxon test scores for Group I and Hadean zircons in various trace elements.

D.2.2 Discriminant Analysis

Discriminant analysis was carried out using the program IBM SPSS Statistics 20. Variables included in the discriminant analysis were U_t, $(Th/U)_t$, Hf, Ce, and P. One discriminant function was found to adequately describe the data. Standardized canonical discriminant function coefficients for Function One are shown below.

Variable	**Function One Coefficient**
U_t	0.983
$(Th/U)_t$	0.233
Hf	0.413
Ce	-0.548
P	-0.629

Table D.6: Discriminant function coefficients for the chapter three Group I/Group II distinction.

Using this discriminant function, 100% of Group I and Group II grains are sorted into their expected (pre-assigned by eye) groups. Leave-one-out cross-validation also correctly sorts 100% of Group I and Group II zircons. Of the 14 Hadean zircons analyzed, 13 are assigned to Group I (the exception is RSES 67-10.11; all casewise results are given below).

Group	Centroid (Function One)
I	-2.651
II	2.027

Table D.7: Group I and II centroids for the discriminant function in table D.6.

Tests of significance reveal a Wilks' Lambda of 0.148 and a chi-squared value of 48.716 (5 degrees of freedom), for which the corresponding p-value is <0.001.

Casewise results are shown below, with normalized probabilities of group membership:

Sample Name	**Category**		**Discriminant Score**	**Probability of Group Membership**	
	By Eye	**From Analysis**	**Function 1**	**Group 1**	**Group 2**
RSES54-15.11	1	1	-1.17	0.9825	0.01753
RSES54-18.11	1	1	-1.29	0.99	0.00997
RSES55-11.3	1	1	-2.36	0.9999	0.00007
RSES55-15.11	1	1	-3.36	1	0
RSES55-15.13	1	1	-3.34	1	0
RSES55-5.13	1	1	-3.43	1	0
RSES56-03.17	1	1	-3.96	1	0
RSES58-16.15	1	1	-2.49	0.99996	0.00004
RSES58-3.13	1	1	-3.87	1	0
RSES59-04.08	1	1	-3.01	1	0
RSES59-17.16	1	1	-2.59	0.99998	0.00002
RSES73-3.7	1	1	-3.24	1	0
RSES73-5.8	1	1	-0.34	0.5354	0.46463
RSES53-3.4	2	2	0.651	0.0109	0.98906

RSES53-15.5	2	2	2.746	0	1
RSES53-16.11	2	2	2.231	1E-05	0.99999
RSES55-13.8	2	2	1.755	6E-05	0.99994
RSES55-3.13	2	2	3.659	0	1
RSES56-01.18	2	2	0.838	0.0046	0.9954
RSES56-10.17	2	2	1.079	0.0015	0.99851
RSES58-13.14	2	2	1.999	2E-05	0.99998
RSES58-15.13	2	2	2.193	1E-05	0.99999
RSES58-17.7	2	2	3.467	0	1
RSES58-5.11	2	2	2.193	1E-05	0.99999
RSES59-10.08	2	2	2.182	1E-05	0.99999
RSES59-14.12	2	2	2.815	0	1
RSES59-6.12	2	2	0.652	0.0109	0.98909
RSES72-1.2	2	2	2.351	0	1
RSES72-12.9	2	2	2.502	0	1
RSES73-9.4	2	2	1.144	0.0011	0.9989
RSES55-3.7		1	-2.98	1	0
RSES55-4.9		1	-1.62	0.9978	0.00219
RSES58-4.16		1	-2.8	0.99999	0.00001
RSES58-6.12		1	-1.16	0.9812	0.01885
RSES58-19.12		1	-2.73	0.99999	0.00001
RSES59-8.14		1	-2.43	0.99995	0.00005
RSES59-18.19		1	-1.79	0.999	0.001
RSES64-1.2		1	-2.22	0.9999	0.00013
RSES64-2.2		1	-1.76	0.9989	0.00114
RSES64-9.2		1	-1.78	0.9989	0.00106

RSES64-19.2		1	-1.82	0.9991	0.00088
RSES67-3.11		1	-8.57	1	0
RSES67-10.11		2	0.074	0.1414	0.85865
RSES67-17.12		1	-2.45	0.99996	0.00004

Table D.8: Casewise results for trace element discrimination function in chapter 3.

D.3 Oxygen Isotopes (section 4.4 of the Results)

Oxygen isotope analyses on concordant 4.0-3.6 Ga zircons were imaged to determine whether the ion probe pits overlap cracks, similarly to our treatment of Ti_{MC} analysis spots. We use the Wilcoxon Rank Sum Test to compare these datasets below. Groups include: definitely on cracks ("rej"), higher-confidence measurements definitely not on cracks ("HC"), and lower-confidence measurements with ambiguous images ("LC").

Groups	**HC vs. rej**	**HC vs. LC**
Test Stat	789	806
Z Score	-2.51	-1.78
P-value	0.012	0.072

Table D.9: Wilcoxon results for high- and low-confidence zircon oxygen isotope analyses from chapter 3.

Among concordant zircons, high-confidence and rejected measurements are distinct, but high- and low-confidence measurements are not distinguishable at the 95% confidence level.

Appendix E: Trace Element Results and Zircon Morphologies for Chapter Three Samples

Sample	206Pb/238U Age (Ma)	207Pb/206Pb Age (Ma)	1 sd	% disc	Age Data From…	REE-Ti accepted?	Group	P	1 s.e.	49Ti	1 s.e.	57Fe	1 s.e.	89Y	1 s.e.
						0-N, 1-Y									
RSES54-15.11a	3672	3897	4	6	This study	1		286	14	5.98	0.51	96	12	532	32
RSES54-15.11b	3672	3897	4	6	This study	1		296	8	4.86	0.47	100	13	591	37
54-15.11 average						*1*	*I*	*291*	*17*	*5.42*	*1.06*	*98*	*18*	*561*	*64*
RSES54-18.11	4077	3906	8	-4	Holden et al. (2009)	1	I	227	9	3.48	0.38	112	14	419	23
RSES55-11.3	3816	3841	6	1	This study	1	I	304	8	4.02	0.42	145	17	654	37
RSES55-15.11	2692	3894	15	45	Holden et al. (2009)	1	I	326	8	3.16	0.40	118	25	931	58
RSES55-15.13	4137	3866	15	-7	Holden et al. (2009)	1	I	346	12	3.31	0.42	81	12	756	52
RSES55-5.13	4128	3816	5	-8	This study	1	I	338	12	3.32	0.86	37	13	482	54
RSES56-03.17	3674	3889	11	6	This study	1	I	239	6	2.19	0.30	87	12	732	45
RSES58-16.15	1452	3816	23	163	Holden et al. (2009)	1	I	267	13	4.75	0.44	109	13	783	47
RSES58-3.13	4030	3902	8	-3	Holden et al. (2009)	1	I	326	26	5.28	0.47	96	12	1107	70
RSES59-04.08	4033	3838	8	-5	This study	1	I	625	15	15.54	0.83	127	15	1541	87
RSES59-17.16	3873	3873	13	0	This study	1	I	181	9	5.89	0.50	117	14	459	29
RSES73-3.7	2887	3831	35	33	This study	1	I	248	7	8.38	0.62	96	12	542	34
RSES73-5.8 average						*1*	*I*	*148*	*8*	*3.45*	*0.75*	*99*	*25*	*327*	*55*
RSES73-5.8 (REE spot A)	3682	3884	4	5	This study	1		146	5	3.15	0.37	87	12	294	18
RSES73-5.8 (REE spot B)	3682	3884	4	5	This study	1		151	6	3.74	0.51	112	14	360	22
RSES53-3.4	3914	3839	5	-2	This study	1		286	11	2.47	0.32	76	10	521	29
RSES53-3.4b	3914	3839	5	-2	This study	1		224	6	2.33	0.31	91	12	588	34
RSES53-3.4 average						*1*	*II*	*255*	*46*	*2.40*	*0.46*	*84*	*19*	*554*	*65*
RSES56-01.18	3885	3843	4	-1	This study	1	II	200	8	1.07	0.30	103	16	491	37
RSES59-10.08 (near age spot)	3438	3859	3	12	This study	1	II	226	10	1.86	0.29	126	15	1382	79
RSES55-3.13	4027	3862	5	-4	This study	1	II	268	14	1.32	0.40	38	10	1350	104
RSES72-1.2 (inner REE spot)	3509	3864	5	10	This study	1	II	179	5	0.93	0.20	112	14	737	41
RSES56-10.17	3924	3870	5	-1	This study	1	II	177	5	1.38	0.29	98	12	746	44
RSES58-5.11	3989	3871	4	-3	This study	1	II	180	10	1.13	0.21	119	19	447	26
RSES59-6.12	4053	3875	6	-4	Holden et al. (2009)	1	II	204	10	1.13	0.23	114	14	643	37
RSES73-9.4 (REE spot A)	3460	3884	3	12	This study	1	II	225	6	3.89	0.41	135	16	655	37
RSES55-13.8	3408	3885	7	14	Holden et al. (2009)	1	II	151	15	0.56	0.23	66	13	252	18

RSES58-13.14	3985	3892	7	-2	This study	1	II	193	14	1.82	0.27	101	12	728	41
RSES58-15.13	3994	3893	4	-3	This study	1	II	209	14	1.80	0.27	105	13	783	42
RSES72-12.9 (REE spot A)	3726	3897	3	5	This study	1	II	145	6	1.85	0.30	113	14	464	28
RSES58-17.7	3908	3910	6	0	Holden et al. (2009)	1	II	204	14	1.02	0.20	85	11	876	49
RSES59-14.12	4154	3910	6	-6	Holden et al. (2009)	1	II	192	10	0.64	0.17	98	12	776	43
RSES53-16.11	3842	3911	5	2	Holden et al. (2009)	1	II	263	7	4.29	0.42	130	16	423	22
RSES53-15.5	3713	3912	5	5	Holden et al. (2009)	1	II	228	9	2.67	0.62	86	11	351	22
RSES55-3.7	4109	4006	10	-3	Holden et al. (2009)	1		283	10	5.13	0.50	100	13	676	44
RSES55-4.9	4215	4133	5	-2	Holden et al. (2009)	1		343	10	2.84	0.38	102	13	828	48
RSES58-4.16	4305	4119	6	-4	Holden et al. (2009)	1		259	14	6.57	0.52	89	11	861	56
RSES59-8.14	4271	4097	6	-4	Holden et al. (2009)	1		359	17	26.05	2.05	442	49	408	27
RSES58-19.12	4033	4059	20	1	Holden et al. (2009)	1		196	9	2.93	0.35	86	11	698	43
RSES58-6.12	4015	4057	8	1	Holden et al. (2009)	1		288	13	5.71	0.48	107	13	529	31
RSES59-18.19	3901	4015	21	3	Holden et al. (2009)	1		158	5	2.15	0.31	96	12	428	25
RSES64-1.2	4110	4155	12	1	Holden et al. (2009)	1		194	5	4.62	0.45	101	13	826	56
RSES64-2.2	4154	4159	7	0	Holden et al. (2009)	1		398	10	2.43	0.33	94	12	1136	72
RSES64-9.2	4074	4048	10	-1	Holden et al. (2009)	1		157	4	5.37	0.49	96	12	406	26
RSES64-19.2	4087	4111	12	1	Holden et al. (2009)	1		179	7	3.91	0.42	122	15	542	34
RSES67-3.11	3937	4040	7	3	Holden et al. (2009)	1		640	29	11.98	1.22	90	17	1158	125
RSES67-10.11	3947	4008	5	2	Holden et al. (2009)	1		170	16	2.43	0.72	24	10	238	24
RSES67-17.12	4108	4107	4	0	Holden et al. (2009)	1		597	18	20.17	0.94	196	22	2272	132
RSES59-14.14	4059	3846	6	-5	Holden et al. (2009)	0		644	24	35.17	1.24	467	100	1368	84
RSES59-08.13	1280	3846	6	200	This study	0		968	28	18.45	0.90	621	57	1637	204
RSES73-7.6 (REE spot A)	3205	3846	2	20	This study	0		2277	54	269.60	3.96	1276	112	1051	58
RSES73-7.6 (REE spot B)	3205	3846	2	20	This study	0		528	13	28.11	1.14	269	28	884	49
RSES72-14.9	3430	3848	7	11	This study	0		448	15	4.67	1.06	91	23	543	77
RSES59-10.08 (near MC	3438	3859	3	12	This study	0		454	11	14.08	0.79	214	23	748	64

Ti spot)															
RSES59-16.01	3841	3860	7	0	This study	0		256	18	10.34	0.74	132	16	223	12
RSES72-1.2 (outer REE spot)	3509	3864	5	10	This study	0		175	5	0.67	0.17	106	13	512	31
RSES73-3.2	3689	3866	4	5	This study	0		407	38	20.28	2.97	235	25	746	42
RSES54-19.5	4038	3869	8	-4	Holden et al. (2009)	0		254	7	3.58	0.39	130	15	1499	94
RSES73-9.4 (REE spot B)	3460	3884	3	12	This study	0		116	4	1.08	0.22	93	12	330	18
RSES56-02.09	3590	3890	5	8	This study	0		116	9	1.63	0.26	96	12	303	17
RSES73-4.7	3851	3894	5	1	This study	0		207	6	2.26	0.39	88	12	747	54
RSES72-12.9 (REE spot B)	3726	3897	3	4	This study	0		334	12	14.18	0.82	171	19	532	31
RSES73-17.10	3884	3905	6	1	This study	0		171	7	1.27	0.23	118	14	640	37
RSES59-16.12	3951	3912	14	-1	Holden et al. (2009)	0		278	11	4.09	0.42	100	13	857	53
RSES54-14.6a	3249	3914	8	20	Holden et al. (2009)	0		3207	247	359.07	18.88	2395	324	3690	268
RSES54-14.6b	3249	3914	8	20	Holden et al. (2009)	0		4496	1097	380.47	97.57	1454	402	1957	390
RSES73-3.1 (REE spot A)	1562	3989	5	155	This study	0		811	20	60.69	1.68	172	19	3097	202
RSES73-3.1 (REE spot B)	1562	3989	5	155	This study	0		355	9	6.00	0.51	148	19	1927	131
RSES58-5.14	4003	4074	6	2	Holden et al. (2009)	0		281	16	14.86	0.78	175	19	688	50
RSES59-4.18	4327	4245	3	-2	Holden et al. (2009)	0		437	11	6.39	0.68	106	15	2033	151
RSES59-8.14	4271	4097	6	-4	Holden et al. (2009)	0		359	17	26.05	2.05	442	49	408	27
RSES59-9.15	4279	4103	9	-4	Holden et al. (2009)	0		364	15	5.83	0.50	130	15	1850	111
RSES64-1.16	3753	4010	6	7	Holden et al. (2009)	0		332	9	6.99	0.61	86	12	1303	88
RSES67-15.16	4301	4192	7	-3	Holden et al. (2009)	0		587	14	109.07	15.85	1894	176	2384	166
RSES67-19.13	3757	4041	7	8	Holden et al. (2009)	0		306	17	3.32	0.80	12	7	558	65

Sample	**139La**	**1 s.e.**	**140Ce**	**1 s.e.**	**141Pr**	**1 s.e.**	**143Nd**	**1 s.e.**	**149Sm**	**1 s.e.**	**151Eu**	**1 s.e.**	**156Gd**	**1 s.e.**
RSES54-15.11a	0.04	0.01	7.76	0.19	0.06	0.04	0.88	0.15	1.68	0.52	0.19	0.05	8.39	0.58
RSES54-15.11b	0.04	0.01	7.42	0.19	0.04	0.01	0.63	0.13	1.42	0.32	0.19	0.04	9.82	0.67
54-15.11 average	*0.04*	*0.02*	*7.59*	*0.36*	*0.05*	*0.04*	*0.76*	*0.27*	*1.55*	*0.62*	*0.19*	*0.06*	*9.11*	*1.34*
RSES54-18.11	0.05	0.01	7.90	0.19	0.05	0.01	0.36	0.09	0.75	0.13	0.05	0.02	5.54	0.41
RSES55-11.3	0.29	0.04	12.00	0.49	0.37	0.05	2.61	0.26	2.17	0.24	0.27	0.07	9.27	0.92
RSES55-15.11	0.04	0.01	7.12	0.18	0.13	0.02	2.15	0.25	3.37	0.30	0.50	0.09	17.70	1.12

RSES55-15.13	0.01	0.01	6.50	0.19	0.02	0.01	0.58	0.13	1.34	0.20	0.19	0.04	9.40	0.86
RSES55-5.13	0.00	#DIV/0!	15.39	0.60	0.12	0.05	1.72	0.46	1.92	0.63	0.04	0.04	8.65	0.94
RSES56-03.17	0.06	0.01	12.56	0.24	0.12	0.02	1.71	0.20	2.66	0.26	0.25	0.04	12.65	1.38
RSES58-16.15	0.03	0.01	9.98	0.21	0.05	0.03	1.18	0.16	1.97	0.21	0.27	0.09	12.51	0.79
RSES58-3.13	0.04	0.01	20.89	0.32	0.13	0.02	2.51	0.24	4.09	0.31	0.58	0.06	20.56	1.20
RSES59-04.08	0.07	0.02	7.81	0.19	0.11	0.02	1.36	0.18	2.63	0.26	0.18	0.04	17.86	1.12
RSES59-17.16	0.05	0.01	6.85	0.18	0.05	0.02	1.00	0.15	1.87	0.21	0.18	0.08	9.03	0.85
RSES73-3.7	0.03	0.01	7.65	0.20	0.04	0.01	0.67	0.13	0.95	0.16	0.20	0.04	8.33	0.58
RSES73-5.8 average	*0.06*	*0.02*	*4.53*	*0.24*	*0.02*	*0.03*	*0.44*	*0.16*	*1.20*	*0.29*	*0.21*	*0.07*	*6.18*	*1.48*
RSES73-5.8 (REE spot A)	0.05	0.01	4.45	0.14	0.00	0.00	0.41	0.10	1.09	0.17	0.20	0.04	5.57	0.99
RSES73-5.8 (REE spot B)	0.06	0.01	4.62	0.15	0.03	0.02	0.47	0.11	1.31	0.18	0.22	0.06	6.80	0.51
RSES53-3.4	0.03	0.01	2.74	0.11	0.01	0.01	0.17	0.10	0.78	0.14	0.11	0.03	6.33	0.57
RSES53-3.4b	0.04	0.01	3.34	0.12	0.02	0.01	0.22	0.07	0.98	0.15	0.18	0.04	8.22	0.61
RSES53-3.4 average	*0.04*	*0.02*	*3.04*	*0.46*	*0.02*	*0.01*	*0.19*	*0.14*	*0.88*	*0.25*	*0.14*	*0.07*	*7.28*	*1.58*
RSES56-01.18	0.04	0.02	2.44	0.23	0.03	0.01	0.48	0.15	0.76	0.19	0.09	0.04	5.82	0.74
RSES59-10.08 (near age spot)	0.04	0.01	4.80	0.15	0.06	0.02	1.21	0.21	4.37	0.78	0.64	0.07	28.62	1.82
RSES55-3.13	0.00	--	5.12	0.25	0.04	0.02	0.92	0.37	3.17	0.65	0.41	0.09	25.01	2.35
RSES72-1.2 (inner REE spot)	0.04	0.01	2.05	0.13	0.01	0.01	0.19	0.08	0.88	0.15	0.10	0.07	8.16	0.89
RSES56-10.17	0.06	0.01	3.41	0.12	0.03	0.01	0.28	0.08	1.57	0.19	0.22	0.04	11.44	0.97
RSES58-5.11	0.05	0.01	3.40	0.12	0.01	0.01	0.25	0.07	0.90	0.14	0.11	0.03	6.29	0.48
RSES59-6.12	0.05	0.01	3.05	0.12	0.01	0.00	0.33	0.09	0.78	0.14	0.17	0.04	8.29	0.63
RSES73-9.4 (REE spot A)	0.75	0.05	11.19	0.23	0.97	0.10	5.54	0.39	3.57	0.30	0.53	0.06	14.50	1.05
RSES55-13.8	0.02	0.01	1.44	0.12	0.01	0.01	0.06	0.06	0.28	0.16	0.07	0.04	2.71	0.39
RSES58-13.14	0.05	0.01	3.24	0.12	0.02	0.01	0.43	0.21	1.98	0.21	0.26	0.04	14.18	0.97
RSES58-15.13	0.05	0.01	3.33	0.12	0.02	0.01	0.64	0.12	1.92	0.21	0.29	0.05	13.54	0.94
RSES72-12.9 (REE spot A)	0.04	0.01	2.72	0.12	0.02	0.01	0.19	0.12	1.05	0.40	0.23	0.07	5.57	0.46
RSES58-17.7	0.05	0.01	2.80	0.11	0.01	0.01	0.13	0.07	1.38	0.28	0.07	0.02	10.70	0.78
RSES59-14.12	0.01	0.01	2.71	0.11	0.01	0.01	0.30	0.11	0.98	0.16	0.09	0.03	9.71	0.73
RSES53-16.11	0.11	0.02	6.79	0.18	0.18	0.03	0.89	0.16	1.19	0.40	0.13	0.03	6.42	0.56
RSES53-15.5	0.03	0.01	3.34	0.12	0.04	0.01	0.43	0.10	1.07	0.16	0.14	0.03	4.97	0.40
RSES55-3.7	0.05	0.01	11.42	0.25	0.08	0.02	1.02	0.17	2.19	0.28	0.49	0.06	12.58	1.04
RSES55-4.9	0.01	0.01	14.70	0.29	0.04	0.01	0.55	0.13	0.99	0.17	0.09	0.03	11.76	0.77
RSES58-4.16	0.04	0.01	4.89	0.15	0.06	0.02	1.26	0.17	2.23	0.23	0.43	0.05	14.50	0.95
RSES59-8.14	0.79	0.05	27.13	0.39	1.24	0.12	8.54	0.49	7.06	0.44	1.77	0.12	16.50	1.54
RSES58-19.12	0.05	0.01	6.55	0.17	0.07	0.02	0.63	0.12	2.06	0.29	0.55	0.06	12.14	0.84
RSES58-6.12	0.34	0.03	7.55	0.26	0.48	0.06	2.86	0.26	2.23	0.30	0.24	0.04	8.46	1.06
RSES59-18.19	0.03	0.01	4.87	0.15	0.05	0.02	0.68	0.13	0.98	0.21	0.21	0.04	6.61	0.49
RSES64-1.2	0.02	0.01	3.70	0.13	0.04	0.01	0.96	0.15	2.99	0.38	0.45	0.06	15.48	1.06
RSES64-2.2	0.04	0.01	7.45	0.19	0.03	0.01	0.81	0.14	1.93	0.22	0.50	0.08	16.89	1.07

RSES64-9.2	0.05	0.01	3.25	0.12	0.03	0.02	0.44	0.11	1.48	0.24	0.32	0.05	7.68	0.59
RSES64-19.2	0.03	0.01	6.55	0.18	0.05	0.01	0.57	0.12	1.55	0.20	0.19	0.04	10.45	0.71
RSES67-3.11	1.84	0.13	35.62	0.71	1.99	0.21	10.65	0.86	8.56	0.89	1.28	0.16	29.53	1.91
RSES67-10.11	0.03	0.02	2.74	0.25	0.03	0.03	0.28	0.24	0.60	0.35	0.29	0.10	6.92	0.98
RSES67-17.12	0.93	0.06	26.88	0.59	1.24	0.12	9.02	0.73	10.48	0.52	1.32	0.10	46.08	2.67
RSES59-14.14	2.29	0.09	51.51	0.56	3.01	0.26	16.86	0.66	10.61	0.95	1.69	0.29	30.73	1.93
RSES59-08.13	1.81	0.09	31.65	0.42	2.19	0.19	13.84	0.60	10.92	0.53	1.87	0.12	34.12	1.91
RSES73-7.6 (REE spot A)	4.12	0.12	139.23	1.15	9.47	0.76	58.90	1.36	34.58	1.17	4.97	0.20	53.53	4.24
RSES73-7.6 (REE spot B)	2.43	0.09	37.77	0.47	3.22	0.28	18.50	0.81	10.36	0.52	1.75	0.12	24.86	1.42
RSES72-14.9	0.03	0.02	8.75	0.47	0.15	0.06	1.11	0.39	1.80	0.50	0.37	0.12	10.88	1.51
RSES59-10.08 (near MC Ti spot)	0.57	0.04	25.20	1.27	0.79	0.09	4.95	0.35	4.31	0.50	0.56	0.10	14.31	1.11
RSES59-16.01	0.31	0.03	16.94	0.46	0.40	0.05	2.26	0.24	1.69	0.21	0.27	0.05	3.46	0.32
RSES72-1.2 (outer REE spot)	0.05	0.01	2.03	0.10	0.02	0.01	0.15	0.06	0.70	0.13	0.08	0.02	6.15	0.51
RSES73-3.2	0.29	0.07	17.72	2.23	0.65	0.14	4.54	0.95	5.09	0.91	0.78	0.14	22.67	8.51
RSES54-19.5	0.06	0.01	13.36	0.35	0.35	0.05	5.77	0.37	8.47	0.68	1.22	0.12	36.55	2.57
RSES73-9.4 (REE spot B)	0.03	0.01	1.82	0.09	0.03	0.01	0.34	0.09	0.47	0.11	0.08	0.02	4.68	0.42
RSES56-02.09	0.04	0.01	1.88	0.09	0.02	0.01	0.21	0.07	0.42	0.10	0.08	0.02	3.52	0.46
RSES73-4.7	0.02	0.01	3.98	0.14	0.03	0.01	0.52	0.11	1.96	0.22	0.24	0.04	13.17	0.91
RSES72-12.9 (REE spot B)	0.36	0.04	17.74	0.44	0.63	0.07	3.03	0.28	2.60	0.26	0.67	0.07	7.02	0.72
RSES73-17.10	0.03	0.01	4.63	0.14	0.04	0.01	0.81	0.15	1.94	0.22	0.20	0.04	10.59	0.76
RSES59-16.12	0.03	0.01	11.73	0.24	0.05	0.01	1.04	0.16	2.30	0.24	0.21	0.04	13.05	0.82
RSES54-14.6a	15.04	0.43	324.95	2.66	23.55	1.95	134.41	4.67	79.03	2.92	14.52	0.38	156.34	9.07
RSES54-14.6b	18.77	4.38	333.90	78.13	30.02	10.32	157.88	40.55	86.78	20.01	15.73	3.98	139.24	48.29
RSES73-3.1 (REE spot A)	3.34	0.11	55.38	0.60	5.37	0.53	34.57	0.99	22.39	0.78	3.72	0.17	75.68	4.13
RSES73-3.1 (REE spot B)	0.07	0.01	14.26	0.27	0.13	0.02	2.37	0.24	4.79	0.35	0.58	0.15	27.82	1.63
RSES58-5.14	0.13	0.02	17.46	0.29	0.25	0.03	1.85	0.20	2.79	0.25	0.40	0.07	12.28	0.76
RSES59-4.18	0.01	0.01	15.31	0.35	0.12	0.03	2.01	0.29	7.48	0.56	0.28	0.06	41.05	2.62
RSES59-8.14	0.79	0.05	27.13	0.39	1.24	0.12	8.54	0.49	7.06	0.44	1.77	0.12	16.50	1.54
RSES59-9.15	0.32	0.03	12.66	0.25	0.40	0.06	3.62	0.30	7.55	0.63	1.08	0.09	41.61	2.43
RSES64-1.16	0.06	0.02	16.32	0.31	0.14	0.03	3.21	0.41	4.59	0.50	1.37	0.11	28.42	1.69
RSES67-15.16	3.44	0.11	51.21	2.79	4.22	0.45	27.96	2.22	22.90	1.26	4.78	0.40	69.03	5.29
RSES67-19.13	0.00	--	10.90	0.47	0.08	0.03	1.22	0.36	2.84	1.06	0.63	0.14	11.80	1.61

Sample	**159Tb**	**1 s.e.**	**161Dy**	**1 s.e.**	**165Ho**	**1 s.e.**	**168Er**	**1 s.e.**	**169Tm**	**1 s.e.**	**172Yb**	**1 s.e.**	**175Lu**	**1 s.e.**
RSES54-15.11a	3.34	0.58	40	1	17	5	78	1	16	4	156	13	35	6
RSES54-15.11b	3.90	0.81	47	3	19	4	84	4	19	4	158	13	36	8
54-15.11 average	*3.62*	*1.06*	*43*	*6*	*18*	*7*	*81*	*6*	*18*	*6*	*157*	*18*	*36*	*10*

RSES54-18.11	2.43	0.64	31	2	14	3	70	1	16	6	144	13	33	9
RSES55-11.3	3.98	0.42	48	1	21	2	97	2	22	5	199	22	44	5
RSES55-15.11	6.90	0.90	78	2	31	3	140	3	30	6	267	22	58	8
RSES55-15.13	4.59	1.07	61	2	27	4	123	2	27	6	234	24	55	13
RSES55-5.13	3.19	0.90	42	4	17	6	85	3	18	20	161	20	40	11
RSES56-03.17	5.07	0.63	61	2	26	3	110	2	24	4	213	26	48	6
RSES58-16.15	5.26	0.77	63	2	26	3	114	4	26	9	228	18	53	8
RSES58-3.13	7.90	0.82	94	2	38	3	169	3	37	5	321	24	72	7
RSES59-04.08	9.29	1.28	120	2	52	5	238	3	52	11	450	35	101	14
RSES59-17.16	3.37	0.54	39	3	15	2	71	1	16	7	144	15	33	5
RSES73-3.7	3.55	0.71	44	1	18	3	84	2	18	4	161	14	37	8
RSES73-5.8 average	*2.38*	*0.94*	*27*	*4*	*11*	*3*	*51*	*7*	*11*	*4*	*104*	*27*	*24*	*10*
RSES73-5.8 (REE spot A)	2.22	0.62	24	1	10	2	46	2	10	2	92	17	21	6
RSES73-5.8 (REE spot B)	2.53	0.67	30	1	12	2	56	1	13	3	116	10	27	7
RSES53-3.4	3.31	2.01	39	1	17	3	79	1	17	4	164	17	36	22
RSES53-3.4b	3.86	1.29	46	1	20	3	84	2	19	4	167	15	38	13
RSES53-3.4 average	*3.58*	*2.52*	*43*	*5*	*18*	*5*	*82*	*4*	*18*	*6*	*166*	*23*	*37*	*26*
RSES56-01.18	2.76	0.90	37	1	17	4	74	2	18	7	163	22	38	13
RSES59-10.08 (near age spot)	11.05	1.93	124	3	45	8	189	3	38	5	305	25	66	12
RSES55-3.13	10.67	4.26	125	4	49	10	200	9	42	10	323	34	71	28
RSES72-1.2 (inner REE spot)	4.39	1.89	55	2	24	4	113	2	25	19	233	28	56	24
RSES56-10.17	4.71	1.40	59	2	24	3	107	3	24	5	206	20	45	13
RSES58-5.11	2.89	0.88	37	1	14	2	65	2	15	4	131	12	30	9
RSES59-6.12	3.98	1.13	50	2	20	4	89	2	21	5	183	16	41	12
RSES73-9.4 (REE spot A)	5.43	0.43	59	2	22	2	89	2	18	2	157	13	33	3
RSES55-13.8	1.38	1.39	19	1	9	5	45	2	12	6	115	17	29	29
RSES58-13.14	5.76	2.85	65	1	23	3	98	2	19	3	165	14	35	17
RSES58-15.13	5.85	1.14	65	2	26	3	105	2	22	4	182	15	40	8
RSES72-12.9 (REE spot A)	2.60	1.61	35	1	15	6	68	4	17	5	149	15	37	23
RSES58-17.7	4.70	2.63	64	2	28	6	136	2	32	10	303	26	74	41
RSES59-14.12	4.42	1.58	56	1	26	4	122	3	29	8	262	23	65	24
RSES53-16.11	2.80	0.53	36	1	14	5	61	3	14	3	127	13	29	5
RSES53-15.5	2.18	0.53	24	1	11	2	54	3	14	3	139	13	38	9
RSES55-3.7	4.52	0.76	55	2	22	3	99	3	22	3	199	19	45	8
RSES55-4.9	5.13	1.20	61	2	27	5	124	3	27	9	231	18	52	12
RSES58-4.16	5.64	0.79	71	2	30	3	134	2	31	4	275	22	64	9
RSES59-8.14	5.13	0.56	45	2	14	1	54	3	12	1	104	11	22	3
RSES58-19.12	5.12	1.00	59	2	25	4	105	2	23	3	187	16	43	8
RSES58-6.12	3.22	0.32	42	1	17	2	78	2	18	3	166	22	38	4

RSES59-18.19	2.82	0.55	34	1	15	3	68	1	15	3	142	13	33	6
RSES64-1.2	6.18	1.07	71	2	29	4	121	4	25	4	213	19	46	8
RSES64-2.2	7.11	1.27	86	2	38	4	174	2	38	6	336	27	79	14
RSES64-9.2	2.99	0.73	33	1	14	2	61	2	13	2	113	10	27	7
RSES64-19.2	3.92	0.92	46	1	17	2	71	1	15	3	123	10	26	6
RSES67-3.11	10.81	0.99	110	7	40	4	163	3	36	5	294	24	63	6
RSES67-10.11	2.66	2.31	22	2	9	5	35	2	7	3	60	10	14	13
RSES67-17.12	18.03	1.63	206	4	81	4	336	4	72	6	596	47	128	12
RSES59-14.14	11.49	0.59	124	3	48	4	202	7	43	8	379	32	82	4
RSES59-08.13	12.89	0.71	143	3	55	3	239	4	54	4	477	35	102	6
RSES73-7.6 (REE spot A)	16.93	0.85	138	6	39	2	145	2	31	2	262	24	52	3
RSES73-7.6 (REE spot B)	9.58	0.68	93	2	30	2	119	2	25	2	214	16	44	3
RSES72-14.9	3.84	1.41	46	3	20	5	92	11	21	7	178	26	46	17
RSES59-10.08 (near MC Ti spot)	5.58	0.45	64	2	25	3	107	2	23	4	198	18	45	4
RSES59-16.01	1.53	0.18	17	1	8	1	38	1	10	2	97	10	24	3
RSES72-1.2 (outer REE spot)	2.89	1.19	39	2	17	3	82	3	18	6	164	16	39	16
RSES73-3.2	9.07	3.44	87	22	28	8	106	13	21	4	172	67	37	14
RSES54-19.5	13.10	0.95	140	3	52	4	214	3	42	5	344	29	75	6
RSES73-9.4 (REE spot B)	2.24	0.61	27	1	11	3	47	1	10	3	87	9	21	6
RSES56-02.09	1.76	0.59	21	1	10	2	44	1	11	3	92	13	22	8
RSES73-4.7	5.30	1.19	63	2	24	3	105	2	23	4	203	17	46	10
RSES72-12.9 (REE spot B)	3.38	0.41	40	3	17	2	84	2	20	2	194	22	49	6
RSES73-17.10	4.08	0.78	52	3	20	2	95	2	22	4	213	18	52	10
RSES59-16.12	5.36	0.90	69	2	29	3	132	2	29	6	255	20	58	10
RSES54-14.6a	51.81	2.54	450	11	132	6	486	5	101	6	846	65	159	8
RSES54-14.6b	42.60	14.36	321	68	75	24	241	50	45	14	399	150	67	24
RSES73-3.1 (REE spot A)	26.65	1.11	281	5	103	4	420	5	88	6	711	50	147	8
RSES73-3.1 (REE spot B)	12.28	1.32	143	3	61	5	275	3	58	15	488	36	106	11
RSES58-5.14	5.03	0.59	58	1	24	2	106	2	23	4	204	16	46	6
RSES59-4.18	15.03	2.20	181	4	70	5	302	5	62	13	515	46	109	16
RSES59-8.14	5.13	0.56	45	2	14	1	54	3	12	1	104	11	22	3
RSES59-9.15	14.97	1.31	170	3	66	6	270	4	57	6	457	33	97	10
RSES64-1.16	10.29	1.40	115	2	47	5	189	3	41	4	325	24	73	10
RSES67-15.16	22.12	1.89	226	7	82	5	329	4	70	7	594	53	130	11
RSES67-19.13	4.30	1.45	60	3	21	8	94	5	20	5	157	23	40	14

Sample	**178Hf**	**1 s.e.**	**232Th**	**1 s.e.**	**238U**	**1 s.e.**	**_**	**Th (t)***	**U (t)***	**Th/U (t)***	**1 s.d.**	**Yb/Gd**	**1 s.d.**	**49Ti**	**1 s.e.**	**Txlln**	**est. 1 sigma**

RSES54-15.11a	10931	533	81	3	224	17		99	485	0.20				5.98	0.51	698	10
RSES54-15.11b	10870	605	84	4	239	6		102	517	0.20				4.86	0.47	681	10
54-15.11 average	*10901*	*808*	*83*	*5*	*231*	*21*		*100*	*501*	*0.20*	*0.02*	*17*	*3*	*5.42*		*689*	*18*
RSES54-18.11	12590	616	34	1	160	7		41	346	0.12	*0.01*	*26*	*3*	3.48	0.38	656	10
RSES55-11.3	12349	603	74	5	118	7		90	251	0.36	*0.03*	*21*	*3*	4.02	0.42	667	10
RSES55-15.11	8687	423	62	5	94	3		75	203	0.37	*0.03*	*15*	*2*	3.16	0.40	649	10
RSES55-15.13	10192	496	37	4	58	2		45	125	0.36	*0.04*	*25*	*3*	3.31	0.42	652	10
RSES55-5.13	11636	679	75	12	116	14		91	245	0.37	*0.08*	*19*	*3*	3.32	0.86	652	10
RSES56-03.17	9536	467	29	1	50	2		35	107	0.33	*0.02*	*17*	*3*	2.19	0.30	623	10
RSES58-16.15	10784	541	59	3	139	8		71	295	0.24	*0.02*	*18*	*2*	4.75	0.44	679	10
RSES58-3.13	9547	469	103	6	238	8		125	516	0.24	*0.02*	*16*	*1*	5.28	0.47	688	10
RSES59-04.08	11475	557	123	3	265	7		148	564	0.26	*0.01*	*25*	*2*	15.54	0.83	781	10
RSES59-17.16	9560	469	30	1	59	2		36	126	0.29	*0.02*	*16*	*2*	5.89	0.50	696	10
RSES73-3.7	9677	532	27	1	49	2		33	104	0.32	*0.02*	*19*	*2*	8.38	0.62	726	10
RSES73-5.8 average	*11110*	*822*	*49*	*9*	*178*	*11*		*59*	*384*	*0.15*	*0.03*	*17*	*6*	*3.45*		*655*	*17*
RSES73-5.8 (REE spot A)	11169	618	43	2	172	5		52	372	0.14				3.15	0.37	649	10
RSES73-5.8 (REE spot B)	11051	537	55	3	183	6		66	396	0.17				3.74	0.51	661	10
RSES53-3.4	12205	616	68	2	267	8		82	569	0.14				2.47	0.32	631	10
RSES53-3.4b	11812	645	79	2	296	13		95	631	0.15				2.33	0.31	627	10
RSES53-3.4 average	*12008*	*935*	*73*	*8*	*282*	*26*		*89*	*600*	*0.15*	*0.02*	*23*	*6*	*2.40*		*629*	*14*
RSES56-01.18	12668	657	46	4	246	21		56	526	0.11	*0.01*	*28*	*5*	1.07	0.30	577	10
RSES59-10.08 (near age spot)	11770	601	154	3	392	14		186	839	0.22	*0.01*	*11*	*1*	1.86	0.29	612	10
RSES55-3.13	13496	800	207	5	481	13		251	1031	0.24	*0.01*	*13*	*2*	1.32	0.40	589	10
RSES72-1.2 (inner REE spot)	13417	654	62	2	324	8		75	694	0.11	*0.00*	*29*	*5*	0.93	0.20	568	10
RSES56-10.17	11600	568	82	5	276	8		99	593	0.17	*0.01*	*18*	*2*	1.38	0.29	592	10
RSES58-5.11	11789	572	93	2	367	8		113	788	0.14	*0.00*	*21*	*2*	1.13	0.21	580	10
RSES59-6.12	12070	586	62	2	247	6		75	532	0.14	*0.01*	*22*	*3*	1.13	0.23	580	10
RSES73-9.4 (REE spot A)	12644	614	126	4	371	9		153	801	0.19	*0.01*	*11*	*1*	3.89	0.41	664	10
RSES55-13.8	14462	896	34	2	226	14		41	488	0.08	*0.01*	*43*	*9*	0.56	0.23	538	10
RSES58-13.14	11694	568	113	4	347	10		138	750	0.18	*0.01*	*12*	*1*	1.82	0.27	610	10
RSES58-15.13	11789	593	121	10	370	13		147	801	0.18	*0.02*	*13*	*1*	1.80	0.27	610	10
RSES72-12.9 (REE spot A)	12136	590	60	6	362	9		73	783	0.09	*0.01*	*27*	*3*	1.85	0.30	612	10
RSES58-17.7	12853	624	88	7	447	10		107	972	0.11	*0.01*	*28*	*3*	1.02	0.20	573	10
RSES59-14.12	13280	654	75	2	375	10		91	816	0.11	*0.00*	*27*	*3*	0.64	0.17	545	10
RSES53-16.11	13845	672	139	3	383	9		168	831	0.20	*0.01*	*20*	*3*	4.29	0.42	671	10
RSES53-15.5	10274	499	109	2	483	22		132	1051	0.13	*0.01*	*28*	*3*	2.67	0.62	637	10
RSES55-3.7	9730	474	76	2	103	8		93	230	0.48	*0.04*	*16*	*2*	5.13	0.50	685	10
RSES55-4.9	13768	669	132	4	175	6		163	405	0.49	*0.02*	*20*	*2*	2.84	0.38	641	10
RSES58-4.16	9290	467	37	3	96	5		45	221	0.25	*0.02*	*19*	*2*	6.57	0.52	705	10

RSES59-8.14	9089	442	381	6	188	5		466	431	1.31	*0.04*	*6*	*1*	26.05	2.05	833	10
RSES58-19.12	8838	476	31	2	51	2		38	115	0.40	*0.03*	*15*	*2*	2.93	0.35	643	10
RSES58-6.12	10792	524	63	2	288	13		76	652	0.14	*0.01*	*20*	*4*	5.71	0.48	694	10
RSES59-18.19	11247	549	20	3	62	2		25	138	0.22	*0.03*	*22*	*2*	2.15	0.31	622	10
RSES64-1.2	9580	520	28	2	61	6		34	142	0.29	*0.03*	*14*	*2*	4.62	0.45	677	10
RSES64-2.2	10480	510	107	6	283	12		131	661	0.24	*0.02*	*20*	*2*	2.43	0.33	630	10
RSES64-9.2	9499	462	33	1	84	3		40	191	0.25	*0.01*	*15*	*2*	5.37	0.49	689	10
RSES64-19.2	10647	548	41	1	108	4		50	249	0.24	*0.01*	*12*	*1*	3.91	0.42	664	10
RSES67-3.11	10705	526	127	8	153	6		155	346	0.54	*0.04*	*10*	*1*	11.98	1.22	757	10
RSES67-10.11	13303	758	35	2	163	19		42	363	0.14	*0.02*	*9*	*2*	2.43	0.72	630	10
RSES67-17.12	11545	561	564	55	374	9		691	861	0.97	*0.10*	*13*	*1*	20.17	0.94	807	10
RSES59-14.14	10690	525	547	22	397	11		662	848	0.91				35.17	1.24	865	10
RSES59-08.13	10967	533	664	9	892	20		803	1903	0.49				18.45	0.90	798	10
RSES73-7.6 (REE spot A)	13201	641	2671	41	1129	30		3231	2408	1.57				269.60	3.96	1146	15
RSES73-7.6 (REE spot B)	13476	654	380	9	719	19		459	1535	0.35				28.11	1.14	841	10
RSES72-14.9	11285	563	107	5	101	6		130	216	0.70				4.67	1.06	678	10
RSES59-10.08 (near MC Ti spot)	11865	598	306	10	427	10		370	914	0.48				14.08	0.79	772	10
RSES59-16.01	13664	663	194	5	371	9		234	796	0.35				10.34	0.74	744	10
RSES72-1.2 (outer REE spot)	13644	662	63	2	334	8		76	716	0.13				0.67	0.17	549	10
RSES73-3.2	13798	702	496	28	627	21		600	1345	0.52				20.28	2.97	807	10
RSES54-19.5	9362	455	139	7	193	7		168	414	0.48				3.58	0.39	658	10
RSES73-9.4 (REE spot B)	13460	654	60	2	280	7		73	603	0.14				1.08	0.22	577	10
RSES56-02.09	12330	601	40	1	209	10		49	451	0.13				1.63	0.26	603	10
RSES73-4.7	11341	562	113	4	424	15		137	917	0.18				2.26	0.39	625	10
RSES72-12.9 (REE spot B)	12309	598	238	7	494	11		289	1070	0.32				14.18	0.82	772	10
RSES73-17.10	10886	529	97	2	357	8		117	774	0.18				1.27	0.23	587	10
RSES59-16.12	10392	519	33	2	66	4		40	144	0.33				4.09	0.42	668	10
RSES54-14.6a	9492	464	3424	122	1336	29		4156	2906	1.69				359.07	18.88	1197	69
RSES54-14.6b	9679	542	1616	366	936	187		1962	2035	0.96				380.47	97.57	1208	371
RSES73-3.1 (REE spot A)	9057	456	716	42	408	14		872	907	0.96				60.69	1.68	929	10
RSES73-3.1 (REE spot B)	9057	441	228	4	346	8		278	769	0.36				6.00	0.51	698	10
RSES58-5.14	9866	480	154	3	145	8		188	331	0.69				14.86	0.78	777	10
RSES59-4.18	11522	562	293	5	379	11		361	910	0.40				6.39	0.68	703	10
RSES59-8.14	9089	442	381	6	188	5		466	431	1.08				26.05	2.05	833	10
RSES59-9.15	9834	486	63	3	87	3		77	200	0.38				5.83	0.50	696	10
RSES64-1.16	10569	526	90	2	119	4		110	265	0.41				6.99	0.61	710	10
RSES67-15.16	8021	408	476	47	277	11		586	654	0.90				109.07	15.85	1006	20
RSES67-19.13	10902	541	78	4	141	7		96	318	0.30				3.32	0.80	652	10

Sample	**Zonation type over REE Spot**	_	**PS Spot In Same Zone as Age Spot?**	**MC vs. PS Ti Measurements Agree?**
			0=no, 1=yes, 2=ambiguous	0=no, 1=yes, 2=MC spot was on a crack
RSES54-15.11a	homogeneous (patchy elsewhere)		1	1
RSES54-15.11b	homogeneous (patchy elsewhere)		1	1
54-15.11 average				
RSES54-18.11	patchy		1	1
RSES55-11.3	patchy		0	1
RSES55-15.11	oscillatory		1	2
RSES55-15.13	patchy		1	1
RSES55-5.13	large dark band (wide concentric zoned zircon)		1	1
RSES56-03.17	bright, cloudy		1	1
RSES58-16.15	patchy		2 (age spot location uncertain)	1
RSES58-3.13	oscillatory (altered elsewhere)		1	1
RSES59-04.08	patchy			0
RSES59-17.16	blurred oscillatory		1	1
RSES73-3.7	original sector or oscillatory; cloudy dark alteration at edges		1	1
RSES73-5.8 average				
RSES73-5.8 (REE spot A)	oscillatory		1	0
RSES73-5.8 (REE spot B)	oscillatory		1	0
RSES53-3.4	homogeneous		1	0
RSES53-3.4b	homogeneous		1	0
RSES53-3.4 average				
RSES56-01.18	bright stripe (homogeneous elsewhere)		1	1
RSES59-10.08 (near age spot)	patchy		0	0
RSES55-3.13	patchy		0	2
RSES72-1.2 (inner REE spot)	homogeneous		1	1
RSES56-10.17	wide dark band (broad concentric zones)		1	1
RSES58-5.11	homogeneous		1	1
RSES59-6.12	broad, faint concentric zonation		1	1
RSES73-9.4 (REE spot A)	homogeneous		1	0
RSES55-13.8	patchy		0	0
RSES58-13.14	homogeneous		1	1
RSES58-15.13	homogeneous regions with patchy areas		1	1
RSES72-12.9 (REE spot A)	homogeneous (some patches elsewhere)		1	0
RSES58-17.7	homogeneous (patchy elsewhere)		1	1
RSES59-14.12	homogeneous; bright streak on one edge		1	1
RSES53-16.11	homogeneous		1	0
RSES53-15.5	homogeneous		1	1

Table E.1: Trace element and morphology results for Hadean and 3.91-3.84 Ga zircons from chapter 3.

Additional Group I CL Images

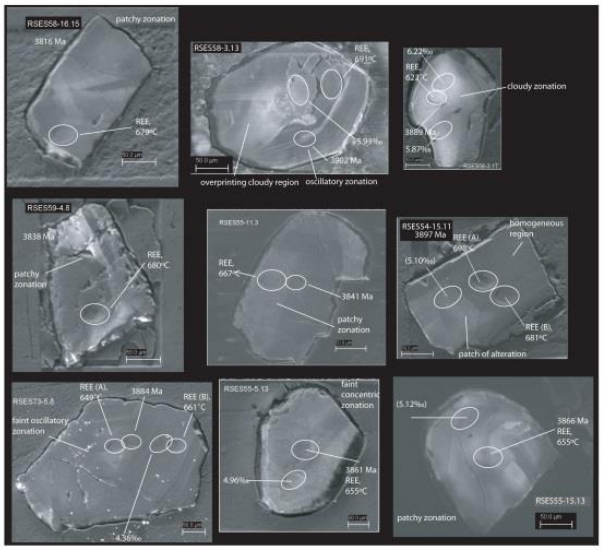

Group II CL Images

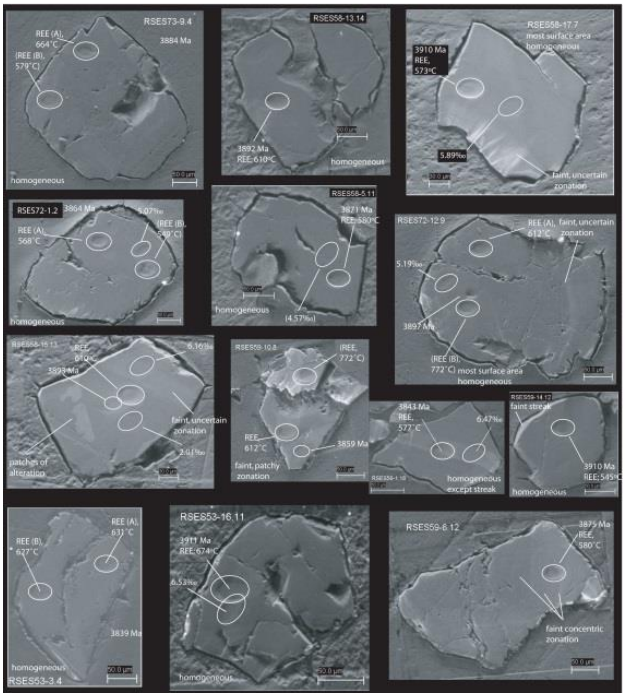

Image E.1: Additional cathodoluminescence images for Group I and II zircons from chapter.

Appendix F: Ch. 4 Lu-Hf-Pb Data and Explanation of Data Reduction

We measured both Lu-Hf systematics and Pb isotopes on a Thermo-Finnigan Neptune (with laser ablation) using the coupled Hf-Pb analysis developed by Woodhead et al. (2004). Our analysis sequence was that of Bell et al. (2011) and consisted of eleven seconds of counting on a Yb-Lu-Hf mass set (masses 171, 173, 174, 175, 176, 177, 178, 179, 181) followed by five seconds counting on a Pb isotope mass set (masses 204, 206, 207, 208). The first two seconds of counting on each mass set were discarded to allow for magnet settling. Baseline corrections were accomplished online, and all other data reduction was accomplished offline. Further data reduction for individual analyses included peak stripping to separate ^{176}Yb, ^{176}Lu, and ^{176}Hf.

Analyses took place at UCLA in seven sessions during the spring of 2013. Lu-Hf standard materials analyzed in each session include the zircon standards Mudtank and AS3; AS3 and NIST 610 glass were used as Pb isotope standards. Lu-Hf standard analyses reproduce both the ^{178}Hf/^{177}Hf of Thirlwall et al. (2004) and the ^{176}Hf/^{177}Hf values of AS3 (Kemp et al., 2009) and Mudtank zircon (Woodhead and Hergt, 2005) typically within ~ 1ε. A small correction factor is calculated for each session based on the standard analyses within that session and used to correct the unknown analyses. Uncertainties in the correction factor were added quadratically to internal uncertainties in the unknowns.

Standard materials used are shown in Table A1:

Quantity	**Standards Used**	**Notes**
^{176}Hf/^{177}Hf	AS3, Mudtank	
^{176}Lu/^{177}Hf	AS3	Not close to accepted values, but had little effect on the unknowns' calculated initial ^{176}Hf/^{177}Hf
^{207}Pb/^{206}Pb	AS3, NIST 610	Only analyses with ^{206}Pb signals > 0.02 V were used to calculate the correction factor
^{208}Pb/^{206}Pb	NIST 610	

Table F.1: Standard materials for Lu-Hf-Pb analyses in chapter four.

As developed in Supplementary File A from Harrison et al. (2008), the variance of the ε_{Hf} is calculated by their equation:

$$\sigma^2_{\varepsilon_o} = \left(10^4 \frac{Hf_t}{Hf_o}\right)^2 \left[\frac{1}{Hf_t^2}\sigma^2_{Hf} + \frac{1}{Hf_o^2}\sigma^2_{Hf_{ch}} + \frac{(e^{\lambda t}-1)^2}{Hf_t^2}\sigma^2_{Lu} + \frac{(e^{\lambda t_o}-1)^2}{Hf_o^2}\sigma^2_{Lu_{ch}} + \sigma^2_{\lambda}\left(\frac{Lu\,te^{\lambda t}}{Hf_t} - \frac{Lu_{ch}\,t_o e^{\lambda t_o}}{Hf_o}\right)^2 + \sigma^2_t\left(\frac{Lu\,\lambda e^{\lambda t}}{Hf_t}\right)^2 \right. \quad \text{(A1)}$$
$$\left. -2\rho_{Hf_{ch},Lu_{ch}}\sigma_{Hf_{ch}}\sigma_{Lu_{ch}}\left(\frac{1}{Hf_o}\right)\left(\frac{(e^{\lambda t_0}-1)}{Hf_o}\right)\right]$$

All uncertainties included in this equation already take account of the reproducibility of the standard materials in each session as described above. All uncertainties are reported as 2σ. The terms in the above equation are defined as:

$Hf = (^{176}Hf/^{177}Hf)_{today} \equiv$ measured $^{176}Hf/^{177}Hf$
$Lu = (^{176}Lu/^{177}Hf)_{today} \equiv$ measured $^{176}Lu/^{177}Hf$
$Hf_{ch} = (^{176}Hf/^{177}Hf)_{today} \equiv$ chondrite Hf today
$Lu_{ch} = (^{176}Lu/^{177}Hf)_{today} \equiv$ chondrite $^{176}Lu/^{177}Hf$ today
$\bar{H}f_t = Hf_{ch} - Lu_{ch}\,(e^{\lambda t} - 1) \equiv$ chondrite Hf at time t
$Hf_o = Hf_{ch} - Lu_{ch}\,(e^{\lambda to} - 1) \equiv$ chondrite initial Hf
$Hf_t = Hf - Lu\,(e^{\lambda t} - 1) \equiv$ sample Hf at time of formation t

All equations and variables are taken from Harrison et al. (2008; Supplementary File A).

CHUR values used are those of Bouvier et al. (2008), the ^{176}Lu decay constant (λ) of 1.867×10^{-11} yr^{-1} is that of Soderlund et al. (2004).

All standard and unknown analyses, marked by session, are shown in the following pages.

$^{207}Pb/^{206}Pb$ ages calculated by SIMS and ICPMS (Fig. A1) generally agree. Exceptions mainly involve:

a) several zircons dated as ca. 3.2-3.3 Ga by SIMS are found by ICPMS to be ca. 3.4 Ga (one is ~3.6 Ga).
b) several zircons in the 3.6-4.0 Ga range as dated by SIMS are found to be either ca. 3.4 or 4.0-4.2 Ga as dated by ICPMS.

These discrepancies do not change our main conclusions, and probably result from sampling of smaller, surficial age domains by SIMS versus the larger volume of material dated by laser ablation ICPMS analyses.

Appendix F References:

Bell, E.A., Harrison, T.M., McCulloch, M.T., Young, E.D., 2011. Early Archean crustal evolution of the Jack Hills Zircon source terrane inferred from Lu-Hf, $^{207}Pb/^{206}Pb$, and $\delta^{18}O$ systematics of Jack Hills zircons. Geochim. Cosmochim. Acta v. 75, p. 4816-4829.

Bouvier A., Vervoort J.D., Patchett P.J., 2008. The Lu-Hf and Sm-Nd isotopic composition of CHUR: constraints from unequilibrated chondrites and implications for the bulk composition of terrestrial planets. Earth Planet. Sci. Lett. v. 273, p. 48–57.

Harrison T.M., Schmitt A.K., McCulloch M.T., Lovera O.M., 2008. Early (≥4.5 Ga) formation of terrestrial crust: Lu-Hf, $\delta^{18}O$, and Ti thermometry results for Hadean zircons. Earth Planet. Sci. Lett. v. 268, p. 476–86.

Kemp, A.I.S., Foster, G.L., Schersten, A., Whitehouse, M.J., Darling, J., Storey, C., 2009. Concurrent Pb–Hf isotope analysis of zircon by laser ablation multi-collector ICP-MS, with implications for the crustal evolution of Greenland and the Himalayas. Chem. Geol. v. 261, p. 244-260.

Soderlund, U., Patchett, J.P., Vervoort, J.D., Isachsen, C.E., 2004. The ^{176}Lu decay constant determined by Lu-Hf and U-Pb isotope systematics of Precambrian mafic intrusions. Earth Planet. Sci. Lett. v. 219, p. 311-324.

Thirlwall, M.F., Anczkiewicz, R., 2004. Multidynamic isotope ratio analysis using MC-ICP-MS and the causes of secular drift in Hf, Nd and Pb isotope ratios. Int. J. Mass Spec. v. 235, p. 59–81.

Woodhead, J.D., Hergt, J.M., 2005. A preliminary appraisal of seven natural zircon reference materials for in situ Hf isotope determination. Geostd. Geoanal. Res. v. 29, p. 183-195.

Woodhead, J.D., Hergt, J.M., Shelley, M., Eggins, S., Kemp, R., 2004. Zircon Hf isotope analysis with an excimer laser, depth profiling, ablation of complex geometries, and concomitant age estimation. Chem. Geol. v. 209, p. 121–135.

Table F2: Lu-Hf-Pb Data For All Standard Materials and Session Average Correction Factors													
Sample name	**Session #**	**178Hf/177HF**	**2 s.e.**	**176Lu/177Hf**	**2 s.e.**	**176Hf/177Hf**	**2 s.e.**	**207Pb/206Pb**	**2 s.e.**	**208Pb/206Pb**	**2 s.e.**	**178Hf V**	**206Pb V**
Mudtank_f01	1	1.46725	0.00006	0.00001	0.00000	0.28253	0.00002	-0.07479	0.05351	0.14065	0.03192	1.78926	0.00019
Mudtank_f02	1	1.46723	0.00006	0.00001	0.00000	0.28253	0.00002	-0.03916	0.04078	0.12379	0.02425	1.83773	0.00020
nist610_f01	1	1.46743	0.00032	0.14788	0.00014	0.28555	0.00370	0.92756	0.00057	2.12512	0.00069	0.07380	0.02493
nist610_f02	1	1.46734	0.00033	0.14791	0.00014	0.29033	0.00367	0.92749	0.00052	2.12549	0.00064	0.07778	0.02599
AS3_f01	1	1.46719	0.00010	0.00136	0.00003	0.28218	0.00002	0.07741	0.00064	0.19325	0.00161	1.24534	0.03215
AS3_f02	1	1.46721	0.00007	0.00094	0.00001	0.28217	0.00002	0.07392	0.00194	0.18390	0.00100	1.28557	0.00710
AS3_f03	1	1.46722	0.00011	0.00062	0.00000	0.28217	0.00003	0.08018	0.00277	0.16443	0.01151	2.35664	0.00884
Mudtank_f03	1	1.46723	0.00005	0.00001	0.00000	0.28248	0.00002	-0.18188	0.10551	0.00717	0.05697	1.74018	0.00013
nist610_f03	1	1.46736	0.00032	0.14849	0.00013	0.28897	0.00349	0.92730	0.00046	2.12551	0.00055	0.07470	0.02513
AS3_f04	1	1.46746	0.00015	0.00130	0.00009	0.28210	0.00004	0.07823	0.00068	0.21263	0.00120	1.17565	0.01155
AS3_f05	1	1.46729	0.00006	0.00145	0.00007	0.28216	0.00002	0.07707	0.00036	0.26459	0.00596	1.46771	0.03968
Mudtank_f04	1	1.46720	0.00005	0.00001	0.00000	0.28248	0.00002	-0.20776	0.07788	0.12318	0.05624	1.84161	0.00012
nist610_f04	1	1.46730	0.00026	0.14940	0.00011	0.28747	0.00270	0.92758	0.00045	2.12533	0.00057	0.07513	0.02437
Mudtank_f06	1	1.46726	0.00005	0.00001	0.00000	0.28250	0.00002	-0.04622	0.10417	0.06742	0.06084	1.35342	0.00012
AS3_f06	1	1.46727	0.00010	0.00172	0.00005	0.28228	0.00003	0.07631	0.00050	0.11419	0.00175	0.86721	0.02012
AS3_f07	1	1.46726	0.00008	0.00189	0.00002	0.28220	0.00003	0.07760	0.00072	0.22220	0.00119	1.41499	0.01956
Mudtank_f07	1	1.46727	0.00006	0.00001	0.00000	0.28252	0.00002	-0.04718	0.06695	0.09597	0.05205	1.28530	0.00012
nist610_f06	1	1.46730	0.00037	0.14884	0.00011	0.28951	0.00500	0.92571	0.00074	2.11418	0.00073	0.06734	0.02190
Mudtank_f08	1	1.46722	0.00006	0.00001	0.00000	0.28251	0.00002	-0.15847	0.08655	0.22283	0.04022	1.36710	0.00012
AS3_f08	1	1.46724	0.00007	0.00087	0.00005	0.28219	0.00002	0.07721	0.00043	1.14790	0.20664	1.41368	0.03002
nist610_f07	1	1.46724	0.00031	0.14899	0.00014	0.28915	0.00284	0.92489	0.00074	2.11260	0.00068	0.06267	0.02072
	1												
Mudtank_m01	2	1.46720	0.00006	0.00001	0.00000	0.28250	0.00001	-0.07064	0.05134	0.11701	0.02455	2.08232	0.00021
Mudtank_m02	2	1.46724	0.00005	0.00001	0.00000	0.28249	0.00002	-0.06826	0.07278	0.15472	0.02385	2.10976	0.00019
AS3_m01	2	1.46720	0.00010	0.00088	0.00001	0.28221	0.00003	0.07562	0.00076	0.20290	0.00071	1.74045	0.00765
AS3_m02	2	1.46721	0.00007	0.00146	0.00006	0.28217	0.00002	0.07698	0.00042	0.19968	0.00349	1.89080	0.03754
nist610_m01	2	1.46720	0.00033	0.14830	0.00014	0.28764	0.00405	0.92746	0.00057	2.12089	0.00069	0.07178	0.02230
Mudtank_m03	2	1.46723	0.00005	0.00001	0.00000	0.28251	0.00001	-0.07714	0.06884	0.15708	0.02925	1.73690	0.00017
AS3_m03	2	1.46723	0.00007	0.00115	0.00004	0.28220	0.00002	0.07614	0.00099	0.15011	0.00382	1.41925	0.01295
nist610_m02	2	1.46706	0.00029	0.14854	0.00013	0.28650	0.00264	0.92686	0.00048	2.11788	0.00062	0.06890	0.02182
Mudtank_m04	2	1.46725	0.00005	0.00001	0.00000	0.28250	0.00002	-0.07829	0.06569	0.17745	0.03453	1.91039	0.00017
AS3_m04	2	1.46723	0.00011	0.00214	0.00012	0.28220	0.00003	0.07921	0.00089	0.79793	0.02792	1.85495	0.01367
nist610_m03	2	1.46743	0.00097	0.14877	0.00018	0.30071	0.00509	0.92747	0.00242	2.11740	0.00195	0.02096	0.00542
Mudtank_m05	2	1.46724	0.00005	0.00001	0.00000	0.28251	0.00001	-0.04823	0.05424	0.12312	0.03812	1.73200	0.00018
nist610_m04	2	1.46716	0.00032	0.14930	0.00011	0.29003	0.00352	0.92847	0.00059	2.12775	0.00061	0.07350	0.02218
AS3_m05	2	1.46727	0.00010	0.00125	0.00001	0.28216	0.00003	0.07678	0.00076	0.16443	0.00075	1.55155	0.01224
AS3_m06	2	1.46724	0.00009	0.00057	0.00004	0.28216	0.00005	0.08248	0.00420	0.14249	0.00583	1.38598	0.00295

Mudtank_m06	2	1.46726	0.00005	0.00001	0.00000	0.28251	0.00002	-0.09594	0.14930	0.14167	0.07238	1.52994	0.00014
AS3_m07	2	1.46732	0.00011	0.00148	0.00008	0.28217	0.00003	0.07833	0.00134	0.18695	0.00070	1.24653	0.00895
nist610_m05	2	1.46753	0.00034	0.14915	0.00011	0.29011	0.00332	0.92743	0.00055	2.12457	0.00060	0.07132	0.02145
Mudtank_m07	2	1.46726	0.00006	0.00001	0.00000	0.28251	0.00001	-0.09980	0.04521	0.08120	0.03021	1.83662	0.00018
	2												
Mudtank_t01	3	1.46723	0.00007	0.00001	0.00000	0.28252	0.00003	-0.13703	0.12394	0.12444	0.13142	1.09131	0.00007
Mudtank_t02	3	1.46723	0.00005	0.00001	0.00000	0.28252	0.00001	-0.07251	0.05284	0.11276	0.03056	2.04544	0.00019
AS3_t01	3	1.46720	0.00007	0.00076	0.00003	0.28217	0.00002	0.07811	0.00094	0.18094	0.00323	1.77243	0.01566
NIST610_t01	3	1.46691	0.00032	0.14781	0.00013	0.29101	0.00355	0.92870	0.00062	2.13118	0.00060	0.08131	0.02474
AS3_t02	3	1.46722	0.00012	0.00115	0.00003	0.28214	0.00004	0.07657	0.00186	0.20196	0.00092	1.44232	0.00695
Mudtank_t03	3	1.46722	0.00005	0.00001	0.00000	0.28252	0.00002	-0.07547	0.06400	0.13145	0.03878	1.65891	0.00016
AS3_t03	3	1.46723	0.00011	0.00061	0.00003	0.28219	0.00003	0.07762	0.00093	0.18828	0.00200	1.95115	0.03029
nist610_t02	3	1.46733	0.00031	0.14802	0.00012	0.29144	0.00396	0.92823	0.00057	2.13066	0.00067	0.07619	0.02314
AS3_t04	3	1.46727	0.00008	0.00165	0.00006	0.28219	0.00003	0.07701	0.00108	0.22962	0.00315	1.33580	0.03123
Mudtank_t04	3	1.46725	0.00005	0.00001	0.00000	0.28253	0.00001	-0.13819	0.06435	0.14535	0.04103	1.48085	0.00013
nist610_t03	3	1.46700	0.00033	0.14839	0.00012	0.29356	0.00561	0.92815	0.00064	2.12835	0.00073	0.06989	0.02209
AS3_t05	3	1.46731	0.00007	0.00099	0.00004	0.28216	0.00002	0.07554	0.00124	0.20068	0.00341	1.67593	0.01928
Mudtank_t05	3	1.46726	0.00005	0.00001	0.00000	0.28252	0.00002	-0.06247	0.06387	0.07110	0.03684	1.62943	0.00014
nist610_t04	3	1.46708	0.00027	0.14856	0.00011	0.28959	0.00355	0.92851	0.00051	2.12963	0.00053	0.07998	0.02471
Mudtank_t06	3	1.46726	0.00006	0.00001	0.00000	0.28249	0.00002	-0.15671	0.07424	0.16922	0.03258	1.57632	0.00014
AS3_t06	3	1.46725	0.00009	0.00130	0.00004	0.28220	0.00003	0.07869	0.00067	0.20686	0.00163	1.70556	0.01865
nist610_t05	3	1.46728	0.00032	0.14917	0.00008	0.28980	0.00265	0.92804	0.00049	2.13107	0.00055	0.07795	0.02363
Mudtank_t07	3	1.46733	0.00006	0.00001	0.00000	0.28250	0.00002	-0.08894	0.06347	0.12427	0.03724	1.75510	0.00017
nsit610_t06	3	1.46732	0.00036	0.14879	0.00015	0.29203	0.00374	0.92858	0.00064	2.12982	0.00077	0.06663	0.02041
AS3_t07	3	1.46732	0.00007	0.00084	0.00001	0.28220	0.00002	0.07987	0.00143	0.12881	0.00181	1.30538	0.00811
	3												
Mudtank_ww01	4	1.46725	0.00006	0.00003	0.00000	0.28254	0.00002	0.01952	0.03558	0.20343	0.02364	1.43197	0.00027
Mudtank_ww02	4	1.46724	0.00005	0.00001	0.00000	0.28251	0.00002	0.00495	0.07927	0.19036	0.05900	1.55736	0.00015
AS3_ww01	4	1.46733	0.00010	0.00082	0.00002	0.28221	0.00003	0.07796	0.00157	0.19650	0.01503	1.37881	0.01700
Mudtank_ww03	4	1.46726	0.00006	0.00001	0.00000	0.28249	0.00002	-0.19164	0.12781	-0.00269	0.10507	1.43483	0.00011
AS3_ww02	4	1.46722	0.00010	0.00088	0.00007	0.28216	0.00002	0.07511	0.00221	0.17652	0.00430	1.43304	0.00699
nist610_ww01	4	1.46729	0.00033	0.14821	0.00013	0.28653	0.00412	0.92781	0.00072	2.12738	0.00080	0.06174	0.01787
Mudtank_ww04	4	1.46730	0.00005	0.00001	0.00000	0.28250	0.00002	-0.05965	0.05963	0.09123	0.05300	1.54488	0.00015
nist610_ww02	4	1.46719	0.00036	0.14829	0.00012	0.28936	0.00332	0.92834	0.00066	2.13073	0.00078	0.06065	0.01855
AS3_ww03	4	1.46737	0.00008	0.00118	0.00001	0.28222	0.00004	0.07651	0.00076	0.17551	0.00109	0.95648	0.01844
AS3_ww04	4	1.46737	0.00008	0.00194	0.00002	0.28226	0.00003	0.07731	0.00035	0.19513	0.00094	1.21893	0.04641
Mudtank_ww05	4	1.46733	0.00005	0.00002	0.00000	0.28251	0.00002	-0.04725	0.06321	0.13273	0.03508	1.74660	0.00017
AS3_ww05	4	1.46736	0.00007	0.00088	0.00001	0.28220	0.00003	0.07570	0.00325	0.20219	0.00290	1.01736	0.00356
AS3_ww06	4	1.46737	0.00007	0.00159	0.00002	0.28221	0.00003	0.07830	0.00045	0.33518	0.00165	1.43522	0.04751

AS3_ww07	4	1.46739	0.00008	0.00079	0.00002	0.28219	0.00003	0.07394	0.00214	0.17332	0.00174	1.16777	0.00662
Mudtank_ww06	4	1.46732	0.00005	0.00001	0.00000	0.28249	0.00002	-0.10958	0.08023	0.19075	0.04269	1.40381	0.00012
AS3_ww08	4	1.46742	0.00007	0.00066	0.00003	0.28214	0.00003	0.07721	0.00294	0.14147	0.00342	1.16830	0.00446
nist610_ww03	4	1.46749	0.00035	0.14872	0.00014	0.29126	0.00541	0.92830	0.00068	2.12914	0.00067	0.06130	0.01848
Mudtank_ww07	4	1.46738	0.00006	0.00001	0.00000	0.28246	0.00002	-0.08362	0.08057	0.13030	0.04981	1.45255	0.00012
Mudtank_ww08	4	1.46739	0.00005	0.00001	0.00000	0.28248	0.00002	-0.08783	0.07475	0.13573	0.04220	1.41156	0.00012
Mudtank_ww09	4	1.46724	0.00006	0.00001	0.00000	0.28250	0.00002	-0.02722	0.08120	0.18560	0.04038	1.54044	0.00012
nist610_ww04	4	1.46722	0.00033	0.14845	0.00014	0.29145	0.00359	0.92798	0.00061	2.12701	0.00074	0.06718	0.02072
AS3_ww09	4	1.46724	0.00008	0.00114	0.00005	0.28217	0.00002	0.07624	0.00076	0.19549	0.00593	1.58880	0.01700
AS3_ww10	4	1.46725	0.00009	0.00114	0.00003	0.28222	0.00003	0.07724	0.00095	0.18443	0.00348	1.26744	0.01554
Mudtank_ww10	4	1.46724	0.00005	0.00001	0.00000	0.28250	0.00002	-0.01219	0.03811	0.13311	0.02967	1.54902	0.00020
nsit610_ww05	4	1.46727	0.00033	0.14916	0.00009	0.29070	0.00286	0.92758	0.00067	2.12370	0.00089	0.06523	0.02013
	4												
Mudtank_rr01	5	1.46722	0.00006	0.00001	0.00000	0.28250	0.00002	-0.05751	0.04641	0.14375	0.02391	1.56820	0.00017
Mudtank_rr02	5	1.46723	0.00005	0.00001	0.00000	0.28251	0.00001	-0.13501	0.08054	0.08810	0.04259	1.93802	0.00014
nist610_rr01	5	1.46714	0.00036	0.14817	0.00014	0.28899	0.00413	0.92742	0.00055	2.12632	0.00063	0.07044	0.02198
AS3_rr01	5	1.46733	0.00011	0.00140	0.00006	0.28215	0.00004	0.07637	0.00141	0.17926	0.00048	1.37196	0.00808
AS3_rr02	5	1.46728	0.00009	0.00014	0.00000	0.28217	0.00002	0.07644	0.00134	0.00216	0.00073	1.64121	0.00951
AS3_rr03	5	1.46728	0.00008	0.00096	0.00007	0.28219	0.00002	0.07681	0.00090	0.16079	0.00233	1.32600	0.01695
nist610_rr02	5	1.46733	0.00035	0.14826	0.00014	0.28958	0.00382	0.92772	0.00063	2.12583	0.00069	0.06753	0.02085
Mudtank_rr03	5	1.46730	0.00009	0.00003	0.00000	0.28259	0.00003	-0.02618	0.08230	0.21361	0.05995	1.09051	0.00008
Mudtank_rr04	5	1.46723	0.00006	0.00001	0.00000	0.28250	0.00002	-0.14679	0.07327	0.14988	0.06029	1.83275	0.00012
AS3_rr04	5	1.46726	0.00007	0.00124	0.00003	0.28216	0.00003	0.08526	0.00228	0.22944	0.00608	1.18237	0.01010
nist610_rr03	5	1.46716	0.00032	0.14856	0.00011	0.28688	0.00466	0.92762	0.00069	2.12455	0.00058	0.06431	0.02000
Mudtank_rr05	5	1.46721	0.00007	0.00001	0.00000	0.28252	0.00002	-0.61683	0.93794	0.19938	0.08398	1.07230	0.00006
nist610_rr04	5	1.46722	0.00036	0.14880	0.00013	0.29086	0.00341	0.92728	0.00061	2.12508	0.00075	0.05807	0.01833
AS3_rr05	5	1.46727	0.00007	0.00087	0.00001	0.28219	0.00003	0.07336	0.00138	0.16888	0.00227	1.08437	0.00624
AS3_rr06	5	1.46725	0.00008	0.00068	0.00003	0.28218	0.00002	0.07689	0.00119	0.17456	0.00200	1.21845	0.01081
nist610_rr05	5	1.46716	0.00042	0.14882	0.00014	0.28954	0.00318	0.92707	0.00069	2.12332	0.00081	0.05615	0.01778
Mudtank_rr06	5	1.46729	0.00006	0.00001	0.00000	0.28251	0.00002	-0.18605	0.18143	0.10449	0.09019	1.15165	0.00008
nist610_rr06	5	1.46725	0.00039	0.14890	0.00014	0.29193	0.00356	0.92770	0.00068	2.12330	0.00084	0.05381	0.01714
	5												
Mudtank_ff01	6	1.46742	0.00007	0.00001	0.00000	0.28266	0.00002	-0.10957	0.14012	0.24026	0.06524	1.25132	0.00011
Mudtank_ff02	6	1.46742	0.00006	0.00001	0.00000	0.28262	0.00002	-0.07747	0.15889	0.05711	0.10053	1.46350	0.00010
Mudtank_ff03	6	1.46743	0.00006	0.00001	0.00000	0.28264	0.00002	-0.12702	0.08949	0.11017	0.05984	1.66268	0.00013
Mudtank_ff04	6	1.46748	0.00006	0.00001	0.00000	0.28266	0.00002	-0.06828	0.10092	0.14317	0.08069	1.59572	0.00011
Mudtank_ff05	6	1.46726	0.00006	0.00001	0.00000	0.28249	0.00002	-0.08412	0.10313	0.19690	0.06161	1.31374	0.00009
Mudtank_ff06	6	1.46729	0.00006	0.00001	0.00000	0.28250	0.00002	-0.39924	0.49549	0.27441	0.08566	1.36425	0.00008
nist610_ff01	6	1.46745	0.00036	0.15001	0.00014	0.29357	0.00733	0.92857	0.00062	2.12713	0.00083	0.05984	0.01823

AS3_ff01	6	1.46733	0.00012	0.00114	0.00016	0.28219	0.00004	0.07748	0.00162	0.22187	0.00925	1.27509	0.00514
AS3_ff02	6	1.46725	0.00009	0.00101	0.00007	0.28219	0.00004	0.07905	0.00154	0.20538	0.00823	1.29820	0.01882
Mudtank_ff07	6	1.46725	0.00006	0.00001	0.00000	0.28251	0.00002	-0.03745	0.16031	0.17673	0.10137	1.12665	0.00010
nist610_ff02	6	1.46720	0.00038	0.15042	0.00012	0.29726	0.00488	0.92822	0.00082	2.12582	0.00062	0.06121	0.01829
Mudtank_ff08	6	1.46726	0.00007	0.00001	0.00000	0.28247	0.00002	-0.82539	1.06806	-0.01622	0.20108	1.35940	0.00009
nist610_ff03	6	1.46718	0.00035	0.15010	0.00011	0.29000	0.00330	0.92831	0.00061	2.12918	0.00077	0.06607	0.02059
AS3_ff03	6	1.46727	0.00008	0.00059	0.00001	0.28219	0.00003	0.07630	0.00075	0.17543	0.00217	1.17040	0.02004
Mudtank_ff09	6	1.46727	0.00006	0.00001	0.00000	0.28252	0.00002	-0.21988	0.25861	0.28598	0.09512	1.22370	0.00007
Mudtank_ff10	6	1.46722	0.00006	0.00001	0.00000	0.28250	0.00002	-0.10133	0.05836	0.21079	0.03443	1.70201	0.00016
nist610_ff04	6	1.46735	0.00031	0.14959	0.00015	0.28977	0.00382	0.92834	0.00055	2.12764	0.00063	0.06368	0.02088
	6												
Mudtank_mm01	7	1.46741	0.00006	0.00001	0.00000	0.28264	0.00002	-0.07391	0.06914	0.12637	0.05431	1.67610	0.00010
Mudtank_mm02	7	1.46752	0.00007	0.00001	0.00000	0.28267	0.00002	-0.14595	0.11957	0.22775	0.05994	1.20197	0.00009
Mudtank_mm03	7	1.46723	0.00005	0.00001	0.00000	0.28249	0.00001	-0.08351	0.04912	0.12283	0.03780	1.84060	0.00015
Mudtank_mm04	7	1.46724	0.00005	0.00001	0.00000	0.28250	0.00001	-0.11642	0.10687	0.17396	0.03815	1.97676	0.00013
nist610_mm01	7	1.46731	0.00024	0.14755	0.00013	0.29084	0.00518	0.93147	0.00043	2.14463	0.00053	0.10211	0.03164
AS3_mm01	7	1.46728	0.00014	0.00129	0.00014	0.28215	0.00003	0.07770	0.00023	0.15051	0.03127	2.08906	0.02095
AS3_mm02	7	1.46725	0.00007	0.00106	0.00011	0.28217	0.00002	0.09032	0.00978	0.21686	0.03071	2.29928	0.03342
AS3_mm03	7	1.46732	0.00008	0.00125	0.00011	0.28223	0.00002	0.08309	0.00161	0.19711	0.00508	1.36860	0.02810
nist610_mm02	7	1.46738	0.00027	0.14830	0.00012	0.28902	0.00454	0.92946	0.00062	2.13490	0.00073	0.07051	0.02044
Mudtank_mm05	7	1.46723	0.00007	0.00001	0.00000	0.28249	0.00002	-0.10778	0.07936	0.15089	0.04296	1.89864	0.00014
Mudtank_mm06	7	1.46727	0.00006	0.00001	0.00000	0.28249	0.00002	-0.27319	0.31818	0.13668	0.05624	1.47026	0.00010
nist610_mm03	7	1.46700	0.00029	0.14827	0.00014	0.28966	0.00513	0.92830	0.00061	2.12596	0.00069	0.06422	0.01916
AS3_mm04	7	1.46728	0.00009	0.00107	0.00003	0.28219	0.00003	0.07816	0.00193	0.17100	0.00610	1.08580	0.00712
nsit610_mm04	7	1.46730	0.00031	0.14876	0.00012	0.28873	0.00361	0.92823	0.00066	2.12462	0.00076	0.06695	0.02024
Mudtank_mm07	7	1.46726	0.00006	0.00001	0.00000	0.28251	0.00002	-0.12654	0.06375	0.12335	0.04270	1.62236	0.00014
nist610_mm05	7	1.46711	0.00035	0.14870	0.00013	0.28990	0.00411	0.92753	0.00064	2.12471	0.00079	0.06522	0.01997
AS3_mm05	7	1.46719	0.00007	0.00134	0.00004	0.28220	0.00002	0.07689	0.00063	0.20590	0.00188	1.14903	0.01884
nist610_mm06	7	1.46678	0.00035	0.14869	0.00015	0.29066	0.00380	0.92776	0.00065	2.12469	0.00075	0.05964	0.01833
Mudtank_mm08	7	1.46724	0.00007	0.00001	0.00000	0.28248	0.00002	-0.07725	0.11860	0.23324	0.07031	1.34657	0.00009
	7												

	Correction Factors					
Sample name	**176Hf/177Hf**	**2 s.d.**	**176Lu/177Hf**	**2 s.d.**	**207Pb/206Pb**	**2 s.d.**
Mudtank_f01	1.000064586					
Mudtank_f02	1.000068414					
nist610_f01					1.019543568	
nist610_f02					1.019469296	

AS3_f01	1.000007483		1.165311155		1.016500097	
AS3_f02	0.999964721		0.799148618			
AS3_f03	0.999989635		0.525737733			
Mudtank_f03	0.999888534					
nist610_f03					1.019263156	
AS3_f04	0.999724211		1.110796321			
AS3_f05	0.999944943		1.235474539		1.012111771	
Mudtank_f04	0.999922117					
nist610_f04					1.01956637	
Mudtank_f06	0.99996691					
AS3_f06	1.000356983		1.473544881		1.002126865	
AS3_f07	1.000093558		1.616554386		1.01902116	
Mudtank_f07	1.000038183					
nist610_f06					1.017514764	
Mudtank_f08	1.00000203					
AS3_f08	1.000061793		0.74042144		1.013882199	
nist610_f07					1.016612091	
Session Avg.	**1.00000E+00**	**1.25030E-04**	**1.08337E+00**	**7.46984E-01**	**1.01596E+00**	**1.04319E-02**
Mudtank_m01	0.999958646					
Mudtank_m02	0.999937698					
AS3_m01	1.000121245		0.753359439			
AS3_m02	0.999962442		1.24857589		1.010865608	
nist610_m01					1.019437154	
Mudtank_m03	1.000027526					
AS3_m03	1.000080321		0.979462629			
nist610_m02					1.018780063	
Mudtank_m04	0.999977763					
AS3_m04	1.000073331		1.827786772			
nist610_m03						
Mudtank_m05	1.000017474					
nist610_m04					1.020542457	
AS3_m05						
AS3_m06	0.999956609		0.484456526			
Mudtank_m06	1.000006331					
AS3_m07	0.99998077		1.264519123			
nist610_m05					1.019398205	
Mudtank_m07	1.000003544					
Session Avg.	**1.000007977**	**0.000110404**	**1.09302673**	**0.934711022**	**1.017804697**	**0.007861413**
Mudtank_t01	1.000052866					

Mudtank_t02	1.000061955					
AS3_t01	0.999990643		0.652892097			
NIST610_t01					1.020795865	
AS3_t02	0.999878107		0.98578988			
Mudtank_t03	1.000038508					
AS3_t03	1.000046972		0.518661279		1.019371391	
nist610_t02					1.020284373	
AS3_t04	1.000035678		1.409528433		1.011321357	
Mudtank_t04	1.000075144					
nist610_t03					1.02019097	
AS3_t05	0.999957269		0.849645814			
Mudtank_t05	1.000056668					
nist610_t04					1.020585875	
Mudtank_t06	0.999936646					
AS3_t06	1.000074753		1.108983486			
nist610_t05					1.020073055	
Mudtank_t07	0.999972156					
nsit610_t06					1.020660604	
AS3_t07	1.000091926		0.719224078			
Session Avg.	**1.000019235**	**0.000125112**	**0.921208618**	**0.694030974**	**1.018926803**	**0.006760378**
Mudtank_ww01	1.00011156					
Mudtank_ww02	1.000020476					
AS3_ww01	1.000113302		0.697661357			
Mudtank_ww03	0.999937036					
AS3_ww02	0.999955614		0.756324381			
nist610_ww01						
Mudtank_ww04	0.999971369					
nist610_ww02						
AS3_ww03	1.000154254		1.009771699			
AS3_ww04	1.000288609		1.656987285		1.015261416	
Mudtank_ww05	0.999997375					
AS3_ww05	1.000084828		0.749149651			
AS3_ww06	1.000117737		1.35955757		1.028205947	
AS3_ww07	1.000056488		0.678443104			
Mudtank_ww06	0.999940388					
AS3_ww08	0.999879111		0.564672167			
nist610_ww03					1.020359383	
Mudtank_ww07	0.999844435					
Mudtank_ww08	0.999904239					

Mudtank_ww09	0.999960114					
nist610_ww04					1.020003095	
AS3_ww09	0.999964177		0.97467285			
AS3_ww10	1.000147547		0.972600926			
Mudtank_ww10	0.999969338					
nsit610_ww05					1.01956328	
Session Avg.	**1.0000209**	**0.000221092**	**0.941984099**	**0.678352471**	**1.020678624**	**0.009370645**
Mudtank_rr01	0.999992076					
Mudtank_rr02	1.000013121					
nist610_rr01					1.019386786	
AS3_rr01	0.999897677		1.19363392			
AS3_rr02	0.999974141		0.117301527			
AS3_rr03	1.000051562		0.817705709			
nist610_rr02					1.019716217	
Mudtank_rr03	1.000279666					
Mudtank_rr04	0.999991762					
AS3_rr04	0.999949448		1.058234688			
nist610_rr03					1.019607989	
Mudtank_rr05	1.000042739					
nist610_rr04						
AS3_rr05	1.000043397		0.747537552			
AS3_rr06	1.000007045		0.577750421			
nist610_rr05						
Mudtank_rr06	1.000026896					
nist610_rr06						
Session Avg.	**0.999999079**	**9.19334E-05**	**0.752027303**	**0.762292553**	**1.019570331**	**0.000335826**
Mudtank_ff01	1.000540348					
Mudtank_ff02	1.00040089					
Mudtank_ff03	1.000460325					
Mudtank_ff04	1.000550131					
Mudtank_ff05	0.999936714					
Mudtank_ff06	0.99996513					
nist610_ff01						
AS3_ff01	1.00004593		0.977728857			
AS3_ff02	1.000052322		0.862798192			
Mudtank_ff07	1.000011463					
nist610_ff02						
Mudtank_ff08	0.999862075					
nist610_ff03					1.0203707	

AS3_ff03	1.000034425		0.506021604		1.002016363	
Mudtank_ff09	1.000051556					
Mudtank_ff10	0.999960716					
nist610_ff04					1.020404027	
Session Avg.	**0.999990495**	**0.000122823**	**0.848534246**	**0.481431403**	**1.014263697**	**0.02121303**
Mudtank_mm01	1.000475784					
Mudtank_mm02	1.000589212					
Mudtank_mm03	0.999926593					
Mudtank_mm04	0.999991848					
nist610_mm01					1.023841096	
AS3_mm01	0.999903936		1.102567327		1.020311976	
AS3_mm02	0.999974994		0.903141497		1.18611275	
AS3_mm03	1.000182105		1.068687473		1.091159874	
nist610_mm02					1.021633179	
Mudtank_mm05	0.999949816					
Mudtank_mm06	0.999935777					
nist610_mm03						
AS3_mm04	1.000057749		0.915324935			
nsit610_mm04					1.020275978	
Mudtank_mm07	1.00002727					
nist610_mm05					1.019515046	
AS3_mm05	1.000079117		1.145650139			
nist610_mm06						
Mudtank_mm08	0.999891859					
Session Avg.	**0.999992824**	**0.00017502**	**1.027074274**	**0.22212236**	**1.054692843**	**0.127147814**

Table F.2: Standard data for all Lu-Hf-Pb analysis sessions in chapter 4.

Sample name	**Session #**	**Lithology**	**178/177**	**2 s.e.**	**207Pb/206Pb**	**2se**	**208Pb/206Pb**	**2 s.d.**	**icp age, Ma**	**2 s.d.**
RSES53-3.1	1	detrital	1.46726	0.00007	0.3482	0.0042	0.2587	0.0308	3699	18.5
RSES53-3.4first10	1	detrital	1.46723	0.00006	0.3719	0.0043	0.0752	0.0005	3799	17.5
rses53-3.4last5	1	detrital	1.46717	0.00011	0.3756	0.0039			3814	16
rses53-3.5	1	detrital	1.46728	0.00006	0.3886	0.0045	0.0997	0.0021	3866	17.5
rses53-4.6	1	detrital	1.46722	0.00005	0.2864	0.0031	0.2069	0.0046	3398	17
rses53-4.6b	1	detrital	1.46724	0.00006	0.2866	0.0033	0.1455	0.0026	3399	18
rses53-4.7	1	detrital	1.46723	0.00006	0.3461	0.0046	0.1912	0.0107	3690	20
rses53-1.11	1	detrital	1.46731	0.00008	0.3470	0.0063	0.1900	0.0032	3694	27.5
rses53-1-19	1	detrital	1.46727	0.00007	0.3164	0.0049	0.0946	0.0038	3552	24

rses53-13.19	1	detrital	1.46727	0.00006	0.3982	0.0042	0.0939	0.0025	3902	16
rses53-16.11	1	detrital	1.46725	0.00006	0.3800	0.0043	0.0681	0.0008	3832	17
rses53-17.10 1-5	1	detrital	1.46718	0.00008	0.4432	0.0049	0.1347	0.0028	4063	16.5
rses53-17.10 6-8	1	detrital	1.46723	0.00013	0.4279	0.0056	0.1534	0.0033	4010	19.5
rses53-13.17	1	detrital	1.46729	0.00008	0.4749	0.0201	0.3919	0.0490	4165	62.5
rses53-15.5	1	detrital	1.46719	0.00007	0.3978	0.0041	0.0735	0.0013	3901	15.5
RSES73-3.2	1	detrital	1.46727	0.00006	0.3845	0.0043	0.0822	0.0027	3850	17
rses73-4.7	1	detrital	1.46724	0.00006	0.3963	0.0041	0.0734	0.0010	3895	16
rses73-5.8	1	detrital	1.46726	0.00006	0.4750	0.0277	0.5021	0.0694	4165	86.5
rses73-13.7	1	detrital	1.46722	0.00007	0.4062	0.0043	0.0693	0.0009	3932	16
rses73-13.7 blk 12	1	detrital	1.46725	0.00016	0.3957	0.0041			3893	16
rses73-12.3 1-6	2	detrital	1.46719	0.00007	0.2829	0.0082	0.4172	0.0074	3379	45.5
rses73-14.3	2	detrital	1.46722	0.00006	0.2659	0.0123	0.4386	0.0089	3282	73
rses73-17.10	2	detrital	1.46725	0.00007	0.3863	0.0061	0.1381	0.0065	3857	24
rses73-17.6	2	detrital	1.46725	0.00007	0.2757	0.0034	0.3017	0.0042	3339	19
rses73-17.7	2	detrital	1.46727	0.00007	0.3233	0.0025	0.1122	0.0022	3586	12
rses73-6.7 1-6	2	detrital	1.46727	0.00009	0.3228	0.0093	0.1446	0.0118	3583	44.5
rses73-6.7 7-10	2	detrital	1.46724	0.00010	0.2938	0.0057	0.2033	0.0092	3438	30.5
rses73-6.4	2	detrital	1.46726	0.00006	0.2826	0.0023	0.1860	0.0039	3377	13
rses73-6.2	2	detrital	1.46718	0.00006	0.2938	0.0178	0.3361	0.0222	3438	94
rses58-1.19	2	detrital	1.46719	0.00007	0.4231	0.0035	0.1778	0.0018	3993	12
rses58-4.19	2	detrital	1.46722	0.00008	0.3995	0.0065	0.1389	0.0025	3907	24.5
rses58-4.7osc	2	detrital	1.46721	0.00007	0.4248	0.0038	0.1690	0.0027	3999	13
rses58-4.7alt	2	detrital	1.46725	0.00008	0.4209	0.0048	0.1694	0.0035	3986	17
rses58-3.13	2	detrital	1.46726	0.00006	0.4308	0.0037	0.0894	0.0033	4020	13
rses58-5.11	2	detrital	1.46726	0.00006	0.3910	0.0030	0.0761	0.0004	3875	12
rses58-8.2	2	detrital	1.46723	0.00006	0.4324	0.0063	0.0608	0.0021	4026	22
rses58-11.3	2	detrital	1.46724	0.00006	0.4292	0.0155	0.3280	0.0362	4015	54
rses58-12.3	2	detrital	1.46728	0.00009	0.3994	0.0056	0.1924	0.0013	3907	21
rses58-13.6	2	detrital	1.46723	0.00006	0.3285	0.0026	0.0893	0.0010	3610	12
rses58-15.12 1-5	2	detrital	1.46720	0.00013	0.3288	0.0032	0.1338	0.0052	3612	15
rses58-15.12 6-10	2	detrital	1.46726	0.00010	0.3281	0.0036	0.1434	0.0040	3608	17
rses58-15.13	2	detrital	1.46723	0.00007	0.3956	0.0031	0.0878	0.0006	3892	12
rses58-16.17	2	detrital	1.46727	0.00006	0.3296	0.0036	0.1316	0.0030	3615	17
rses58-18.17	2	detrital	1.46723	0.00007	0.4382	0.0037	0.1264	0.0007	4046	13
rses58-19.19	2	detrital	1.46725	0.00007	0.3908	0.0182	0.1190	0.0051	3874	70.5
rses58-17.7	2	detrital	1.46721	0.00006	0.4007	0.0031	0.0553	0.0004	3912	12
rses58-16.2	2	detrital	1.46725	0.00007	0.4170	0.0044	0.0756	0.0010	3972	16
rses58-15.1	2	detrital	1.46727	0.00007	0.3804	0.0053	0.0990	0.0050	3833	21

rses58-10.15	2	detrital	1.46723	0.00007	0.4133	0.0037	0.1235	0.0020	3958	13.5
rses58-13.14	2	detrital	1.46725	0.00006	0.3986	0.0031	0.0966	0.0010	3904	12
rses58-13.9	2	detrital	1.46720	0.00009	0.4430	0.0037	0.1731	0.0014	4062	12.5
rses58-17.2	2	detrital	1.46725	0.00005	0.4137	0.0039	0.1579	0.0032	3960	14
rses59-4.17	3	detrital	1.46720	0.00007	0.3537	0.0029	0.2144	0.0006	3723	12.5
rses59-6.18	3	detrital	1.46723	0.00006	0.3600	0.0026	0.1257	0.0029	3750	11
rses59-8.17	3	detrital	1.46724	0.00006	0.3596	0.0026	0.1644	0.0007	3748	11
rses59-10.16	3	detrital	1.46720	0.00006	0.3275	0.0024	0.1083	0.0013	3605	11
rses59-10.19	3	detrital	1.46721	0.00007	0.4374	0.0037	0.2696	0.0085	4043	13
rses59-13.17	3	detrital	1.46724	0.00007	0.3729	0.0038	0.2043	0.0028	3803	15.5
rses59-15.16	3	detrital	1.46725	0.00006	0.3346	0.0023	0.1127	0.0004	3638	11
rses59-14.14	3	detrital	1.46730	0.00008	0.3903	0.0042	0.1583	0.0044	3872	16
rses59-16.14	3	detrital	1.46723	0.00007	0.4147	0.0046	0.1264	0.0018	3963	17
rses59-16.12	3	detrital	1.46724	0.00008	0.4005	0.0157	0.2060	0.0120	3911	59
rses59-14.12	3	detrital	1.46728	0.00008	0.4009	0.0027	0.0585	0.0002	3913	10
rses59-17.13	3	detrital	1.46729	0.00007	0.4128	0.0128	0.1431	0.0011	3956	46.5
rses59-17.15	3	detrital	1.46724	0.00006	0.4058	0.0034	0.1331	0.0022	3931	13
rses59-17.16	3	detrital	1.46729	0.00007	0.4158	0.0060	0.1631	0.0014	3967	21.5
rses59-17.7	3	detrital	1.46725	0.00006	0.3235	0.0023	0.1127	0.0004	3587	11
rses59-16.1	3	detrital	1.46720	0.00009	0.3567	0.0079	0.0831	0.0025	3736	33.5
rses59-16.1 2-3	3	detrital	1.46721	0.00010	0.2745	0.0079	0.0612	0.0012	3332	45
rses59-16.3	3	detrital	1.46726	0.00011	0.4089	0.0038	0.0802	0.0008	3942	14
rses59-16.5	3	detrital	1.46721	0.00006	0.4105	0.0029	0.0928	0.0022	3948	11
rses59-16.6	3	detrital	1.46723	0.00005	0.3354	0.0023	0.0862	0.0006	3642	11
rses59-15.1	3	detrital	1.46727	0.00008	0.3331	0.0024	0.1266	0.0082	3631	11
rses59-15.9	3	detrital	1.46722	0.00007	0.3921	0.0031	0.0945	0.0021	3879	12
rses59-14.7	3	detrital	1.46725	0.00007	0.3302	0.0024	0.1092	0.0043	3618	11
rses59-9.11	3	detrital	1.46726	0.00008	0.3315	0.0027	0.1216	0.0041	3624	12.5
res59-9.11 9-10	3	detrital	1.46720	0.00015	0.3402	0.0033	0.1546	0.0009	3664	15
rses59-5.9	3	detrital	1.46725	0.00007	0.3440	0.0042	0.1674	0.0071	3681	19
rses59-4.8	3	detrital	1.46727	0.00007	0.4109	0.0049	0.1432	0.0066	3950	18
rses59-4.7	3	detrital	1.46721	0.00007	0.3654	0.0029	0.1704	0.0009	3772	12
rses59-3.15	3	detrital	1.46722	0.00007	0.3764	0.0034	0.1951	0.0038	3817	14
rses59-6.12	3	detrital	1.46726	0.00008	0.3906	0.0026	0.0757	0.0007	3873	10
rses59-8.11	3	detrital	1.46724	0.00006	0.4132	0.0037	0.1146	0.0045	3958	13.5
rses59-9.14	3	detrital	1.46724	0.00007	0.4468	0.0037	0.2087	0.0079	4075	12
rses59-6.4	3	detrital	1.46725	0.00007	0.3946	0.0042	0.1845	0.0012	3889	16
rses72-1.2	3	detrital	1.46725	0.00006	0.3889	0.0026	0.0602	0.0005	3867	10
rses72-1.3	3	detrital	1.46728	0.00006	0.3303	0.0025	0.1201	0.0028	3619	12

rses72-3.2	3	detrital	1.46727	0.00007	0.3327	0.0023	0.1125	0.0014	3630	11
rses72-4.2	3	detrital	1.46726	0.00006	0.4139	0.0028	0.0621	0.0010	3960	10
rses72-9.3	3	detrital	1.46732	0.00006	0.4216	0.0034	0.0589	0.0003	3988	12
rses72-13.1	3	detrital	1.46724	0.00007	0.3918	0.0029	0.1316	0.0010	3878	11
rses72-15.7	3	detrital	1.46721	0.00007	0.3235	0.0024	0.1560	0.0034	3587	11
rses72-17.8	3	detrital	1.46724	0.00007	0.3307	0.0022	0.0712	0.0005	3620	10
rses72-12.9	3	detrital	1.46725	0.00007	0.4013	0.0028	0.0577	0.0017	3914	10.5
rses72-14.9	3	detrital	1.46725	0.00007	0.3577	0.0114	0.2440	0.0139	3740	48.5
rses72-1.2 pyr	3	detrital	1.46729	0.00007	0.3891	0.0026	0.0924	0.0016	3868	10
rses55-5.6	4	detrital	1.46724	0.00007	0.3722	0.0127	0.1552	0.0277	3800	52
rses55-4.6	4	detrital	1.46727	0.00006	0.4456	0.0111	0.2323	0.0259	4071	37.5
rses55-6.8	4	detrital	1.46729	0.00012	0.3698	0.0067	0.1182	0.0115	3791	27.5
rses55-6.12	4	detrital	1.46729	0.00007	0.4162	0.0042	0.1330	0.0030	3969	15
rses55-5.13	4	detrital	1.46728	0.00007	0.3989	0.0039	0.1859	0.0034	3905	15
rses55-3.13a	4	detrital	1.46726	0.00006	0.3931	0.0045	0.1157	0.0053	3883	17
rses55-3.13b	4	detrital	1.46724	0.00008	0.4030	0.0070	0.1669	0.0137	3920	26
rses55-3.13b 1-2	4	detrital	1.46729	0.00010	0.3899	0.0039	0.1390	0.0062	3871	15
rses55-4.19	4	detrital	1.46729	0.00006	0.3215	0.0030	0.0571	0.0004	3577	14
rses55-6.19	4	detrital	1.46736	0.00007	0.4267	0.0040	0.2386	0.0012	4006	14
rses55-7.20	4	detrital	1.46730	0.00007	0.4219	0.0040	0.1474	0.0036	3989	14
rses55-5.20	4	detrital	1.46724	0.00007	0.4897	0.0171	0.3964	0.0447	4211	52
res55-8.14	4	detrital	1.46736	0.00007	0.3320	0.0031	0.0712	0.0003	3626	14
rses55-9.15	4	detrital	1.46730	0.00007	0.3264	0.0031	0.0892	0.0014	3600	15
rses55-12.13	4	detrital	1.46733	0.00010	0.3810	0.0040	0.1219	0.0060	3836	16
rses55-13.13	4	detrital	1.46729	0.00008	0.3928	0.0059	0.1536	0.0123	3882	22.5
rses55-15.13	4	detrital	1.46731	0.00008	0.4510	0.0053	0.1613	0.0015	4089	17.5
rses55-19.19	4	detrital	1.46732	0.00006	0.4128	0.0041	0.0713	0.0005	3956	15
rses55-14.20	4	detrital	1.46735	0.00006	0.3270	0.0030	0.1075	0.0007	3603	14
rses55-15.11core	4	detrital	1.46728	0.00007	0.3975	0.0064	0.1792	0.0027	3900	24
rses55-15.11outer	4	detrital	1.46739	0.00007	0.3924	0.0043	0.1784	0.0034	3880	16.5
rses55-15.9	4	detrital	1.46735	0.00007	0.3995	0.0054	0.0911	0.0058	3907	20.5
rses55-13.7	4	detrital	1.46734	0.00007	0.4316	0.0041	0.0919	0.0025	4023	14
rses55-11.11	4	detrital	1.46735	0.00007	0.3598	0.0034	0.1044	0.0010	3749	14
rses55-11.3	4	detrital	1.46735	0.00007	0.3756	0.0037	0.1479	0.0011	3814	15
rses55-12.1	4	detrital	1.46738	0.00008	0.3878	0.0049	0.1042	0.0043	3862	19
rses55-12.1 8-10	4	detrital	1.46738	0.00011	0.3806	0.0042	0.1923	0.0120	3834	17
rses55-13.8	4	detrital	1.46734	0.00007	0.3952	0.0037	0.1219	0.0017	3891	14
rses55-13.8 1-2	4	detrital	1.46747	0.00013	0.3945	0.0041	0.0908	0.0021	3888	16
blob1-7.2	4	metaigneous -- 'Blob' granite	1.46722	0.00007	0.1773	0.0024	0.3429	0.0092	2628	22.5

blob1-7.3	4	metaigneous -- 'Blob' granite	1.46723	0.00007	0.1784	0.0054	0.3071	0.0082	2638	50
blob1-7.9	4	metaigneous -- 'Blob' granite	1.46726	0.00006	0.1663	0.0023	0.2964	0.0089	2521	23
blob1-7.10	4	metaigneous -- 'Blob' granite	1.46724	0.00009	0.1884	0.0118	0.5579	0.0154	2728	103.5
blob1-1.1	4	metaigneous -- 'Blob' granite	1.46726	0.00009	0.3999	0.0079	1.5308	0.0193	3909	29.5
blob1-1.2 (guess at ID)	4	metaigneous -- 'Blob' granite	1.46729	0.00008	0.3918	0.0096	1.6133	0.0292	3878	36.5
blob1-1.9 (guess at ID)	4	metaigneous -- 'Blob' granite	1.46726	0.00010	0.2726	0.0151	0.9232	0.0404	3321	87
blob1-8.9	4	metaigneous -- 'Blob' granite	1.46725	0.00006	0.3807	0.0061	1.4790	0.0168	3835	24
blob1-9.10	4	metaigneous -- 'Blob' granite	1.46723	0.00006	0.3280	0.0155	1.1902	0.0418	3608	72.5
blob1-9.8	4	metaigneous -- 'Blob' granite	1.46742	0.00011	0.3943	0.0087	1.5786	0.0259	3888	33.5
rses54-1.19	5	detrital	1.46725	0.00006	0.3313	0.0006	0.1101	0.0007	3623	3
rses54-2.16	5	detrital	1.46727	0.00006	0.3326	0.0004	0.1250	0.0010	3629	2
rses54-6.17	5	detrital	1.46728	0.00009	0.2830	0.0014	0.1897	0.0067	3380	8
rses54-8.16	5	detrital	1.46724	0.00008	0.3523	0.0016	0.3176	0.0073	3717	7
rses54-6.12	5	detrital	1.46720	0.00005	0.3434	0.0012	0.1011	0.0033	3678	5
rses54-7.5	5	detrital	1.46725	0.00007	0.3421	0.0005	0.1040	0.0009	3672	2
rses54-9.4	5	detrital	1.46726	0.00007	0.4262	0.0016	0.1907	0.0020	4004	6
rses54-3.9	5	detrital	1.46726	0.00006	0.4335	0.0009	0.1009	0.0006	4030	3
rses54-11.12	5	detrital	1.46731	0.00006	0.3199	0.0041	0.0951	0.0076	3569	20
rses54-12.11	5	detrital	1.46724	0.00007	0.3326	0.0003	0.1012	0.0004	3629	1
rses54-15.11dark	5	detrital	1.46723	0.00008	0.4042	0.0016	0.0780	0.0010	3925	6
rses54-15.11light	5	detrital	1.46722	0.00006	0.3770	0.0041	0.0975	0.0033	3820	16.5
rses54-17.17	5	detrital	1.46726	0.00008	0.4531	0.0081	0.1769	0.0171	4095	26.5
rses54-17.18	5	detrital	1.46724	0.00006	0.4175	0.0012	0.1054	0.0033	3973	4
rses54-16.20	5	detrital	1.46721	0.00006	0.4178	0.0008	0.1739	0.0010	3974	3
rses54-18.11	5	detrital	1.46728	0.00008	0.4176	0.0025	0.1073	0.0030	3974	9
rses54-18.11lines	5	detrital	1.46722	0.00007	0.4346	0.0155	0.2381	0.0400	4033	53
rses54-16.14	5	detrital	1.46722	0.00006	0.3593	0.0015	0.1431	0.0017	3747	6
rses54-14.19	5	detrital	1.46724	0.00007	0.3524	0.0005	0.1709	0.0088	3717	2
rses54-19.5	5	detrital	1.46728	0.00008	0.4181	0.0024	0.2229	0.0005	3976	9
rses54-17.1	5	detrital	1.46725	0.00008	0.3645	0.0094	0.3017	0.0207	3769	39.5
rses56_1-18	5	detrital	1.46725	0.00007	0.3874	0.0006	0.0658	0.0009	3861	2
rses56_2-18	5	detrital	1.46723	0.00007	0.3934	0.0019	0.1486	0.0017	3884	7
rses56_3-17	5	detrital	1.46726	0.00007	0.3836	0.0028	0.1971	0.0016	3846	11
rses56_2-17	5	detrital	1.46727	0.00007	0.3943	0.0031	0.1455	0.0022	3888	12
rses56-5.16	5	detrital	1.46725	0.00006	0.4225	0.0016	0.1296	0.0019	3991	6
rses56-6.12	5	detrital	1.46728	0.00006	0.3048	0.0009	0.1468	0.0005	3495	5
rses56-5.2	5	detrital	1.46726	0.00007	0.3043	0.0038	0.2144	0.0074	3492	19
rses56-8.10	5	detrital	1.46724	0.00006	0.2821	0.0011	0.1978	0.0036	3375	6
rses56-7.6	5	detrital	1.46724	0.00006	0.4014	0.0006	0.0635	0.0005	3914	2

rses56-9.10	5	detrital	1.46730	0.00007	0.3773	0.0018	0.0913	0.0011	3821	7
rses56-6.2	5	detrital	1.46726	0.00007	0.4005	0.0061	0.0951	0.0020	3911	12.5
rses56-7.12	5	detrital	1.46725	0.00007	0.4148	0.0011	0.1167	0.0018	3964	4
rses56-2.9	5	detrital	1.46726	0.00007	0.3925	0.0012	0.0624	0.0006	3881	5
rses56-10.11	5	detrital	1.46724	0.00015	0.3960	0.0024	0.2125	0.0023	3894	9
rses56-14.14	5	detrital	1.46729	0.00007	0.4423	0.0014	0.0894	0.0011	4060	5
rses56-14.9	5	detrital	1.46724	0.00006	0.3587	0.0004	0.1440	0.0011	3744	2
rses56-17.14	5	detrital	1.46716	0.00008	0.3634	0.0055	0.0857	0.0029	3764	23
rses56-10.17	5	detrital	1.46728	0.00007	0.3904	0.0004	0.0862	0.0006	3873	2
rses56-14.19	5	detrital	1.46725	0.00007	0.4436	0.0006	0.0850	0.0003	4064	2
su1x_5-4a	6	metaigneous -- near 'Blob' granite contact	1.46736	0.00014	0.2926	0.0301	0.5649	0.0509	3432	160.5
su1x_5-4b	6	metaigneous -- near 'Blob' granite contact	1.46723	0.00008	0.1985	0.0048	0.3257	0.0196	2814	39.5
su1x-3.5	6	metaigneous -- near 'Blob' granite contact	1.46726	0.00008	0.3256	0.0263	0.7205	0.0424	3597	124.5
su1x-4.6	6	metaigneous -- near 'Blob' granite contact	1.46724	0.00007	0.2250	0.0096	0.3591	0.0152	3017	68.5
su1x-4.5a	6	metaigneous -- near 'Blob' granite contact	1.46731	0.00007	0.2190	0.0080	0.3985	0.0107	2973	59
su1x-5.6	6	metaigneous -- near 'Blob' granite contact	1.46728	0.00008	0.3335	0.0130	0.6596	0.0166	3633	59.5
su1x-3.2	6	metaigneous -- near 'Blob' granite contact	1.46734	0.00009	0.2494	0.0134	0.4180	0.0221	3181	85.5
su1x-6.5	6	metaigneous -- near 'Blob' granite contact	1.46729	0.00008	0.2629	0.0150	0.4311	0.0234	3264	90
su1x-7.3	6	metaigneous -- near 'Blob' granite contact	1.46727	0.00007	0.2603	0.0136	0.4932	0.0189	3249	82.5
JHO3008x-1.6	7	metaigneous	1.46724	0.00007	0.1732	0.0212	0.1212	0.0048	2589	0
JHO3008x-2.5	7	metaigneous	1.46724	0.00004	0.1861	0.0226	0.1860	0.0040	2708	0
JHO3008x-2.4	7	metaigneous	1.46723	0.00006	0.1907	0.0241	0.2086	0.0129	2748	0
JHO3008x-3.3	7	metaigneous	1.46722	0.00007	0.1740	0.0210	0.1749	0.0032	2597	0
JHO3008x-4.1	7	metaigneous	1.46724	0.00006	0.1859	0.0231	0.2525	0.0115	2706	0
JHO3008x-4.4	7	metaigneous	1.46731	0.00012	0.2053	0.0249	0.3074	0.0081	2869	0
JHO3008x-6.6	7	metaigneous	1.46724	0.00007	0.1875	0.0231	0.1655	0.0073		

Sample name	**176Hf/177Hf**	**2 s.d.**	**176Lu/177Hf**	**Hf (t)**	**Hf (t) CHUR**	**Hf (t) DM**	**eHf**	**2 s.d.**	**TDM Felsic**	**2 s.d.**
RSES53-3.1	0.28025	0.00004	0.00082	0.28019	0.28038	0.28048	-6.77	2.28	4120	78
RSES53-3.4first10	0.28016	0.00004	0.00033	0.28013	0.28032	0.28040	-6.48	1.80	4246	73
rses53-3.4last5	0.28007	0.00009	0.00031	0.28004	0.28031	0.28039	-9.34	3.30	4406	158
rses53-3.5	0.28021	0.00004	0.00071	0.28016	0.28027	0.28035	-3.98	2.14	4120	73
rses53-4.6	0.28038	0.00004	0.00101	0.28032	0.28058	0.28072	-9.52	2.36	4008	74
rses53-4.6b	0.28038	0.00004	0.00067	0.28033	0.28058	0.28072	-8.95	2.05	4020	75
rses53-4.7	0.28009	0.00004	0.00122	0.28000	0.28039	0.28049	-13.72	2.77	4415	77
rses53-1.11	0.28024	0.00004	0.00098	0.28017	0.28039	0.28049	-7.84	2.50	4150	82
rses53-1-19	0.28036	0.00004	0.00077	0.28031	0.28048	0.28060	-6.22	2.14	3986	75
rses53-13.19	0.28021	0.00004	0.00052	0.28017	0.28025	0.28032	-2.67	1.94	4107	72

rses53-16.11	0.28015	0.00004	0.00028	0.28013	0.28029	0.28038	-5.86	1.76	4248	72
rses53-17.10 1-5	0.28012	0.00005	0.00101	0.28004	0.28014	0.28019	-3.33	2.72	4193	85
rses53-17.10 6-8	0.28013	0.00005	0.00091	0.28006	0.28017	0.28024	-4.05	2.69	4205	94
rses53-13.17	0.28013	0.00004	0.00150	0.28000	0.28007	0.28011	-2.28	3.49	4144	100
rses53-15.5	0.28020	0.00004	0.00050	0.28017	0.28025	0.28032	-2.85	1.99	4118	76
RSES73-3.2	0.28020	0.00004	0.00052	0.28016	0.28028	0.28036	-4.43	1.94	4156	72
rses73-4.7	0.28020	0.00004	0.00040	0.28017	0.28025	0.28033	-2.87	1.87	4127	74
rses73-5.8	0.28016	0.00004	0.00031	0.28013	0.28007	0.28011	2.25	1.83	4087	113
rses73-13.7	0.28010	0.00007	0.00081	0.28004	0.28023	0.28030	-6.52	3.21	4286	136
rses73-13.7 blk 12	0.27856	0.00151	0.00110	0.27848	0.28025	0.28033	-63.20	53.90	7034	2596
rses73-12.3 1-6	0.28040	0.00004	0.00077	0.28035	0.28060	0.28073	-8.66	2.29	3978	84
rses73-14.3	0.28046	0.00005	0.00225	0.28031	0.28066	0.28081	-12.37	4.86	3924	109
rses73-17.10	0.28024	0.00004	0.00190	0.28010	0.28028	0.28036	-6.35	4.69	4072	73
rses73-17.6	0.28041	0.00004	0.00075	0.28036	0.28062	0.28076	-9.32	2.18	3983	68
rses73-17.7	0.28038	0.00004	0.00058	0.28034	0.28046	0.28057	-4.17	2.05	3932	69
rses73-6.7 1-6	0.28041	0.00004	0.00056	0.28038	0.28046	0.28057	-3.03	2.05	3873	82
rses73-6.7 7-10	0.28048	0.00005	0.00528	0.28013	0.28056	0.28069	-15.32	10.95	3820	101
rses73-6.4	0.28043	0.00004	0.00127	0.28034	0.28060	0.28073	-9.07	3.06	3939	75
rses73-6.2	0.28072	0.00004	0.00465	0.28041	0.28056	0.28069	-5.30	9.63	3382	120
rses58-1.19	0.28009	0.00004	0.00074	0.28003	0.28018	0.28025	-5.55	2.39	4292	68
rses58-4.19	0.28003	0.00004	0.00048	0.27999	0.28024	0.28032	-8.97	1.97	4436	70
rses58-4.7osc	0.28020	0.00004	0.00040	0.28017	0.28018	0.28025	-0.49	1.99	4087	76
rses58-4.7alt	0.28017	0.00004	0.00049	0.28013	0.28019	0.28026	-1.97	2.06	4140	74
rses58-3.13	0.28004	0.00005	0.00036	0.28001	0.28017	0.28023	-5.50	2.23	4364	93
rses58-5.11	0.28013	0.00004	0.00031	0.28011	0.28026	0.28034	-5.55	1.86	4261	73
rses58-8.2	0.28003	0.00011	0.00012	0.28002	0.28016	0.28022	-4.91	3.91	4373	193
rses58-11.3	0.28019	0.00004	0.00042	0.28016	0.28017	0.28023	-0.34	1.89	4088	85
rses58-12.3	0.28010	0.00004	0.00108	0.28002	0.28024	0.28032	-7.85	3.03	4297	76
rses58-13.6	0.28038	0.00004	0.00090	0.28032	0.28044	0.28055	-4.30	2.49	3916	66
rses58-15.12 1-5	0.28045	0.00004	0.00086	0.28039	0.28044	0.28055	-1.87	2.59	3798	80
rses58-15.12 6-10	0.28040	0.00005	0.00095	0.28033	0.28044	0.28055	-3.96	2.91	3891	96
rses58-15.13	0.28017	0.00003	0.00035	0.28015	0.28025	0.28033	-3.73	1.78	4176	65
rses58-16.17	0.28034	0.00004	0.00086	0.28028	0.28044	0.28055	-5.82	2.50	4002	73
rses58-18.17	0.28007	0.00004	0.00066	0.28002	0.28015	0.28021	-4.76	2.30	4304	71
rses58-19.19	0.28016	0.00004	0.00069	0.28011	0.28026	0.28034	-5.69	2.32	4215	100
rses58-17.7	0.28020	0.00004	0.00060	0.28016	0.28024	0.28031	-2.93	2.12	4116	66
rses58-16.2	0.28017	0.00004	0.00023	0.28016	0.28020	0.28027	-1.53	1.69	4143	67
rses58-15.1	0.28013	0.00004	0.00066	0.28008	0.28029	0.28038	-7.40	2.26	4276	74
rses58-10.15	0.28009	0.00005	0.00029	0.28007	0.28021	0.28028	-5.09	2.18	4304	94

rses58-13.14	0.28007	0.00006	0.00037	0.28004	0.28024	0.28032	-7.35	2.43	4368	105
rses58-13.9	0.28017	0.00004	0.00217	0.28000	0.28014	0.28020	-4.85	5.48	4104	73
rses58-17.2	0.28010	0.00004	0.00036	0.28007	0.28021	0.28028	-4.75	1.89	4279	72
rses59-4.17	0.28024	0.00004	0.00152	0.28013	0.28037	0.28046	-8.34	3.41	4126	74
rses59-6.18	0.28032	0.00004	0.00133	0.28022	0.28035	0.28044	-4.61	3.11	3981	72
rses59-8.17	0.28023	0.00004	0.00156	0.28012	0.28035	0.28044	-8.36	3.52	4140	75
rses59-10.16	0.28041	0.00004	0.00061	0.28036	0.28045	0.28056	-2.92	2.11	3878	76
rses59-10.19	0.28017	0.00004	0.00091	0.28009	0.28015	0.28021	-2.01	2.62	4126	78
rses59-13.17	0.28010	0.00004	0.00083	0.28003	0.28031	0.28040	-9.91	2.42	4357	76
rses59-15.16	0.28021	0.00005	0.00062	0.28017	0.28042	0.28053	-9.09	2.46	4217	98
rses59-14.14	0.28012	0.00004	0.00114	0.28003	0.28027	0.28035	-8.43	2.94	4292	80
rses59-16.14	0.28012	0.00004	0.00070	0.28007	0.28020	0.28027	-4.93	2.31	4243	79
rses59-16.12	0.28004	0.00004	0.00085	0.27998	0.28024	0.28031	-9.32	2.50	4406	97
rses59-14.12	0.28018	0.00004	0.00067	0.28013	0.28024	0.28031	-3.99	2.25	4162	77
rses59-17.13	0.28005	0.00004	0.00068	0.28000	0.28021	0.28028	-7.39	2.28	4366	90
rses59-17.15	0.28006	0.00004	0.00129	0.27996	0.28023	0.28030	-9.53	3.16	4372	74
rses59-17.16	0.28005	0.00004	0.00069	0.28000	0.28020	0.28027	-7.34	2.24	4371	76
rses59-17.7	0.28034	0.00004	0.00063	0.28029	0.28046	0.28057	-5.88	2.20	4013	81
rses59-16.1	0.28021	0.00004	0.00120	0.28012	0.28036	0.28045	-8.48	3.14	4185	88
rses59-16.1 2-3	0.28045	0.00008	0.00690	0.28000	0.28063	0.28077	-22.23	12.43	3919	146
rses59-16.3	0.28007	0.00005	0.00040	0.28004	0.28022	0.28029	-6.39	2.06	4344	83
rses59-16.5	0.28018	0.00004	0.00054	0.28014	0.28021	0.28029	-2.73	2.03	4142	73
rses59-16.6	0.28030	0.00004	0.00082	0.28024	0.28042	0.28053	-6.39	2.30	4057	71
rses59-15.1	0.28030	0.00004	0.00100	0.28023	0.28043	0.28054	-7.02	2.59	4058	76
rses59-15.9	0.28017	0.00004	0.00034	0.28014	0.28026	0.28034	-4.28	1.84	4196	72
rses59-14.7	0.28026	0.00004	0.00102	0.28019	0.28044	0.28055	-8.89	2.60	4141	74
rses59-9.11	0.28029	0.00004	0.00081	0.28023	0.28043	0.28054	-7.27	2.33	4090	76
res59-9.11 9-10	0.28026	0.00005	0.00106	0.28019	0.28041	0.28051	-7.86	2.97	4117	100
rses59-5.9	0.28030	0.00004	0.00102	0.28022	0.28039	0.28050	-6.14	2.60	4048	75
rses59-4.8	0.28009	0.00004	0.00137	0.27999	0.28021	0.28028	-8.02	3.33	4298	78
rses59-4.7	0.28007	0.00004	0.00031	0.28005	0.28033	0.28042	-10.08	1.84	4412	74
rses59-3.15	0.28008	0.00004	0.00046	0.28004	0.28030	0.28039	-9.27	1.96	4385	74
rses59-6.12	0.28015	0.00004	0.00043	0.28012	0.28027	0.28034	-5.25	1.89	4228	70
rses59-8.11	0.28012	0.00004	0.00060	0.28008	0.28021	0.28028	-4.73	2.14	4244	75
rses59-9.14	0.28009	0.00004	0.00126	0.27999	0.28013	0.28019	-4.87	3.23	4245	78
rses59-6.4	0.28014	0.00004	0.00083	0.28008	0.28025	0.28033	-6.23	2.45	4235	77
rses72-1.2	0.28017	0.00004	0.00050	0.28013	0.28027	0.28035	-4.95	2.01	4199	74
rses72-1.3	0.28034	0.00004	0.00063	0.28029	0.28044	0.28054	-5.12	2.11	3999	75
rses72-3.2	0.28032	0.00004	0.00074	0.28026	0.28043	0.28054	-5.86	2.23	4032	74

rses72-4.2	0.28014	0.00004	0.00052	0.28010	0.28021	0.28028	-3.78	2.02	4208	73
rses72-9.3	0.28009	0.00004	0.00013	0.28008	0.28019	0.28025	-3.74	1.75	4282	73
rses72-13.1	0.28003	0.00004	0.00068	0.27998	0.28026	0.28034	-10.11	2.20	4445	72
rses72-15.7	0.28040	0.00004	0.00148	0.28030	0.28046	0.28057	-5.58	3.26	3891	74
rses72-17.8	0.28022	0.00004	0.00046	0.28019	0.28044	0.28054	-8.90	1.95	4213	74
rses72-12.9	0.28021	0.00004	0.00049	0.28017	0.28024	0.28031	-2.48	2.02	4109	75
rses72-14.9	0.28005	0.00004	0.00057	0.28001	0.28036	0.28045	-12.44	2.11	4472	90
rses72-1.2 pyr	0.28023	0.00004	0.00084	0.28017	0.28027	0.28035	-3.62	2.41	4085	73
rses55-5.6	0.28031	0.00007	0.00082	0.28025	0.28031	0.28040	-2.21	2.97	3964	130
rses55-4.6	0.28005	0.00007	0.00056	0.28001	0.28013	0.28019	-4.42	2.78	4321	125
rses55-6.8	0.28028	0.00007	0.00077	0.28022	0.28032	0.28041	-3.51	2.98	4029	126
rses55-6.12	0.28008	0.00007	0.00050	0.28004	0.28020	0.28027	-5.63	2.74	4312	122
rses55-5.13	0.28005	0.00007	0.00066	0.28000	0.28024	0.28032	-8.63	2.85	4394	120
rses55-3.13a	0.28018	0.00006	0.00053	0.28014	0.28026	0.28034	-4.37	2.71	4177	119
rses55-3.13b	0.28020	0.00007	0.00063	0.28015	0.28023	0.28031	-3.07	2.85	4125	124
rses55-3.13b 1-2	0.28020	0.00007	0.00099	0.28013	0.28027	0.28035	-5.05	3.35	4140	132
rses55-4.19	0.28033	0.00007	0.00023	0.28031	0.28046	0.28058	-5.43	2.58	4033	120
rses55-6.19	0.28013	0.00007	0.00074	0.28008	0.28018	0.28024	-3.52	2.94	4198	120
rses55-7.20	0.28001	0.00007	0.00067	0.27996	0.28019	0.28025	-8.07	2.86	4427	119
rses55-5.20	0.28004	0.00006	0.00041	0.28001	0.28004	0.28008	-1.06	2.65	4278	129
res55-8.14	0.28034	0.00006	0.00081	0.28028	0.28043	0.28054	-5.29	2.90	3990	118
rses55-9.15	0.28041	0.00007	0.00131	0.28032	0.28045	0.28056	-4.70	3.48	3877	122
rses55-12.13	0.28021	0.00007	0.00120	0.28012	0.28029	0.28037	-5.96	3.44	4131	122
rses55-13.13	0.28022	0.00007	0.00079	0.28017	0.28026	0.28034	-3.36	3.00	4089	124
rses55-15.13	0.28008	0.00007	0.00082	0.28002	0.28012	0.28017	-3.69	3.05	4259	122
rses55-19.19	0.28015	0.00007	0.00034	0.28013	0.28021	0.28028	-2.98	2.62	4189	120
rses55-14.20	0.28039	0.00006	0.00071	0.28034	0.28045	0.28056	-3.78	2.81	3909	119
rses55-15.11core	0.28008	0.00007	0.00052	0.28004	0.28025	0.28032	-7.45	2.74	4348	122
rses55-15.11outer	0.28004	0.00007	0.00032	0.28002	0.28026	0.28034	-8.76	2.64	4428	122
rses55-15.9	0.28012	0.00007	0.00037	0.28009	0.28024	0.28032	-5.34	2.65	4268	122
rses55-13.7	0.28013	0.00007	0.00058	0.28008	0.28016	0.28023	-2.89	2.78	4203	120
rses55-11.11	0.28029	0.00006	0.00129	0.28019	0.28035	0.28044	-5.52	3.47	4032	118
rses55-11.3	0.28004	0.00007	0.00053	0.28000	0.28031	0.28039	-10.89	2.74	4455	120
rses55-12.1	0.28007	0.00007	0.00063	0.28002	0.28027	0.28035	-8.94	2.83	4380	121
rses55-12.1 8-10	0.28016	0.00008	0.00131	0.28006	0.28029	0.28038	-8.29	3.84	4235	141
rses55-13.8	0.28023	0.00007	0.00140	0.28012	0.28025	0.28033	-4.70	3.72	4081	121
rses55-13.8 1-2	0.28013	0.00008	0.00056	0.28009	0.28026	0.28033	-5.85	3.11	4252	141
blob1-7.2	0.28076	0.00006	0.00083	0.28072	0.28110	0.28132	-13.33	2.73	3633	118
blob1-7.3	0.28072	0.00007	0.00127	0.28066	0.28109	0.28131	-15.41	3.04	3705	128

blob1-7.9	0.28075	0.00007	0.00117	0.28069	0.28117	0.28140	-16.80	2.92	3697	119
blob1-7.10	0.28075	0.00007	0.00152	0.28067	0.28103	0.28124	-12.66	3.30	3611	159
blob1-1.1	0.28070	0.00007	0.00165	0.28058	0.28024	0.28032	11.92	4.11	3201	126
blob1-1.2 (guess at ID)	0.28072	0.00007	0.00123	0.28063	0.28026	0.28034	13.00	3.50	3182	129
blob1-1.9 (guess at ID)	0.28073	0.00007	0.00127	0.28065	0.28064	0.28078	0.62	3.39	3402	154
blob1-8.9	0.28076	0.00007	0.00194	0.28062	0.28029	0.28037	11.63	4.52	3123	127
blob1-9.10	0.28072	0.00007	0.00126	0.28063	0.28044	0.28055	6.72	3.38	3303	140
blob1-9.8	0.28068	0.00008	0.00191	0.28054	0.28026	0.28033	10.03	4.77	3249	150
rses54-1.19	0.28031	0.00003	0.00098	0.28024	0.28043	0.28054	-6.99	2.90	4053	59
rses54-2.16	0.28027	0.00003	0.00067	0.28023	0.28043	0.28054	-7.29	2.27	4112	59
rses54-6.17	0.28037	0.00004	0.00111	0.28030	0.28060	0.28073	-10.59	3.07	4037	64
rses54-8.16	0.28019	0.00004	0.00208	0.28005	0.28037	0.28047	-11.58	5.63	4215	64
rses54-6.12	0.28039	0.00003	0.00252	0.28021	0.28040	0.28050	-6.61	6.66	3875	60
rses54-7.5	0.28031	0.00003	0.00045	0.28028	0.28040	0.28050	-4.21	1.89	4017	59
rses54-9.4	0.28010	0.00003	0.00072	0.28005	0.28018	0.28024	-4.60	2.54	4255	61
rses54-3.9	0.28009	0.00003	0.00051	0.28005	0.28016	0.28022	-3.79	2.12	4263	61
rses54-11.12	0.28040	0.00003	0.00104	0.28033	0.28047	0.28058	-5.04	3.02	3905	63
rses54-12.11	0.28036	0.00004	0.00129	0.28027	0.28043	0.28054	-5.65	3.65	3949	65
rses54-15.11dark	0.28002	0.00003	0.00037	0.28000	0.28023	0.28030	-8.38	1.87	4436	63
rses54-15.11light	0.28002	0.00003	0.00047	0.27998	0.28030	0.28039	-11.34	1.92	4492	57
rses54-17.17	0.28007	0.00003	0.00126	0.27997	0.28012	0.28017	-5.07	3.95	4269	67
rses54-17.18	0.28010	0.00003	0.00082	0.28004	0.28020	0.28027	-5.79	2.73	4279	59
rses54-16.20	0.28020	0.00003	0.00137	0.28009	0.28020	0.28027	-3.77	4.09	4099	58
rses54-18.11	0.28008	0.00004	0.00072	0.28003	0.28020	0.28027	-6.06	2.57	4306	65
rses54-18.11lines	0.28015	0.00003	0.00112	0.28006	0.28016	0.28022	-3.43	3.52	4161	81
rses54-16.14	0.28036	0.00003	0.00239	0.28019	0.28035	0.28044	-5.86	6.45	3903	62
rses54-14.19	0.28027	0.00003	0.00118	0.28019	0.28037	0.28047	-6.49	3.43	4072	60
rses54-19.5	0.28013	0.00003	0.00139	0.28002	0.28020	0.28026	-6.33	4.18	4227	61
rses54-17.1	0.28002	0.00004	0.00046	0.27999	0.28034	0.28043	-12.49	2.01	4511	75
rses56_1-18	0.28016	0.00003	0.00056	0.28012	0.28027	0.28035	-5.47	2.14	4212	59
rses56_2-18	0.28005	0.00003	0.00073	0.27999	0.28026	0.28034	-9.46	2.47	4410	57
rses56_3-17	0.28009	0.00003	0.00078	0.28004	0.28028	0.28037	-8.86	2.64	4343	64
rses56_2-17	0.28016	0.00003	0.00107	0.28008	0.28026	0.28033	-6.35	3.27	4208	59
rses56-5.16	0.28015	0.00003	0.00058	0.28010	0.28019	0.28025	-3.02	2.22	4184	59
rses56-6.12	0.28045	0.00003	0.00061	0.28041	0.28052	0.28064	-4.01	2.15	3850	62
rses56-5.2	0.28044	0.00003	0.00094	0.28038	0.28052	0.28064	-5.12	2.76	3863	63
rses56-8.10	0.28042	0.00003	0.00089	0.28036	0.28060	0.28074	-8.60	2.61	3958	62
rses56-7.6	0.28018	0.00003	0.00046	0.28014	0.28024	0.28031	-3.40	1.97	4161	59
rses56-9.10	0.28019	0.00003	0.00088	0.28013	0.28030	0.28039	-6.18	2.81	4175	62

rses56-6.2	0.28013	0.00003	0.00070	0.28007	0.28024	0.28031	-5.91	2.46	4254	62
rses56-7.12	0.28009	0.00004	0.00081	0.28002	0.28020	0.28027	-6.44	2.76	4306	64
rses56-2.9	0.28015	0.00003	0.00041	0.28012	0.28026	0.28034	-5.01	1.90	4225	61
rses56-10.11	0.28017	0.00004	0.00108	0.28009	0.28025	0.28033	-5.67	3.47	4177	81
rses56-14.14	0.28003	0.00004	0.00082	0.27997	0.28014	0.28020	-6.14	2.84	4362	65
rses56-14.9	0.28036	0.00003	0.00227	0.28019	0.28035	0.28045	-5.68	6.15	3906	62
rses56-17.14	0.28009	0.00003	0.00050	0.28006	0.28034	0.28043	-10.03	2.01	4378	64
rses56-10.17	0.28018	0.00003	0.00065	0.28013	0.28027	0.28034	-4.72	2.33	4171	61
rses56-14.19	0.28008	0.00003	0.00140	0.27997	0.28014	0.28019	-6.10	4.25	4280	59
su1x_5-4a	0.28076	0.00005	0.00211	0.28062	0.28056	0.28069	2.24	3.43	3299	182
su1x_5-4b	0.28072	0.00005	0.00122	0.28066	0.28097	0.28117	-11.28	2.35	3634	93
su1x-3.5	0.28072	0.00004	0.00273	0.28053	0.28045	0.28056	2.72	4.30	3312	148
su1x-4.6	0.28069	0.00004	0.00098	0.28064	0.28084	0.28102	-7.14	2.07	3602	99
su1x-4.5a	0.28071	0.00004	0.00108	0.28064	0.28087	0.28105	-7.93	2.09	3598	91
su1x-5.6	0.28074	0.00006	0.00198	0.28060	0.28043	0.28053	6.23	3.60	3254	119
su1x-3.2	0.28078	0.00005	0.00191	0.28066	0.28073	0.28089	-2.36	3.08	3378	121
su1x-6.5	0.28073	0.00004	0.00167	0.28063	0.28067	0.28082	-1.70	2.80	3432	119
su1x-7.3	0.28077	0.00004	0.00162	0.28067	0.28068	0.28083	-0.38	2.71	3359	111
JHO3008x-1.6	0.28070	0.00004	0.00096	0.28066	0.28112	0.28135	-16.56	1.98	3755	72
JHO3008x-2.5	0.28070	0.00004	0.00209	0.28060	0.28104	0.28125	-15.86	2.75	3705	67
JHO3008x-2.4	0.28069	0.00004	0.00160	0.28060	0.28102	0.28122	-14.76	2.39	3724	68
JHO3008x-3.3	0.28071	0.00004	0.00069	0.28067	0.28112	0.28134	-15.73	1.85	3744	71
JHO3008x-4.1	0.28070	0.00004	0.00307	0.28054	0.28104	0.28126	-17.82	3.86	3711	78
JHO3008x-4.4	0.28101	0.00007	0.00635	0.28066	0.28094	0.28113	-9.96	7.54	3096	119
JHO3008x-6.6	0.28072	0.00004	0.00171	0.28072	0.28279	0.28329	-73.08	1.78	4522	70

Table F.3: Lu-Hf-Pb data for unknowns from chapter four.

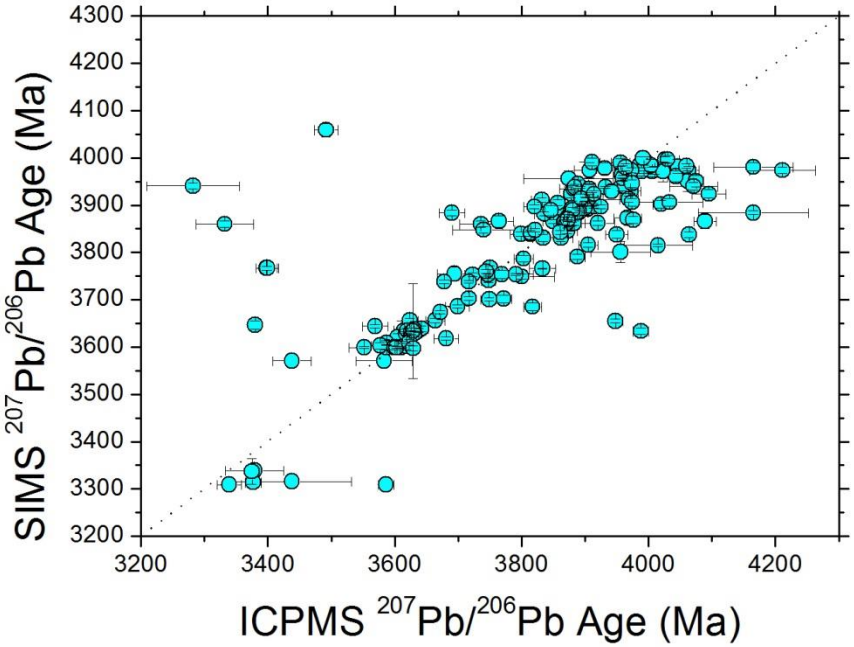

Fig. F.1: SIMS vs. ICP-MS age comparison. Most ages match well, with a few exceptions mostly <3.4 or >4 Ga in either SIMS or ICP-MS age.

Appendix G: Trace Element and Oxygen Isotope Data for Chapters Four and Five

Study or Date	Sample	207Pb/206Pb Age (Ma)	1 sd	55Mn	1 s.d.	P	1 s.d.	49Ti	1 s.d.	57Fe	1 s.d.	89Y	1 s.d.
This Study	RSES51_7_2	3351				376	36						
This Study	RSES51_3_10	3363				628	118						
This Study	RSES51_3_8	3392				231	16						
This Study	RSES51_5_4	3459				488	48						
This Study	RSES51_4_2	3686				306	20						
This Study	RSES51_3_12	3704				157	25						
This Study	RSES51_4_7	3754				266	27						
This Study	RSES51_4_5	3829				419	54						
This Study	RSES51_1_6	3864				353	12						
This Study	RSES59-5.9	3618				328	8						
This Study	RSES59-10.16	3621				179	7						
This Study	RSES59-15.1	3629				442	9						
This Study	RSES59-15.16	3635				343	7						
This Study	RSES59-16.3	3639				200	7						
This Study	RSES59-16.6	3639				528	6						
This Study	RSES59-3.15	3685				228	13						
This Study	RSES59-4.7	3702				213	9						
This Study	RSES59-4.17	3753				585	14						
This Study	RSES59-13.17	3787				265	6						
This Study	RSES51_4-1	3395	2			452							
This Study	RSES51_16-1	3397	2			226							
This Study	RSES51_11-1	3408	3			434							
This Study	RSES51_10-6	3456	2			863							
This Study	RSES51_7-1	3459	72			255							
This Study	RSES51_2-10	3534	3			219							
This Study	RSES51_3-5	3538	3			164							
This Study	RSES51_3-1	3547	2			391							

This Study	RSES51_14-1	3631	3			1018							
This Study	RSES51_3-7	3633	1			333							
This Study	RSES51_17-11	3764	1			1220							
This Study	RSES51_10-12	3783	11			263							
This Study	RSES51_17-1	3950	3			281							
This Study	RSES51_17-2	3976	5			114							
This Study	RSES51_10-1	3982	5			451							
crowley '05	24-L14	3340	28										
crowley '05	29-MEW14	3491	20										
crowley '05	30-MEW3	3524	22										
crowley '05	29-M16	3570	21										
peck '01	W74-35	3279											
peck '01	W74-19	3376											
peck '01	W74-7	3386											
peck '01	W74-34	3455											
peck '01	W74-6	3509											
peck '01	W74-20	3604											
This Study	RSES55-5.13	3816	5			338	12	3.32	0.86	37.09	13.48	482.19	53.63
This Study	RSES58-16.15	3816	23			267	13	4.75	0.44	109.21	13.25	782.57	46.57
This Study	RSES73-3.7	3831	35			248	7	8.38	0.62	95.66	12.46	542.13	33.65
This Study	RSES59-04.08	3838	8			625	15	15.54	0.83	126.87	15.04	1541.18	87.36
This Study	RSES55-11.3	3841	6			304	8	4.02	0.42	145.19	16.77	654.40	37.42
This Study	RSES55-15.13	3866	15			346	12	3.31	0.42	80.98	11.87	756.07	52.26
This Study	RSES59-17.16	3873	13			181	9	5.89	0.50	117.07	14.09	458.78	28.82
This Study	RSES73-5.8 average	*3884*	*4*			148	8	3.45	0.75	99.38	24.83	327.24	54.69
This Study	RSES56-03.17	3889	11			239	6	2.19	0.30	86.64	11.80	732.05	45.28
This Study	RSES55-15.11	3894	15			326	8	3.16	0.40	118.19	24.69	931.04	58.49
This Study	rses54-15.11 average	*3897*	*4*			291	17	5.42	1.06	98.45	18.07	561.33	64.06
This Study	RSES58-3.13	3902	8			326	26	5.28	0.47	95.67	12.12	1106.52	69.92
This Study	RSES54-18.11	3906	8			227	9	3.48	0.38	112.40	13.68	419.04	22.75

This Study	rses100-7.18	3908	5	0.23	0.07	246	13	2.96	0.70	89.75	7.34	558.57	56.67
This Study	rses100-7.19	3912	7	0.51	0.17	214	12	5.20	1.48	106.03	12.40	345.88	51.35
This Study	rses100-17.1	3936	4	0.41	0.05	313	10	4.81	0.38	109.93	11.12	800.93	84.92
This Study	rses100-1.12	3946	7	0.52	0.15	214	10	5.05	1.23	107.56	10.60	533.10	69.80
This Study	rses100-16.3	3973	4	0.35	0.10	220	10	3.96	0.95	94.75	11.48	273.33	30.04
This Study	ANU33-12-14	4001				192	2	5.25	0.32			735.58	1.80
This Study	ANU33-7-15	4004				293	3	2.84	0.23			867.41	1.96
This Study	RSES55-3.7	4006	10			283	10	5.13	0.50	99.64	12.98	676.36	44.27
This Study	RSES67-10.11	4008	5			170	16	2.43	0.72	23.69	10.44	237.76	23.65
This Study	rses100-6.13	4011	14	0.40	0.12	205	9	4.20	1.40	118.32	10.57	485.91	60.72
This Study	RSES59-18.19	4015	21			158	5	2.15	0.31	95.93	12.33	427.98	24.70
This Study	ANU32-1-7	4021				316	3	3.00	0.24			734.57	1.80
This Study	rses100-20.17b	4024	11	2.19	0.28	302	16	15.05	1.57	202.25	11.51	610.11	55.08
This Study	ANU31-1-14	4034				123	2	2.17	0.20			526.86	1.52
This Study	ANU31-10-11	4040				203	3	7.62	0.38			446.25	1.40
This Study	RSES67-3.11	4040	7			640	29	11.98	1.22	89.85	16.88	1158.39	124.63
This Study	RSES64-9.2	4048	10			157	4	5.37	0.49	95.66	12.39	405.90	25.66
This Study	rses60_4-19	4049	14	0.36	0.04	398	6	5.10	0.40	103.38	10.64	1580.70	154.82
This Study	rses100-4.19	4051	6	0.34	0.12	240	10	3.08	0.98	138.78	25.67	329.17	42.30
This Study	rses100-8.6	4054	7	0.12	0.05	132	8	6.05	1.00	107.19	8.06	101.80	9.48
This Study	ANU33-5-3	4054				402	4	3.64	0.26			1599.50	2.66
This Study	rses100-1.11	4055	10	0.68	0.15	326	11	3.58	0.91	108.97	9.51	1413.17	150.05
This Study	RSES58-6.12	4057	8			288	13	5.71	0.48	107.08	13.02	529.19	30.56
This Study	RSES58-19.12	4059	20			196	9	2.93	0.35	85.78	11.15	698.47	42.91
This Study	rses60_7-17	4061	5	0.42	0.05	304	10	4.84	0.66	113.24	11.43	1450.68	141.97
This Study	rses60_8-10bright	4062	7	0.46	0.08	333	8	4.71	0.38	118.48	11.90	1015.04	99.35
This Study	rses60_8-10dark	4062	7	0.52	0.10	145	2	4.76	0.38	102.93	10.55	290.14	28.74
This Study	ANU33-13-6	4063				183	2	7.33	0.37			745.27	1.81
This Study	ANU31-12-12	4064				203	3	3.57	0.26			809.59	1.89
This Study	ANU33-6-14	4065				104	2	4.25	0.28			254.77	1.06

This Study	ANU32-11-5	4068				233	3	2.35	0.21			1064.66	2.17
This Study	rses100-1.18	4069	8	0.42	0.15	271	12	2.18	0.93	120.53	12.84	1014.01	144.73
This Study	rses100-13.4	4069	6	0.54	0.07	286	7	4.55	0.51	109.25	5.23	1323.54	118.83
This Study	ANU32-6-9	4070				407	4	7.62	0.38			984.48	2.08
This Study	ANU33-14-9-1	4084				194	2	3.99	0.28			594.60	1.62
This Study	ANU33-14-9-2	4084				170	2	4.12	0.28			616.26	1.65
This Study	rses60_7-5	4085	7	2.36	0.21	265	12	9.58	1.49	118.83	11.91	2323.35	231.18
This Study	rses100-15.2	4089	8	0.29	0.12	301	15	5.14	1.37	91.79	10.72	1500.33	220.05
This Study	ANU32-6-15	4092				182	2	4.40	0.29			704.93	1.76
This Study	RSES59-8.14	4097	6			359	17	26.05	2.05	441.78	49.15	407.66	26.71
This Study	RSES67-17.12	4107	4			597	18	20.17	0.94	196.02	21.71	2271.71	132.18
This Study	ANU31-15-8	4111				140	2	2.90	0.24			716.39	1.78
This Study	ANU31-8-4	4111				253	3	8.58	0.40			1227.76	2.33
This Study	RSES64-19.2	4111	12			179	7	3.91	0.42	121.51	14.74	541.76	34.00
This Study	rses100-16.2	4114	13	0.50	0.85	121	52	10.16	10.16	43.73	38.13	477.69	291.73
This Study	ANU33-11-15	4117				273	3	3.09	0.24			1957.78	2.94
This Study	ANU31-4-10	4118				373	3	6.47	0.35			879.28	1.97
This Study	RSES58-4.16	4119	6			259	14	6.57	0.52	89.40	11.48	861.12	55.91
This Study	ANU31-14-3	4121				79	2	3.82	0.27			660.31	1.71
This Study	ANU31-4-14	4121				202	3	5.00	0.31			762.38	1.83
This Study	ANU31-14-7	4127				662	5	11.62	0.47			3689.18	4.03
This Study	rses100-6.1	4132	21	0.35	0.13	282	12	7.66	1.57	120.56	11.69	748.90	105.15
This Study	RSES55-4.9	4133	5			343	10	2.84	0.38	102.17	13.47	827.85	48.29
This Study	rses100-4.6	4145	23	0.37	0.13	271	9	6.36	1.12	113.96	9.04	402.99	42.82
This Study	ANU32-6-10	4152				265	3	4.65	0.30			1271.65	2.37
This Study	RSES64-1.2	4155	12			194	5	4.62	0.45	101.49	12.86	825.69	56.38
This Study	RSES64-2.2	4159	7			398	10	2.43	0.33	94.48	12.21	1135.61	72.26
This Study	rses60_5-15	4160	4	0.69	0.12	218	4	5.05	0.42	119.51	11.95	594.46	58.48
This Study	ANU33-15-11	4196				192	2	3.26	0.25			644.98	1.69

Sample	139La	1 s.d.	140Ce	1 s.d.	141Pr	1 s.d.	143Nd	1 s.d.	149Sm	1 s.d.	151Eu	1 s.d.	156Gd	1 s.d.	159Tb	1 s.d.	161Dy	1 s.d.	165Ho	1 s.d.
RSES51_7_2	0.16		20.32		0.14		0.77		2.54		0.22		11.60		4.01		47		18	
RSES51_3_10	0.32		10.28		0.19		0.75		1.12		0.17		8.20		3.39		41		20	
RSES51_3_8	0.07		12.06		0.04		0.67		1.29		0.18		7.84		2.76		35		15	
RSES51_5_4	0.17		7.72		0.10		0.66		1.26		0.06		10.11		4.49		58		27	
RSES51_4_2	0.10		14.35		0.11		1.28		2.58		0.38		16.05		5.96		70		28	
RSES51_3_12	1.32		36.95		0.63		3.40		1.90		0.56		6.75		2.04		22		9	
RSES51_4_7	0.12		11.41		0.06		0.81		1.42		0.40		10.44		3.86		44		19	
RSES51_4_5	0.15		8.73		0.16		1.28		2.01		0.31		8.94		3.10		35		15	
RSES51_1_6	0.06		2.13		0.09		1.26		2.89		0.41		14.98		6.38		90		47	
RSES59-5.9	0.01		18.78		0.07		1.45		2.72		0.43		23.39		9.50		114		46	
RSES59-10.16	0.02		5.20		0.04		1.07		2.26		0.23		13.61		5.26		62		25	
RSES59-15.1	0.00		6.41		0.02		0.43		1.08		0.06		10.12		5.15		73		33	
RSES59-15.16	0.02		12.17		0.06		1.38		2.76		0.39		16.20		7.05		81		34	
RSES59-16.3	0.02		3.42		0.02		0.42		0.77		0.06		5.44		2.28		30		13	
RSES59-16.6	0.02		7.03		0.03		0.57		1.50		0.17		13.62		6.29		84		37	
RSES59-3.15	0.01		18.73		0.01		1.31		2.03		0.24		9.34		3.60		41		19	
RSES59-4.7	0.06		8.41		0.08		1.28		2.12		0.27		11.07		3.54		40		16	
RSES59-4.17	0.00		14.48		0.09		2.11		6.54		0.18		38.47		14.70		169		67	
RSES59-13.17	0.04		10.74		0.06		1.09		2.26		0.27		12.30		5.09		58		23	
RSES51_4-1	0.05		14.32		0.04		1.15		2.02		0.00		11.36		4.35		50		25	
RSES51_16-1	0.10		18.49		0.21		1.27		2.05		0.30		8.86		3.27		41		17	
RSES51_11-1	0.07		33.71		0.34		7.44		12.45		0.84		59.17		19.88		209		76	
RSES51_10-6	0.04		29.94		0.09		1.72		3.41		0.79		23.19		9.88		117		51	
RSES51_7-1	0.06		11.04		0.05		0.75		1.88		0.29		9.86		4.19		52		21	
RSES51_2-10	0.04		4.87		0.04		0.37		1.03		0.41		7.58		3.46		46		20	

RSES51_3-5	0.07		10.01		0.03		0.43		1.19		0.20		6.47		2.60		33		14	
RSES51_3-1	0.61		27.78		1.00		4.65		3.79		0.65		12.86		4.90		54		20	
RSES51_14-1	0.92		30.07		1.36		7.85		5.74		0.96		19.37		9.08		119		52	
RSES51_3-7	0.07		7.52		0.04		0.51		1.16		0.22		12.43		6.02		82		35	
RSES51_17-11	0.96		54.14		1.46		9.11		8.60		0.94		36.85		16.75		210		89	
RSES51_10-12	0.13		5.74		0.05		0.62		1.83		0.26		9.01		4.08		48		20	
RSES51_17-1	0.04		12.48		0.24		4.87		8.64		0.46		39.74		14.29		155		61	
RSES51_17-2	0.03		3.18		0.02		0.38		0.50		0.11		2.82		1.21		15		6	
RSES51_10-1	0.26		29.38		0.62		3.87		3.30		0.65		11.59		4.44		56		24	
24-L14	0.02		13.20		0.13		2.04		3.95		0.57		21.50		6.99		85		32	
29-MEW14	0.03		6.90		0.10		0.87		1.37		0.70		8.61		2.98		37		14	
30-MEW3	0.07		4.79		0.03		0.56		2.82		0.19		20.30		7.36		85		30	
29-M16	0.03		3.89		0.02		0.27		0.78		0.34		6.96		2.92		38		17	
W74-35	5.10		25.40		2.30		11.20		4.90		0.80		8.80		2.20		23		8	
W74-19	0.40		30.40		0.90		4.90		4.10		0.70		16.00		5.40		60		22	
W74-7	0.40		33.80		0.60		3.80		4.20		0.30		27.40		8.90		103		39	
W74-34			11.80		0.10		1.10		3.40		0.20		21.10		8.00		108		43	
W74-6	0.90		16.30		0.70		7.00		9.80		1.20		42.80		11.30		117		39	
W74-20	2.00		33.80		2.40		12.80		7.80		1.60		19.70		6.30		67		22	
RSES55-5.13	0.00		15.39	0.60	0.12	0.05	1.72	0.46	1.92	0.63	0.04	0.04	8.65	0.94	3.19	0.90	42	4	17	6
RSES58-16.15	0.03	0.01	9.98	0.21	0.05	0.03	1.18	0.16	1.97	0.21	0.27	0.09	12.51	0.79	5.26	0.77	63	2	26	3
RSES73-3.7	0.03	0.01	7.65	0.20	0.04	0.01	0.67	0.13	0.95	0.16	0.20	0.04	8.33	0.58	3.55	0.71	44	1	18	3
RSES59-04.08	0.07	0.02	7.81	0.19	0.11	0.02	1.36	0.18	2.63	0.26	0.18	0.04	17.86	1.12	9.29	1.28	120	2	52	5
RSES55-11.3	0.29	0.04	12.00	0.49	0.37	0.05	2.61	0.26	2.17	0.24	0.27	0.07	9.27	0.92	3.98	0.42	48	1	21	2
RSES55-15.13	0.01	0.01	6.50	0.19	0.02	0.01	0.58	0.13	1.34	0.20	0.19	0.04	9.40	0.86	4.59	1.07	61	2	27	4
RSES59-17.16	0.05	0.01	6.85	0.18	0.05	0.02	1.00	0.15	1.87	0.21	0.18	0.08	9.03	0.85	3.37	0.54	39	3	15	2
RSES73-5.8 average	0.06	0.02	4.53	0.24	0.02	0.03	0.44	0.16	1.20	0.29	0.21	0.07	6.18	1.48	2.38	0.94	27	4	11	3
RSES56-03.17	0.06	0.01	12.56	0.24	0.12	0.02	1.71	0.20	2.66	0.26	0.25	0.04	12.65	1.38	5.07	0.63	61	2	26	3
RSES55-15.11	0.04	0.01	7.12	0.18	0.13	0.02	2.15	0.25	3.37	0.30	0.50	0.09	17.70	1.12	6.90	0.90	78	2	31	3

rses54-15.11 average	0.04	0.02	7.59	0.36	0.05	0.04	0.76	0.27	1.55	0.62	0.19	0.06	9.11	1.34	3.62	1.06	43	6	18	7
RSES58-3.13	0.04	0.01	20.89	0.32	0.13	0.02	2.51	0.24	4.09	0.31	0.58	0.06	20.56	1.20	7.90	0.82	94	2	38	3
RSES54-18.11	0.05	0.01	7.90	0.19	0.05	0.01	0.36	0.09	0.75	0.13	0.05	0.02	5.54	0.41	2.43	0.64	31	2	14	3
rses100-7.18	0.03	0.03	5.34	0.30	0.04	0.02	0.82	0.42	1.00	0.30	0.33	0.17	6.16	0.64	3.25	1.67	38	2	16	5
rses100-7.19	0.07	0.05	9.43	1.01	0.20	0.09	0.74	0.67	2.53	0.76	0.34	0.23	6.65	1.43	1.99	1.83	29	2	12	5
rses100-17.1	0.06	0.01	10.74	0.94	0.05	0.01	0.74	0.11	1.99	0.20	0.23	0.03	11.82	0.81	4.99	0.69	63	2	27	3
rses100-1.12	0.05	0.03	10.32	0.56	0.12	0.06	0.95	0.39	0.81	0.36	0.30	0.21	9.89	1.24	3.25	1.37	39	5	18	8
rses100-16.3	0.05	0.03	5.57	0.36	0.03	0.03	0.23	0.23	0.24	0.17	0.00		4.28	0.59	1.43	1.46	20	2	9	7
ANU33-12-14	0.02	0.00	6.28	0.20	0.05	0.01	0.70	0.08	1.93	0.12	0.25	0.04	11.01	0.52	4.33	0.14	56	1	22	0
ANU33-7-15	0.01	0.00	8.69	0.24	0.02	0.01	0.69	0.08	1.50	0.11	0.08	0.02	11.18	0.52	5.05	0.15	64	1	26	0
RSES55-3.7	0.05	0.01	11.42	0.25	0.08	0.02	1.02	0.17	2.19	0.28	0.49	0.06	12.58	1.04	4.52	0.76	55	2	22	3
RSES67-10.11	0.03	0.02	2.74	0.25	0.03	0.03	0.28	0.24	0.60	0.35	0.29	0.10	6.92	0.98	2.66	2.31	22	2	9	5
rses100-6.13	0.04	0.03	10.12	0.52	0.06	0.04	1.12	0.40	1.73	1.17	0.27	0.19	9.90	1.20	3.34	1.42	41	4	15	11
RSES59-18.19	0.03	0.01	4.87	0.15	0.05	0.02	0.68	0.13	0.98	0.21	0.21	0.04	6.61	0.49	2.82	0.55	34	1	15	3
ANU32-1-7	0.04	0.01	11.23	0.27	0.05	0.01	1.08	0.10	1.86	0.12	0.16	0.03	11.06	0.52	4.47	0.14	57	1	23	0
rses100-20.17b	0.50	0.08	13.12	1.16	0.52	0.10	4.61	1.64	2.74	0.79	0.42	0.12	12.61	1.36	3.71	1.34	46	2	17	5
ANU31-1-14	0.01	0.00	3.32	0.15	0.03	0.01	0.59	0.07	1.35	0.10	0.29	0.04	8.16	0.45	3.05	0.11	40	1	15	0
ANU31-10-11	0.29	0.02	8.08	0.23	0.46	0.03	2.93	0.17	3.42	0.16	0.35	0.05	6.13	0.39	2.41	0.10	30	1	13	0
RSES67-3.11	1.84	0.13	35.62	0.71	1.99	0.21	10.65	0.86	8.56	0.89	1.28	0.16	29.53	1.91	10.81	0.99	110	7	40	4
RSES64-9.2	0.05	0.01	3.25	0.12	0.03	0.02	0.44	0.11	1.48	0.24	0.32	0.05	7.68	0.59	2.99	0.73	33	1	14	2
rses60_4-19	0.07	0.01	13.53	1.18	0.12	0.03	1.66	0.19	3.72	0.31	0.44	0.05	23.30	1.55	9.92	1.06	128	4	53	5
rses100-4.19	0.05	0.03	5.32	0.41	0.00		0.50	0.29	0.68	0.70	0.00		4.66	0.73	1.60	0.96	22	2	9	9
rses100-8.6	0.06	0.03	0.82	0.12	0.03	0.02	0.27	0.16	0.36	0.18	0.21	0.08	2.31	0.55	1.18	0.69	9	1	3	2
ANU33-5-3	0.04	0.01	17.72	0.34	0.14	0.02	2.32	0.15	4.82	0.19	0.62	0.07	29.65	0.85	11.16	0.22	133	2	52	1
rses100-1.11	0.07	0.04	12.72	0.55	0.10	0.04	2.37	0.55	3.80	0.70	0.42	0.13	21.97	1.76	8.64	2.04	107	4	45	8
RSES58-6.12	0.34	0.03	7.55	0.26	0.48	0.06	2.86	0.26	2.23	0.30	0.24	0.04	8.46	1.06	3.22	0.32	42	1	17	2
RSES58-19.12	0.05	0.01	6.55	0.17	0.07	0.02	0.63	0.12	2.06	0.29	0.55	0.06	12.14	0.84	5.12	1.00	59	2	25	4
rses60_7-17	0.09	0.01	12.67	1.11	0.20	0.04	3.99	0.41	7.57	0.57	0.98	0.09	36.87	2.76	12.67	1.11	135	4	48	4
rses60_8-10bright	0.09	0.02	13.77	1.20	0.06	0.02	1.39	0.17	2.86	0.35	0.25	0.04	17.86	1.20	6.76	0.76	84	3	34	4

rses60_8-10dark	0.06	0.01	4.52	0.40	0.03	0.01	0.31	0.08	0.75	0.10	0.20	0.04	4.69	0.39	1.98	0.50	24	1	10	1
ANU33-13-6	0.00	0.00	5.38	0.19	0.05	0.01	0.48	0.07	1.35	0.10	0.20	0.04	10.28	0.50	4.28	0.14	58	1	23	0
ANU31-12-12	0.04	0.01	10.64	0.27	0.05	0.01	0.87	0.09	2.10	0.13	0.27	0.04	12.97	0.56	5.30	0.15	65	1	25	0
ANU33-6-14	bd	0.00	2.78	0.14	0.02	0.01	0.29	0.05	0.54	0.06	0.07	0.02	4.20	0.32	1.64	0.08	19	1	8	0
ANU32-11-5	0.01	0.00	10.51	0.26	0.02	0.01	0.58	0.07	1.48	0.11	0.17	0.03	12.71	0.56	5.61	0.16	78	2	33	0
rses100-1.18	0.01	0.01	13.00	0.87	0.00		1.08	0.48	2.36	0.71	0.20	0.11	13.55	1.96	5.29	2.41	66	4	29	11
rses100-13.4	0.09	0.02	12.55	0.41	0.13	0.03	3.30	0.32	5.73	0.42	0.57	0.07	25.56	1.13	9.51	0.95	112	2	42	3
ANU32-6-9	0.21	0.02	4.69	0.18	0.07	0.01	0.97	0.09	1.84	0.12	0.27	0.04	13.25	0.57	5.48	0.15	72	1	30	0
ANU33-14-9-1	0.03	0.01	6.88	0.21	0.07	0.01	1.04	0.10	2.13	0.13	0.24	0.04	10.17	0.50	3.87	0.13	45	1	18	0
ANU33-14-9-2	0.01	0.00	6.94	0.21	0.05	0.01	1.07	0.10	2.06	0.13	0.47	0.06	12.55	0.55	4.50	0.14	50	1	19	0
rses60_7-5	0.10	0.01	6.45	0.57	0.33	0.07	4.79	0.46	7.81	0.58	1.21	0.09	38.31	2.58	14.99	1.21	185	5	74	6
rses100-15.2	0.07	0.04	6.79	0.50	0.41	0.15	5.73	1.07	7.92	1.52	0.94	0.39	23.77	2.55	11.11	2.15	114	9	46	9
ANU32-6-15	0.03	0.01	12.55	0.29	0.12	0.02	2.16	0.14	3.06	0.15	0.43	0.05	12.95	0.56	5.08	0.15	57	1	22	0
RSES59-8.14	0.79	0.05	27.13	0.39	1.24	0.12	8.54	0.49	7.06	0.44	1.77	0.12	16.50	1.54	5.13	0.56	45	2	14	1
RSES67-17.12	0.93	0.06	26.88	0.59	1.24	0.12	9.02	0.73	10.48	0.52	1.32	0.10	46.08	2.67	18.03	1.63	206	4	81	4
ANU31-15-8	0.05	0.01	6.32	0.20	0.29	0.02	4.44	0.20	4.66	0.19	1.02	0.08	16.76	0.64	5.63	0.16	57	1	21	0
ANU31-8-4	0.04	0.01	15.08	0.32	0.13	0.02	2.79	0.16	4.31	0.18	0.89	0.08	21.70	0.73	8.24	0.19	98	2	40	0
RSES64-19.2	0.03	0.01	6.55	0.18	0.05	0.01	0.57	0.12	1.55	0.20	0.19	0.04	10.45	0.71	3.92	0.92	46	1	17	2
rses100-16.2	0.75	0.75	5.84	2.42	0.82	0.89	5.65	5.65	0.00		0.00		13.94	11.15	4.29	5.31	48	15	15	
ANU33-11-15	0.01	0.00	10.96	0.27	0.07	0.01	1.85	0.13	4.83	0.19	0.41	0.05	34.48	0.92	13.35	0.24	168	2	64	1
ANU31-4-10	0.03	0.01	4.14	0.17	0.04	0.01	0.47	0.07	1.28	0.10	0.17	0.03	9.97	0.49	4.46	0.14	60	1	27	0
RSES58-4.16	0.04	0.01	4.89	0.15	0.06	0.02	1.26	0.17	2.23	0.23	0.43	0.05	14.50	0.95	5.64	0.79	71	2	30	3
ANU31-14-3	0.03	0.01	3.33	0.15	0.21	0.02	4.00	0.19	5.34	0.20	0.98	0.08	17.62	0.65	5.64	0.16	55	1	19	0
ANU31-4-14	0.01	0.00	10.37	0.26	0.03	0.01	0.60	0.07	1.41	0.10	0.27	0.04	11.14	0.52	4.45	0.14	60	1	24	0
ANU31-14-7	0.08	0.01	40.31	0.52	0.53	0.03	9.28	0.29	13.26	0.32	2.01	0.12	66.86	1.28	24.86	0.33	307	3	119	1
rses100-6.1	0.02	0.02	13.05	0.65	0.17	0.07	1.19	0.80	2.81	1.03	0.63	0.18	16.23	1.48	4.28	2.91	63	3	22	8
RSES55-4.9	0.01	0.01	14.70	0.29	0.04	0.01	0.55	0.13	0.99	0.17	0.09	0.03	11.76	0.77	5.13	1.20	61	2	27	5
rses100-4.6	0.10	0.04	7.08	0.87	0.09	0.05	1.07	0.34	1.51	0.40	0.12	0.06	8.77	1.29	2.67	0.91	31	4	12	3
ANU32-6-10	0.02	0.01	5.48	0.19	0.05	0.01	1.12	0.10	2.98	0.15	0.47	0.06	20.58	0.71	7.88	0.18	103	2	40	0

RSES64-1.2	0.02	0.01	3.70	0.13	0.04	0.01	0.96	0.15	2.99	0.38	0.45	0.06	15.48	1.06	6.18	1.07	71	2	29	4
RSES64-2.2	0.04	0.01	7.45	0.19	0.03	0.01	0.81	0.14	1.93	0.22	0.50	0.08	16.89	1.07	7.11	1.27	86	2	38	4
rses60_5-15	0.07	0.01	9.94	0.87	0.09	0.02	1.40	0.19	2.30	0.22	0.56	0.06	11.35	0.92	4.39	0.56	50	2	21	2
ANU33-15-11	0.02	0.00	8.69	0.24	0.05	0.01	2.48	0.15	2.22	0.13	0.23	0.04	12.48	0.55	4.49	0.14	51	1	20	0

Sample	**168Er**	**1 s.d.**	**169Tm**	**1 s.d.**	**172Yb**	**1 s.d.**	**175Lu**	**1 s.d.**	**178Hf**	**1 s.d.**	**232Th**	**1 s.d.**	**238U**	**1 s.d.**	**Th(t)**	**U(t)**	**Th/U (t)**	**T (celsius)**
RSES51_7_2	83		18		155		33		11750				58			109		721
RSES51_3_10	97		23		208		47		11184				122			229		741
RSES51_3_8	68		16		132		30		11184				44			84		712
RSES51_5_4	125		28		250		54		12127				337			650		689
RSES51_4_2	131		29		243		55		10367				99			203		692
RSES51_3_12	49		12		110		22		9990				144			295		655
RSES51_4_7	82		18		156		36		9551				68			142		676
RSES51_4_5	66		14		131		32		9488				92			195		714
RSES51_1_6	260		67		649		158		7449				201			431		733
RSES59-5.9	196		41		349		85		13284		222		451		265	905	0.29	662
RSES59-10.16	110		23		191		43		7907		25		70		31	141	0.22	694
RSES59-15.1	171		36		318		80		14472		137		375		164	755	0.22	563
RSES59-15.16	154		33		285		71		13123		157		429		187	865	0.22	619
RSES59-16.3	64		15		131		31		10377		16		53		19	106	0.18	687
RSES59-16.6	169		38		340		79		11803		73		238		87	480	0.18	622
RSES59-3.15	80		17		153		38		10377		131		154		158	314	0.50	661
RSES59-4.7	65		14		107		25		10653		78		115		94	236	0.40	651
RSES59-4.17	289		60		468		110		12632		354		409		427	850	0.50	659
RSES59-13.17	103		21		181		41		10331		67		109		80	229	0.35	676
RSES51_4-1	113		20		179		43		10594		64		92		75	174	0.43	645
RSES51_16-1	81		17		148		37		11252		94		45		112	86	1.30	699
RSES51_11-1	309		62		490		109		11382		192		120		227	227	1.00	705
RSES51_10-6	237		53		478		119		12212		240		452		285	870	0.33	681

RSES51_7-1	97		21		181		42		9971		67		155		79	298	0.27	694
RSES51_2-10	99		24		222		54		9971		71		195		84	383	0.22	650
RSES51_3-5	60		14		125		29		11951		54		160		65	314	0.21	660
RSES51_3-1	88		20		166		39		10457		331		197		394	388	1.02	806
RSES51_14-1	250		55		470		106		13397		276		490		331	986	0.34	817
RSES51_3-7	165		38		334		80		12684		138		492		165	991	0.17	630
RSES51_17-11	387		83		697		156		14247		523		654		630	1364	0.46	820
RSES51_10-12	93		21		181		41		9909		29		102		35	213	0.16	685
RSES51_17-1	252		51		420		91		10409		99		96		121	211	0.57	682
RSES51_17-2	30		7		63		15		9950		12		30		14	67	0.22	685
RSES51_10-1	116		26		226		55		9375		270		237		329	526	0.63	786
24-L14	150		31		282		55		8864		104		103		123	193	0.64	
29-MEW14	69		15		155		33		9879		54		135		65	262	0.25	
30-MEW3	128		25		226		45		9989		136		270		162	529	0.31	
29-M16	88		21		231		50		9578		49		138		59	274	0.21	
W74-35					103		33				144		170		169	314	0.54	
W74-19					183		44				609		245		720	463	1.56	
W74-7					314		73				130		141		154	267	0.58	
W74-34					359		87				103		216		122	416	0.29	
W74-6					218		52				207		216		246	422	0.58	
W74-20					182		43				640		233		765	466	1.64	
RSES55-5.13	85	3	18	20	161	20	40	11	11636	679	75	12	116	14	91	245	0.37	652
RSES58-16.15	114	4	26	9	228	18	53	8	10784	541	59	3	139	8	71	295	0.24	679
RSES73-3.7	84	2	18	4	161	14	37	8	9677	532	27	1	49	2	33	104	0.32	726
RSES59-04.08	238	3	52	11	450	35	101	14	11475	557	123	3	265	7	148	564	0.26	781
RSES55-11.3	97	2	22	5	199	22	44	5	12349	603	74	5	118	7	90	251	0.36	667
RSES55-15.13	123	2	27	6	234	24	55	13	10192	496	37	4	58	2	45	125	0.36	652
RSES59-17.16	71	1	16	7	144	15	33	5	9560	469	30	1	59	2	36	126	0.29	696
RSES73-5.8 average	51	7	11	4	104	27	24	10	11110	822	49	9	178	11	59	384	0.15	655
RSES56-03.17	110	2	24	4	213	26	48	6	9536	467	29	1	50	2	35	107	0.33	623

RSES55-15.11	140	3	30	6	267	22	58	8	8687	423	62	5	94	3	75	203	0.37	649
rses54-15.11 average	81	6	18	6	157	18	36	10	10901	808	83	5	231	21	100	501	0.20	690
RSES58-3.13	169	3	37	5	321	24	72	7	9547	469	103	6	238	8	125	516	0.24	688
RSES54-18.11	70	1	16	6	144	13	33	9	12590	616	34	1	160	7	41	346	0.12	656
rses100-7.18	72	5	18	9	162	18	42	22	7187	352	38	2	123	6	47	266	0.18	644
rses100-7.19	47	3	8	6	86	25	20	18	7766	199	122	6	180	17	148	392	0.38	686
rses100-17.1	120	3	26	4	229	13	52	7	10574	424	45	1	102	4	54	223	0.24	680
rses100-1.12	72	5	17	12	145	19	34	14	7035	169	37	3	108	6	45	237	0.19	684
rses100-16.3	42	2	10		86	15	18	19	8435	270	20	3	63	11	24	140	0.17	666
ANU33-12-14	103	2	22	0	190	3	42	1	8464	22	41	1	110	1	51	245	0.21	687
ANU33-7-15	125	2	26	0	230	3	51	1	10436	24	51	1	89	1	63	199	0.31	641
RSES55-3.7	99	3	22	3	199	19	45	8	9730	474	76	2	103	8	93	230	0.40	685
RSES67-10.11	35	2	7	3	60	10	14	13	13303	758	35	2	163	19	42	363	0.12	630
rses100-6.13	66	3	14	10	117	15	31	13	7132	390	54	3	118	14	66	263	0.25	670
RSES59-18.19	68	1	15	3	142	13	33	6	11247	549	20	3	62	2	25	138	0.18	622
ANU32-1-7	111	2	23	0	213	3	47	1	8569	22	44	1	128	1	54	287	0.19	645
rses100-20.17b	72	2	16	4	133	16	28	10	8558	177	194	19	335	16	237	752	0.32	778
ANU31-1-14	75	1	17	0	163	3	39	1	8854	23	40	1	130	1	49	292	0.17	622
ANU31-10-11	67	1	16	0	167	3	40	1	10274	24	37	1	127	1	46	287	0.16	718
RSES67-3.11	163	3	36	5	294	24	63	6	10705	526	127	8	153	6	155	346	0.45	757
RSES64-9.2	61	2	13	2	113	10	27	7	9499	462	33	1	84	3	40	191	0.21	689
rses60_4-19	245	5	54	5	472	25	109	11	9751	392	92	3	179	5	113	405	0.28	685
rses100-4.19	40	3	10		94	15	24	14	8269	194	42	3	129	7	52	292	0.18	647
rses100-8.6	13	1	3	1	22	5	5	3	7883	166	1	0	10	3	1	22	0.07	698
ANU33-5-3	237	2	48	1	401	4	86	1	8193	22	90	1	125	1	110	283	0.39	659
rses100-1.11	186	6	40	13	318	27	71	17	7416	167	90	11	127	25	109	289	0.38	658
RSES58-6.12	78	2	18	3	166	22	38	4	10792	524	63	2	288	13	76	652	0.12	694
RSES58-19.12	105	2	23	3	187	16	43	8	8838	476	31	2	51	2	38	115	0.33	643
rses60_7-17	190	4	38	3	314	20	68	5	10156	402	97	3	155	5	119	352	0.34	681
rses60_8-10bright	148	3	31	4	274	15	60	6	10930	434	80	3	140	6	98	319	0.31	679

rses60_8-10dark	45	1	10	2	94	7	21	5	9621	373	17	1	56	2	21	127	0.16	680
ANU33-13-6	111	2	24	0	215	3	48	1	9209	23	37	1	108	1	45	245	0.19	714
ANU31-12-12	117	2	24	0	214	3	46	1	9227	23	57	1	122	1	69	277	0.25	658
ANU33-6-14	36	1	7	0	70	2	15	0	8900	23	10	0	22	0	12	51	0.23	671
ANU32-11-5	164	2	36	0	312	4	69	1	10242	24	55	1	155	1	67	353	0.19	628
rses100-1.18	129	5	30	17	245	37	60	27	8003	435	68	4	162	11	83	368	0.23	622
rses100-13.4	171	3	37	5	284	16	65	7	7377	262	78	4	88	3	95	199	0.48	676
ANU32-6-9	139	2	30	0	265	4	59	1	8655	22	40	1	124	1	49	282	0.17	717
ANU33-14-9-1	81	1	17	0	148	3	34	1	7288	20	39	1	83	1	47	190	0.25	666
ANU33-14-9-2	87	1	18	0	165	3	35	1	7785	21	39	1	76	1	48	175	0.28	668
rses60_7-5	328	6	70	4	583	31	126	9	8936	351	140	3	237	10	171	542	0.32	737
rses100-15.2	180	6	41	17	320	36	73	16	6541	168	44	3	87	6	54	198	0.27	685
ANU32-6-15	102	2	21	0	187	3	41	1	8354	22	75	1	204	1	92	467	0.20	673
RSES59-8.14	54	3	12	1	104	11	22	3	9089	442	381	6	188	5	466	431	1.08	833
RSES67-17.12	336	4	72	6	596	47	128	12	11545	561	564	55	374	9	691	861	0.80	807
ANU31-15-8	93	2	19	0	179	3	41	1	6846	20	73	1	113	1	89	260	0.34	642
ANU31-8-4	194	2	43	1	398	4	93	1	8136	22	30	0	75	1	37	173	0.21	728
RSES64-19.2	71	1	15	3	123	10	26	6	10647	548	41	1	108	4	50	249	0.20	664
rses100-16.2	82	19	11		161	156	40	51	4592	544	0		17	17	0	39	0.00	742
ANU33-11-15	293	3	58	1	480	5	101	1	9053	23	70	1	129	1	86	297	0.29	647
ANU31-4-10	131	2	30	0	285	4	68	1	10184	24	63	1	232	1	77	536	0.14	704
RSES58-4.16	134	2	31	4	275	22	64	9	9290	467	37	3	96	5	45	221	0.20	705
ANU31-14-3	84	1	17	0	164	3	37	1	9524	23	67	1	149	1	83	344	0.24	663
ANU31-4-14	114	2	24	0	211	3	46	1	9661	24	30	0	64	1	37	147	0.25	683
ANU31-14-7	544	4	112	1	968	7	204	2	8602	22	248	1	255	2	304	590	0.52	754
rses100-6.1	99	9	24	7	187	21	42	28	7313	178	70	7	143	10	86	332	0.26	718
RSES55-4.9	124	3	27	9	231	18	52	12	13768	669	132	4	175	6	163	405	0.40	641
rses100-4.6	52	2	13	7	109	17	24	8	8422	372	24	9	55	4	29	129	0.23	703
ANU32-6-10	186	2	39	0	345	4	76	1	8504	22	52	1	156	1	64	363	0.18	678
RSES64-1.2	121	4	25	4	213	19	46	8	9580	520	28	2	61	6	34	142	0.24	677

RSES64-2.2	174	2	38	6	336	27	79	14	10480	510	107	6	283	12	131	661	0.20	630
rses60_5-15	90	2	19	2	165	12	37	5	9018	374	55	2	119	4	67	279	0.24	684
ANU33-15-11	92	2	19	0	175	3	39	1	9805	24	81	1	200	1	100	473	0.21	651

Sample	**Yb/Gd (N)**	**Gd/Gd***	**Ce/Ce***	**Eu/Eu***	**Dy/Dy***	**La/CI**	**Ce/CI**	**Pr/CI**	**Nd/CI**	**Sm/CI**	**Eu/CI**	**Gd/CI**	**Tb/CI**	**Dy/CI**	**Ho/CI**	**Er/CI**	**Tm/CI**	**Yb/CI**	**Lu/CI**
RSES51_7_2	17	1	34	1	1	1	33	1	2	17	45	58	111	189	330	516	713	963	1327
RSES51_3_10	31	1	10	1	1	1	17	2	2	8	20	41	94	168	355	604	911	1290	1867
RSES51_3_8	21	1	56	1	1	0	20	0	1	9	23	39	77	142	272	428	622	817	1201
RSES51_5_4	31	1	15	1	1	1	13	1	1	9	23	51	125	237	499	780	1113	1552	2175
RSES51_4_2	19	1	34	1	1	0	23	1	3	17	46	81	166	283	508	821	1152	1512	2193
RSES51_3_12	20	0	10	2	1	6	60	7	7	13	34	34	57	88	170	305	483	686	862
RSES51_4_7	18	1	32	1	1	0	19	1	2	10	25	52	107	180	341	513	724	966	1458
RSES51_4_5	18	1	14	1	1	1	14	2	3	14	36	45	86	143	266	415	566	813	1276
RSES51_1_6	54	1	7	1	1	0	3	1	3	20	52	75	177	366	859	1625	2688	4029	6331
RSES59-5.9	18	1	219	1	1	0	31	1	3	18	49	118	264	463	830	1228	1651	2171	3397
RSES59-10.16	17	1	42	1	1	0	8	0	2	15	40	68	146	251	463	690	904	1183	1719
RSES59-15.1	39	1		1	1	0	10	0	1	7	19	51	143	296	603	1069	1449	1973	3206
RSES59-15.16	22	1	87	1	1	0	20	1	3	19	49	81	196	328	615	961	1312	1769	2836
RSES59-16.3	30	1	47	1	1	0	6	0	1	5	14	27	63	122	240	401	584	811	1250
RSES59-16.6	31	1	65	1	1	0	11	0	1	10	27	68	175	342	679	1053	1532	2114	3165
RSES59-3.15	20	1	456	1	1	0	31	0	3	14	36	47	100	169	341	499	669	948	1523
RSES59-4.7	12	1	28	1	1	0	14	1	3	14	38	56	98	162	288	405	544	662	992
RSES59-4.17	15	2		1	1	0	24	1	5	44	117	193	408	686	1226	1809	2391	2909	4410
RSES59-13.17	18	1	58	1	1	0	18	1	2	15	40	62	141	235	425	641	841	1122	1653
RSES51_4-1	19	1	85	1	1	0	23	0	3	14	36	57	121	204	455	705	795	1113	1703
RSES51_16-1	21	1	31	1	1	0	30	2	3	14	37	45	91	169	311	504	687	921	1485
RSES51_11-1	10	1	53	1	1	0	55	4	16	84	222	297	552	849	1390	1933	2463	3045	4350
RSES51_10-6	25	1	124	1	1	0	49	1	4	23	61	117	274	477	926	1480	2140	2972	4740
RSES51_7-1	23	1	49	1	1	0	18	1	2	13	33	50	117	211	382	605	843	1125	1682

RSES51_2-10	36	1	27	1	1	0	8	0	1	7	18	38	96	188	371	616	958	1377	2175
RSES51_3-5	24	1	54	1	1	0	16	0	1	8	21	33	72	135	246	374	556	774	1167
RSES51_3-1	16	1	9	2	1	3	45	11	10	26	68	65	136	220	368	549	781	1030	1556
RSES51_14-1	30	0	7	2	1	4	49	15	17	39	102	97	252	484	945	1560	2182	2922	4220
RSES51_3-7	33	1	35	1	1	0	12	0	1	8	21	62	167	335	631	1032	1528	2075	3217
RSES51_17-11	23	1	11	1	1	4	88	16	20	58	154	185	465	853	1620	2419	3329	4327	6253
RSES51_10-12	25	1	17	1	1	1	9	1	1	12	33	45	113	194	366	582	833	1121	1649
RSES51_17-1	13	1	31	1	1	0	20	3	11	58	154	200	397	630	1103	1573	2055	2609	3629
RSES51_17-2	28	1	32	1	1	0	5	0	1	3	9	14	34	63	110	186	268	393	599
RSES51_10-1	24	1	18	2	1	1	48	7	8	22	59	58	123	227	442	728	1041	1403	2213
24-L14	16	1	63	1	1	0	22	1	4	27	71	108	194	344	582	938	1220	1752	2212
29-MEW14	22	1	31	1	1	0	11	1	2	9	24	43	83	150	255	431	596	963	1332
30-MEW3	14	2	25	1	1	0	8	0	1	19	50	102	204	346	545	800	988	1404	1804
29-M16	41	1	38	1	1	0	6	0	1	5	14	35	81	155	300	552	832	1435	1984
W74-35	14	0	2	2		22	41	25	25	33	88	44	61	92	140	0	0	640	1300
W74-19	14	1	12	2		2	50	10	11	28	73	80	150	244	395	0	0	1137	1756
W74-7	14	1	17	1		2	55	6	8	28	75	138	247	419	711	0	0	1950	2936
W74-34	21	1		1		0	19	1	2	23	61	106	222	439	778	0	0	2230	3468
W74-6	6	1	5	1		4	27	8	15	66	175	215	314	476	702	0	0	1354	2072
W74-20	11	1	4	2		8	55	26	28	53	139	99	175	273	405	0	0	1130	1720
RSES55-5.13	23	1		1	1	0	25	1	4	13	34	43	88	172	305	530	737	1003	1600
RSES58-16.15	23	1	64	1	1	0	16	0	3	13	35	63	146	256	478	710	1042	1417	2119
RSES73-3.7	24	1	54	1	1	0	12	0	1	6	17	42	99	177	330	526	718	999	1484
RSES59-04.08	31	1	21	1	1	0	13	1	3	18	47	90	258	489	937	1487	2090	2794	4029
RSES55-11.3	26	1	9	1	1	1	20	4	6	15	39	47	110	194	376	606	868	1233	1774
RSES55-15.13	31	1	105	1	1	0	11	0	1	9	24	47	127	248	483	769	1090	1456	2185
RSES59-17.16	20	1	36	1	1	0	11	0	2	13	33	45	94	158	276	441	635	895	1320
RSES73-5.8 average	21	1	35	1	1	0	7	0	1	8	21	31	66	111	196	319	457	644	953
RSES56-03.17	21	1	35	1	1	0	20	1	4	18	48	64	141	249	466	686	945	1323	1912

RSES55-15.11	19	1	24	1	1	0	12	1	5	23	60	89	192	317	564	875	1209	1660	2305
rses54-15.11 average	21	1	41	1	1	0	12	1	2	10	28	46	101	176	326	506	701	975	1426
RSES58-3.13	19	1	73	1	1	0	34	1	5	28	73	103	219	383	698	1055	1470	1992	2863
RSES54-18.11	32	1	37	1	1	0	13	1	1	5	13	28	67	126	256	440	647	896	1318
rses100-7.18	32	1	38	1	1	0	9	0	2	7	18	31	90	153	285	448	710	1003	1678
rses100-7.19	16	1	20	2	1	0	15	2	2	17	45	33	55	117	220	292	325	535	796
rses100-17.1	24	1	48	1	1	0	18	1	2	13	36	59	138	255	491	752	1040	1420	2073
rses100-1.12	18	1	33	1	1	0	17	1	2	5	14	50	90	157	325	452	694	903	1354
rses100-16.3	25	1	35	1	1	0	9	0	1	2	4	22	40	80	166	266	382	536	730
ANU33-12-14	21	1	51	1	1	0	10	1	2	13	34	55	120	226	399	645	892	1183	1680
ANU33-7-15	25	1	141	1	1	0	14	0	2	10	27	56	140	259	476	780	1033	1428	2059
RSES55-3.7	20	1	42	1	1	0	19	1	2	15	39	63	126	222	402	619	875	1236	1818
RSES67-10.11	11	2	21	1	1	0	4	0	1	4	11	35	74	91	163	219	292	372	579
rses100-6.13	15	1	48	1	1	0	17	1	2	12	31	50	93	165	281	412	578	727	1235
RSES59-18.19	27	1	31	1	1	0	8	1	1	7	17	33	78	137	271	422	612	884	1309
ANU32-1-7	24	1	66	1	1	0	18	1	2	13	33	56	124	231	419	696	931	1324	1867
rses100-20.17b	13	1	6	1	1	2	21	6	10	19	49	63	103	188	305	449	635	829	1132
ANU31-1-14	25	1	40	1	1	0	5	0	1	9	24	41	85	165	275	471	682	1010	1562
ANU31-10-11	34	0	5	2	1	1	13	5	6	23	61	31	67	121	241	422	656	1037	1591
RSES67-3.11	12	1	5	2	1	8	58	21	23	58	153	148	300	445	734	1022	1429	1826	2522
RSES64-9.2	18	1	22	1	1	0	5	0	1	10	26	39	83	136	248	381	521	703	1066
rses60_4-19	25	1	34	1	1	0	22	1	4	25	66	117	276	519	965	1532	2173	2931	4344
rses100-4.19	25	1	#NUM!	1	1	0	9	0	1	5	12	23	45	89	169	250	411	582	942
rses100-8.6	12	1	5	1	1	0	1	0	1	2	6	12	33	36	56	83	109	138	216
ANU33-5-3	17	1	57	1	1	0	29	2	5	33	86	149	310	541	940	1479	1915	2493	3438
rses100-1.11	18	1	37	1	1	0	21	1	5	26	68	110	240	434	820	1164	1602	1975	2836
RSES58-6.12	24	1	4	2	1	1	12	5	6	15	40	43	89	171	307	487	707	1032	1537
RSES58-19.12	19	2	27	1	1	0	11	1	1	14	37	61	142	240	450	659	910	1164	1713
rses60_7-17	11	1	23	1	1	0	21	2	9	51	135	185	352	549	869	1186	1532	1947	2728

rses60_8-10bright	19	1	49	1	1	0	22	1	3	19	51	90	188	339	610	923	1257	1704	2380
rses60_8-10dark	25	1	24	1	1	0	7	0	1	5	13	24	55	97	182	279	397	582	846
ANU33-13-6	26	1	92	1	1	0	9	1	1	9	24	52	119	236	425	695	976	1333	1935
ANU31-12-12	20	1	63	1	1	0	17	0	2	14	37	65	147	266	456	729	978	1326	1839
ANU33-6-14	21	1		1	1		5	0	1	4	10	21	46	76	139	227	293	436	602
ANU32-11-5	30	1	146	1	1	0	17	0	1	10	26	64	156	318	596	1022	1437	1937	2776
rses100-1.18	22	1	#NUM!	1	1	0	21	0	2	16	42	68	147	269	526	806	1212	1519	2384
rses100-13.4	14	1	28	1	1	0	20	1	7	39	102	128	264	454	757	1070	1473	1765	2609
ANU32-6-9	25	1	9	1	1	1	8	1	2	12	33	67	152	294	543	870	1198	1648	2356
ANU33-14-9-1	18	1	37	1	1	0	11	1	2	14	38	51	107	184	319	509	665	918	1353
ANU33-14-9-2	16	1	76	1	1	0	11	1	2	14	37	63	125	204	348	544	713	1023	1382
rses60_7-5	19	1	9	1	1	0	11	4	10	53	139	193	416	751	1354	2047	2814	3624	5025
rses100-15.2	17	1	10	2	1	0	11	4	13	54	141	119	309	465	828	1124	1641	1985	2935
ANU32-6-15	18	1	49	1	1	0	20	1	5	21	55	65	141	231	409	640	836	1160	1640
RSES59-8.14	8	1	7	2	1	3	44	13	19	48	126	83	143	181	251	339	463	647	895
RSES67-17.12	16	1	6	1	1	4	44	13	20	71	187	232	501	837	1466	2097	2887	3704	5135
ANU31-15-8	13	1	13	2	1	0	10	3	10	32	83	84	156	233	381	584	777	1111	1633
ANU31-8-4	23	1	49	1	1	0	25	1	6	29	77	109	229	400	721	1213	1715	2471	3735
RSES64-19.2	15	2	40	1	1	0	11	1	1	10	28	53	109	187	303	444	585	766	1043
rses100-16.2	14	1	2		1	3	10	9	12	0	0	70	119	194	264	511	443	1002	1591
ANU33-11-15	17	2	84	1	1	0	18	1	4	33	86	173	371	685	1172	1829	2312	2982	4058
ANU31-4-10	35	1	31	1	1	0	7	0	1	9	23	50	124	245	484	820	1210	1770	2732
RSES58-4.16	23	1	23	1	1	0	8	1	3	15	40	73	157	290	541	836	1227	1706	2549
ANU31-14-3	11	1	11	2	1	0	5	2	9	36	95	89	157	224	343	523	698	1016	1499
ANU31-4-14	23	1	126	1	1	0	17	0	1	10	25	56	124	244	437	713	973	1308	1856
ANU31-14-7	18	1	46	1	1	0	66	6	20	90	237	336	690	1247	2161	3399	4478	6010	8166
rses100-6.1	14	1	57	1	1	0	21	2	3	19	50	82	119	254	391	621	951	1163	1676
RSES55-4.9	24	1	167	1	1	0	24	0	1	7	18	59	142	249	497	775	1078	1437	2093
rses100-4.6	15	1	18	1	1	0	12	1	2	10	27	44	74	128	226	323	505	677	969

ANU32-6-10	21	1	39	1	1	0	9	1	2	20	53	103	219	417	728	1163	1547	2142	3044
RSES64-1.2	17	1	32	1	1	0	6	0	2	20	53	78	172	288	523	756	1019	1324	1858
RSES64-2.2	25	1	48	1	1	0	12	0	2	13	35	85	198	349	684	1085	1513	2090	3142
rses60_5-15	18	1	30	1	1	0	16	1	3	16	41	57	122	201	374	565	756	1023	1497
ANU33-15-11	17	1	66	1	1	0	14	1	5	15	40	63	125	209	370	572	769	1089	1576

Table G.1: Trace elements in Jack Hills zircons from this and previous studies, which are considered in chapters 4 and 5.

Sample Name	**(207/206)Pb Age, Ma**	**1 s.d.**	**% discord.**	**d18O**	**1 s.d.**	**Clean=1, Bad=0, ambiguous=2**
RSES67_13_14	4.020	0.006	2	4.4	0.7	0
RSES67_3_2	4.008	0.006	-2	4.4	0.7	0
RSES67_17_14	4.021	0.010	1	4.6	0.7	0
RSES64_17_19	4.009	0.015	-1	4.7	0.4	0
RSES61_2_6	4.024	0.014	0	4.7	0.2	0
RSES67_3_2R	4.008	0.006	-2	4.9	0.7	0
RSES60_15_15	4.028	0.012	-1	4.9	0.5	0
RSES67_19_12	4.130	0.005	3	4.9	0.7	0
RSES65_15_8	4.152	0.003	2	5.0	0.4	0
RSES67_13_14R	4.020	0.006	2	5.0	0.7	0
RSES65_8_13	4.090	0.004	1	5.1	0.4	0
rses_55_new_8_9	4.205	0.006	9	5.3	0.4	0
RSES67_12_6R	4.087	0.004	2	5.3	0.7	0
RSES61_10_7	4.078	0.009	0	5.5	0.2	0
rses_55_new_11_6	4.073	0.009	-8	5.6	0.4	0
RSES64_1_2	4.155	0.012	1	5.7	0.4	0
rses_57_13_8	4.102	0.007	-7	5.7	0.3	0
RSES66_5_16	4.178	0.009	2	5.8	0.3	0
RSES59_9_9	4.028	0.011	-4	5.9	0.2	0
RSES_58_6_16	4.074	0.007	-7	5.9	1.1	0
RSES59_18_9	4.099	0.009	4	5.9	0.2	0
RSES59_14_18	4.067	0.008	9	6.0	0.2	0
RSES61_16_10	4.032	0.006	0	6.0	0.2	0
RSES62_5_10	4.059	0.009	6	6.0	0.8	0

RSES61_13_14	4.017	0.010	2	6.0	0.2	0
RSES61_4_9	4.078	0.005	2	6.0	0.2	0
RSES66_10_10	4.010	0.007	0	6.1	0.3	0
rses_57_18_5	4.019	0.003	-4	6.1	0.3	0
RSES63_5_3	4.069	0.015	-3	6.1	0.2	0
rses_55_new_10_9	4.088	0.008	-8	6.2	0.4	0
RSES_58_5_14	4.074	0.006	2	6.2	1.1	0
RSES64_6_13	4.060	0.007	14	6.2	0.4	0
RSES61_4_10	4.017	0.005	1	6.3	0.2	0
RSES67_12_6	4.087	0.004	2	6.4	0.7	0
RSES64_9_2	4.048	0.010	-1	6.4	0.4	0
RSES_58_13_15	4.020	0.014	-5	6.5	1.1	0
RSES61_12_8	4.080	0.010	0	6.5	0.2	0
RSES_58_13_17	4.051	0.010	7	6.7	1.1	0
RSES62_18_20	4.024	0.016	3	6.8	0.8	0
RSES64_2_2	4.159	0.007	0	7.0	0.4	0
RSES67_3_11	4.040	0.007	3	7.3	0.7	0?
RSES67_16_6	4.038	0.006	0	7.3	0.7	0 (probably)
RSES67_3_11R	4.040	0.007	3	7.3	0.7	0?
RSES67_16_2	4.029	0.005	0	7.5	0.7	0 (probably)
rses_55_new_16_11	4.140	0.009	1	5.2	0.4	1
rses_55_new_17_8	4.021	0.008	-4	4.9	0.4	1
rses_57_15_11	4.048	0.009	0	5.9	0.3	1
rses_57_15_16	4.082	0.004	-1	5.5	0.3	1
rses_57_19_15	4.021	0.007	-5	6.6	0.3	1
rses_57_2_13	4.016	0.006	-7	6.6	0.3	1
RSES_58_19_12	4.059	0.020	1	6.5	1.1	1
RSES_58_3_16	0.000	0.000		6.0	1.1	1
RSES_58_6_12	4.057	0.008	1	6.8	1.1	1
RSES_58_7_9	4.025	0.021	-9	5.2	1.1	1
RSES59_12_2	4.025	0.005	3	5.6	0.2	1
RSES59_17_1	4.077	0.006	-4	5.9	0.2	1
RSES59_18_19	4.015	0.021	3	6.1	0.2	1
RSES59_4_18	4.245	0.003	-2	5.4	0.2	1
RSES59_9_15	4.103	0.009	-4	5.5	0.2	1

RSES60_4_19	4.049	0.014	0	4.8	0.5	1
RSES60_5_15	4.160	0.004	-1	4.9	0.5	1
RSES60_6_7	4.002	0.006	-2	5.3	0.5	1
RSES60_7_17	4.061	0.005	-3	4.5	0.5	1
RSES60_7_5	4.085	0.007	-1	4.5	0.5	1
RSES60_8_10	4.062	0.007	-3	5.3	0.5	1
RSES61_1_20	4.134	0.007	0	7.2	0.2	1
RSES61_14_16	4.174	0.011	2	6.3	0.3	1
RSES61_5_15	4.042	0.013	2	5.7	0.2	1
RSES61_8_11	4.151	0.007	-1	5.5	0.2	1
RSES61_9_19	4.031	0.007	1	7.3	0.2	1
RSES62_10_8	4.050	0.015	1	6.6	0.8	1
RSES62_2_17	4.018	0.013	1	5.6	0.8	1
RSES62_6_10	4.054	0.017	3	6.0	0.8	1
RSES62_9_18	4.097	0.011	6	5.3	0.8	1
RSES63_1_11	4.097	0.008	-4	4.2	0.2	1
RSES63_16_1	4.094	0.023	-4	6.2	0.2	1
RSES63_6_4	4.043	0.009	-5	7.1	0.2	1
RSES64_1_16	4.010	0.006	7	7.0	0.4	1
RSES64_1_3	4.066	0.010	0	5.9	0.4	1
RSES64_11_14	4.029	0.006	2	6.3	0.4	1
RSES64_12_11	4.039	0.014	7	6.4	0.4	1
RSES64_19_2	4.111	0.012	1	5.8	0.4	1
RSES64_2_13	4.027	0.012	3	5.7	0.4	1
RSES64_5_2	4.031	0.011	1	5.6	0.4	1
RSES64_6_1	4.096	0.015	-1	6.2	0.4	1
RSES64_6_7	4.062	0.013	0	6.2	0.4	1
RSES64_7_16	4.011	0.010	0	6.3	0.4	1
RSES65_11_6	4.015	0.004	4	6.4	0.4	1
RSES65_14_9	4.041	0.005	2	5.2	0.4	1
RSES65_20_1	4.029	0.005	4	4.7	0.4	1
RSES66_1_9	4.068	0.013	5	5.7	0.3	1
RSES66_14_12	4.069	0.009	-1	4.7	0.3	1
RSES66_6_1	4.143	0.004	3	5.5	0.3	1
RSES66_9_2	4.038	0.014	1	5.9	0.3	1

RSES67_11_7	4.110	0.008	2	7.3	0.7	1
RSES67_11_7R	4.110	0.008	2	6.5	0.7	1
RSES67_14_16	4.067	0.004	8	4.8	0.7	1
RSES67_14_16R	4.067	0.004	8	5.3	0.7	1
RSES67_17_12	4.107	0.004	0	6.0	0.7	0 or 1 (prob. 1)
RSES67_19_5	4.151	0.005	3	5.1	0.7	1
rses_55_11_15_dup	4.040	0.014	0	7.1	0.3	2
rses_55_6_15_dup	4.017	0.019	-7	4.8	0.3	2
rses_55_new_10_2	4.036	0.010	-9	5.0	0.4	2
rses_55_new_11_15	4.040	0.014	0	6.5	0.4	2
rses_55_new_19_1	4.128	0.006	-7	5.4	0.4	2
rses_55_new_3_1	4.016	0.008	-1	5.8	0.4	2
rses_55_new_3_7	4.006	0.010	-3	5.8	0.4	2
rses_55_new_4_9	4.133	0.005	-2	5.6	0.4	2
rses_55_new_6_15	4.017	0.019	-7	4.3	0.4	2
rses_57_1_3	4.039	0.007	-1	6.2	0.3	2
rses_57_19_12	4.124	0.006	-5	6.2	0.3	2
RSES_58_3_4	4.133	0.007	-5	5.6	1.1	2
RSES_58_4_16	4.119	0.006	-4	6.4	1.1	2
RSES59_11_7	4.016	0.006	-3	5.7	0.2	2
RSES59_2_17	4.048	0.008	3	5.5	0.2	2
RSES59_4_11	4.003	0.008	-6	6.0	0.2	2
RSES59_5_2	4.004	0.004	-1	5.5	0.2	2
RSES59_8_14	4.097	0.006	-4	5.5	0.2	2
RSES59_8_4	4.108	0.005	-8	5.9	0.2	2
RSES60_10_19	4.023	0.008	-2	5.2	0.5	2
RSES60_16_1	4.162	0.005	8	4.9	0.5	2
RSES60_6_18	4.020	0.007	3	5.3	0.5	2
RSES60_7_19	4.128	0.015	-1	5.7	0.5	2
RSES60_8_8	4.041	0.006	0	5.1	0.5	2
RSES61_10_8	4.028	0.011	0	5.5	0.2	2
RSES61_12_10	4.088	0.008	2	5.8	0.2	2
RSES61_12_13	4.127	0.006	4	6.5	0.2	2
RSES61_13_11	4.015	0.008	0	5.1	0.2	2
RSES61_15_11	4.023	0.018	3	6.8	0.2	2

RSES61_16_1	4.082	0.009	0	5.1	0.2	2
RSES61_18_8	4.102	0.013	1	5.7	0.2	2
RSES61_5_9	4.112	0.006	1	5.9	0.2	2
RSES61_8_2	4.033	0.010	0	6.2	0.2	2
RSES62_15_17	4.064	0.016	6	6.8	0.8	2
RSES62_2_7	4.057	0.005	2	5.4	0.8	2
RSES62_20_18	4.075	0.012	2	7.2	0.8	2
RSES62_6_12	4.031	0.008	3	7.1	0.8	2
RSES63_14_5	4.145	0.013	-5	6.1	0.2	2
RSES64_10_7	4.018	0.006	3	6.5	0.4	2
RSES64_5_13	4.091	0.024	-1	5.0	0.4	2
RSES65_10_12	0.000	0.000		5.5	0.4	2
RSES65_18_9	4.105	0.009	2	5.6	0.4	2
RSES65_3_6	4.022	0.007	1	5.4	0.4	2
RSES65_9_1	4.018	0.005	-1	3.1	0.4	2
RSES66_12_18	4.029	0.008	0	6.3	0.3	2
RSES66_13_14	4.004	0.009	7	5.9	0.3	2
RSES66_3_16	4.129	0.005	-1	5.8	0.3	2
RSES66_5_18	4.173	0.007	3	6.1	0.3	2
RSES66_6_12	4.110	0.012	-1	6.4	0.3	2
RSES67_10_11	4.008	0.005	2	7.1	0.7	2
RSES67_10_11R	4.008	0.005	2	7.0	0.7	2
RSES67_15_16	4.192	0.007	-3	5.8	0.7	2
RSES67_19_13	4.041	0.007	8	6.6	0.7	2

Sample Name	**Texture (from CL imaging)**	**Size (um)**	**Grain rounding**
RSES67_13_14	unclear; probably patches	50x125 to 125x125	subrounded then broken
RSES67_3_2	faint osc+sect; alteration possible	125x200	subrounded
RSES67_17_14	osc + sect; altered?	150x150	subrounded
RSES64_17_19			
RSES61_2_6			
RSES67_3_2R	faint osc+sect; alteration possible	125x200	subrounded
RSES60_15_15	patchy; original osc?		
RSES67_19_12	dark interior; conc. Zones; v. bright rim	75x125	rounded then broken

RSES65_15_8			
RSES67_13_14R	unclear; probably patches	50x125 to 125x125	subrounded then broken
RSES65_8_13			
rses_55_new_8_9			
RSES67_12_6R	cloudy; indeterminate/some osc-iness	75x150	angular
RSES61_10_7			
rses_55_new_11_6			
RSES64_1_2			
rses_57_13_8	bright osc with dark rim		
RSES66_5_16			
RSES59_9_9			
RSES_58_6_16	faint; patchy?	175x175	
RSES59_18_9	patchy		
RSES59_14_18	osc (?)		
RSES61_16_10			
RSES62_5_10			
RSES61_13_14			
RSES61_4_9			
RSES66_10_10			
rses_57_18_5	altered? Part cloudy; part discontinuous stripes		
RSES63_5_3	patches; spot in dark patch	125x125, necks to 75	
rses_55_new_10_9			
RSES_58_5_14	faint	175X250	
RSES64_6_13			
RSES61_4_10			
RSES67_12_6	cloudy; indeterminate/some osc-iness	75x150	angular
RSES64_9_2	osc		
RSES_58_13_15	patchy over osc		
RSES61_12_8			
RSES_58_13_17	patchy		
RSES62_18_20			
RSES64_2_2			
RSES67_3_11	concentric zones + ropy (alteration?) texture	main: 125x125	angular
RSES67_16_6	complicated; looks like alteration	125x125	angular
RSES67_3_11R	concentric zones + ropy (alteration?) texture	main: 125x125	angular

RSES67_16_2	homogeneous	150x100	rounded
rses_55_new_16_11			
rses_55_new_17_8			
rses_57_15_11	bright sector; altered away from pits?		
rses_57_15_16	osc; alteration away from oxygen (age?)		
rses_57_19_15	osc		
rses_57_2_13	patches?		
RSES_58_19_12	patchy, cloudy		
RSES_58_3_16		100x200	anhedral angular
RSES_58_6_12	homogeneous?	100x150	angular
RSES_58_7_9	osc; core?	150x200	subangular
RSES59_12_2			
RSES59_17_1			
RSES59_18_19	osc		
RSES59_4_18			
RSES59_9_15	cloudy		
RSES60_4_19	faintly cloudy		
RSES60_5_15	homogeneous		
RSES60_6_7	osc	125x300	subrounded
RSES60_7_17	osc		
RSES60_7_5	osc		
RSES60_8_10	look at pic more		
RSES61_1_20			
RSES61_14_16			
RSES61_5_15			
RSES61_8_11			
RSES61_9_19			
RSES62_10_8			
RSES62_2_17			
RSES62_6_10			
RSES62_9_18			
RSES63_1_11	altered? Complicated & uncertain	150x175	angular
RSES63_16_1	cloudy interior, osc rim	125x250	subangular then broken
RSES63_6_4	patches; spot in bright patch	mostly 100x200	subrounded; broken chunk
RSES64_1_16			

RSES64_1_3			
RSES64_11_14	v. faint		
RSES64_12_11	osc		
RSES64_19_2			
RSES64_2_13	osc; core?		
RSES64_5_2			
RSES64_6_1			
RSES64_6_7			
RSES64_7_16	osc+sect		
RSES65_11_6			
RSES65_14_9			
RSES65_20_1			
RSES66_1_9			
RSES66_14_12			
RSES66_6_1			
RSES66_9_2			
RSES67_11_7	homo.; faint stripes across spot	150x150	subrounded
RSES67_11_7R	homo.; faint stripes across spot	150x150	subrounded
RSES67_14_16	patchy (one spot in dark, one spot in ~light)	125x150	subangular
RSES67_14_16R	patchy (one spot in dark, one spot in ~light)	125x150	subangular
RSES67_17_12	faint osc linear	125x150 (necks to 75)	angular, likely broken
RSES67_19_5	osc conc, ~faint	150x150	subangular
rses_55_11_15_dup			
rses_55_6_15_dup			
rses_55_new_10_2			
rses_55_new_11_15			
rses_55_new_19_1			
rses_55_new_3_1	faint osc; dark/disrupted rim?	125x250	anhedral subrounded
rses_55_new_3_7	faint; homogeneous?	150x150	anhedral subangular
rses_55_new_4_9	unclear;	175x200	anhedral subrounded
rses_55_new_6_15	unclear;	175x200	anhedral subrounded
rses_57_1_3	osc linear		
rses_57_19_12	patchy		
RSES_58_3_4	homogeneous?	150x200	anhedral subangular
RSES_58_4_16	osc	150x300	rounded

RSES59_11_7			
RSES59_2_17	cloudy/patchy		
RSES59_4_11			
RSES59_5_2	homogeneous		
RSES59_8_14	stripey		
RSES59_8_4			
RSES60_10_19	osc; other…		
RSES60_16_1	osc; altered		
RSES60_6_18	patchy/cloudy		
RSES60_7_19	osc		
RSES60_8_8	not in mount		
RSES61_10_8			
RSES61_12_10			
RSES61_12_13			
RSES61_13_11			
RSES61_15_11			
RSES61_16_1	not in mount		
RSES61_18_8			
RSES61_5_9			
RSES61_8_2			
RSES62_15_17			
RSES62_2_7			
RSES62_20_18			
RSES62_6_12			
RSES63_14_5	cloudy interior, osc or altered rim	main: 125x150	angular
RSES64_10_7	faint osc + bright stripe		
RSES64_5_13			
RSES65_10_12			
RSES65_18_9			
RSES65_3_6			
RSES65_9_1	not in mount		
RSES66_12_18			
RSES66_13_14			
RSES66_3_16			
RSES66_5_18			

RSES66_6_12			
RSES67_10_11	faint rimming osc; brighter region in center	100x175	subangular
RSES67_10_11R	faint rimming osc; brighter region in center	100x175	subangular
RSES67_15_16	patchy/altered	125x125	angular, concave
RSES67_19_13	faint osc conc; bright outer rim (altered?)	125x125	subangular

Table G.2: Oxygen isotope and morphology data for Hadean zircons in supplemental oxygen isotope dataset used in chapters four and five. Oxygen isotope data collected by Dr. Haibo Zhou; imaging by Elizabeth Bell.

Appendix H: Xenon Isotope Data from Chapter Five

								Component Fractions			based on 238U	
Sample	**131Xe/ 134Xe**	**1 s.d.**	**132Xe/1 34Xe**	**1 s.d.**	**131/134 % err**	**7/6 age (ma)**	**% conc**	**U238**	**Pu244**	**U235**	**(Pu/8U)o**	**1 s.d.**
ANU 31-4.10	0.1944	0.0088	0.6782	0.0185	5	4118	93	0.55	0.12	0.34	0.0022	0.0001
ANU 33-13.6	0.1814	0.0101	0.6615	0.0221	6	4063	92	0.63	0.05	0.33	0.0012	0.0001
ANU 33-13.6	0.2184	0.0114	0.6703	0.0231	5	4063	92	0.43	0.14	0.43	0.0051	0.0003
ANU 33-12.14	0.1979	0.0088	0.6380	0.0183	4	4001	97	0.56	0.01	0.43	0.0004	0.0000
ANU 33-12.14	0.2206	0.0028	0.6530	0.0059	1	4001	97	0.43	0.09	0.47	0.0057	0.0001
ANU 31-12.12	0.1782	0.0074	0.6489	0.0163	4	4064	93	0.65	0.01	0.34	0.0001	0.0000
ANU 33-7.15	0.2075	0.0046	0.6514	0.0095	2	4004	98	0.50	0.06	0.43	0.0033	0.0001
ANU 33-15.11	0.1962	0.0060	0.7048	0.0138	3	4196	96	0.52	0.20	0.28	0.0021	0.0001
ANU 33-11.15	0.2135	0.0048	0.6599	0.0099	2	4117	96	0.46	0.10	0.44	0.0022	0.0001
ANU 31-10.11	0.1620	0.0076	0.6609	0.0172	5	4040	93	0.72	0.01	0.26	0.0003	0.0000
ANU 31-14.3	0.2033	0.0067	0.6426	0.0134	3	4121	95	0.53	0.03	0.44	0.0006	0.0000
ANU 31-15.8	0.1996	0.0081	0.6444	0.0167	4	4111	95	0.55	0.03	0.42	0.0006	0.0000
ANU 31-8.4	0.1415	0.0125	0.5910	0.0257	9	4111	94	0.88	-0.23	0.34	-0.0028	-0.0003

	based on 235U						
Sample	**(Pu/U)o**	**% diff 235/238 Pu est.**	**U-Xe Age (Ma)**	**1 s.d. to value**	**U-Xe/Pb-Pb % disc**	**d18O**	**1 s.d.**
ANU 31-4.10	0.0014	-36	2912	153	41	5.0	0.9
ANU 33-13.6	0.0009	-24	3304	215	23	5.8	0.8

ANU 33-13.6	0.0020	-60	1934	121	110		
ANU 33-12.14	0.0002	-47	2414	128	66	7.1	0.6
ANU 33-12.14	0.0021	-63	1785	28	124		
ANU 31-12.12	0.0001	-24	3283	160	24	5.5	0.9
ANU 33-7.15	0.0016	-53	2183	58	83	6.2	0.8
ANU 33-15.11	0.0014	-31	3174	116	32	6.8	0.5
ANU 33-11.15	0.0009	-58	2037	55	102	6.5	0.7
ANU 31-10.11	0.0003	10	4339	233	-7	4.6	0.9
ANU 31-14.3	0.0003	-53	2266	89	82	5.9	0.9
ANU 31-15.8	0.0003	-49	2402	116	71	5.5	0.9
ANU 31-8.4	-0.0028	1	4128	405	0	4.6	0.9

Table H.1: Xenon isotope and age data for Jack Hills zircons. U-Pb age data from Trail et al. (2007).

Appendix I: Parameters Used in Subduction Models

Our models are run in a Cartesian coordinate system, using a box 700 km high and 2000 km in length. The upper 100 km contains tracers of "sticky air" to create a free slip surface for the lithosphere. The remaining 600 km represent the crust and upper mantle and are broken into the lithosphere (populated by "crust" tracers, although no distinction is made between crust and lithospheric mantle) and the ambient mantle (populated by "mantle" tracers). Initial geometry of the models consists of lithospheric plates of various dimensions at the top of the modeled earth (below the sticky air in the model box).

Quantity	**Value**
Lower Plate	
thickness	varied
length	900 km
initial deflection	200 km
radius of curvature	400 km
internal friction coefficient	0
cohesion	$6x10^{-8}$
viscosity	varied
Upper Plate	
thickness	varied
length	
internal friction coefficient	0
cohesion	$6x10^{-8}$
viscosity	varied
Ambient Mantle	
reference T	1650 K
reference viscosity	$2x10^{20}$ Pa s
internal friction coefficient	0.5
cohesion	$6x10^{-7}$
Other	
T at base of lithosphere	1600 K
T at surface	300 K
thermal diffusivity	$1x10^{-6}$ m^2/s
initial plate gap	50 km

Table I.1: Various properties of the models in chapter 6 and their initial geometries.

References

Abbott, D., Burgess, L., Longhi, J., Smith, W.H.F., 1994. An empirical thermal history of the Earth's upper mantle. Journ. Geophys. Res.99, 13,835-13,850.

Abbott, S.S., Harrison, T.M., Schmitt, A.K., Mojzsis, S.J. 2012. Ti-U-Th-Pb depth profiling of Hadean zircons: A search for evidence of ancient extraterrestrial impacts. Proc. Nat. Acad. Sci. 109, 13486-13492.

Abramov, O., Kring, D.A., Mojzsis, S.J., 2013. The impact environment of the Hadean Earth. In press at Chemie der Erde.

Abramov, O., Mojzsis, S.J., 2009. Microbial habitability of the Hadean Earth during the late heavy bombardment. Nature 459, 419-422.

Aikman, A.B., 2007. Tectonics of the eastern Tethyan Himalaya. Ph.D. thesis. Australian National University.

Amelin, Y.V., 1998. Geochronology of the Jack Hills detrital zircons by precise U-Pb isotope dilution analysis of crystal fragments. Chem. Geol. 146, 25-38.

Amelin, Y.V., Lee, D.C., Halliday, A.N., 2000. Early-Middle Archean crustal evolution deduced from Lu-Hf and U-Pb isotopic studies of single zircon grains. Geochim. Cosmochim. Acta 64, 4205-4225.

Amelin, Y.V., Lee, D.C., Halliday, A.N., Pidgeon, R.T., 1999. Nature of the Earth's earliest crust from hafnium isotopes in single detrital zircons. Nature 399, 252–255.

Belousova, E.A., Griffin, W.L., O'Reilly, S.Y., Fisher, N.I., 2002. Igneous zircon: trace element composition as an indicator of source rock type. Contrib. Mineral. Petrol.143, 602–622.

Bennett, V.C., McCulloch, M.T., Nutman, A.P., and Kinny, P.D., 1990. Combined Sm-Nd isotopic systematics and U-Pb zircon characteristics in the Narryer Gneiss Complex, Western Australia: Implications for Archean crustal genesis. Intl. Archean Symp. 3rd, 9-10.

Bindeman, I.N., Schmitt, A.K., Valley, J.W., 2006. U–Pb zircon geochronology of silicic tuffs from the Timber Mountain/Oasis Valley caldera complex, Nevada: rapid generation of large volume magmas by shallow-level remelting. Contrib. Mineral. Petrol. 152, 649-665.

Blichert-Toft, J., Albarède, F., 2008. Hafnium in Jack Hills zircons and the formation of the Hadean crust. Earth Planet. Sci. Lett. 265, 686–702.

Booth, A. L., Y. Kolodny, C. P. Chamberlain, M. McWilliams, A. K. Schmitt, and J. Wooden (2005), Oxygen isotopic composition and U-Pb discordance in zircon, Geochim. Cosmochim. Acta, 69, 4895–4905.

Bouvier A., Vervoort J.D., Patchett P.J., 2008. The Lu-Hf and Sm-Nd isotopic composition of CHUR: constraints from unequilibrated chondrites and implications for the bulk composition of terrestrial planets. Earth Planet. Sci. Lett. 273, 48–57.

Bouvier, A., Wadhwa, M., 2010. The age of the Solar System redefined by the oldest Pb–Pb age of a meteoritic inclusion. Nat. Geo. 3, 637-641.

Bowring, S.A., and Williams, I.S., 1999. Priscoan (4.00-4.03 Ga) orthogneisses from northwestern Canada.Contrib. Mineral. Petrol. 134, 3-16.

Boyet, M., Carlson, R.W., 2005. ^{142}Nd evidence for early (>4.53 billion years ago) global differentiation of the silicate Earth. Science 309, 576–581.

Caro, G., Bennett, V.C., Bourdon, B., Harrison, T.M., von Quadt, A., Mojzsis, S.J., Harris, J.W., 2008. Application of precise ^{142}Nd/^{144}Nd analysis of small samples to inclusions in diamonds (Finsch, South Africa and Hadean zircons (Jack Hills, Western Australia). Chem. Geol. 247, 253-265.

Caro, G., Bourdon, B., Birck, J., Moorbath, S., 2003. Sm-Nd evidence from Isua metamorphosed sediments for early differentiation of the Earth's mantle. Nature 423, 428-432.

Cates, N.L., Mojzsis, S.J., 2009. Metamorphic zircon, trace elements, and Neoarchean metamorphism in the ca. 3.75 Ga Nuvvuagittuq supracrustal belt, Quebec (Canada). Chem. Geol. 261, 98-113.

Cates, N.L., Ziegler, K., Schmitt, A.K., Mojzsis, S.J., 2013. Reduced, reused and recycled: Detrital zircons define a maximum age for the Eoarchean (ca. 3750–3780 Ma) Nuvvuagittuq Supracrustal Belt, Québec (Canada). Earth Planet. Sci. Lett. 362, 283–293.

Cavosie, A.J., Quintero, R.R., Radovan, H.A., Moser, D.E., 2010. A record of ancient cataclysm in modern sand: Shock microstructures in detrital minerals from the Vaal River, Vredefort Dome, South Africa. GSA Bulletin 122, 1968-1980.

Cavosie, A.J., Valley, J.W., Wilde, S.A., E.I.M.F., 2005. Magmatic δ^{18}O in 4400-3900 Ma detrital zircons: A record of the alteration and recycling of crust in the Early Archean. Earth Planet. Sci. Lett. 235, 663-681.

Cavosie, A.J., Wilde, S.A., Liu, D., Weiblen, P.W., Valley, J.W., 2004. Internal zoning and U-Th-Pb chemistry of Jack Hills detrital zircons: a mineral record of early Archean to Mesoproterozoic (4348-1576 Ma) magmatism. Precambr. Res. 135, 251-279.

Choukroun, M., O'Reilly, S.Y., Griffin, W.L., Pearson, N.J., Dawson, J.B., 2005. Hf isotopes of MARID (mica-amphibole-rutile-ilmenite-diopside) rutile trace metasomatic processes in the lithospheric mantle. Geology 33, 45-48.

Claiborne, L.L., Miller, C.F., Wooden, J.L., 2010. Trace element composition of igneous zircon: a thermal and compositional record of the accumulation and evolution of a large silicic batholith, Spirit Mountain, Nevada. Contrib. Mineral. Petrol. 160, 511-531.

Cohen, B.A., Swindle, T.D., Kring, D.A., 2000. Support for the lunar cataclysm hypothesis from lunar meteorite impact melt ages. Science 290, 1754-1756.

Collins, W.J., Belousova, E.A., Kemp, A.I.S., Murphy, J.B., 2011. Two contrasting Phanerozoic orogenic systems revealed by Hf isotopic data. Nat. Geosci. 4, 333-337.

Compston, W., Pidgeon, R.T., 1986. Jack Hills, evidence of more very old detrital zircons in Western Australia. Nature 321, 766–769.

Condie, K.C., 1993. Chemical composition and evolution of the upper continental crust: contrasting results from surface samples and shales. Chem. Geol. 104, 1–37.

Condie, K.C., 2008. Did the character of subduction change at the end of the Archean? Constraints from convergent-margin granitoids. Geology 36, 611-614.

Connelly, J.N., Amelin, Y., Krot, A.N., Bizzarro, M., 2008. Chronology of the solar system's oldest solids. Astrophys. J. 675, L121–L124.

Coogan, L.A., Hinton, R.W., 2006. Do the trace elements compositions of detrital zircons require Hadean continental crust? Geology 34, 633-636.

Corfu, F., Hanchar, J.M., Hoskin, P.W.O., Kinny, P., 2003. Atlas of zircon textures. In Hanchar, J.M., Hoskin, P.W.O, eds., Zircon. Rev. Mineral. 53, 469-500.

Crowley J.L., Myers J.S., Sylvester P.J., Cox R.A., 2005. Detrital zircon from the Jack Hills and Mount Narryer, Western Australia: Evidence for diverse >4.0 Ga source rocks. J. Geol. 113, 239–63.

Crowther, S.A., Mohapatra, R.K., Turner, G., Blagburn, D.J., Kehm, K., Gilmour, J.D., 2008. Characteristics and applications of RELAX, an ultrasensitive resonance ionization mass spectrometer for xenon. Journ. Anal. Atom. Spec. 27, 938-947.

Darling, J., Storey, C., Hawkesworth, C., 2009.Impact melt sheet zircons and their implications for the Hadean crust. Geology 37, 927-930.

Darling, J.R., Moser, D.E., 2012. Impact induced crustal differentiation: New insights from the Sudbury Structure. LPSC XLIII.

Dauphas, N., Chaussidon, M. 2011. A perspective from extinct radionuclides on a young stellar object: the sun and its accretion disk. Ann. Revs. Earth Planet. Sci. 39, 351-386.

Dauphas, N., Marty, B., 2002. Inference on the Nature and the Mass of Earth's Late Veneer from Noble Metals and Gases. J. Geophys. Res. 107, 12-1 – 12-7.

Davies, G.F., 1992. On the emergence of plate tectonics. Geology 20, 963-966.

Davies, G.F., 2006. Gravitational depletion of the early Earth's upper mantle and the viability of early plate tectonics. Earth Planet. Sci. Lett. 243, 376-382.

Debaille, V., O'Neill, C., Brandon, A.D., Haenecour, P., Yin, Q.-Z., Mattielli, N., Treiman, A.H., 2013.Stagnant-lid tectonics in early Earth revealed by ^{142}Nd variations in late Archean rocks. In press at Earth Planet. Sci. Lett.

DeCelles, P.G., Ducea, M.N., Kapp, P., and Zandt, G., 2009, Cyclicity in Cordilleran orogenic systems: Nat. Geosci., 2, 251–257.

DeLaeter, J.L., Fletcher, I.R., Bickle, M.J., Myers, J.S., Libby, W.G., Williams, I.R., 1985. Rb-Sr, Sm-Nd and Pb-Pb geochronology of ancient gneisses from Mt. Narryer, Western Australia. Australian J. Earth Sci. 32, 349-358.

Dhuime, B., Hawkesworth, C.J., Cawood, P.A., Storey, C.D., 2012. A change in the geodynamics of continental growth 3 billion years ago. Science 335, 1334-1336.

Dickinson, W.R., 2008. Impact of differential zircon fertility of granitoid basement rocks in North America on age populations of detrital zircons and implications for granite petrogenesis. Earth Planet. Sci. Lett. 275, 80-92.

England, P., Houseman, G., 1989. Extension during continental convergence, with application to the Tibetan Plateau. Journ. Geophys. Res. 94, no. B12, 17,561-17,579.

Ferry, J.M., Watson, E.B., 2007.New thermodynamic models and revised calibrations for the Ti-in-zircon and Zr-in-rutile thermometers.Contrib. Mineral. Petrol. 154, 429-437.

Finch, R.J., Hanchar, J.M., 2003.Structure and chemistry of zircon and zircon-group minerals. In Hanchar, J.M., Hoskin, P.W.O, eds., Zircon. Rev. Mineral. 53, 1-25.

Fletcher, I.R., Rosman, K.J.R., Libby, W.G., 1988. Sm-Nd, Pb-Pb and Rb-Sr geochronology of the Manred Complex, Mount Narryer, Western Australia. Precambr. Res. 38, 343-354.

Fu, B., Page, F.Z., Cavosie, A.J., Fournelle, J., Kita, N.T., Lackey, J.S., Wilde, S.A., Valley, J.W., 2008. Ti-in-zircon thermometry: applications and limitations. Contrib. Mineral. Petrol. 156, 197-215.

Fung, A.T., Haggerty, S.E., 1995. Petrography and mineral compositions of eclogites from the Koidu Kimberlite Complex, Sierra Leone. Journ. Geophys. Res.100, 20,451-20,473.

Gerya, T.V., 2011. Intra-oceanic subduction zones. In D. Brown and P.D. Ryan (eds.), Arc-Continent Collision, Frontiers in Earth Sciences, Springer-Verlag Berlin Heidelberg 2011.

Gerya, T.V., Connolly, J.A.D., Yuen, D.A., 2008. Why is terrestrial subduction one-sided? Geology36 43–46.

Gilmour, J.D.; Lyon, I.C.; Johnston, W.A.; Turner, G.; 1994. RELAX: an ultrasensitive, resonance ionization mass spectrometer for xenon. Rev. Sci. Instrum. 65, 617-625.

Gomes, R., Levison, H.F., Tsiganis, K., Morbidelli, A., 2005. Origin of the cataclysmic Late Heavy Bombardment period of the terrestrial planets. Nature 435: 466-469.

Grange, M.L., Wilde, S.A., Nemchin, A.A., Pidgeon, R.T., 2010. Proterozoic events recorded in quartzite cobbles at Jack Hills, Western Australia: New constraints on sedimentation and source of >4 Ga zircons. Earth Planet Sci. Lett. 292, 158-169.

Gregory, R. T., Taylor, H. P., Jr., 1981. An oxygen isotope profile in a section of Cretaceous oceanic crust, Samail Ophiolite, Oman: Evidence for δ18O buffering of the oceans by deep (>5 km) seawater-hydrothermal circulation. J. Geophys. Res. 86, 2737-2755.

Grieve, R.A.F., Cintala, M.J., Therriault, A.M., 2006. Large-scale impacts and the evolution of the Earth's crust: The early years. In Reimold W.U., Gibson, R.L. (eds.), Processes of the Early Earth. Geological Society of America Special Paper 405, 22-31.

Griffin, W.L., Belousova, E.A., Shee, S.R., Pearson, N.J., O'Reilly, S.Y., 2004. Archean crustal evolution in the northern Yilgarn Craton: U–Pb and Hf-isotope evidence from detrital zircons. Precam. Res. 131, 231-282.

Grimes, C.B., John, B.E., Kelemen, P.B., Mazdab, F.K.,Wooden, J.L., Cheadle, M.J.,Hanghøj, K., Schwartz, J.J., 2007. Trace element chemistry of zircons from oceanic crust: A method for distinguishing detrital zircon provenance. Geology 35, 643–646.

Guitreau, M., Blichert-Toft, J., Martin, H., Mojzsis, S.J., Albarede, F., 2012. Hafnium isotope evidence from Archean granitic rocks for deep-mantle origin of continental crust. Earth Planet. Sci. Lett. 337–338, 211–223.

Hall, C.E., Gurnis, M., Sdrolias, M., Lavier L.L.,Muller, R.D., 2003.Catastrophic initiation of subduction following forced convergence across fracture zones. Earth Planet. Sci. Lett.212, 15-30.

Hamilton, W.B., 1998. Archean magmatism and deformation were not products of plate tectonics. Precam. Res. 91, 143-179.

Harrison T.M., Schmitt A.K., McCulloch M.T., Lovera O.M., 2008. Early (≥4.5 Ga) formationof terrestrial crust: Lu-Hf, δ18O, and Ti thermometry results for Hadean zircons. Earth Planet. Sci. Lett.268, 476–86.

Harrison, T.M., 2009. The Hadean crust: Evidence from >4 Ga zircons. Annu. Rev. Earth. Planet. Sci. 37, 479-505.

Harrison, T.M., Blichert-Toft, J., Müller,W., Albarede, F., Holden, P., Mojzsis, S.J., 2005. Heterogeneous Hadean hafnium: evidence of continental crust by 4.4–4.5 Ga. Science 310, 1947–1950.

Harrison, T.M., Schmitt, A.K., 2007. High sensitivity mapping of Ti distributions in Hadean zircons. Earth Planet. Sci. Lett. 261, 9-19.

Harrison, T.M., Watson, B.E., Aikman, A.B., 2007. Temperature spectra of zircon crystallization in plutonic rocks. Geology 35, 635-638.

Hartmann, W.K., 1975. Lunar "cataclysm": A misconception? Icarus 24: 181–187.

Hassani, R.,Jongmans, D., 1997. Study of plate deformation and stress in subduction processes using two-dimensional numerical models. Journ.Geophys. Res.102, 17,951-17,965.

Herzberg, C., Condie, K., Korenaga, J., 2010. Thermal history of the Earth and its petrological expression. Earth Planet. Sci. Lett. 292, 79-88.

Holden, P., Lanc, P., Ireland, T.R., Harrison, T.M., Foster, J.J., Bruce, Z., 2009. Mass-spectrometric mining of Hadean zircons by automated SHRIMP multi-collector and single-collector U/Pb zircon age dating: The first 100,000 grains. Int. J. Mass Spec. 286, 53-63.

Holzheid, A., Sylvester, P., O'Neill, H. St C., Rubie, D.C., Palme, H., 2000. Evidence for a late chondritic veneer in the Earth's mantle from high-pressure partitioning of palladium and platinum. Nature 406, 396-399.

Hopkins, M., Harrison, T.M., Manning, C.E. 2008. Low heat flow inferred from >4 Gyr zircons suggests Hadean plate boundary interactions. Nature 456, 493-496.

Hopkins, M., Harrison, T.M., Manning, C.E. 2010. Constraints on Hadean geodynamics from mineral inclusions in >4 Ga zircons. Earth Planet. Sci. Lett. 298, 367-376.

Hoskin, P.W.O., 2005. Trace-element composition of hydrothermal zircon and the alteration of Hadean zircon from the Jack Hills, Australia. Geochim. Cosmochim. Acta 69, 637-648.

Hoskin, P.W.O., Black, L.P., 2000. Metamorphic zircon formation by solid-state recrystallization of protolith igneous zircon.J. Meta. Geol. 18, 423-439.

Hoskin, P.W.O., Kinny, P.D., Wyborn, B., Chappell, B.W., 2000. Identifying accessory mineral saturation during differentiation of granitoid magmas: an integrated approach. J. Pet. 41, 1365-1396.

Hoskin, P.W.O., Schaltegger, U., 2003. The composition of zircon and igneous and metamorphic petrogenesis. In Hanchar, J.M., Hoskin, P.W.O., eds., Zircon. Rev. Mineral. 53, 343-385.

Hudson, G.B., Kennedy, B.M., Podosek, F.A., Hohenberg, C.M., 1989. The early solar system abundance of 244Pu as inferred from the St. Severin Chondrite. Proc. 19th Lunar and Planetary Sci. Conf., 547-557.

Iizuka, T., Komiya, T., Johnson, S.P., Kon, Y., Maruyama, S., Hirata, T., 2009. Reworking of Hadean crust in the Acasta gneisses, northwestern Canada: Evidence from in-situ Lu–Hf isotope analysis of zircon. Chem. Geol. 259, 230–239.

Jones, J.H., Burnett, D.S., 1987. Experimental geochemistry of Pu and Sm and the thermodynamics of trace element partitioning. Geochim. Cosmochim. Acta 51, 769-782.

Kemp, A.I.S., Wilde, S.A., Hawkesworth, C.J., Coath, C.D., Nemchin, A., Pidgeon, R.T., Vervoort, J.D., DuFrane, S.A., 2010. Hadean crustal evolution revisited: New constraints from Pb-Hf isotope systematics of the Jack Hills zircons. Earth Planet. Sci. Lett. 296, 45-56.

Kersting, A.B., Efurd, D.W., Finnegan, D.L., Rokop, D.J., Smith, D.K., and Thompson, J.L. 1999. Migration of plutonium in groundwater at the Nevada Test Site. Nature 397, 56-59.

Kinny, P.D., Williams, I.S., Froude, D.O., Ireland, T.R., Compston, W., 1988. Early Archaean zircon ages from orthogneisses and anorthosites at Mount Narryer, Western Australia. Precambr. Res. 38, 325-341.

Klecka, W.R., 1980. Discriminant Analysis.Quantitative Applications in the Social Sciences (ed. J.L. Sullivan), Sage Publications, Beverly Hills, CA, 70 p.

Kleine, T., Touboul, M., Bourdon, B., Nimmo, F., Mezger, K., Palme, H., Jacobsen, S.B., Yin, Q.-Z., Halliday, A.N., 2009. Hf–W chronology of the accretion and early evolution of asteroids and terrestrial planets. Geochim. Cosmochim. Acta 73, 5150–5188.

Kober, B., Pidgeon, R.T., Lippolt, H.J., 1989. Single-zircon dating by stepwise Pb-evaporation constrains the Archean history of detrital zircons from the Jack Hills, Western Australia. Earth Planet. Sci. Lett. 91, 286-296.

Koelling, D.D., 1985. Cerium compounds in the fashion of the light actinides. Physica 130B, 135-137.

Korenaga, J., 2008. Urey ratio and the structure and evolution of Earth's mantle.Rev. Geophys. 46, 2007RG000241.

Korenaga, J., 2013. Initiation and evolution of plate tectonics on Earth: theories and observations. Annu. Rev. Earth Planet. Sci. 41, 117-151.

Kring, D.A., Cohen, B.A., 2002. Cataclysmic bombardment throughout the inner solar system 3.9-4.0 Ga. Journ.Geophys.Res. 107, no.E2, 5009.

Langmuir, D. 1978. Uranium solution-mineral equilibria at low temperatures with application to sedimentary ore deposits. Geochim. Cosmochim. Acta 42, 547-69.

Linnen, R.L., Keppler, H., Melt composition control of Zr/Hf fractionation in magmatic processes. Geochim. Cosmochim. Acta 66, 3293-3301.

Liu, L., Stegman, D.R., 2011. Segmentation of the Farallon slab. Earth Planet. Sci. Lett. 311, 1-10.

Lugmair, G.W., Marti, K., 1977. Sm-Nd-Pu timepieces in the Angra dos Reis meteorite. Earth Planet. Sci. Lett. 35, 273-284.

Maas, R., McCulloch, M.T., 1992. The provenance of Archean clastic metasediments in the Narryer Gneiss Complex, Western Australia: Trace element geochemistry, Nd isotopes, and U-Pb ages for detrital zircons. Geochim. Cosmochim. Acta 55, 1915-1932.

Maher, K., Bargar, J.R., Brown, G.E., Jr., 2013. Environmental speciation of actinides. Inorg. Chem. 52, 3510–3532.

Martin, H., 1986. Effect of steeper Archean geothermal gradient on geochemistry of subduction-zone magmas. Geology 14, 753-756.

Maurer P., Eberhardt P., Geiss I., Grögler N., Stettler A., Brown G.M., Peckett A., and Krähenbühl U. (1978) Pre-Imbrian craters and basins: Ages, compositions and excavation depths of Apollo 16 breccias. Geochim.Cosmochim. Acta 42, 1687-1720.

McClave, J.T., Sincich, T., 2006.Statistics, 10th edition.Pearson/Prentice Hall, Upper Saddle River, NJ, 935 p.

McLennan, S.M., Taylor, S.R., 1982. Geochemical constraints on the growth of the continental crust. J. Geol. 90, 347-361.

Mezger, K., Krogstad, E.J., 1997. Interpretation of discordant U-Pb zircon ages: An evaluation. J. Meta. Geol. 15, 127-140.

Mojzsis, S.J., Harrison, T.M., Pidgeon, R.T., 2001. Oxygen-isotope evidence from ancient zircons for liquid water at the Earth's surface 4300 Myr ago. Nature 409, 178–181.

Molnar, P., England, P., Martinod, J., 1993. Mantle dynamics, uplift of the Tibetan Plateau, and the Indian Monsoon. Revs. Geophys. 31, 357-396.

Muehlenbacks, K., Clayton, R.N., 1976. Oxygen isotope composition of the oceanic crust and its bearing on seawater. Journ. Geophys. Res. 81, 4365-4369.

Murrell, M.T., Burnett, D.S., 1983. The behavior of a~tinides, phosphorus, and rare earth elements during chondrite metamorphism. Geochim. Cosmochim. Acta 47, 1999-2014.

Myers, J.S., 1988a. Early Archaean Narryer Gneiss Complex, Yilgarn Craton, Western Australia. Precambr. Res. 38, 297-307.

Myers, J.S., 1988b. Oldest known terrestrial anorthosite at Mount Narryer, Western Australia. Precambr. Res. 38, 309-323.

Naeraa, T., Schersten, A., Rosing, M.T., Kemp, A.I.S., Hofmann, J.E., Kokfelt, T.F.,Whitehouse, M.J., 2012. Hafnium isotope evidence for a transition in the dynamics of continental growth 3.2 Gyr ago. Nature 485, 627-630.

Nebel-Jacobsen, Y., Munker, C., Nebel, O., Gerdes, A., Mezger, K., Nelson, D.R., 2010. Reworking of Earth's first crust: Constraints from Hf isotopes in Archean zircons from Mt. Narryer, Australia. Precambr. Res.182, 175-186.

Nutman, A.P., 2006. Antiquity of the oceans and continents. Elements 2, 223-227.

Nutman, A.P., Kinny, P.D., Compston, W., Williams, I.S., 1991. SHRIMP U-Pb zircon geochronology of the Narryer Gneiss Complex, Western Australia. Precambr. Res. 52, 275-300.

O'Neil, J., Boyet, M., Carlson, R.W., Paquette, J.-L., 2013. Half a billion years of reworking of Hadean mafic crust to produce the Nuvvuagittuq Eoarchean felsic crust. Earth Planet. Sci. Lett. 379, 13–25.

O'Neil, J., Carlson, R.W., Francis, D., Stevenson, R.K., 2008. Neodymium-142 evidence for Hadean mafic crust. Science 321, 1828-1831.

O'Neill, C., Lenardic, A., Moresi, L., Torsvik, T.H., Lee, C.-T. A., 2007. Episodic Precambrian subduction. Earth Planet. Sci. Lett. 262, 552-562.

Ozima, M.; Podosek, F.A.; 2002. Noble Gas Geochemistry, 2nd ed. Cambridge University

Paces, J. B., J. D. Miller, 1993. Precise U-Pb ages of Duluth Complex and related mafic intrusions, northeastern Minnesota: Geochronological insights into physical, petrogenetic, and paleomagnetic and tectonomagnetic processes associated with the 1.1 Ga mid-continent rift system, J. Geophys. Res. 98, 13,997–14,013.

Peck, W.H., Valley, J.W., Wilde, S.A., Graham, C.M., 2001. Oxygen isotope ratios and rare earth elements in 3.3-4.4 Ga zircons: Ion microprobe evidence for high $\delta^{18}O$ continental crust and oceans in the Early Archean. Geochim. Cosmochim. Acta 65, 4215-4299.

Pidgeon, R.T., Nemchin, A.A., Hitchen, G.J., 1998. Internal structures of zircons from Archaean granites from the Darling Range batholith: implications for zircon stability and the interpretation of zircon U-Pb ages. Contrib. Mineral. Petrol. 32, 288-299.

Pietranik, A.B., Hawkesworth, C.J., Storey, C.D., Kemp, A.I.S., Sircombe, K.N., Whitehouse, M.J., Bleeker, W., 2008. Episodic, mafic crust formation from 4.5 to 2.8 Ga: New evidence from detrital zircons, Slave craton, Canada. Geology 36, 875-878.

Rey, P.F., Coltice, N., 2008. Neoarchean lithospheric strengthening and the coupling of Earth's geochemical reservoirs. Geology 36, 635-638.

Rudnick, R.L., Gao, S., 2003. Composition of the continental crust. In Rudnick, R.L., ed., The Crust, Treatise on Geochemistry 3, 1-64.

Ryder G., Koeberl C., Mojzsis S. (2000) Heavy Bombardment of the Earth at ~3.85: The search for petrographic and geochemical evidence. Origin of the Earth and Moon.Tucson, AZ, Univ. Press Tucson. pp. 475-492.

Ryder, G., 2002. Mass flux in the ancient Earth-Moon system and benign implications for the origin of life on Earth. J. Geophys. Res. 107, 6-1 – 6-13.

Sarbas, B., 2008. The GEOROC database as part of a growing geoinformatics network. In: Brady, S.R., Sinha, A.K., and Gundersen, L.C. (editors): Geoinformatics 2008—Data to Knowledge, Proceedings: U.S. Geological Survey Scientific Investigations Report 2008-5172, 42-43.

Scholl, D.W., von Huene, R., 2010. Subduction zone recycling processes and the rock record of crustal suture zones. Can. J. Earth Sci. 47, 633-654.

Shirey, S.B., Richardson, S.H., 2011. Start of the Wilson Cycle at 3 Ga shown by diamonds from subcontinental mantle. Science 333, 434-436.

Shukolyukov, Y.A.; Fugzan, M.M.; Paderin, I.P.; Sergeev, S.A.; Krylov, D.P.; 2009. Unusually high thermal stability of the uranium-xenon isotopic system in nonmetamict zircons. Doklady Earth Sciences 424, 814-817.

Sizova, E., Gerya, T., Brown, M., Perchuk, L.L., 2010. Subduction styles in the Precambrian: Insight from numerical experiments. Lithos 116, 209-229.

Sleep, N.H., 2000. Evolution of the mode of convection within terrestrial planets. J. Geophys. Res. 105, 17563-17568.

Sobolev, S.V., Babeyko, A.Y., 2005. What drives orogeny in the Andes? Geology33, 617-620.

Soderlund, U., Patchett, J.P., Vervoort, J.D., Isachsen, C.E., 2004. The ^{176}Lu decay constant determined by Lu-Hf and U-Pb isotope systematics of Precambrian mafic intrusions. Earth Planet. Sci. Lett. 219, 311-324.

Spaggiari, C.V., Pidgeon, R.T., Wilde, S.A., 2007. The Jack Hills greenstone belt, Western Australia Part 2: Lithological relationships and implications for the deposition of ≥4.0 Ga detrital zircons. Precambr. Res. 155, 261-286.

Staudigal, H., Plank, T., White, W., Schmincke, H.-U., 1996. Geochemical Fluxes During Seafloor Alteration of the Basaltic Upper Oceanic Crust, DSDP Sites 417 and 418. In Bebout, E., Scholl, W., Kirby, H., Platt, P. (Eds.) Subduction: Top to Bottom, Geophysical Monograph 96, American Geophysical Union.

Stegman, D.R., Farrington, R., Capitanio, F.A.,Schellart, W.P., 2010. A regime diagram for subduction styles from 3-D numerical models of free subduction. Tectonophys.483, 29–45.

Stern, R.J., 2004. Evidence from ophiolites, blueschists, and ultrahigh-pressure metamorphic terranes that the modern episode of subduction tectonics began in Neoproterozoic time. Geology 33, 557-560.

Stern, R.J., 2007. When and how did plate tectonics begin? Theoretical and empirical considerations. Chinese Science Bulletin 52, 578-591.

Stern, R.J., Tsujimori, T., Harlow, G., and Groat, L.A., 2013. Plate tectonic gemstones. In press at Geology.

Tackley, P.J., 2008. Modelling compressible mantle convection with large viscosity contrasts in a three-dimensional spherical shell using the yin-yang grid. Phys. Earth Planet. Int. 171 7-18.

Taylor, D.J., McKeegan, K.D., Harrison, T.M., 2008. ^{176}Lu-^{177}Hf zircon evidence for rapid lunar differentiation. Earth Planet. Sci. Lett., 279, 157-164.

Taylor, S.R., McLennan, S.M., 1985. The Continental Crust: its Composition and Evolution. Blackwell, Oxford, UK, 311 p.

Tera, F., Papanastassiou D.A, Wasserburg G., 1974. Isotopic evidence for a terminal lunar cataclysm. Earth Planet. Sci. Lett., 22, 1-21.

Thern, E.R., Nelson, D.R., 2012. Detrital zircon age structure within ca. 3 Ga metasedimentary rocks, Yilgarn Craton: Elucidation of Hadean source terranes by principal component analysis. Precam. Res. 214-215, 28-43.

Thirlwall, M.F., Anczkiewicz, R., 2004. Multidynamic isotope ratio analysis using MC-ICP-MS and the causes of secular drift in Hf, Nd and Pb isotope ratios. Int. J. Mass Spec. 235, 59–81.

Touboul, M., Puchtel, I.S., Walker, R.J., 2012. ^{182}W Evidence for Long-Term Preservation of Early Mantle Differentiation Products. Science 335, 1065-1069.

Trail, D., Mojzsis, S.J., Harrison, T.M., 2007a. Thermal events documented in Hadean zircons by ion microprobe depth profiles. Geochim.Cosmochim. Acta 71, 4044-4065.

Trail, D., Mojzsis, S.J., Harrison, T.M., Schmitt, A.K., Watson, E.B., Young E.D., 2007b. Constraints on Hadean zircon protoliths from oxygen isotopes, REEs and Ti-thermometry. Geochem. Geophys. Geosyst. 8, Q06014.

Turner G. (1977) Potassium-argon chronology of the moon.Phys. Chem. Earth 10, 145-195.

Turner, G., Busfield, A., Crowther, S.A., Harrison, T.M., Mojzsis, S.J., Gilmour, J.D., 2007. Pu-Xe, U-Xe, U-Pb chronology and isotope systematics of ancient zircons from Western Australia. Earth. Planet. Sci. Lett. 261, 491-499.

Turner, G., Harrison, T.M., Holland, G., Mojzsis, S.J., Gilmour, J.D., 2004. Extinct 244Pu in ancient zircons. Science 306, 89-91.Valley, J.W., 2003. Oxygen isotopes in zircon. In Hanchar, J.M., Hoskin, P.W.O., eds., Zircon. Rev. Mineral. 53, 343-385.

Valley, J.W., 2003. Oxygen isotopes in zircon. In Hanchar, J.M., Hoskin, P.W.O., eds., Zircon. Rev. Mineral. 53, 343-385.

Valley, J.W., Cavosie, A.J., Fu, B., Peck, W.H., Wilde, S.A., 2006. Comment on "Heterogeneous Hadean hafnium: Evidence of continental crust at 4.4-4.5 Ga." Science 312, 1139a.

van Hunen, J., van den Berg, A.P., 2008. Plate tectonics on the early Earth: Limitations imposed by strength and buoyancy of subducted lithosphere. Lithos 103, 217-234.

Vavra, G., Gebauer, D., Schmid, R., Compston, W., 1996. Multiple zircon growth and recrystallization during polyphase Late Carboniferous to Triassic metamorphism in granulites of the Ivrea Zone (Southern Alps): an ion microprobe (SHRIMP) study. Contrib. Mineral. Petrol. 122, 337-358.

Vavra, G., Schmid, R., Gebauer, D., 1999. Internal morphology, habit and U-Th-Pb microanalysis of amphibolite-to-granulite facies zircons: geochronology of the Ivrea Zone (Southern Alps). Contrib. Mineral. Petrol. 34, 380-404.

Veizer, J., Ala, D., Azmy, K., Bruckschen, P., Buhl, D., Bruhn, F., Carden, G.A.F., Diener, A., Ebneth, S., Godderis, Y., Jasper, T., Korte, C., Pawellek, F., Podlaha, O.G., Strauss, H., 1999. $^{87}Sr/^{86}Sr$, $\delta^{13}C$ and $\delta^{18}O$ evolution of Phanerozoic seawater. Chem. Geol. 161, 59-88.

Vogt, K., Gerya, T.V., Castro, A., 2012. Crustal growth at active continental margins: Numerical modeling. Phys. Earth Planet. Int. 192–193, 1–20.

Wan, Y., Liu, D., Dong, C., Liu, S., Wang, S., Yang, E., 2011. U-Th-Pb behavior of zircons under high-grade metamorphic conditions: A case study of zircon dating of meta-diorite near Qixia, eastern Shandong. Geoscience Frontiers 2, 137-146.

Warren, P.H., 1989. Growth of the continental crust: a planetary-mantle perspective. Tectonophys. 161, 165–199.

Wasserburg, G.J., Tera, F., Papanastassiou, D.A., Huneke, J.C., 1977. Isotopic and chemical investigations of Angra Dos Reis. Earth Planet. Sci. Lett. 35, 294-316.

Watson, E.B., Harrison, T.M., 2005. Zircon thermometer reveals minimum melting conditions on earliest Earth. Science 308, 841–844.

Wielicki, M.T., Harrison, T.M., and Schmitt, A.K. 2012. Geochemical signatures and magmatic stability of impact produced zircons. Earth Planet. Sci. Lett. 321-322, 20-31.

Williams, I.R., Myers, J.S., 1987. Archean geology of the Mount Narryer region, Western Australia. W. Aust. Geol. Surv. Rep., 22: 32 pp.

Woodhead, J.D., Hergt, J.M., 2005. A preliminary appraisal of seven natural zircon reference materials for in situ Hf isotope determination. Geostd. Geoanal. Res. 29, 183-195.

Woodhead, J.D., Hergt, J.M., Shelley, M., Eggins, S., Kemp, R., 2004. Zircon Hf isotope analysis with an excimer laser, depth profiling, ablation of complex geometries, and concomitant age estimation. Chem. Geol. 209, 121–135.

Xie, L., Zhang, Y., Zhang, H., Sun, J., Wu, F., 2008. In situ simultaneous determination of trace elements, U-Pb and Lu-Hf isotopes in zircon and baddeleyite. Chinese Science Bulletin 53, 1565-1573.

Xie, S., Tackley, P.J., 2004. Evolution of U-Pb and Sm-Nd systems in numerical models of mantle convection and plate tectonics Journ. Geophys. Res.109, B11204, doi:10.1029/2004JB003176.